Expeditious Thermal(Photo) Induced Functionalization/Annulation: *En route* to N-Heterocycles

A dissertation submitted in partial fulfilment for the degree of

Doctor of Philosophy

Submitted by

TAMANNA KHANDELIA

Roll No. 186122116

Department of Chemistry

Indian Institute of Technology Guwahati

January 2024

DEDICATED

TO

MY FAMILY

INDIAN INSTITUTE OF TECHNOLOGY GUWAHATI

Department of Chemistry

STATEMENT

I do hereby declare that the matter embodied in this thesis is the result of investigations carried out by me in the Department of Chemistry, Indian Institute of Technology Guwahati, India, under the guidance of Prof. Bhisma K. Patel. This thesis has been submitted by me to the Department of Chemistry, Indian Institute of Technology Guwahati for the award of the Doctor of Philosophy.

In keeping with the general practice of reporting scientific observations, due acknowledgements have been made wherever the work described is based on the findings of other investigators. I further declare that this work has not been submitted anywhere else for any degree, diploma, associateship or membership etc. of any Institute or University to the best of my knowledge.

Tamanna Khandelia

January 2024 **Tamanna Khandelia**

IIT Guwahati

INDIAN INSTITUTE OF TECHNOLOGY GUWAHATI

Department of Chemistry

CERTIFICATE

This is to certify that Tamanna Khandelia has been working under my supervision since March, 2019 as a regular Ph.D. student. Her thesis entitled "**Expeditious Thermal(Photo) Induced Functionalization/Annulation: *En route* to N-Heterocycles**" is an authentic record of the results obtained from the research work in the Department of Chemistry, Indian Institute of Technology Guwahati, Assam, India. I am forwarding her thesis to submit for the Ph.D. (Science) degree from this institute. I certify that she has fulfilled all the requirements according to the rules of this institute regarding the investigations embodied in her thesis and this work has not been submitted elsewhere for a degree.

January 2024

Prof. Bhisma K. Patel
(Thesis Supervisor)
Department of Chemistry
IIT Guwahati

ACKNOWLEDGEMENT

With an extreme sense of gratitude and excitement, I take this opportunity to thank all the individuals who have helped and encouraged me during my Ph.D. studies. I thank IITG for the friendly environment it has provided which helped me enormously. I thank everyone from the bottom of my heart.

Firstly, I extend my sincere and immense gratitude to my supervisor, Prof. Bhisma K. Patel Sir. It was an inestimable privilege for me to have the opportunity to work under his supervision. I will always be grateful for his guidance, scientific ideas, support, encouragement, motivation throughout my journey in IITG. I thank him for everything and trusting me which gave me strength to work efficiently and responsibly.

I would like to express my deepest gratitude to my doctoral committee members, Prof. Bhubaneswar Mandal Sir, Prof. Subhas Chandra Pan Sir and Dr. Dipankar Srimani Sir for their continuous guidance in each and every step of my Ph.D. work. It is my pleasure to thank them for their valuable suggestions which added towards the improvement of my thesis. Also, I thank Prof. Siddhartha Sankar Ghosh Sir for the collaborative work done with him for one of my works.

I would also like to express my special and profound thanks to IITG for all the instrument facilities without which the work included in this thesis would not have been possible. Together with this I would also like to thank all the instrument operators for their carefulness and patience which leads to swift and correct analysis of the samples. I would like to thank Rinki Brahma for helping me with Single Crystal XRD studies. I also thank all the staff members of Chemistry department and IITG for their help whenever I was in need.

I extend my gratitude to INSPIRE for fellowship and SERB for funding and providing all the requirements.

I have been indeed fortunate enough to work with very experienced lab seniors Suresh Rajamanickam, Bilal A Mir, Subhendu Ghosh, Anjali Dahiya, Amitava Rakshit, Tipu Alam, Nikita Chakraborty, Ashish Kumar Sahoo, Binoyargha Dam, Kamal Krishna Rajbongshi, Bhaskar Deka. I would like to thank my senior Subhendu Ghosh for his valuable guidance and support in each and every step of my Ph.D. work. I also thank my friends and lab juniors Hirendra Nath Dhara, Bubul Das, Pritishree Panigrahi, Raju Mandal, Dinabandhu Barik,

Shalini Gupta, Deepjyoti Boruah, Supriya Manna for their help, motivation and always ready to help behaviour. I express my gratitude to all my friends in IITG Suravi Paul, Rabu Ranjan Changmai, Anisha Mondal, Mongoli Brahma and all my batch mates for making the journey easy for me and always extending a helping hand.

I cannot stop thanking my family for the endless love and care they have showered upon me. My parents have always supported me in all my endeavours of life because of which I could reach here. My mother has been the pillar of strength throughout my journey of Ph.D. with all her motivational words, life lessons, care, love, endless warmth and incomparable support. Also, my siblings Sneha and Harsh equally made the journey very easy for me. The warm bond we exchange with each other strengthened me to handle many difficult situations in an effective manner. I thank my family for the support, love and affection.

Finally, I thank the Almighty for blessing me with good health during the Ph.D. studies and for everything it has given me.

Tamanna Khandelia

SYNOPSIS

The content of the thesis has been divided into four chapters based on the research conducted and productive results obtained. The research idea included in the thesis streamlines the synthesis of aromatic and non-aromatic N-heterocycles. These chapters contribute towards the facile formation of C–C, C–N, C–O and C–S bonds using *o*-alkynylanilines, maleimides, 2-aryl quinoxalines, (benz)imidazoles, boronic acids and disulfides.

Chapter I gives an introduction to transition metal induced (thermal) and photochemical construction of C–C and C–Heteroatom bonds. The mechanism involved in both transition metal induced (thermal) and photochemical approach are discussed. Both the processes are explained in details with the help of suitable examples.

Chapter II describes a Cu(I) mediated cascade cyclization/annulation of unprotected *o*-alkynylanilines with maleimides in one-pot. The protocol offers sequential formation of one C–N and two C–C bonds to deliver fused benzo[*a*]carbazoles having free NH skeletons. The annulated products display fluorescence emission in the range of 485–502 nm with a large Stokes shift and fluorescence lifetime of ~17 ns. The annulated benzo[*a*]carbazoles display AEE behavior in the ethanol/hexane system and possesses marigold-flower like morphology at the aggregated state. Cell viability assays enumerate biocompatible of AEEgens, while their high intracellular fluorescence depicts cell imaging applicability.

Chapter III describes a $Cu(OTf)_2$ mediated regioselective de-aromatized aryl-hydroxylation across $C(sp^2)$=N bond of 2-aryl quinoxalines and bis-N-arylation of (benz)imidazoles using aryl boronic acids. For dearomative aryl-hydroxylation, the C-center should be electrophilic (*ca.* 0.08), N-center nucleophilic (*ca.* –0.50), and the $C(sp^2)$=N bond should be polarized (Δe = 0.609).

Chapter IV describes a visible light-driven di-functionalization of maleimide with disulfide and *in situ*-generated singlet oxygen to offer selective 1,2-thiohydroxylation under additive-free conditions. Here, the disulfide plays dual role of photosensitizer and the coupling reagent. Notably, the hydroxyl functionality originates from the *in situ* generated singlet oxygen followed by HAT from H_2O (moisture).

Chapters II, III, and IV comprise of introduction, previous work, present work, experimental section, references, spectral data and a few representative spectra.

CHAPTER I: An Overview of Thermal(Photo) Induced Functionalization/Annulation: Formation of C–C and C–Heteroatom Bonds

Organic synthesis is the root of the advancements made in synthesis of many important natural products, drugs, and organic materials. Since the foundation of organic chemistry, there has been a continuous effort made by synthetic chemists to develop molecules efficiently. With this quest, the construction of C–C, C–N, C–O, C–S and other C–heteroatom bonds in an efficient manner becomes a challenge for organic chemists.

Heterocycles form an integral part of pharmaceutical and functional materials and 59 % of FDA-approved drugs are made up of nitrogen heterocycles. Both saturated and unsaturated heterocycles form numerous pertinent drugs as they improve the solubility, polarity, lipophilicity, and hydrogen bonding capacity of the drugs and optimize their application. Moreover, the heteroatom in heterocycles provides scope for further modification of the molecule. The biochemicals present in the human body are mainly composed of heterocycles for example nucleic acid, glucose, bilirubin, biliverdin etc. Considering the importance and applications of heterocycles, their synthesis has been highly sought after and has been challenging the synthetic chemists.

As the research work included in the thesis is based on the principles of transition metal (copper) mediated and photocatalytic synthesis of N-Heterocycles, this section has been divided into two segments such as (a) transition metal assisted synthesis (b) photocatalytic synthesis.

(a) Transition Metal Assisted Synthesis

Until very recently, the C–H bond breaking was considered a challenging task. The introduction of Transition Metal (TM) catalyzed C–H activation has changed the scenario and has been one of the pioneer processes for the activation of C–H bonds since the last three decades. The method has been widely utilized for the synthesis and functionalization of organic molecules in a regioselective and stereoselective manner. Moreover, it is a step and atom economical method to reach the target molecule as compared to the traditional cross-coupling which require prefunctionalization of starting materials in addition to the requirement of additives.

The process of TM catalyzed C–H functionalization involves the activation of the substrate with the TM catalyst leading to the formation of a reactive organometallic species. The substrate coordinates to the metal either as an alkene/arene complex intermediate or a transition state (M–C bond formation). This intermediate or transition state then reacts with the second component to deliver the final functionalized (Scheme I.1. a) or annulated product (Scheme I.1. b).

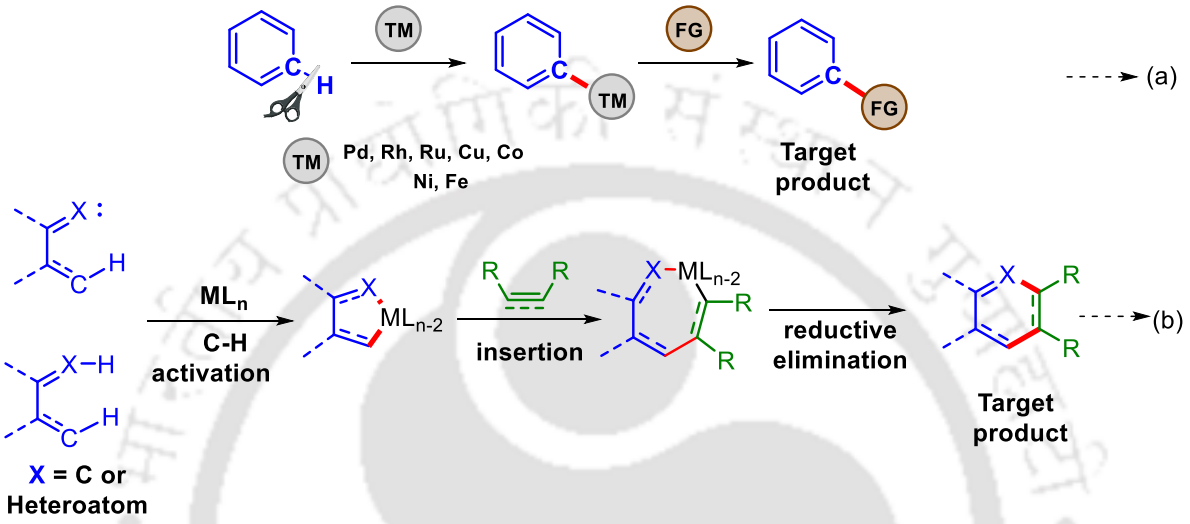

Scheme I.1. *(a) C–H functionalization and (b) C–H annulation*

The transition metal catalyzed/mediated organic synthetic strategy has been widely employed for the synthesis of heterocycles. Among the transition metals, copper salts are less expensive and more abundant as compared to 4d and 5d transition metals.

(b) Photocatalytic Synthesis

Photocatalysis has been growing at a fast pace to synthesize complex organic molecules. In an attempt to move towards a sustainable approach to organic synthesis, photocatalysis has met the goals of environment friendliness with the utilization of visible light under mild conditions. Moreover, photochemistry provides access to complex molecules which are difficult to synthesize via the thermal pathway.

A photochemical process generally includes an external organic or inorganic photocatalyst. In other photochemical processes, the reaction does not depend on any external photocatalyst and is self-sufficient to absorb the visible light. Accordingly, the process may be (a) photo-redox catalysis (b) Energy Transfer (EnT) catalysis (c) EDA complex driven synthesis (d) Self photoexcitation driven synthesis.

(a) Photo-redox Catalysis

The photo-redox catalysis involves photocatalyst. There is transfer of a single electron (SET) either to the excited photocatalyst from the substrate or from the excited photocatalyst to the substrate depending upon the reductive or oxidative process involved (Figure I.1).

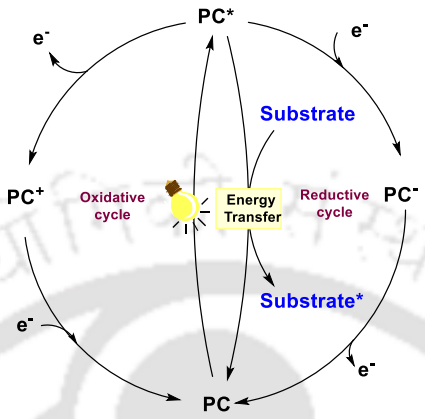

Figure I.1. *Photo-redox catalysis*

(b) Energy Transfer (EnT) Catalysis

In general, a substrate is photoexcited from the ground state S_0 to its excited state S_1 by the absorption of photons. Subsequently, the excited S_1 state undergoes an intersystem crossing (ISC) to reach T_1 which is a rapid process. Moreover, the relaxation from T_1 to S_0 is spin forbidden and thus the substrate stays in the T_1 state for longer time and majority of the reactions occur from the T_1 state.

The Energy Transfer (EnT) Catalysis involves photocatalyst. In the process of Energy Transfer (EnT) catalysis, a similar concept of excitation is applied and a triplet energy sensitiser (photocatalyst) transfers its triplet energy to the substrate and excites the substrate to its triplet state in an overall spin allowed process. The process of EnT from the triplet energy to the substrate is exergonic (E_T(substrate) ≤ E_T(sensitiser)). A collision between the two leads to the energy transfer (Figure I.2).

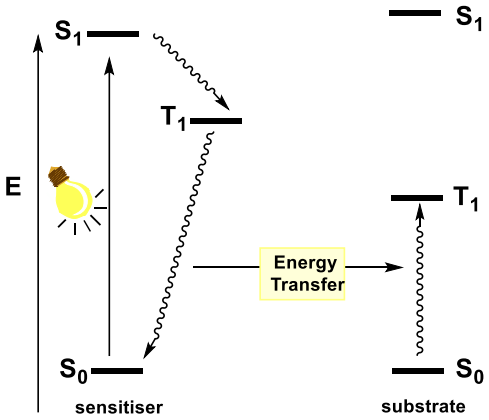

Figure I.2. *Energy Transfer (EnT) catalysis*

The excited triplet state (T_1) has different reactivity as compared to the ground state. Most organic molecules require UV light for excitation, which makes the application a difficult

process. To circumvent this difficulty, photosensitisers are used to reach the triplet state in a milder condition by the absorption of visible light.

(c) EDA Complex Driven Synthesis

The EDA complex driven synthesis does not involve photocatalyst. There is formation of transient electron donor-acceptor (EDA) complex between an electron donor (D) and electron acceptor (A). This EDA complex absorbs light which triggers an intramolecular single electron transfer (SET) to form a charged species D+· and A–· and deliver the target product under mild conditions (Scheme I.2).

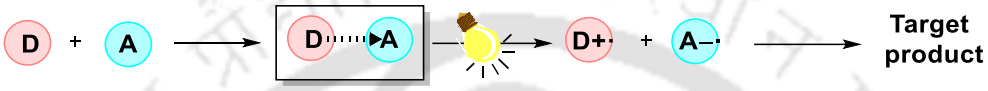

Scheme I.2. *EDA complex driven synthesis*

(d) Self Photoexcitation Driven Synthesis

The self photoexcitation driven synthesis does not involve photocatalyst. The reagent itself is photoexcited and assists the photochemical reaction via homolytic cleavage to form radicals (Scheme I.3).

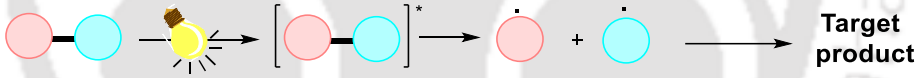

Scheme I.3. *Self-photoexcitation driven synthesis*

CHAPTER 2: Copper(I) Mediated Cascade Annulation *via* Dual C–H/C–H Activation: Access to Benzo[*a*]carbazolic AEEgens

Abstract: *This chapter focuses on the synthesis of benzo[a]carbazoles and its applications. A Cu(I) mediated cascade annulation is introduced for the cyclization of unprotected o-alkynylanilines with maleimides in one-pot. This cascade annulation involves the sequential formation of one C–N and two C–C bonds to deliver fused benzo[a]carbazoles having free NH skeletons. The annulated products display excellent photophysical properties and have been utilized for cell imaging.*

The interest in developing pharmacologically and functionally pertinent π-extended nitrogen-containing polyaromatic hydrocarbons (NPAHs) *via* one-pot cascade-annulation has

increased largely in contemporary organic synthesis. In this context, benzo[*a*]carbazole fused NPAHs have shown phenomenal applications in the field of medicinal and functional materials chemistry.

Due to the importance of benzo[*a*]carbazoles there has been a pursuit among researchers to synthesize them elegantly. The reported methods mainly utilize 4d- and 5d- transition-metals such as Rh, Pd and Au. Thus, the discovery of methods utilizing cheaper 3d metals to access the functionalized benzo[*a*]carbazoles is highly sought after. There is no report on dehydrogenative annulation of maleimide with an unprotected 2-alkanylaniline using copper salt to deliver benzo[*a*]carbazole. This chapter describes the synthesis of benzo[*a*]pyrrolo[3,4-*c*]carbazole-1,3(2*H*,8*H*)-dione (**3**) from *o*-alkynylanilines (**1**) and maleimides (**2**) using Cu(I) salt (Scheme II.1). The oxidative annulation involves an intramolecular cyclization followed by an intermolecular dual C–C bond formation.

The best optimized condition was the use of *o*-alkynylaniline (1 equiv), maleimide (1.5 equiv), $Cu(CH_3CN)_4BF_4$ (1.5 equiv), $AgNO_3$ (30 mol%), NaOAc (1.5 equiv), dry 1,2-DCE (1.5 mL) at 110 °C for 15 h under N_2 atmosphere. With this optimized reaction condition in hand, the scope and generality of the reaction condition was tested. Various substituted *o*-alkynylaniline with substitution in both the aryl rings and *N*-substituted and free N–H maleimides adhered to the protocol (Scheme II.1).

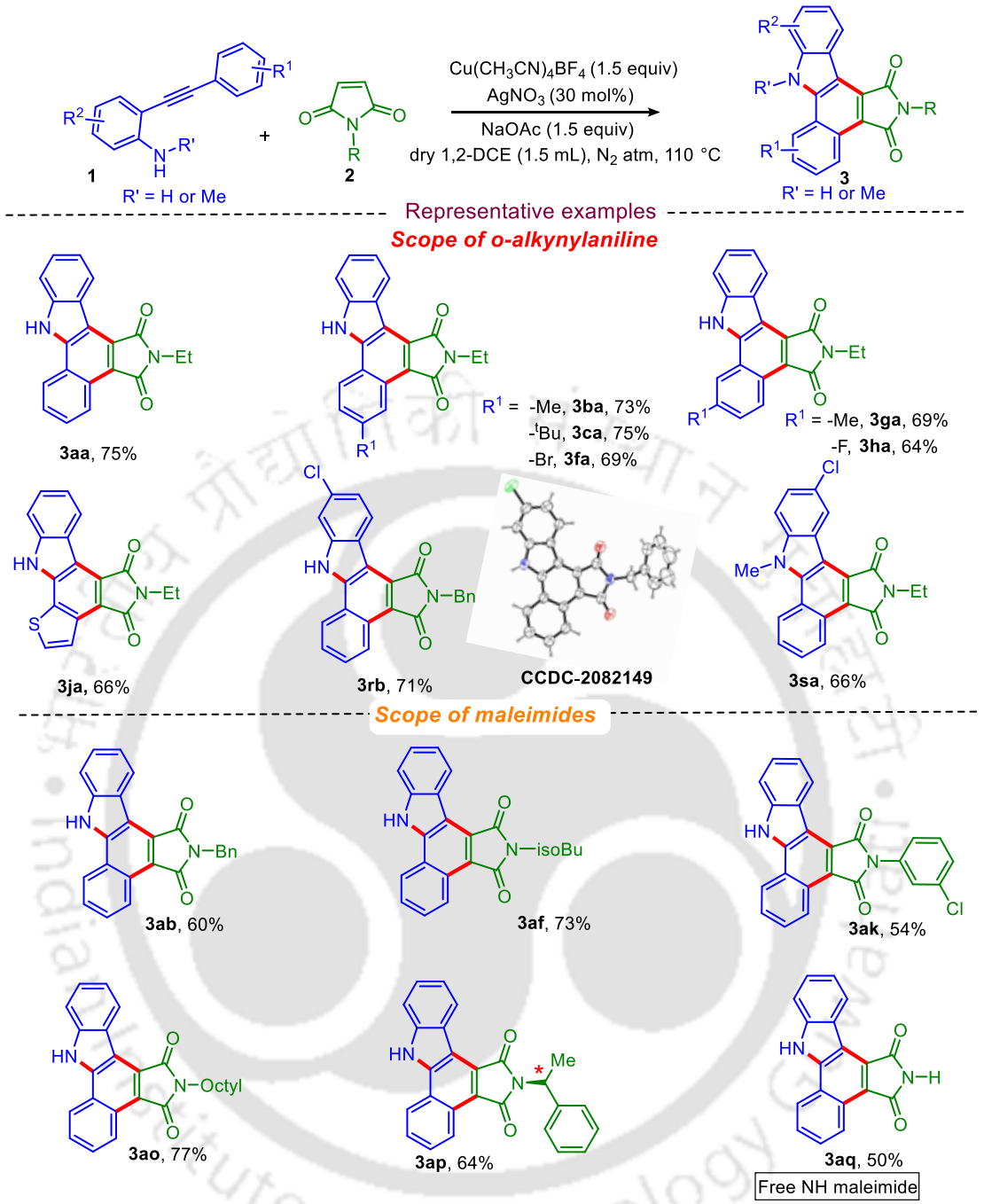

Reaction conditions: **1** (0.35 mmol), **2** (0.53 mmol), $Cu(CH_3CN)_4BF_4$ (1.5 equiv), $AgNO_3$ (30 mol%), NaOAc (1.5 equiv), dry 1,2-DCE (1.5 mL) at 110 °C for 15 h under N_2 atmosphere.

Scheme II.1. *Synthesis of benzo[a]carbazoles*

To understand the mechanism several studies were conducted. Based on these mechanistic studies, HRMS analysis of reaction aliquots, and earlier reports a plausible mechanism for this transformation is proposed in Scheme II.2. At first in the presence of silver salt, a transient silver-amine complex **I** is formed to prevent the transition metal poisoning from free $–NH_2$ of

1a. Then, the Cu/Ag salts polarize the triple bond of 2-(phenylethynyl)aniline to promote a 5-endo dig cyclization followed by nucleophilic substitution of metal to provide a C3-cuprated indole species (**C**). The coordination of *N*-ethylmaleimide (**2a**) to intermediate **C** and subsequent migratory insertion into the reactive Cu–C bond give the intermediate **E**. Further, the copper metal gets inserted into the *ortho*-C–H of the C-2 phenyl ring to deliver a seven-membered cupracycle **F**. Then the reductive elimination, followed by the oxidation of **G** afforded the annulated product (**3aa**).

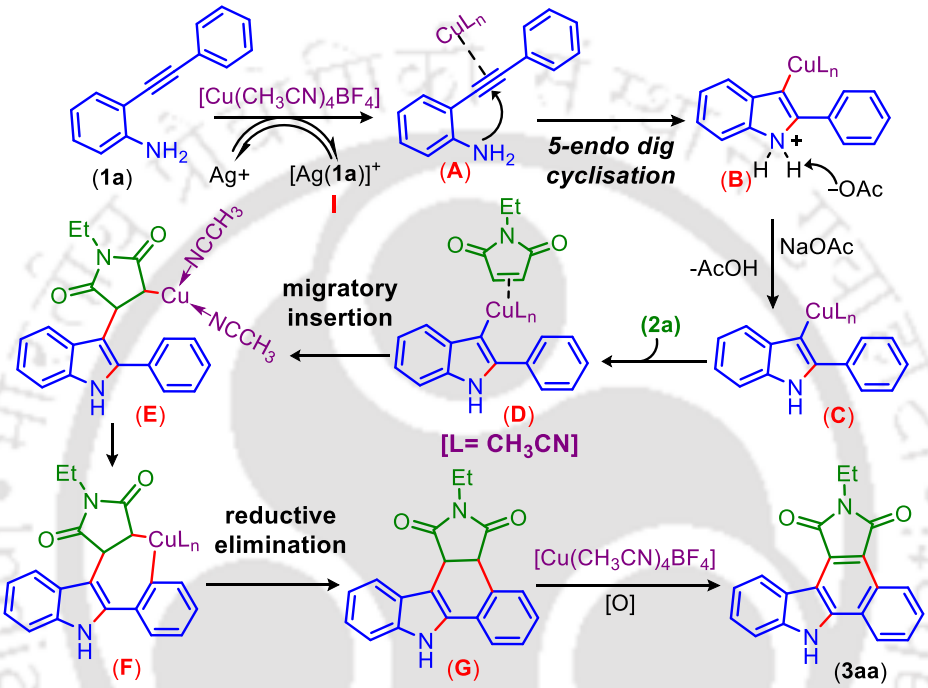

Scheme II.2. *Plausible mechanism for cascade-annulation*

Several post-synthetic studies and applications of the synthesized annulated products were conducted such as (i) electronic structure study via density functional theory (DFT) calculation, (ii) investigation of photophysical properties including aggregation-enhanced emission (AEE) phenomenon, (iii) biological studies and applications. The annulated products display admirable photophysical properties with fluorescence emission in the range of 485–502 nm with a fluorescence lifetime of ~17 ns. The annulated benzo[*a*]carbazoles display AEE behavior in ethanol/hexane system. Cell viability assays enumerate biocompatiblity of AEEgens, and their high intracellular fluorescence depicts cell imaging applicability.

In summary, a copper(I) mediated dual annulation involving dual C–C bonds formation is reported. The cascadic intramolecular and intermolecular C–H/C–H cyclization of *o*-alkynylanilines with maleimides leads to highly fluorescent benzo[*a*]carbazoles. The protocol offers two consecutive ring construction involving one new C–N and two C–C bonds formation

in a single pot with diverse functional group tolerance. The synthesized annulated products displayed strong emission in the green region. The annulated compounds display AEE behavior in the ethanol/hexane solvent system The compounds are biocompatible and convenient for the cellular imaging of HeLa cell lines.

CHAPTER 3: Dearomative Bis-Functionalization of Quinoxalines and Bis-*N*-Arylation of (Benz)imidazoles via Cu(II) Mediated Addition of Boronic Acids

Abstract: *This chapter describes a $Cu(OTf)_2$ mediated regioselective de-aromatized aryl-hydroxylation across $C(sp^2)$=N bond of 2-aryl quinoxalines and bis-N-arylation of (benz)imidazoles using aryl boronic acids. It has been calculated that for dearomative aryl-hydroxylation, the C-center should be electrophilic (ca. 0.08), N-center nucleophilic (ca. –0.50), and the $C(sp^2)$=N bond should be polarized (Δe = 0.609).*

The strategy of difunctionalization across C–C unsaturated bonds has emerged as a straightforward approach to enhance molecular complexity. Significant effort has been devoted towards bi-functionalization employing transition metal or photocatalytic approaches. Whereas bis-functionalization across $C(sp^2)$=N bond in an aromatic heterocyclic system is far less explored as the addition leads to dearomatization and thus the approach requires sophisticated reaction protocols. In this context, regioselective de-aromatized bis-functionalization of the $C(sp^2)$=N bond under mild conditions is a challenging and demanding task for synthetic chemists.

The utility of C–C bonds containing compounds is enhanced through the incorporation of heteroatoms. Among all carbon-heteroatom bond-forming reactions, the construction of C–N and C–O bonds have gained much attention due to their prevalence in the structural core of numerous natural products, pharmaceuticals, and polymeric materials. These bonds are constructed via nucleophilic substitutions and transition metal-catalyzed cross-coupling reactions. In this context, C–N cross-coupling reactions such as Buchwald-Hartwig, Ullmann, and Chan-Evans-Lam (CEL) which utilizes transition-metal catalyst are well established. But these C–N cross-couplings require a free N–H group along with the usage of suitable ligands, base and transition metals. Thus, the regioselective C(aryl)–N bond formation across the $C(sp^2)$=N bond of heteroarenes is an alternative avenue to classical C–N bond forming

reactions. In this context, there were reports on synthesis of quaternized salts (via C–N bond formation) without losing their aromaticity.

Quinoxaline being a privileged class of N-containing heterocycles, this chapter focuses on the C–N bond formation in this moiety. Substituted quinoxaline (**1**) (having two types of $C(sp^2)$=N bonds), upon reaction with boronic acid (**2**) in the optimized reaction condition delivered a dearomatized aryl-hydroxylated product *viz.* 1,3-diphenyl-1,2-dihydroquinoxalin-2-ol (**3aa**) (Scheme III.1).

The best optimized condition was the use of 2-aryl quinoxaline (1 equiv), boronic acid (1.6 equiv), $Cu(OTf)_2$ (1.2 equiv), toluene (1.5 mL), at 90 °C for 15 h. With the optimized condition in hand, the scope of the reaction was checked with various substituted 2-(hetero)arylquinoxalines (**1**) and arylboronic acids (**2**) (Scheme III.1). All reacted well to give an array of hydroxyarylated quinoxalines in good yields.

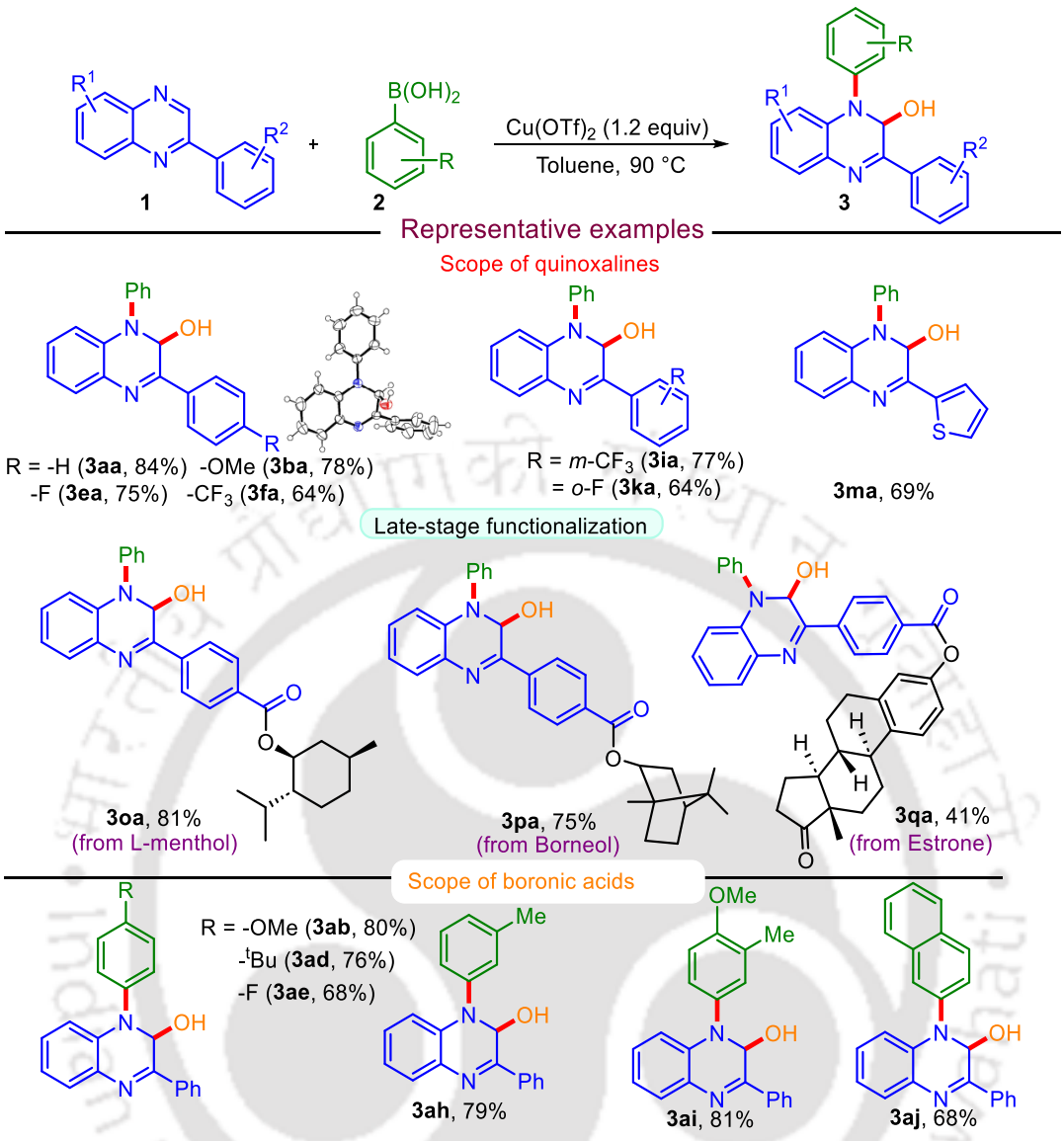

Reaction conditions: **1** (0.35 mmol), **2** (0.56 mmol), $Cu(OTf)_2$ (1.2 equiv), toluene (1.5 mL) at 90 °C for 15 h.

Scheme III.1. *Synthesis of hydroxyarylated quinoxalines*

Now, a query arises whether a similar addition across C(sp^2)=N bonds having a diverse steric and electronic environment in quinoxaline analogues will occur? To find this out, atomic charge distribution calculations on various substrates were carried out. From the atomic charge distribution pattern of **1a**, the sterically less hindered C(sp^2)=N bond has a Mulliken charge of –0.528 and 0.081 respectively at the N and C atoms, with a charge difference of 0.609. Thus, the essential requirement hydroxy arylation is, the C-center should be electrophilic (*ca.* 0.08), N-center nucleophilic (*ca.* –0.50), and the C(sp^2)=N bond should be sufficiently polarized (Δe = 0.609) which is not the case with quinoxaline analogous substrates.

When (benz)imidazoles (**9**) were subjected to the present conditions all provided bis-arylated quaternized products **10** (Scheme III.2). Variously substituted benzimidazole, imidazole and boronic acids delivered the bis-arylated quaternized products in good yields.

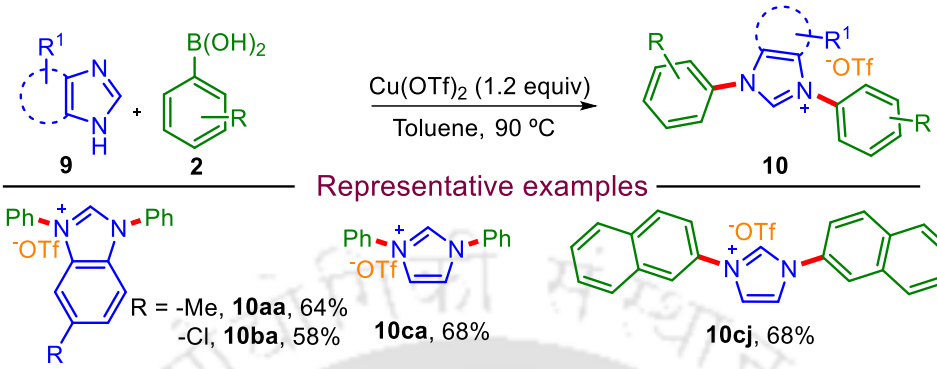

Reaction conditions: **9** (0.35 mmol), **2** (0.88 mmol), $Cu(OTf)_2$ (1.2 equiv), toluene (1.5 mL) at 90 °C for 15 h.

Scheme III.2*. Synthesis of bis-N-arylated (benz)imidazoles.*

Based on previous reports, results obtained from the control reactions and high-resolution mass spectrometry (HRMS) analysis of the reaction aliquots, a plausible mechanism is proposed (Scheme III.3). Initially, $Cu(OTf)_2$ forms a complex **A** with 2-phenylquinoxaline. Trans-metalation of the phenyl ring of the boronic acid with **A** resulted in another intermediate (**B**). The Cu(II) complex (**B**) is oxidized to Cu(III) by $Cu(OTf)_2$ via disproportionation reaction to give **C**. This is followed by migration of the Cu bound –OH group to the C3 position of **1a** with the formation of the Cu–N bond to give **D**. Next, reductive elimination of **D** offers the final product **3aa** with the release of reduced species **E**. Similarly, the mechanism for the formation of **10** involves transmetallation, coordination, oxidation and reductive elimination where Chan-Evans-Lam (CEL) reaction delivers the N-arylated (benz)imidazole (Scheme III.3).

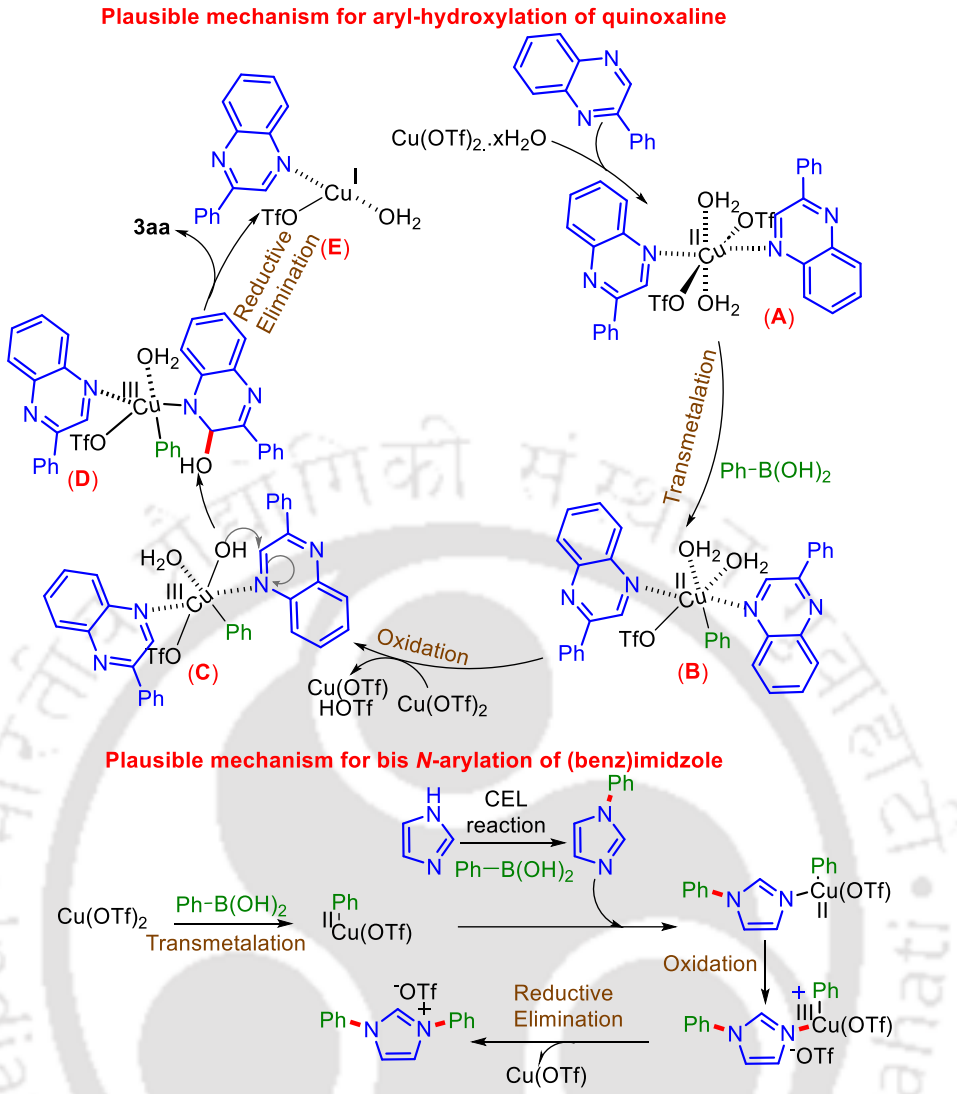

Scheme III.3. *Plausible mechanism.*

In conclusion, this work presents a $Cu(OTf)_2$ mediated addition of phenylboronic acid to $C(sp^2)$=N bond embedded in 2-aryl quinoxaline to deliver dearomatized bifunctionalized (hydroxyarylated) quinoxalines. The essential requirement for aryl-hydroxylation is that the $C(sp^2)$=N bond should be sufficiently polarized (Δe = 0.609) (C-center electrophilic (*ca.* 0.08), N-center nucleophilic (*ca.* –0.50) and sterically unhindered. Under similar conditions, (benz)imidazole undergo *bis*-N-arylation. Mechanistic investigation indicates copper bound aryl and –OH group addition to the selective C=N bond.

CHAPTER 4: Photo-Induced 1,2-Thiohydroxylation of Maleimide Involving Disulfide and Singlet Oxygen

Abstract: *This chapter focuses on visible light-driven di-functionalization of maleimides with disulfides. The protocol utilizes in situ generated singlet oxygen which offers selective 1,2-thiohydroxylation under additive-free conditions. Here, the disulfide plays dual role of photosensitizer and as a coupling reagent. Notably, the hydroxyl functionality originates from the in situ generated singlet oxygen followed by HAT from H_2O in moisture.*

The recent times of modern organic synthesis has witnessed the rapid application of photo-catalysis. It offers sustainable and eco-friendly conditions to access drugs, natural products, and agrochemicals. Many photochemical strategies are associated with developing biologically and functionally pertinent organosulfur compounds. The organosulfur compounds having alkyl-aryl C–S and vicinal C–S/C–O linked candidates have gained much attention due to their prevalence in many commercial drugs. In this context, the intricate structure of sulfur compounds and their multiple valences have attracted researchers to synthesize numerous sulfur-linked targets using thiols as one of the precursors. But the stench and toxic behaviour of thiols and the requirement of oxidant and metal for the generation of thiyl radical make this route unfavourable for accessing C–S bonds. To overcome this, disulfides have been used as an alternative thiolating reagent to facilitate C–S bond formation. Moreover, under the irradiation of light of appropriate wavelength organic disulfides undergo homolytic cleavage, generating thiyl radical (RS•). Thus, a sustainable and mild disulfide mediated protocol is highly looked for.

The alkene di-functionalization strategy is renowned to open up a new path to access complex molecular entities via the simultaneous installation of two distinct functionalities. Lately, this strategy rapidly evolves under metal and photocatalysis to synthesize numerous functional materials. Despite notable achievement in this arena, the di-functionalization of maleimide under sustainable photocatalysis is highly sought after. As maleimides and succinimides are biologically pertinent scaffolds therefore great efforts have been devoted towards their functionalization. Apart from this, maleimides are also explored as powerful di-functionalization handles to access substituted maleimides.

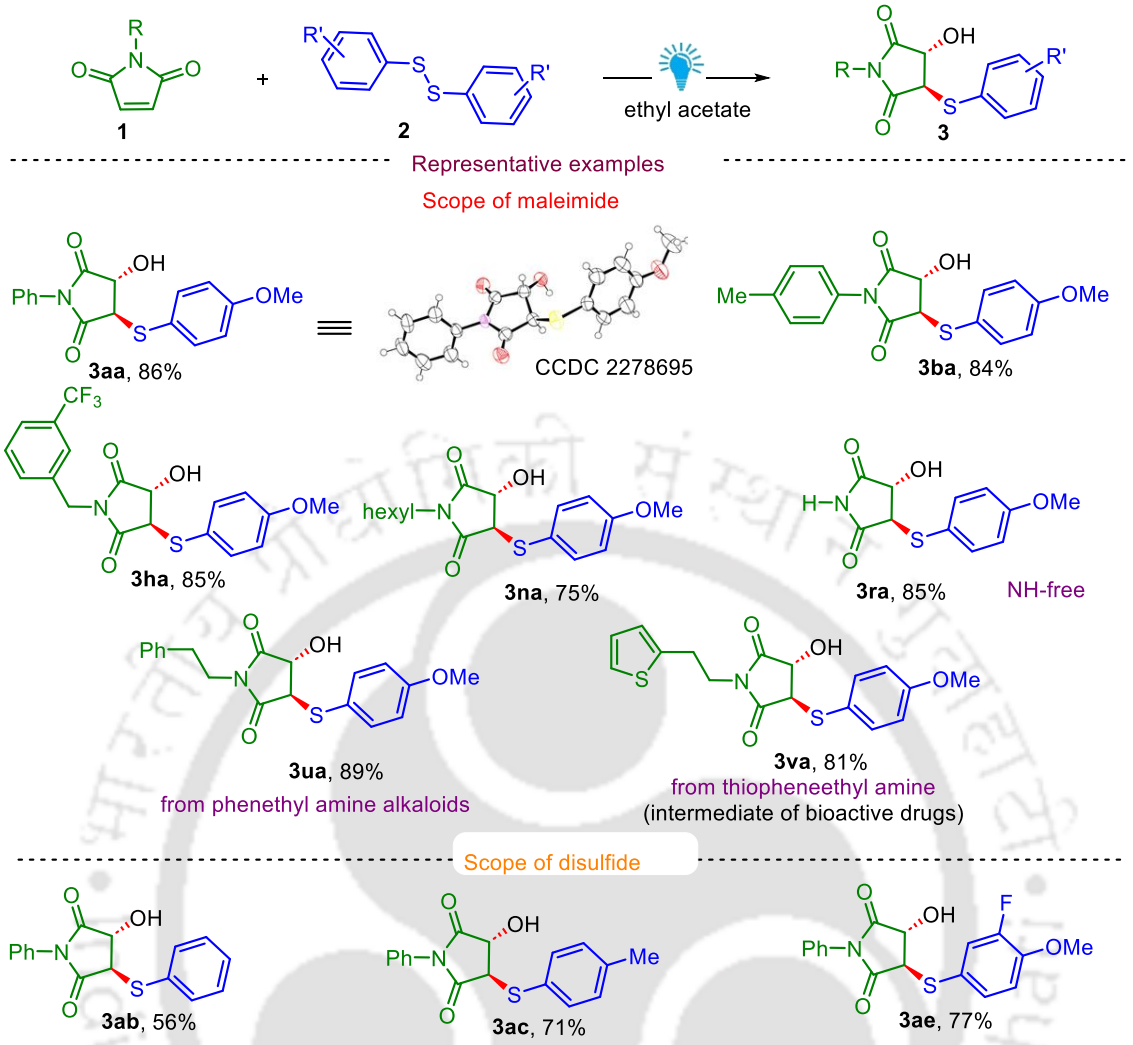

Reaction conditions: **1** (0.25 mmol), **2** (0.125 mmol), ethylacetate (2 mL) for 9 h in an open-air under 5W x 4 blue LEDs ($\lambda_{em,max}$ = 419 nm).

Scheme IV.1*. Synthesis of 1,2-thiohydroxylated maleimide*

There have been reports of difunctionalization of maleimide in metal catalyzed thermal conditions and photochemical approach with the usage of organic and inorganic photocatalysts. Thiyl radicals are powerful hydrogen atom transfer (HAT) catalysts in a photo redox process and can add across C=C double bond. Despite the remarkable achievements, to the best of our knowledge the di-functionalized succinimides are less scrutinized under sustainable photocatalysis. With this vision of di-functionalization of maleimide under a sustainable additive-free photocatalysis, N-phenylmaleimide (**1a**) (1 equiv.) and 1,2-bis(4-methoxyphenyl)disulfane (**2a**) (0.5 equiv., λ_{ab} = 400–440 nm) were reacted in ethyl acetate under blue light ($\lambda_{em,max}$ = 419 nm) irradiation to deliver a di-functionalized thio-hydroxylated

maleimide (**3aa**) or (3*S*,4*R*)-3-hydroxy-4-((4-methoxyphenyl)thio)-1-phenylpyrrolidine-2,5-dione in trans selective form (Scheme IV.1).

The, best optimized condition was the use of maleimide (1 equiv) and disulfane (0.5 equiv) in ethyl acetate under the exposure of blue LEDs (4 x 5W, $\lambda_{em,max}$ = 419 nm) in an open air. By executing the optimized reaction conditions, the scope of the strategy was extended towards diversely substituted maleimides and disulfides (Scheme IV.1). Various substituted N-phenyl maleimides, N-benzyl maleimides, N-alkyl maleimides including long alky chains, free NH maleimide and unsubstituted, mono and disubstituted disulfides delivered the 1,2-thiohydroxylated products in good yields.

Based on the mechanistic studies and literature precedence a plausible reaction mechanism is depicted in Scheme IV.2. Initially, under blue light irradiation, the disulfide (**2a**) is excited and cleaved to thiyl radical (**A**) with the generation of singlet oxygen ($^1O_2$) from triplet oxygen ($^3O_2$). The thiyl radical **A** then underwent radical addition to the C=C bond of N-phenyl maleimide **1a** to form the radical species **B**. Which then reacts with the singlet oxygen to afford a peroxy radical species **C**. A subsequent protonation from H_2O with the generation of H_2O_2 delivers a peroxy intermediate **D** which subsequently lead to the hydroxyl thiolated adduct **3aa**.

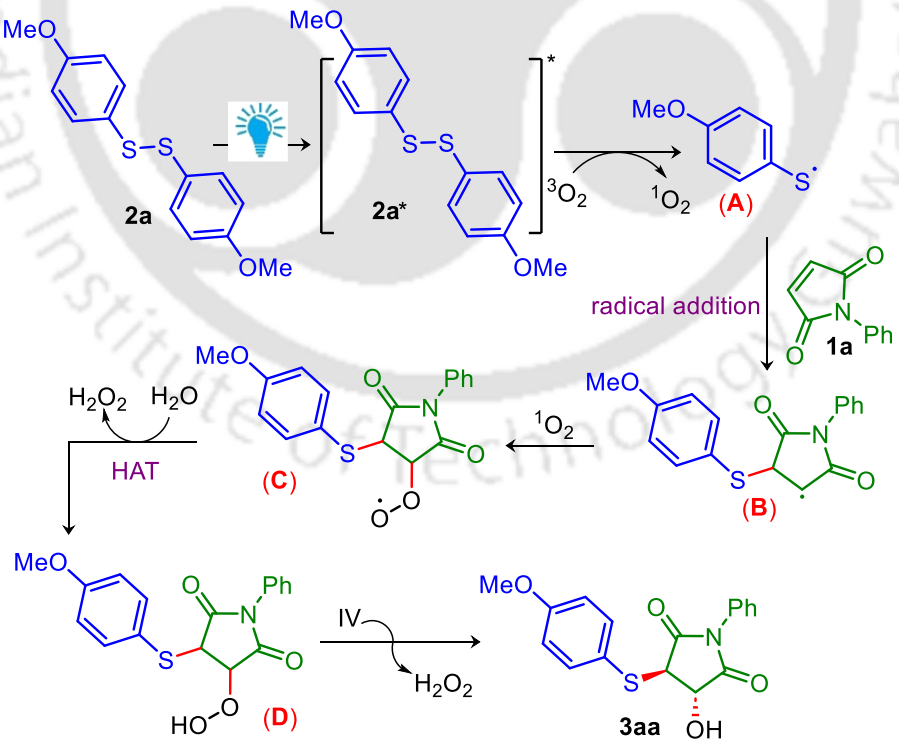

Scheme IV.2. *Plausible mechanism of thiohydroxylation*

In summary, a visible-light-induced 1,2-thiohydroxylation of maleimides has been accomplished using disulfides in green solvent ethyl acetate under mild conditions. The hydroxyl group originates from the singlet oxygen generated *in situ* from the atmospheric oxygen and photo activated disulfide. The mechanism involves the formation of peroxy radical followed by HAT from H_2O via water oxidation. External photocatalyst free, decent yield and 1,2-thiohydroxylation in a simple ease technique are salient features of this protocol.

CONTENTS

An Overview of Thermal(Photo) Induced Functionalization/Annulation: Formation of C–C and C–Heteroatom Bonds

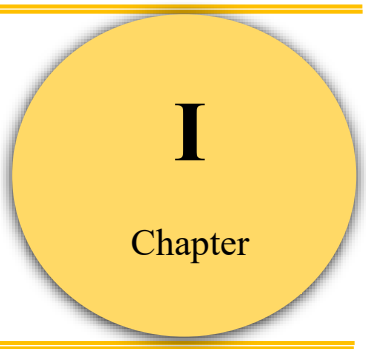

ABSTRACT

An introduction to transition metal induced (thermal) and photochemical construction of C–C and C–Heteroatom bonds is provided in this chapter. The mechanism involved in both transition metal induced (thermal) and photochemical approach are discussed. Both the processes are explained in details with the help of suitable examples.

I.1. Introduction

The dawn of organic chemistry lies in an effort to comprehend the chemistry of life. Inadvertently, organic chemistry is applied in universal activities of living beings such as medication, food, bridging of brain cells by neurotransmitters (serotonin), etc. The advancements made in organic chemistry is an effort towards the well-being of mankind and move towards an economic side. Organic chemistry has its contribution towards synthesizing new molecules with various utilities in the field of agrochemicals, pharmaceuticals and functional materials in an atom and step economical manner. With the advent of studying and synthesizing new molecules together with introduction of newer methods for the synthesis of organic molecules, organic chemistry has progressed significantly.

Organic compounds which exist ubiquitously in the ecosystem constitute mainly of carbon and hydrogen atoms. The synthesis of these compounds requires the activation of the C–H and C–C bonds (C–C, C=C, C≡C) which are inert due to their high bond dissociation energy (BDE) and non-polar nature. Modification and synthesis of organic molecules require the alteration of the ubiquitous C–H bonds, C–C bonds (C–C, C=C, C≡C) and other C–heteroatom bonds.

Heterocycles form an integral part of pharmaceutical and functional materials; and 59 % of FDA approved drugs are made up of nitrogen heterocycles.[1] Both saturated and unsaturated heterocycles form numerous pertinent drugs as they improve the solubility, polarity, lipophilicity and hydrogen bonding capacity of the drugs and optimize their application. Moreover, the heteroatom in the heterocycle provide scope for further modification of the molecule. The biochemicals present in the human body are mainly composed of heterocycles for eg nucleic acid, glucose, bilirubin, biliverdin etc. Considering the importance and applications of heterocycles, their synthesis has been highly sought after and has been challenging the synthetic chemists.[2]

Among the various methods of heterocycle synthesis (C–C and C–Heteroatom bond formation), transition metal (TM) catalyzed/mediated organic synthesis is one of the most pronounced methods.[3] Together with this, various other methods have been developed including the concept of photochemistry,[4] electrochemistry,[5] etc. Also, organic molecules have been synthesized in the absence of any metal in a metal free concept.[6] Since the works reported in this thesis include the concept of transition metal TM (Copper) mediated and photochemical synthesis of N-heterocycles, detailed explanation of these two concepts is provided below.

I.2. Transition Metal Assisted Synthesis

The construction of C–C, C–N, C–O, C–S and other C–heteroatom bonds with the usage of Transition Metal (TM) (Pd, Rh, Ru, Cu, Co, Ni, Ir, Fe, etc.) has become one of the inevitable processes for organic chemists.[7] Until very recently, the C–H bond breaking was considered a challenging task. The introduction of TM catalyzed C–H activation has changed the scenario and is one of the pioneer processes for the activation of C–H bonds since the last three decades.[8] The method has been widely utilized for the synthesis and functionalization of organic molecules in regioselective and stereoselective manners.[9] Moreover, it is a step and atom economical method to reach the target molecule as compared to the traditional cross coupling reactions which require prefunctionalization of starting materials in addition to the requirement of additives (Scheme I.2.1).[10]

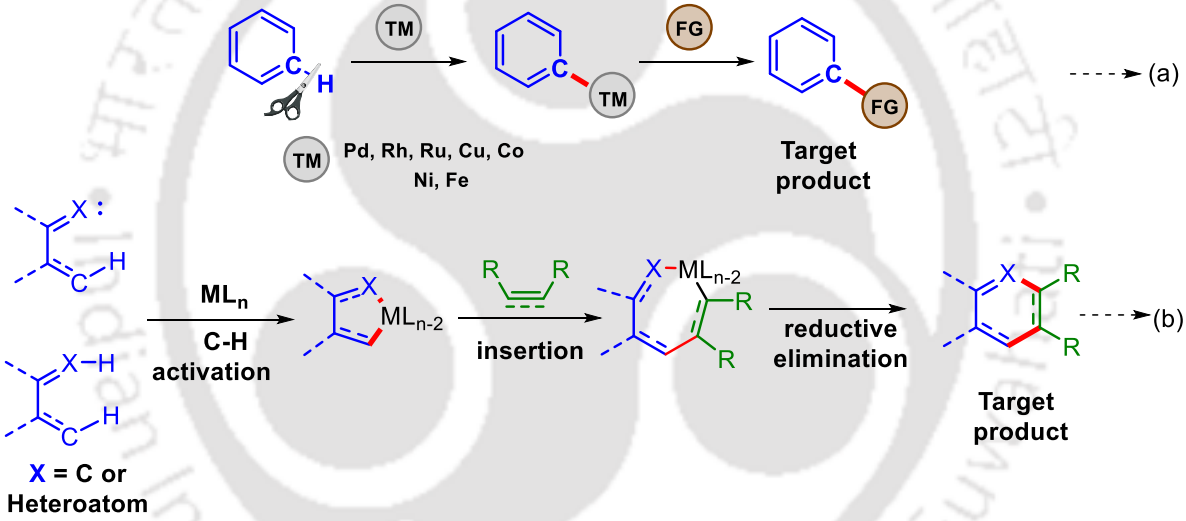

Scheme I.2.1. *Transition metal assisted (a) C–H functionalization and (b) C–H annulation*

I.2.1. Challenges in Transition Metal Assisted Synthesis

With the accomplishment made in the field of Transition Metal Assisted Synthesis, there were many challenges attached to the process (Scheme I.2.1.1).[11] Such as (a) ubiquitous nature of C–H bond (b) diverse reactivity of the substrate (c) regioselectivity and (d) stereoselectivity

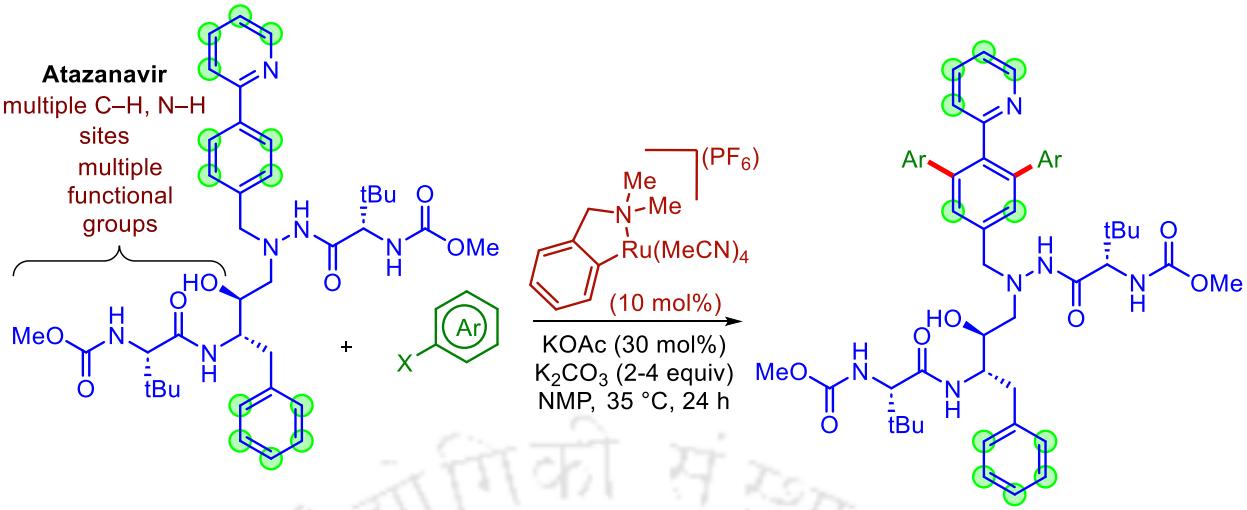

Scheme I.2.1.1. *Overview of synthetic challenge*

(a) Ubiquitous Nature of C–H Bond: The C–H bond is ubiquitous in nature and thus the selective activation of a particular C–H bond is a difficult task. This challenge increases with the increasing complexity of molecules (as the number and variety of C–H bonds increases), thereby limiting the availability of methods.

(b) Diverse Reactivity of the Substrate: Many other side reactions may take place, thus proper optimisation of reaction condition (solvent, additive, temperature, etc.) is required to make the process a sustainable one. This challenge increases with the increasing functional groups in a molecule. As the number of functional groups increases, the number of inhibitory catalytic cycles increases and Lewis-basic coordination of functional groups to the catalyst hinders the yield of the target molecule. Further, some of the functional groups may be intolerant to the catalyst, solvent or additive. The optimized reaction condition serves as a guide for complex molecules to future scientists.

(c) Regioselectivity: There may be possibility of formation of two regioisomers with equal ease. But the preference of formation of one of the products (target product) over the other makes the reaction worthy and an atom economic one. The centre of reaction of the two possible sites may be very similar but the reaction condition must be able to choose a single site to offer the target product.

(d) Stereoselectivity: There may be two equal faces or centre of reaction for the formation of two stereoisomers. While one of the isomers of the molecule may be a drug, the other may

be harmful to the human body. Thus, the reaction condition must be potential enough to synthesize a single stereoisomeric target product for the reaction to be economic and worthy.

I.2.2. Mechanism of Transition Metal Assisted Synthetic Pathways

The reactions which play a key role in the Transition Metal assisted synthetic pathways are as follows: (a) oxidative addition (b) reductive elimination (c) insertion (d) sigma bond metathesis and (e) electrophilic metallation.[12]

(a) Oxidative Addition: In oxidative addition (OA), molecules add to low valent metal complex to deliver a metal complex with an increased oxidation state (Scheme I.2.2.1). Molecules (A–B) such as H–H or CH_3–I add to ML_n to produce $ML_n(A)(B)$. Here, the A–B bond breaks to form bonds to the metal as M–A and M–B. During the process of OA, the oxidation state, electron count and coordination number of the TM complex all increase by two. Since the metal electron count of the TM complex increases by two, a vacant 2e site is needed for OA to take place. The complex must have a more stable two unit more positive oxidation state. In OA, two electron transfer from M into the A–B σ*, and the A–B σ bonding pair donates two electrons to the TM. This leads to the cleavage of A–B bond and formation of two new M–A and M–B bonds. OA is favoured in complexes with low oxidation state of the metal.

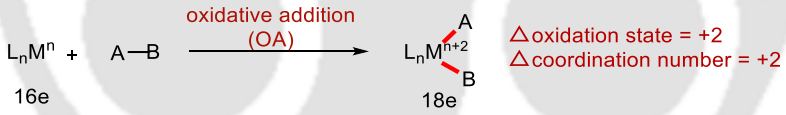

Scheme I.2.2.1. *Oxidative addition*

(b) Reductive Elimination: In reductive elimination (RE), molecules are released from the TM complex with the formation of new bonds (Scheme I.2.2.2). It is the reverse procedure of OA. The reaction leads to the release of A–B from the complex $ML_n(A)(B)$. During the process of RE, the oxidation state, electron count, and coordination number of the TM complex all decrease by two. The complex must have a more stable two unit less positive oxidation state. In a catalytic cycle, RE is often the last step of the cycle and ML_n fragment survive to re-enter the catalytic cycle. In general, a reactant often binds to a TM via OA and the product is released from the TM complex via reductive elimination.

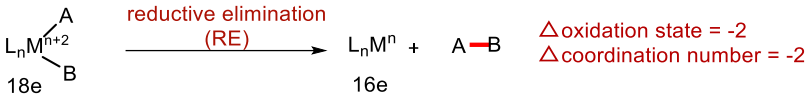

Scheme I.2.2.2. *Reductive elimination*

(c) Insertion: In the process of insertion a π bound 2e ligand is inserted into M–X bond of the TM complex with the formation of new bonds with both M and X. As for example A=B adds to M–X bond to produce M–(AB)–X. There are two types of insertion (i) 1,1-insertion (ii) 1,2-insertion.

(i) 1,1-Insertion: In 1,1 insertion M and X are bound to the same atom of AB (Scheme I.2.2.3). As for example, CO is always inserted in the 1,1-insertion fashion where both M and X are bound to the CO carbon.

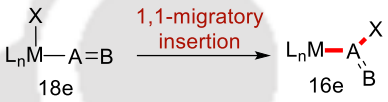

Scheme I.2.2.3. *1,1-insertion*

(ii) 1,2-Insertion: In 1,2 insertion M and X end up binding to adjacent atoms of AB (Scheme I.2.2.4). For example, ethylene is always inserted in the 1,2-insertion fashion where both M and X are bound to the adjacent atoms of the ligand as MCH_2CH_2X.

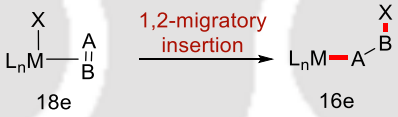

Scheme I.2.2.4. *1,2-insertion*

(d) Sigma Bond Metathesis: Some of the apparent OA/RE sequences take the route of sigma bond metathesis rather than undergoing OA and RE (Scheme I.2.2.5). This process is visible for d^0 metal complexes where OA is forbidden and would lead to d^{-2} which is practically not possible. For d^2–d^{10} TMs, both OA and sigma bond metathesis are permitted, but the processes cannot be distinguished as both the products and kinetics are exactly the same. A d^0 metal complex reacts with H_2 via sigma bond metathesis.

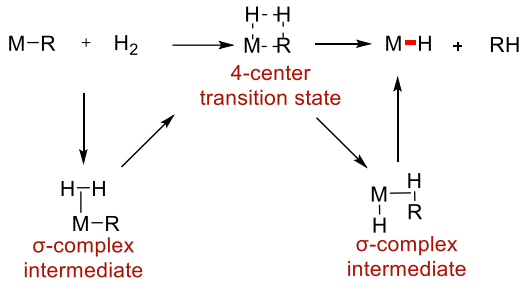

Scheme I.2.2.5. *Sigma bond metathesis*

(e) Electrophilic Metallation: In this process, the TM directly attacks the reagent (alkenes or arenes) to form an intermediate and further loss of proton deliver the σ-organyl complex (Scheme I.2.2.6). This process is visible for TM having higher oxidation states.

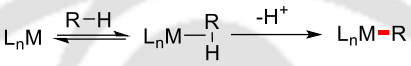

Scheme I.2.2.6. *Electrophilic metallation*

I.2.3. Transition Metal Assisted C–H Activation

The C–H bonds are ubiquitously present in organic molecules. These C–H bonds are unfunctional due to their high bond dissociation energy (85–120 kcal/mol) and non-polar nature (pKa > 35). Due to the high bond dissociation energy, C–H bonds are thermodynamically stable and less reactive. This stability of C–H bonds imposes a challenge upon the synthetic chemists which has been overcome by the usage of transition metal. The molecular orbital diagram of C–H bond activation by TM in shown in Figure I.2.3.1.

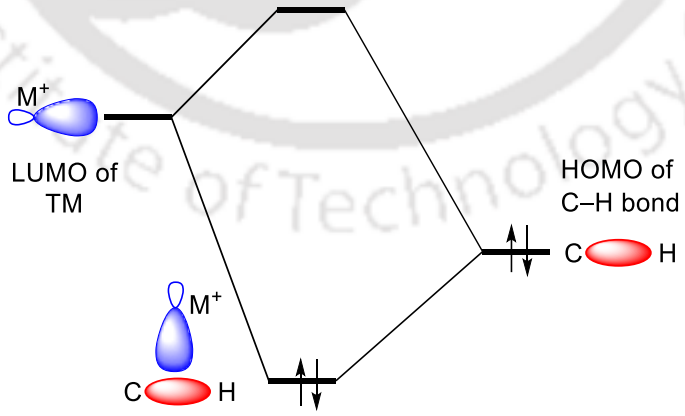

Figure I.2.3.1. *Molecular orbital diagram of C–H bond activation by TM.*

Transition metal complexes react with C–H bonds of alkanes and arenes to form a reactive M–C bond. This M–C bond subsequently undergoes reactions with electrophiles and nucleophiles to form C–C and C–Heteroatom bonds.[13]

I.2.3.1. Approach to C–H Activation

Considering the various challenges of C–H activation, the foremost approach toward C–H activation includes the involvement of directing groups. Other approaches include direct C–H activation without the involvement of directing groups, electronically directed C–H activation etc. Based on these factors the approach towards C–H activation is divided into the following categories (a) directing group enabled C–H activation (b) cross-dehydrogenative coupling (CDC) (c) combination of DG enabled and CDC approach and others.[14]

(a) Directing Group Enabled C–H Activation: The challenge of the ubiquitousness of C–H bonds is overcome by the usage of directing groups (DGs) (Scheme 1.2.3.1.1). The mechanism of DG-enabled C–H activation involves the coordination of the DG to the TM and subsequent activation of the proximal C–H bonds via agostic interaction. With the concomitant activation of the proximal C–H bond, the metallacycle is coordinated by 2π– unsaturated units followed by insertion into the C–Metal bond and subsequent reductive elimination.

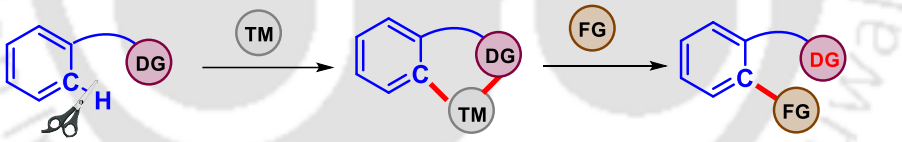

Scheme I.2.3.1.1. *Directing group enabled C–H activation*

(b) Cross-Dehydrogenative Coupling (CDC): This process leads to the formation of C–C or C–Heteroatom in a direct approach via the coupling of two C–H or Heteroatom–H bonds in the presence of oxidants (Scheme 1.2.3.1.2). Various combination of sp^3–sp^3, sp^3–sp^2, sp^3–sp, sp^2–sp^2, sp^2–sp, sp–sp C–H bonds have been involved in the CDC approach. It is one of the most challenging and elegant method of C–H activation of two simple reagents/arenes. This approach requires the introduction of newer strategies to accomplish reactivity and selectivity.

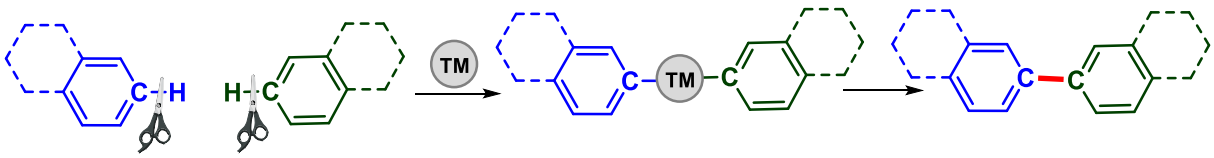

Scheme I.2.3.1.2. *Cross-dehydrogenative coupling (CDC)*

(c) Combination of DG Enabled and CDC Approach and Others: The CDC approach may be assisted by a directing group many a times (Scheme 1.2.3.1.3). Also, sometimes the electronic nature of the substrates with heteroatom assists the process (electrophilic metallation).[14d] The distal C–H bond is activated with the assistance of electronic nature of the substrate and the TM.

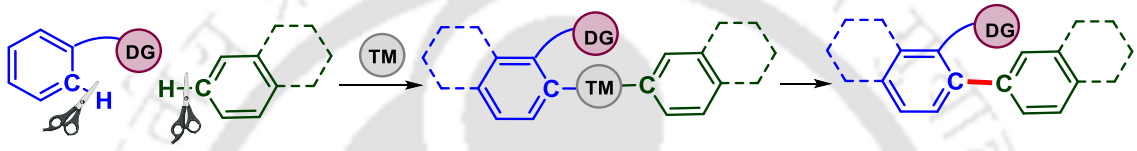

Scheme I.2.3.1.3. *Combination of DG enabled and CDC approach*

I.2.4. Copper Catalyzed/Mediated Annulation and Functionalization Reactions

The strategy of transition metal-catalyzed/mediated annulation and functionalization has been commonly employed for the synthesis of heterocycles.[15] Among the transition metals, copper salts are less expensive as compared to other 4d and 5d transition metals. Apart from being environmentally benign and relatively more abundant compared to that of 4d and 5d transition metals, they are endowed with many beneficial chemical properties. As a result of which, various works revolve around the centre of copper catalyzed C–H activation.[16]

To understand the complex reactions that take place with the usage of copper salts, it is very important to understand the various aspects of copper at the elemental state. Further, the changes in oxidation states of the copper catalyst in the mechanistic cycle of C–H activation must be studied mindfully. The mechanism involves the shuttling of the oxidation states of copper in between Cu(I)/Cu(II)/Cu(III) and accordingly, the process may generally be either (a) one electron process (b) two electron process (c) combination of one and two electron process as described below.[17]

(a) One Electron Process: This process involves a Cu(II)/Cu(I) catalytic cycle (Scheme 1.2.4.1). Initially, the Cu(II) salt gets reduced to its Cu(I) form via the acceptance of 1e from the substrate (R–H) thereby forming a **R**· radical. This radical substrate (**R**·) may then undergo

two possible pathways. One is that it undergoes cyclization and oxidation to deliver the final heterocycle. The other possibility is that the radical substrate (**R·**) may undergo a modification to **R´·** before the cyclization and oxidation to deliver an altered heterocycle.

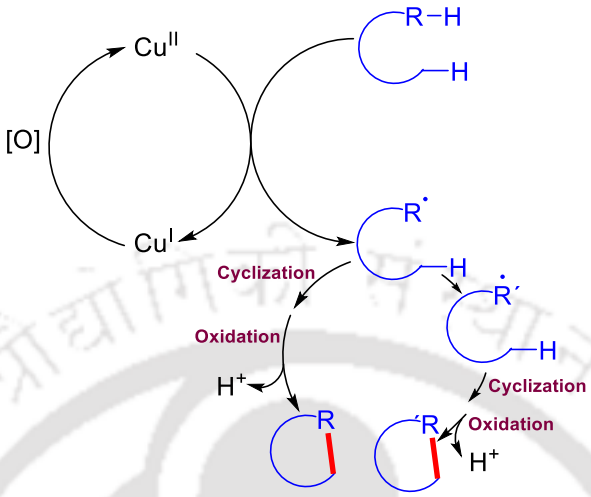

Scheme I.2.4.1. *One electron process*

(b) Two Electron Process: This process involves a Cu(I)/Cu(III) catalytic cycle (Scheme 1.2.4.2). Initially, the Cu(I) salt reacts with the halogenated substrate R(H)(X) to undergo an oxidative addition and C–H functionalization to form a Cu(III) organocopper intermediate. This Cu(III) undergoes reductive elimination to deliver the final heterocycle.

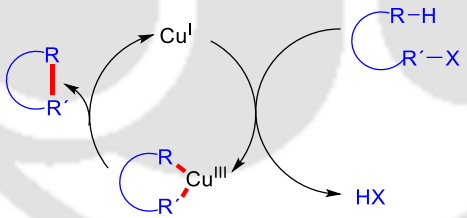

Scheme I.2.4.2. *Two electron process*

(c) Combination of One and Two Electron Process: This process involves a Cu(I)/Cu(II)/Cu(III) catalytic cycle (Scheme 1.2.4.3). Initially, the Cu(II) salt undergoes ligand exchange and C–H functionalization to form another Cu(II) intermediate. This Cu(II) intermediate undergoes oxidation to form Cu(III) intermediate with the assistance of another Cu(II) species (disproportionation reaction). The Cu(III) intermediate undergoes reductive elimination to deliver the final heterocycle and Cu(I). The catalytic cycle continues with the reoxidation of Cu(I) to Cu(II).

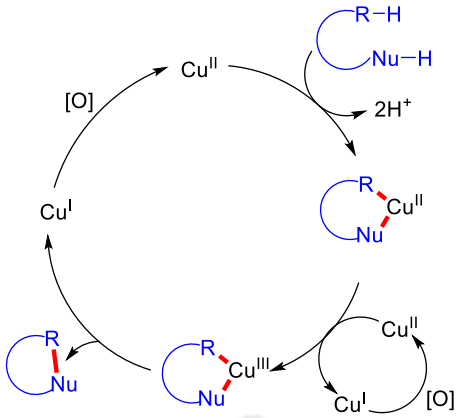

Scheme I.2.4.3. *Combination of one and two electron process*

I.2.4.A. Copper Catalyzed/Mediated Annulation Reactions

Annulation, in organic chemistry describes the method of building a ring onto a pre-existing system either cyclic or acyclic. Over the past years, transition metal catalyzed C–H annulation for synthesis of saturated and π conjugated heterocyclic compounds has become an emerging research strategy in the domain of organic synthesis.[18] Particularly, annulation reactions afford an efficient and atom-economic way for the construction of products with relatively complex cyclic scaffolds from simpler starting materials. Annulated compounds are of importance in many fields and their bright fluorescent property may be utilized for various applications.

Depending on the reacting sites of the reactants, several types of annulation reactions were reported in last few decades by the groups of Antonchick, Patil, Jiang, Zou, Cao and others. Herein, a brief description of copper catalyzed/mediated heterocycle synthesis is provided.

In 2015, Antonchick *et al.* developed a copper-catalyzed [2+1] annulation reaction to generate cyclopropanes from acetophenone and maleimides. The dehydrogenative annulation involves a double C–H bond functionalization at the α position of the ketone using di-tertbutylperoxide as the oxidant (Scheme 1.2.4.A.1).[19]

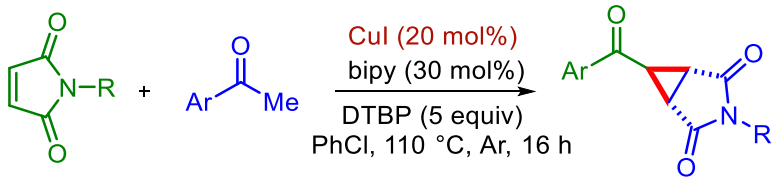

Scheme I.2.4.A.1. *Cu(I) catalyzed synthesis of cyclopropanes*

In 2016, the same group reported the [1+1+1] cyclotrimerization for the synthesis of cyclopropanes via copper catalysis. The protocol synthesizes cyclopropane by the functionalization of C(sp^3)–H bonds (Scheme 1.2.4.A.2).[20]

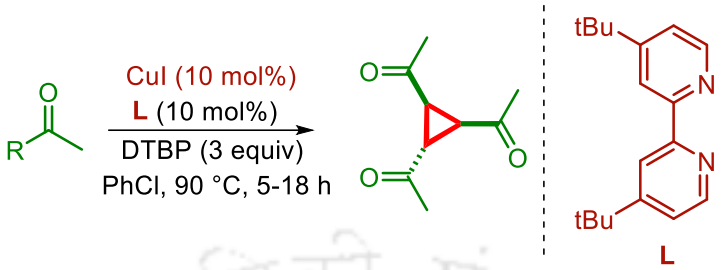

Scheme I.2.4.A.2. *Cu(I) catalyzed synthesis of cyclopropanes*

In 2018, Patil *et al.* reported a copper catalyzed intramolecular [4+2] cycloaddition to access N-doped polycyclic aromatic hydrocarbons (PAHs). The reaction is proposed to proceed via initial amino-cupration followed by C–H activation and reductive elimination sequence to produce the ionic N-doped PAHs. The synthesized PAHs exhibit intense fluorescence (Scheme 1.2.4.A.3).[21]

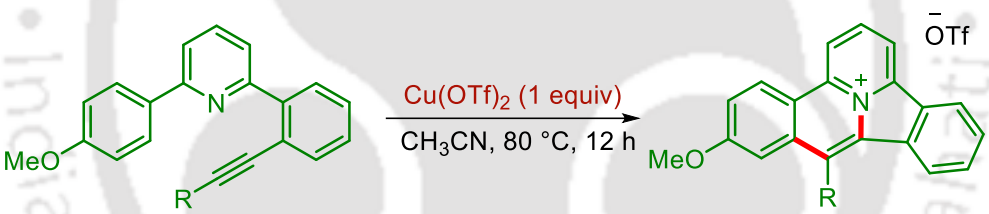

Scheme I.2.4.A.3. *Cu(II) mediated synthesis of polycyclic aromatic hydrocarbons*

In 2018, Jiang's group developed substituted quinazoline derivatives via a copper catalyzed pathway which displayed solid state blue emission (Scheme 1.2.4.A.4).[22]

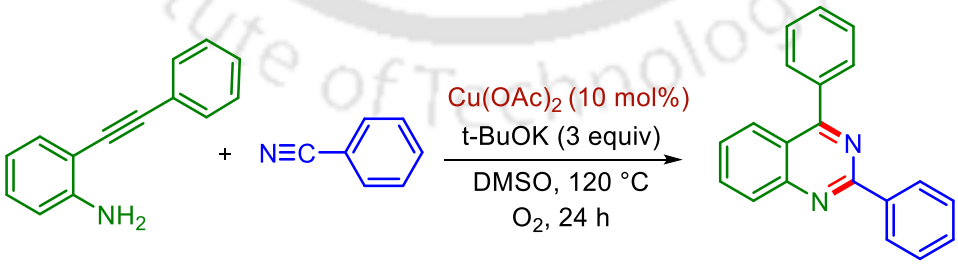

Scheme I.2.4.A.4. *Cu(II) catalyzed synthesis of quinazoline derivatives*

In 2020, Zou *et. al.* developed a method for the synthesis of 2,3-diaroylquinolines under Cu catalysis using sulfoxonium ylides and anthranils in [4+1+1] annulation. The catalytic cycle includes the activation of copper powder to active Cu(II) species with the assistance of Ag salts and O_2 (Scheme 1.2.4.A.5).[23]

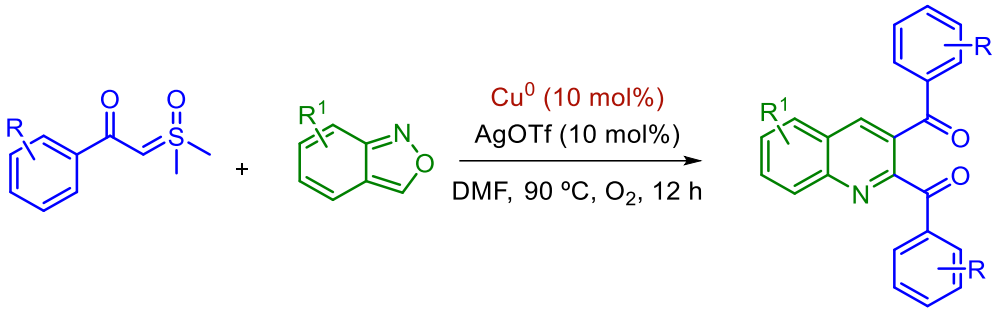

Scheme I.2.4.A.5. *Cu(0) catalyzed synthesis of 2,3-diaroylquinolines*

In 2020, Cao *et. al.* discovered a site selective pathway to construct 5-hydroxyalkyl-substituted imidazoles through a three-component reaction of amidines, ynals and water (Scheme 1.2.4.A.6).[24]

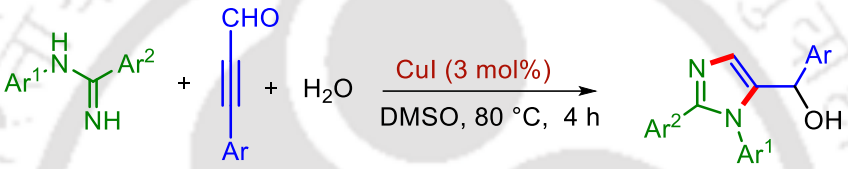

Scheme I.2.4.A.6. *Cu(I) catalyzed synthesis of 5-hydroxyalkyl-substituted imidazoles*

In 2020, Zhou *et al.* developed an economical synthetic methodology to synthesize a privileged isoquinolinone framework via copper catalysis. The protocol synthesizes benzo[3,4]indolo[1,2-b]isoquinoline-8-ones via intramolecular *cis*-addition of N-acyl-8-ethynyl-1-naphthylamine followed by reductive elimination. The prepared compounds are strongly emissive under UV light (Scheme 1.2.4.A.7).[25]

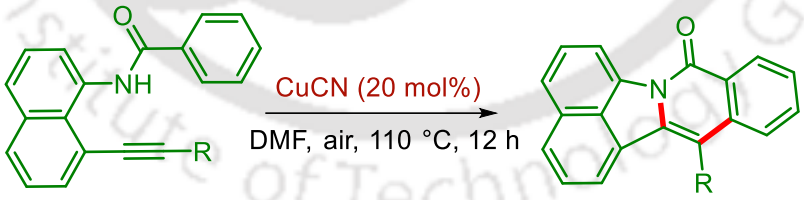

Scheme I.2.4.A.7. *Cu(I) catalyzed synthesis of isoquinolinones*

In 2022, Duan and Guo *et. al.* developed a three-component reaction for the synthesis of imidazoles and dihydroimidazoles under Cu catalysis. The protocol efficiently utilizes α, β-unsaturated ketoximes, amines and paraformaldehyde to achieve the target annulated products. The reaction condition is controlled to deliver the hydrogenated and dehydrogenated imidazoles (Scheme 1.2.4.A.8).[26]

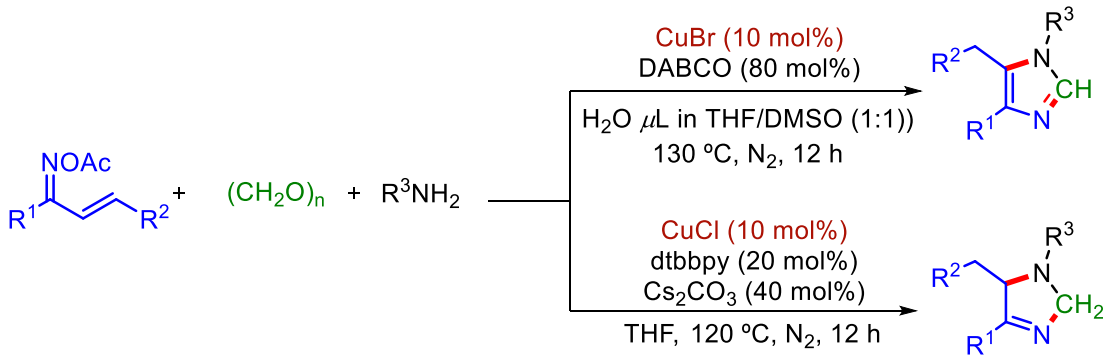

Scheme I.2.4.A.8. *Cu(I) catalyzed synthesis of of imidazoles and dihydroimidazoles*

I.2.4.B. Copper Catalyzed Functionlization Reactions

The controlled functionalization of organic substrates in the presence of various other reactive functional groups is one of the most important tools in organic synthesis. Some of the copper catalyzed functionalization reactions are discussed below.

In 2015, Kuninobu and Kanai *et. al.* developed a copper catalyzed activation of C(sp^3)–H bond to synthesize tertiary carbamates. The protocol utilizes isocyanates as the source of amides to successfully synthesize N,N carbamates (Scheme 1.2.4.B.1).[27]

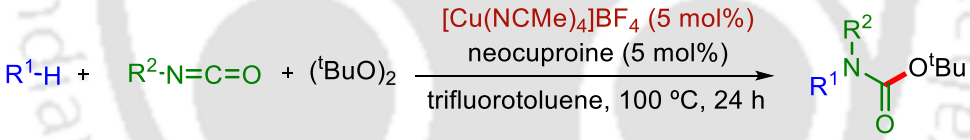

Scheme I.2.4.B.1. *Cu(I) catalyzed synthesis of tertiary carbamates*

In 2016, Su *et. al.* developed a copper catalyzed protocol for the *β*-functionalization of saturated ketones using various N, O and C nucleophiles (Scheme 1.2.4.B.2).[28]

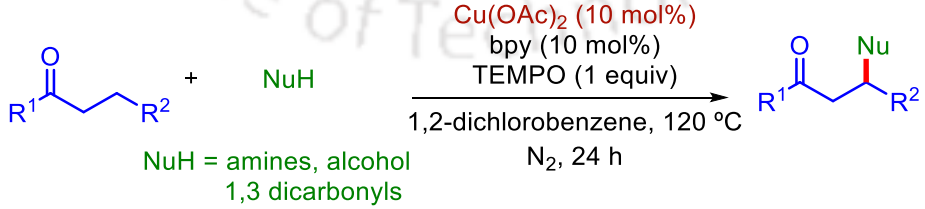

Scheme I.2.4.B.2. *Cu(II) catalyzed β-functionalization of saturated ketones*

In 2016, Mohr *et. al.* introduced *γ*–Alkylation of dienol ethers under Cu(II) catalysis using *α*–halocarbonyl compounds in a regioselective and stereoselective manner. This protocol is a

solution to the challenge of 1,6-dicarbonyl structure synthesis even with quaternary centres (Scheme 1.2.4.B.3).[29]

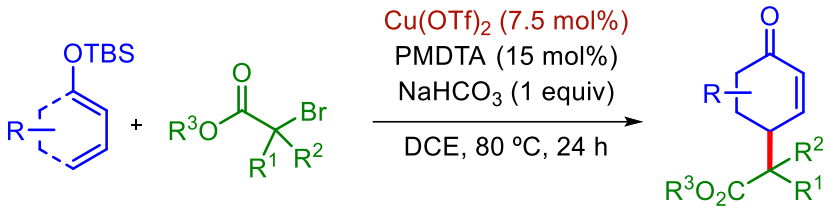

Scheme I.2.4.B.3. *Cu(II) catalyzed synthesis of 1,6-dicarbonyls*

In 2017, Yu *et. al.* developed a copper catalyzed protocol for the activation of remote C(sp^3)–H bond. The process brominated the γ–methylene C(sp^3)–H bonds of aliphatic amides or amines (nosyl protected) using NBS as the brominating reagent. The mechanism includes the formation of azidyl radical, 1,5 HAT and bromination to reach the final product (Scheme 1.2.4.B.4).[30]

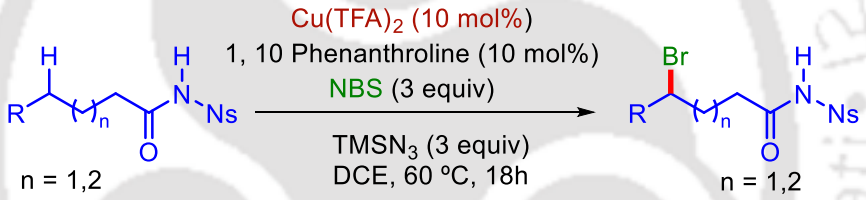

Scheme I.2.4.B.4. *Cu(II) catalyzed activation of remote C(sp^3)–H bond*

In 2018, Mei *et. al.* developed an electrochemical method for the amination of arenes under Cu catalysis without the usage of stoichiometric oxidants. The mechanism involves single-electron-transfer (SET) with the involvement of Cu(III). Initially, the Cu(II) salt coordinates with arenes and amines to form a Cu(II) complex. This, Cu(II) is then oxidized to Cu(III) as a part of anodic oxidation. This is followed by two simultaneous SET processes delivering Cu(I) species together with intramolecular amine transfer to synthesize the aminated target product. The catalytic cycle is completed by another anodic oxidation to oxidize Cu(I) to Cu(II) (Scheme 1.2.4.B.5).[31]

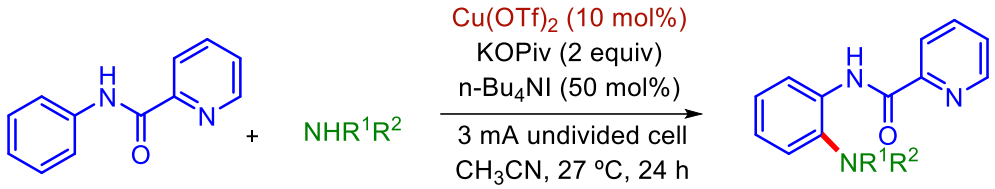

Scheme I.2.4.B.5. *Cu(II) catalyzed amination of arenes*

In 2019, Dong *et. al.* developed a coper catalyzed method for the desaturation of cyclic ketones, lactones and lactams to their α, β-unsaturated counterparts. The conversion is achieved in a mild condition without the use of any acid or base (Scheme 1.2.4.B.6).[32]

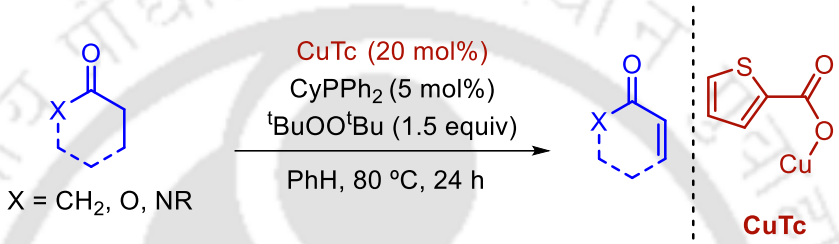

Scheme I.2.4.B.6. *Cu(I) catalyzed desaturation of cyclic ketones, lactones and lactams*

In 2021, Hu *et. al.* developed a copper catalyzed method for the activation of C(sp^3)–H and aliphatic carboxylic acids towards the formation of C–S bonds. The mechanism includes the formation of N centred radical via a SET from the Cu(I) complex. The N centred radical then abstracts the H of alkyl–H and alkyl–COOH (which undergoes decarboxylation) to form alkyl radicals. Further, the somophile of RSO_2Ph traps the alkyl radicals to deliver the final product and PhSO· radical. This PhSO· radical undergoes FAT from Cu(II)F and the catalyst regenerates (Scheme 1.2.4.B.7).[33]

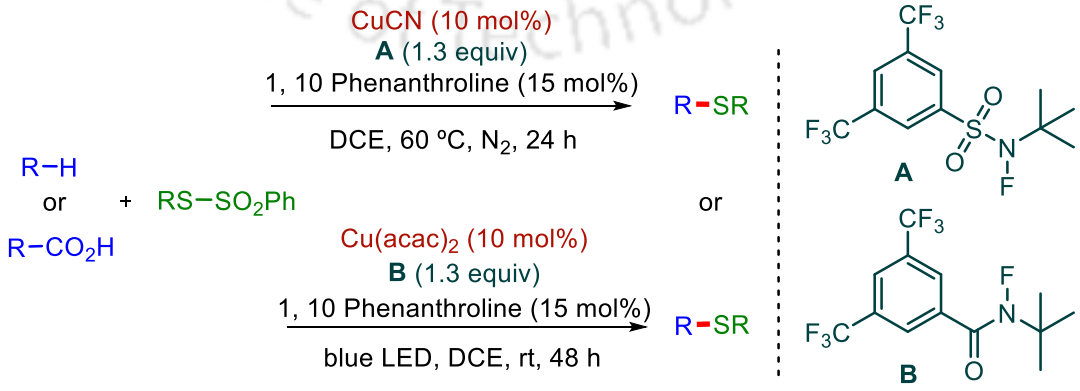

Scheme I.2.4.B.7. *Cu catalyzed activation of C(sp^3)–H and aliphatic carboxylic acids*

In 2023, Duan *et. al.* developed a method for asymmetric arylation of C(sp^2)–H bond under Cu catalysis using diaryliodonium salts. The process synthesizes chiral *ortho*-aryl phosphonic diamides in an enantioselective manner upto 92% ee. In addition, C3 arylation of diarylphosphine oxidated indoles is obtained in an enantioselective manner (Scheme 1.2.4.B.8).[34]

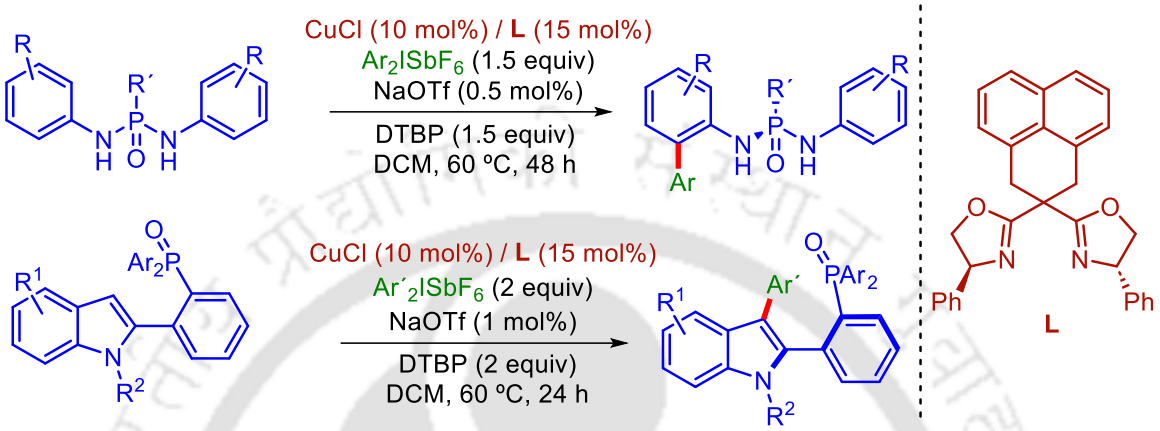

Scheme I.2.4.B.8. *Cu(I) catalyzed asymmetric arylation of C(sp^2)–H bond*

Copper has been successfully used for the asymmetric hydrogenation of the C=O bond of an exocyclic α, β-unsaturated pentanones with the aid of H_2. Considering the selective asymmetric hydrogenation of the C=O bond of an exocyclic α, β-unsaturated pentanones, it was not possible until 2010, when Zhou group have introduced chiral Ir catalysis for its reduction. This protocol replaces Ir and Ru and introduces copper which is comparatively much cheaper (Scheme 1.2.4.B.9).[35]

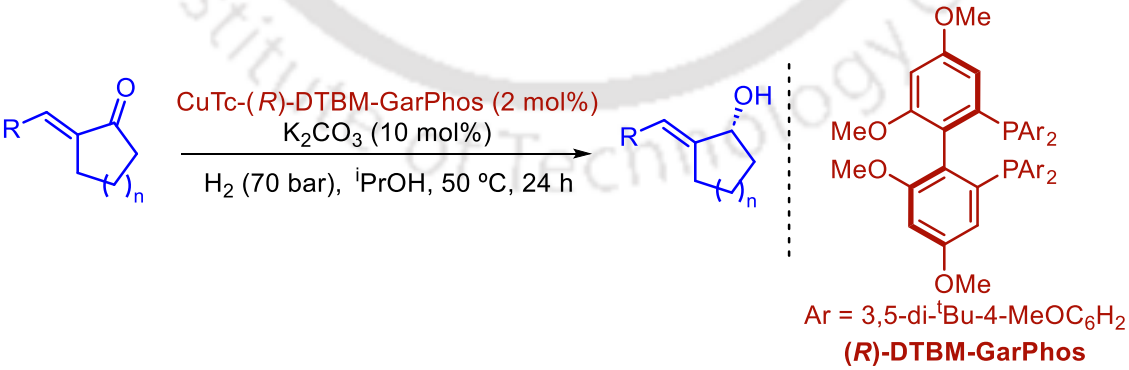

Scheme I.2.4.B.9. *Cu(I) catalyzed asymmetric hydrogenation of the C=O bond*

I.3. Photocatalytic Synthesis

Photocatalysis has been growing at a fast pace to synthesize complex organic molecules.[36] In an attempt to move towards a sustainable approach to organic synthesis, photocatalysis has met the goals of environment friendliness with the utilization of visible light under mild conditions. As green and sustainability are two very important concepts, photochemical processes are highly sought after. Moreover, photochemistry provides access to complex molecules which are difficult to synthesize via the thermal pathway. This is because chemical reactivity of the substrate in its excited state is different from its ground state.

In general, a substrate is photoexcited from the ground state S_0 to its excited state S_1 by the absorption of photons. Subsequently, the excited S_1 state undergoes an intersystem crossing (ISC) to reach T_1 which is a rapid process. Moreover, the relaxation from T_1 to S_0 is spin forbidden and thus the substrate stays in the T_1 state for longer time and majority of the reactions occur from the T_1 state (Figure 1.3.1).

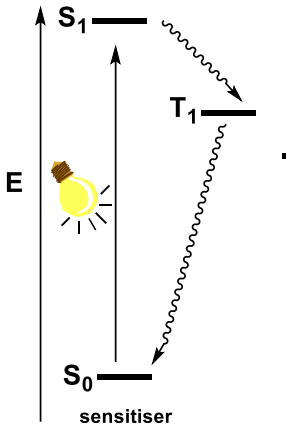

Figure 1.3.1. *Photo excitation of substrates*

I.3.1 Classification of Photocatalytic Synthesis

The photochemical process of organic synthesis generally relies on the usage of exogenous photocatalysts (PC). These photocatalysts harvest the energy of photons to activate the substrate and trigger a chemical reaction via the generation of reactive radicals. The photochemical approach may involve either the transfer of electrons or sensitisation of the triplet states with the usage of photocatalysts. In other photochemical processes, the reaction does not depend on any external photocatalyst and is self-sufficient to absorb the visible light. Accordingly, the process may be (a) photo-redox catalysis (b) Energy Transfer (EnT) catalysis (c) EDA complex driven synthesis (d) Self photoexcitation driven synthesis.

(a) Photo-Redox Catalysis

A photo-redox catalysis includes an external organic or inorganic photoredox catalyst. The photo-redox catalysis involves the transfer of a single electron (SET) either to the excited

photocatalyst from the substrate or from the excited photocatalyst to the substrate depending upon the reductive or oxidative process involved (Figure 1.3.1.1).[37]

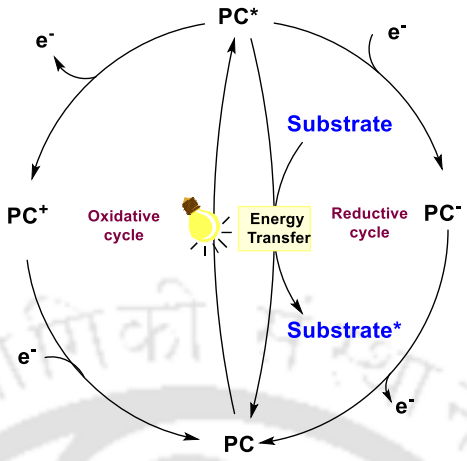

Figure 1.3.1.1. *Photo-redox catalytic pathway*

To illustrate the concept of photo-redox catalysis, some of the examples are described below:

In 2022, Liu and Deng *et. al.* developed a cooperated method of bronsted base, cobalt and photocatalyst for the alkylation of allylic C(sp^3)–H bonds using protic C(sp^3)–H bonds (Scheme 1.3.1.1).[38]

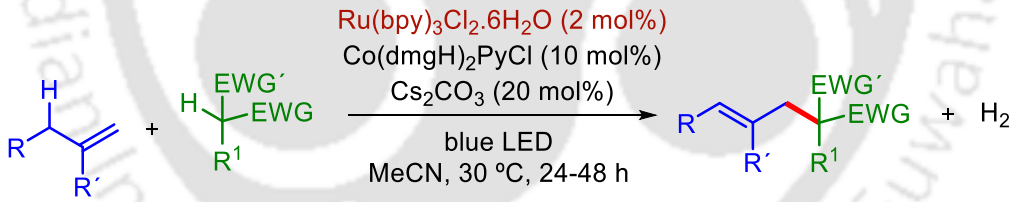

Scheme 1.3.1.1. *Ru(II) catalyzed alkylation of allylic C(sp^3)–H bonds*

In 2022, Nicewicz *et. al.* utilized acridinium photocatalyst together with pyridine-N-oxide for functionalization of C(sp^3)–H bonds (Scheme 1.3.1.2).[39]

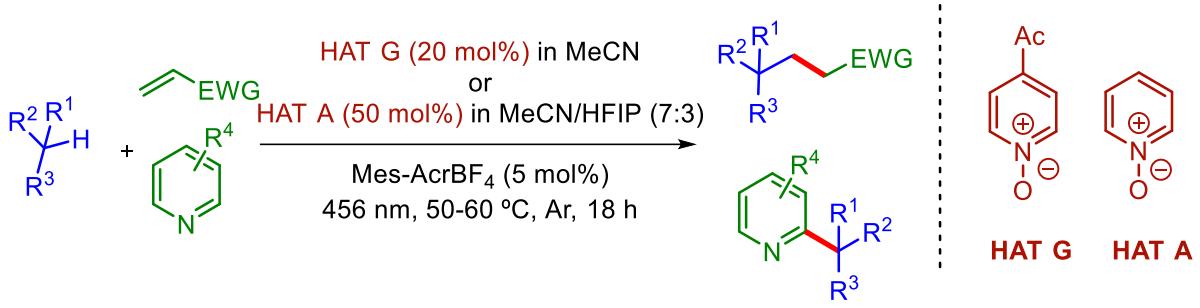

Scheme 1.3.1.2. *Acridinium catalyzed functionalization of C(sp^3)–H bonds*

In 2023, Zhang, Wang and Zhang *et. al.* developed a nickel/tungsten photoredox process, for the synthesis of amides using aldehydes and nitroarenes. The protocol enables the synthesis of C–N bonds in a mild condition. The mechanism involves a direct formation of amines via nitro arene reduction and formation of acyl radicals (Scheme 1.3.1.3).[40]

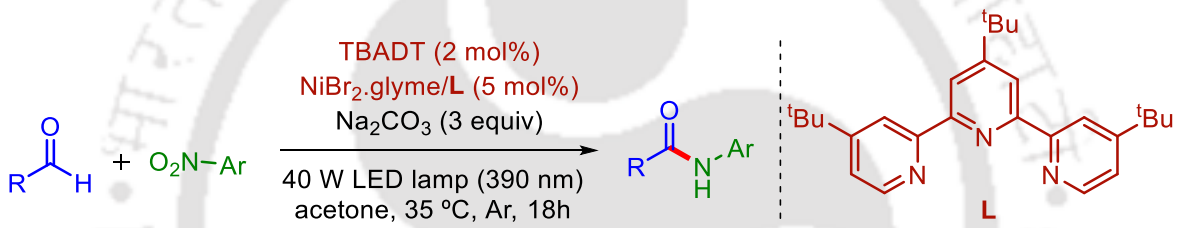

Scheme 1.3.1.3. *Nickel/tungsten photoredox catalytic synthesis of amides*

In 2023, Ritter *et. al.* reported a photochemical process for the C–H fluorination of azaarenes via a concerted nucleophilic substitution using selectfluor. The process is a first efficacious nucleophilic oxidative fluorination of quinolines (Scheme 1.3.1.4).[41]

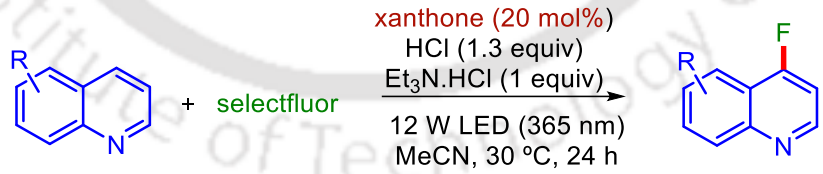

Scheme 1.3.1.4. *Xanthone catalyzed synthesis of fluorinated azaarenes*

(b) Energy Transfer (EnT) Catalysis

Apart from these electron transfer, there is also transfer of energy between the triplet state of the excited photocatalyst to the substrate, thereby exciting it to the triplet state which enables the chemical reaction.

In the process of Energy Transfer (EnT) catalysis, the general concept of photo excitation is applied and a triplet energy sensitiser (photocatalyst) transfers its triplet energy to the substrate and excites the substrate to its triplet state in an overall spin allowed process. The process of EnT from the triplet energy to the substrate is exergonic (E_T(substrate) ≤ E_T(sensitiser)). A collision between the two leads to the energy transfer (Figure 1.3.1.2).[42]

The excited triplet state (T_1) has different reactivity as compared to the ground state. Most organic molecules require UV light for excitation, which makes the application a difficult process. To circumvent this difficulty, photosensitisers are used to reach the triplet state in a milder condition by the absorption of visible light.

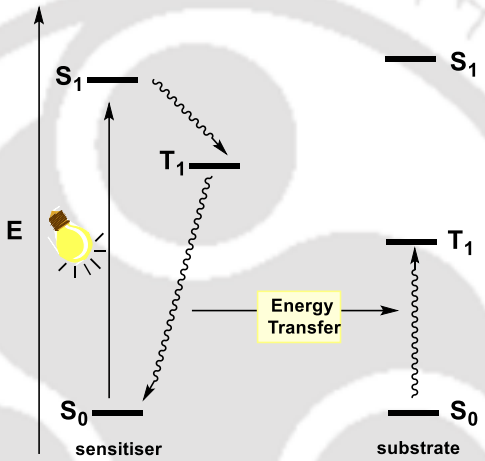

Figure. 1.3.1.2. *Energy transfer pathway*

To illustrate the concept of Energy Transfer (EnT) catalysis, some of the examples are described below:

In 2014, Chen and Xiao *et. al.* synthesized 2-substituted indoles in a photocatalytic energy transfer enabled pathway. The product involves an intramolecular cyclization of styryl azides for the synthesis of 2-substituted indoles under Ru catalysis (Scheme 1.3.1.5).[43]

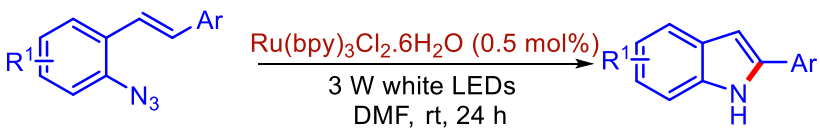

Scheme 1.3.1.5. *Ru(II) catalyzed synthesis of 2-substituted indoles*

In 2014, Yoon *et. al.* reported an energy transfer enabled photocatalytic procedure for the activation of vinyl azides. The protocol generates reactive nitrenes for the formation of C–N bonds to deliver pyrrole derivatives (Scheme 1.3.1.6).[44]

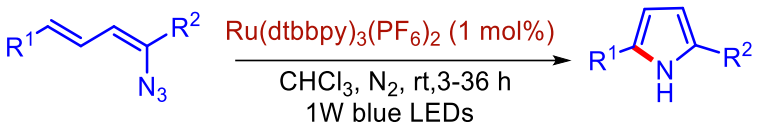

Scheme 1.3.1.6. *Ru(II) catalyzed synthesis of pyrroles*

Also in 2023, Mi and Luo *et. al.* developed a stereoselective method for the hydroxylation of *β*-ketocarbonyls under chiral amine and Ru photocatalysis. The *α* hydroxylated products are obtained in an enamine-singlet oxygen coupled process together with the participation of HFIP solvent (Scheme 1.3.1.7).[45]

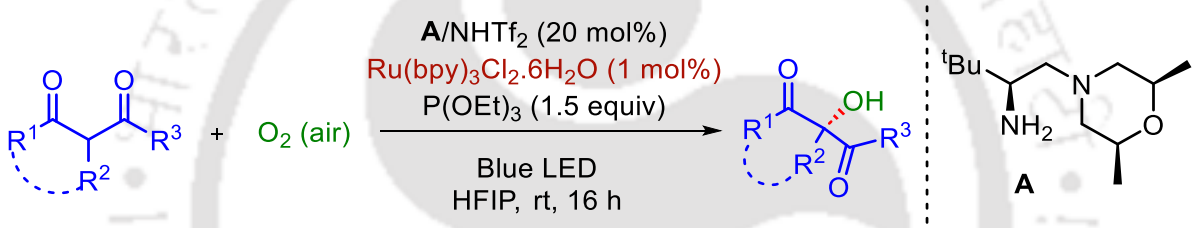

Scheme 1.3.1.7. *Ru(II) catalyzed hydroxylation of β-ketocarbonyls*

(c) EDA Complex Driven Synthesis

In this process, there is a formation of transient electron donor-acceptor (EDA) complex between an electron donor substrate (**D**, Lewis base) and electron acceptor substrate (**A**, Lewis acid) in the ground state. The substrates **A** and **D** may not absorb light by themselves but the EDA complex absorbs. This EDA complex absorbs light which triggers an intramolecular single electron transfer (SET) to form a charged species **D**+· and **A**–· and deliver the target product under mild conditions (Scheme 1.3.1.8).[46]

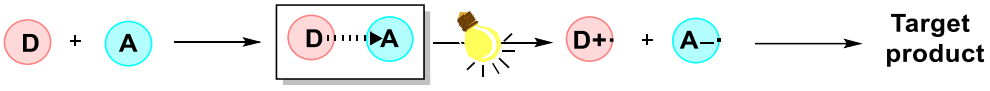

Scheme 1.3.1.8. *Electron donor-acceptor (EDA) complex formation*

New molecular orbitals are generated by the electronic coupling of frontier orbitals of **D** and **A** (HOMO/LUMO). The newly generated EDA complex is characterized by the appearance of

new absorption band. This absorption band is the charge transfer band ($h\nu_{CT}$) with the absorption of light by the new chemical entity ($\Psi_{GS} \rightarrow \Psi_{ES}$ electronic transition). Here, Ψ is the associated wave function. This electronic transition takes place in the visible region. With the increase in population of the Ψ_{ES} an intramolecular electron transfer takes place from **D** to **A**, thereby generating radical ion pair and subsequent reactions.

To illustrate the concept of synthesis driven by light irradiation of EDA complex, some of the examples are described below:

In 2015, Melchiorre *et. al.* developed a metal free photochemical strategy for the alkylation of indoles. The alkylation takes place at ambient temperature via the formation of electron donor acceptor (EDA) complex between the donor 1H-indoles and acceptor benzyl bromides (Scheme 1.3.1.9).[47]

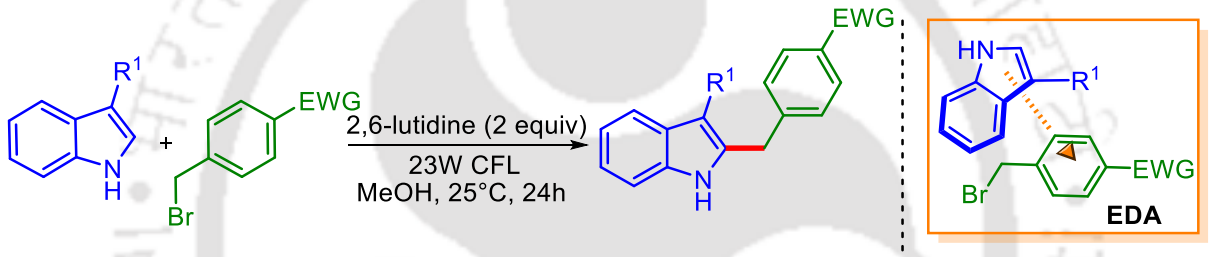

Scheme 1.3.1.9. *alkylation of indoles driven by light irradiation of EDA complex*

In 2015, Leonori *et. al.* reported the generation of nitrogen-centered iminyl radical for the iminohydroxylation cyclization. The protocol involves the formation of an EDA complex between triethyl amine and O-aryl oximes under visible light irradiation (Scheme 1.3.1.10).[48]

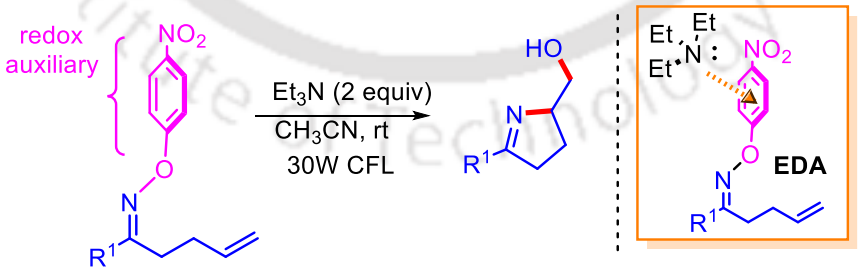

Scheme 1.3.1.10. *iminohydroxylation cyclization driven by light irradiation of EDA complex*

In 2016, Yu *et. al.* reported a double radical isocyanide insertion into perfluoroalkyl iodides for the synthesis of 2-fluoroalkylated 3-iodoquinoxalines under visible light irradiation. The

mechanism involves the formation of an EDA complex between secondary amine and perfluoroalkyl iodide and subsequent electron transfer processes (Scheme 1.3.1.11).[49]

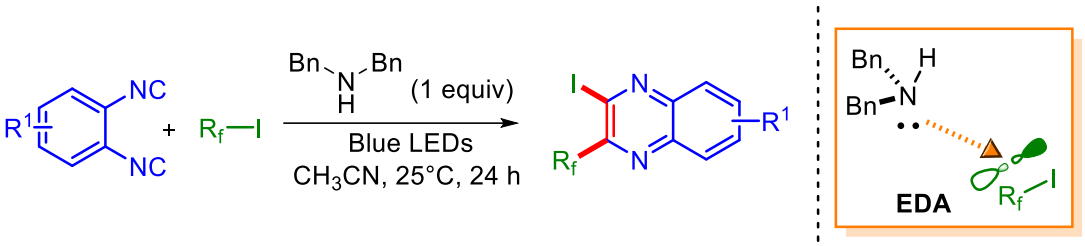

Scheme 1.3.1.11. *2-fluoroalkylated 3-iodoquinoxaline synthesis driven by light irradiation of EDA complex*

In 2017, Chen *et. al.* introduced a metal free C(sp^3)–C(sp^3) cleavage for the generation of alkoxy radicals under visible light irradiation. The mechanism involves the formation of an EDA complex of N-alkoxyl derivatives and Hantzsch ester for C(sp^3)–C(sp^3) allylation/alkenylation (Scheme 1.3.1.12).[50]

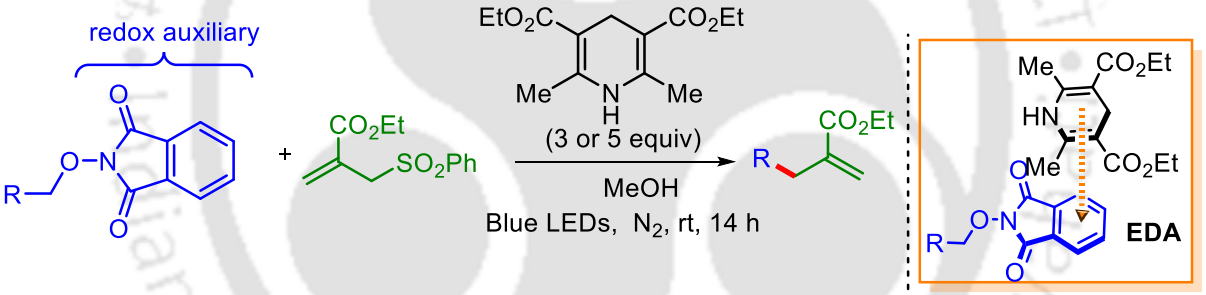

Scheme 1.3.1.12. *C(sp^3)–C(sp^3) Allylation/Alkenylation driven by light irradiation of EDA complex*

In 2019, Chen *et. al.* introduced an intermolecular radical addition of alkyl boronic acids to α-ketoacids under visible light irradiation to synthesize diversely substituted lactates. The process is assisted by the *in situ* formation of boron complex (Scheme 1.3.1.13).[51]

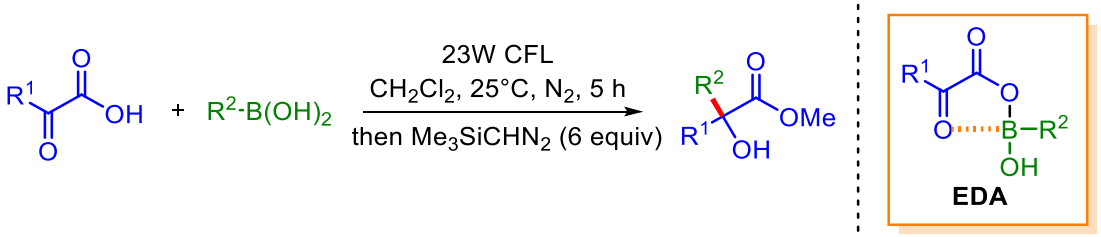

Scheme 1.3.1.13. *Lactate synthesis driven by light irradiation of EDA complex*

(d) Self Photoexcitation Driven Synthesis

Also, sometimes the reagent itself is photoexcited and assists the photochemical reaction via homolytic cleavage to form radicals (Scheme 1.3.1.14).[52]

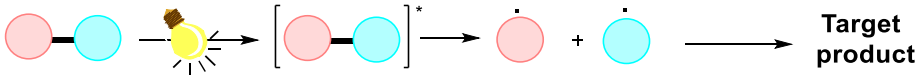

Scheme 1.3.1.14. *Photoexcitation of the reagent*

To illustrate the concept of synthesis driven by self-excitation of the reagent, some of the examples are described below:

In 2014, Luo *et. al.* described a photolytic protocol for the imidation of arenes and heteroarenes with the usage of *N*-bromosaccharin. This visible light promoted protocol generates N radical in the absence of any photocatalyst (Scheme 1.3.1.15).[53]

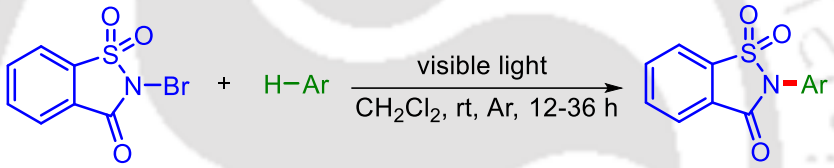

Scheme 1.3.1.15. *Imidation of arenes and heteroarenes driven by self-excitation of N-bromosaccharin*

In 2023, Kokotos *et. al.* developed a photochemical approach for aminochlorination of alkenes in the absence of any photocatalyst. Here, *N*-chlorosulfonamide undergoes self-photo excitation and act as both nitrogen and chlorine source (Scheme 1.3.1.16).[54]

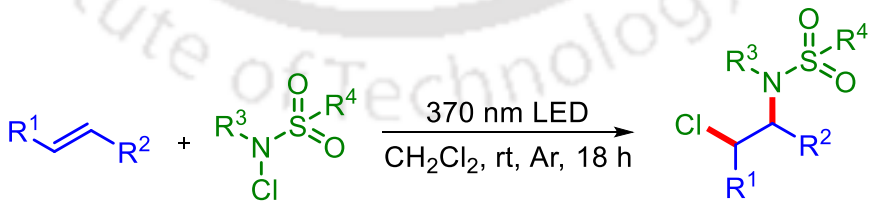

Scheme 1.3.1.16. *Aminochlorination of alkenes driven by self-excitation of N-*chlorosulfonamide

I.4. Motivation of Work

With the allure of annulation, functionalization and photochemistry I delved into my research journey. In annulation and functionalization, the promise of constructing complex structures from simpler components ignites curiosity, while photochemistry sparks with its transformative power, harnessing light to initiate reactions and unveil new sustainable chemical pathways. The pursuit of understanding these realms motivated me to explore the research area with full interest and sincerity. The motivation is about the potential to innovate, to contribute to fields ranging from drug discovery to materials sciences, and ultimately, to leave an indelible mark on the tapestry of scientific knowledge.

I.5. References

1. (a) Vitaku, E.; Smith, D. T.; Njardarson, J. T. *J. Med. Chem.* **2014**, *57*, 10257. (b) Heravi, M. M.; Zadsirjan, V. *RSC Adv.* **2020**, *10*, 44247.

2. (a) Iwumene, N. U. N.; Moseley, D. F.; Pullin, R. D. C.; Willis, M. C. *Chem. Sci.* **2022**, *13*, 1504. (b) Malarney, K. P.; KC, S.; Schmidt, V. A. *Org. Biomol. Chem*. **2021**, *19*, 8425. (c) Lindsay, V. N. G.; Viart, H. M. -F.; Sarpong, R. *J. Am. Chem. Soc*. **2015**, *137*, 8368.

3. (a) Yeung, C. S.; Dong, V. M. *Chem. Rev*. **2011**, *111*, 1215. (b) Sun, C. -L.; Li, B. -J.; Shi, Z. -J. *Chem. Rev*. **2011**, *111*, 1293. (c) Huang, H.; Ji, X.; Wu, W.; Jiang, H. *Chem. Soc. Rev*. **2015**, *44*, 1155.

4. (a) Douglas, N. H.; Nicewicz, D. A. *Chem. Rev*. **2022**, *122*, 1925. (b) Murray, P. R. D.; Leibler, I. N. -M.; Hell, S. M.; Villalona, E.; Doyle, A. G.; Knowles, R. R. *ACS Catal.* **2022**, *12*, 13732.

5. a) Baroliya, P. K.; Dhaker, M.; Panja, S.; Al-Thabaiti, S. A.; Albukhari, S. M.; Alsulami, Q. A.; Dutta, A.; Maiti, D. *ChemSusChem*, **2023**, e202202201. (b) Ma, C.; Fang, P.; Mei, T. -S. *ACS Catal.* **2018**, *8*, 7179.

6. Ashitha, K. T.; Krishna, A.; D, B.; Somappa, S. B. *Org. Chem. Front*. **2022**, *9*, 5306.

7. (a) Yeung, C. S.; Dong, V. M. *Chem. Rev*. **2011**, *111*, 1215. (b) Pati, B. V.; Puthalath, N. N.; Banjare, S. K.; Nanda, T.; Ravikumar, P. C. *Org. Biomol. Chem*. **2023**, *21*, 2842.

8. (a) Kuhl, N.; Hopkinson, M. N.; Delord, J. W. Glorius, F. *Angew. Chem., Int. Ed.* **2012**, *51*, 10236. (b) Negishi, E.-i. *Angew. Chem., Int. Ed.* **2011**, *50*, 6738.

9. (a) Liu, C. -X.; Zhang, W. -W.; Yin, S. -Y.; Gu, Q.; You, S. -L. *J. Am. Chem. Soc.* **2021**, *143*, 14025. (b) Giri, R.; Shi, B. -F.; Engle, K. M.; Maugelc, N.; Yu, J. -Q. *Chem. Soc. Rev*. **2009**, *38*, 3242.

10. (a) Stille, J. K. *Angew. Chem., Int. Ed.* **1986**, *25*, 508. (b) Negishi, E. -i.; Hu, Q.; Huang, Z.; Qian, M.; Wang, G. *Aldrichimica Acta* **2005**, *38*, 71. (c) Surry, D. S.; Buchwald, S. L. *Angew. Chem., Int. Ed.* **2008**, *47*, 6338. (d) Hartwig, J. F. *Nature* **2008**, *455*, 314. (e) Suzuki, A. *Angew. Chem., Int. Ed.* **2011**, *50*, 6723.

11. Docherty, J. H.; Lister, T. M.; Mcarthur, G.; Findlay, M. T.; -Legarda, P. D.; Kenyon, J.; Choudhary, S.; Larrosa, I. *Chem. Rev*. **2023**, *123*, 7692.

12. Labinger, J. A.; Bercaw, J. E. *Nature* **2002**, *417*, 507.

13. (a) Liu, B.; Yang, L.; Li, P.; Wang, F.; Li, X. *Org. Chem. Front*., **2021**, *8*, 1085. (b) Chen, Z.; Wang, B.; Zhang, J.; Yu, W.; Liu, Z.; Zhang, Y. *Org. Chem. Front*., **2015**, *2*, 1107. (c) Dyker, G. *Angew. Chem., Int. Ed.* **1999**, *38*, 1698.

14. (a) Davies, H. M. L.; Morton, D. *J. Org. Chem*. **2016**, *81*, 343. (b) Huang, C. -Y.; Kang, H.; Li, J.; Li, C. -J. *J. Org. Chem*. **2019**, *84*, 12705. (c) Kuhl, N.; Hopkinson, M. N.; Wencel-Delord, J.; Glorius, F. *Angew. Chem., Int. Ed*. **2012**, *51*, 10236. (d) Ghosh, S.; Khandelia, T.; Patel, B. K. *Org. Lett*. **2021**, *23*, 7370.

15. (a) Liu, B.; Yang, L.; Li, P.; Wang, F.; Li, X. *Org. Chem. Front*., **2021**, *8*, 1085.

16. (a) Aneeja, T.; Neetha, M.; Afsina, C. M. A.; Anilkumar, G. *RSC Adv*. **2020**, *10*, 34429. (b) Guo, X. -X.; Gu, D. -W.; Wu, Z.; Zhang, W. *Chem. Rev*. **2015**, *115*, 1622. (c) Ni, Z.; Zhang, Q.; Xiong, T.; Zheng, Y.; Li, Y.; Zhang, H.; Zhang, J.; Liu, Q. *Angew. Chem., Int. Ed*. **2012**, *51*, 1244.

17. (a) Guo, X. -X.; Gu, D. -W.; Wu, Z.; Zhang, W. *Chem. Rev*. **2015**, *115*, 1622. (b) Zhang, Q.; Wang, T.; Zhang, X.; Tong, S.; Wu, Y. D.; Wang, M. X. *J. Am. Chem. Soc.* **2019**, *141*, 18341. (c) Zhang, Q.; Liu, Y.; Wang, T.; Zhang, X.; Long, C.; Wu, Y.-D.; Wang, M.-X. *J. Am. Chem. Soc.* **2018**, *140*, 5579.

18. (a) Font, M.; Gulias, M.; Mascarenas, J. L. *Angew. Chem., Int. Ed*. **2022**, *61*, e202112848. (b) Nandakumar, A.; Midya, S. P.; Landge, V. G.; Balaraman, E. *Angew. Chem., Int. Ed*. **2015**, *54*, 11022.

19. Manna, S.; Antonchick, A. P. *Angew. Chem., Int. Ed.* **2015**, *54*, 14845.

20. Manna, S.; Antonchick, A. P. *Angew. Chem., Int. Ed.* **2016**, *55*, 5290.

21. Mule, R. D.; Shaikh, A.C.; Gade, A. B.; Patil, N. T. *Chem. Commun*., **2018**, *54*, 11909.

22. Wang, X.; He, D.; Huang, Y.; Fan, Q.; Wu, W.; Jiang, H. *J. Org. Chem*. **2018**, *83*, 5458.

23. Zhu, S.; Shi, K.; Zhu, H.; Jia, Z. K.; Xia, X. F.; Wang, D.; Zou, L. H. *Org. Lett*. **2020**, *22*, 1504.

24. Liu, W.; He, J.; Liu, X.; Yu, Y.; Pei, Y.; Zhu, B.; Cao, H. *J. Org. Chem*. **2020**, *85*, 14954.

25. Hua, Y.; Chen, Z. Y.; Diao, H.; Zhang, L.; Qiu, G.; Gao, X.; Zhou H. *J. Org. Chem.* **2020**, *85*, 9614.

26. Xu, G.; Jia, C.; Wang, X.; Yan, H.; Zhang, S.; Wu, Q.; Zhu, N.; Duan, J.; Guo, K. *Org. Lett.* **2022**, *24*, 1060.

27. Chikkade, P. K.; Kuninobu, Y.; Kanai, M. *Chem. Sci.* **2015**, *6*, 3195.

28. Jie, X.; Shang, Y.; Zhang, X.; Su, W. *J. Am. Chem. Soc.* **2016**, *138*, 5623.

29. Chen, X.; Liu, X.; Mohr, J. T. *J. Am. Chem. Soc*. **2016**, *138*, 6364.

30. Liu, T.; Myers, M. C.; Yu, J. -Q. *Angew. Chem., Int. Ed.* **2017**, *56*, 306.

31. Yang, Q. -L.; Wang, X. -Y.; Lu, J. -Y.; Zhang, L. -P.; Fang, P.; Mei, T. -S. *J. Am. Chem. Soc*. **2018**, *140*, 11487.

32. Chen, M.; Dong, G. *J. Am. Chem. Soc*. **2019**, *141*, 14889.

33. Mao, R.; Bera, S.; Turla, A. C.; Hu, X. *J. Am. Chem. Soc*. **2021**, *143*, 14667.

34. Yan, S. -B.; Wang, R.; Li, Z. -G; Li, A. -N.; Wang, C.; Duan, W. -L. *Nat Commun.* **2023,** *14*, 2264.

35. Guan, J.; Chen, J.; Luo, Y.; Guo, L.; Zhang, W. *Angew. Chem., Int. Ed*. **2023**, *62*, e202306380.

36. Capaldo, L.; Ravelli, D.; Fagnoni, M. *Chem. Rev.* **2022**, *122*, 1875.

37. Douglas, N. H.; Nicewicz, D. A. *Chem. Rev*. **2022**, *122*, 1925.

38. Dong, M. -Y.; Han, C. -Y.; Li, D. -S.; Hong, Y.; Liu, F.; Deng, H. -P. *ACS Catal.* **2022**, *12*, 9533.

39. Schlegel, M.; Qian, S.; Nicewicz, D. A. *ACS Catal.* **2022**, *12*, 10499.

40. Sang, J. -W.; Li, Q.; Zhang, C.; Zhang, Y.; Wang, J.; Zhang, W. -D. *Org. Lett.* **2023**, *25*, 4592.

41. Zhang, L.; Yan, J.; Ahmadli, D.; Wang, Z.; Ritter, T. *J. Am. Chem. Soc.* **2023**, *145*, 20182.

42. (a) Zhou, Q. -Q.; Zou, Y. -Q.; Lu, L. -Q.; Xiao, W. -J. *Angew. Chem., Int. Ed.* **2019**, *58*, 1586. (b) Deng, Z.; Zhu, Z.; Ru, Z.; Zou, X.; Ouyang, X.; Li, H.; Yang, X.; Zhou, P.; Tian, S.; Ma, X.; Song, R.; Sun, Q.; Lin, C.; Shu, C. *ACS Catal.* **2023**, *13*, 13232.

43. Xia, X. -D.; Xuan, J.; Wang, Q.; Lu, L.-Q.; Chen, J. -R. Xiao, W.-J. *Adv. Synth. Catal.* **2014**, *356*, 2807.

44. Farney, E. P.; Yoon, T. P.; *Angew. Chem., Int. Ed.* **2014**, *53*,793.

45. Cai, M.; Xu, K.; Jia, H.; Zhang, L.; Mi, X.; Luo, S. *ACS Catal.* **2023**, *13*, 7538.

46. Crisenza, G. E. M.; Mazzarella, D.; Melchiorre, P. *J. Am. Chem. Soc.* **2020**, *142*, 5461.

47. Kandukuri, S. R.; Bahamonde, A.; Chatterjee, I.; Jurberg, I. D.; Escudero-Adán, E. C.; Melchiorre, P. *Angew. Chem., Int. Ed.* **2015**, *54*, 1485.

48. Davies, J.; Booth, S. G.; Essafi, S.; Dryfe, R. A. W.; Leonori, D. *Angew. Chem., Int. Ed.* **2015**, *54*, 14017.

49. Sun, X.; Wang, W.; Li, Y.; Ma, J.; Yu, S. *Org. Lett*. **2016**, *18*, 4638.

50. Zhang, J.; Li, Y.; Xu, R.; Chen, Y. *Angew. Chem., Int. Ed.* **2017**, *56*, 12619.

51. Xie, S.; Li, D.; Huang, H.; Zhang, F.; Chen, Y. *J. Am. Chem. Soc.* **2019**, *141*, 16237.

52. Wei, Y.; Zhou, Q. -Q.; Tan, F.; Lu, L. -Q.; Xiao, W. -J. *Synthesis* **2019**, *51*, 3021.

53. Song, L.; Zhang, L.; Luo, S.; Cheng, J.-P. *Chem. -Eur. J.* **2014**, *20*, 14231.

54. Constantinou, C. T.; Gkizis, P. L.; Lagopanagiotopoulou, O. T. G.; Skolia, E.; Nikitas, N. F.; Triandafillidi, I.; Kokotos, C. G. *Chem. Eur. J.* **2023**, *29*, e202301268.

Copper(I) Mediated Cascade Annulation via Dual C–H/C–H Activation: Access to Benzo[*a*]carbazolic AEEgens

II

Chapter

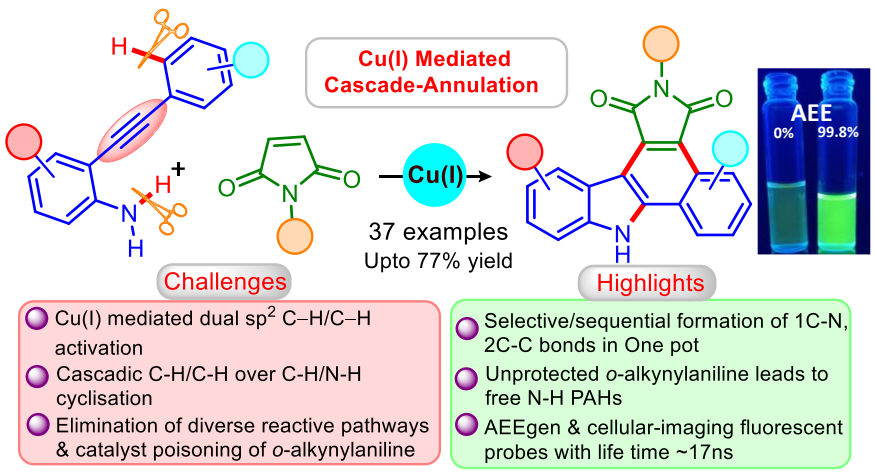

ABSTRACT

A Cu(I) mediated cascade cyclization/annulation of unprotected o-alkynylanilines with maleimides in one-pot is developed. The protocol offers sequential formation of one C–N and two C–C bonds to deliver fused benzo[a]carbazoles having free NH skeletons. The annulated products display fluorescence emission in the range of 485–502 nm with a large Stokes shift and fluorescence lifetime of ~17 ns. The annulated ***3aa*** *display AEE behavior in the ethanol/hexane system and possesses marigold-flower like morphology at the aggregated state. Cell viability assays enumerate biocompatible of AEEgens, while their high intracellular fluorescence depicts cell imaging applicability.*

Reference:

Khandelia, T.; Ghosh, S.; Panigrahi, P.; Shome, R.; Ghosh, S. S.; Patel, B. K. *J. Org. Chem.* **2021**, *86*, 16948.

II.1. Introduction

The upsurge of interest in the advancement of pharmacologically and functionally pertinent π-extended nitrogen-containing polyaromatic hydrocarbons (NPAHs) *via* one-pot cascade-annulation has come to the limelight in modern organic synthesis.[1] In this web of synthesis, transition metal-catalyzed cascade C–H activation/annulation proceeds with minimal step and maximum atom economy to acquire such functionalized NPAHs.[2] In this regard, several pioneering works have been reported utilizing expensive 4d- and 5d- metals.[3] However, from the fundamental and application perspective, their high cost, low Earth abundance, and toxic nature demand the use of earth-abundant and innocuous 3d metals.[4] In this context, despite the significant advances made in C–H activation using 3d metals, Cu salts are far less scrutinized for the cascade annulation.[5]

II.1.1. Importance of Benzo[*a*]carbazole Fused NPAHs

The benzo[*a*]carbazole fused NPAHs have shown prodigious activity as potential anti-cancer and antiangiogenic agents in medicinal chemistry.[6] Primarily, maleimide fused carbazole scaffolds are potent core in numerous natural products having medicinal properties.[7] Furthermore, in material sciences the functionalized π-conjugated benzo[*a*]carbazoles are the key building blocks for the construction of numerous organic functional materials such as organic light-emitting diodes (OLED), organic photovoltaic cells (OPV), organic field-effect transistors (OFET), and dye-sensitized solar cells (DSSC) (Figure II.1.1.1).[8] Moreover, since the introduction of the revolutionary phenomenon of AIE by Tang and co-workers, there has been a surging interest in NPAHs for their widespread application.[9]

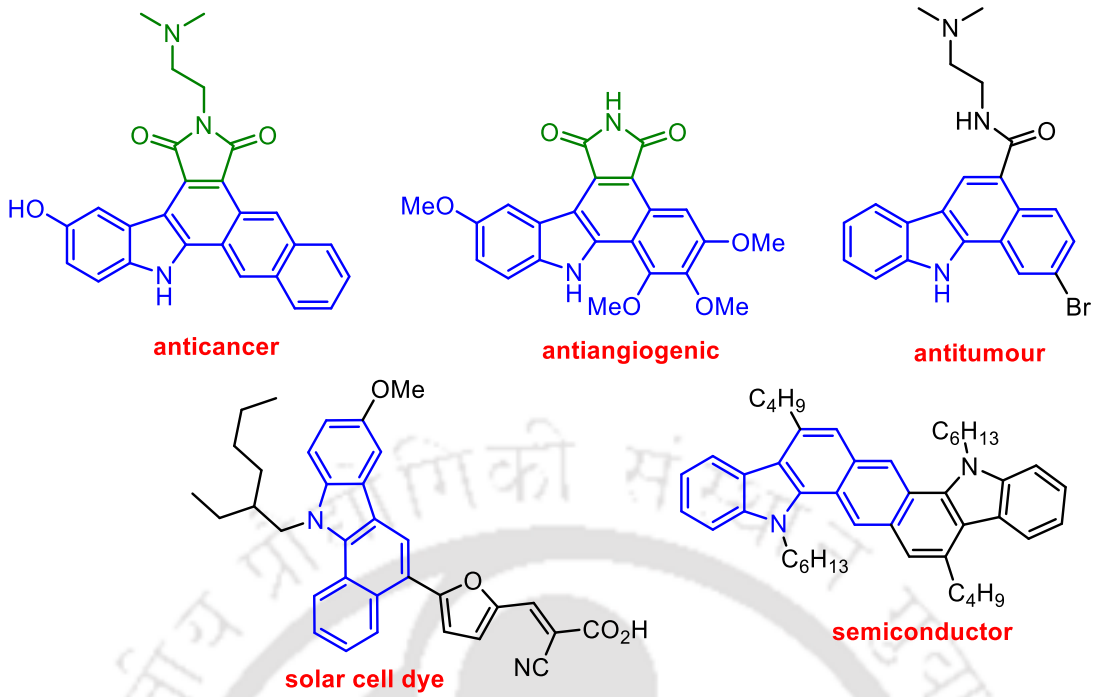

Figure II.1.1.1. *Benzo[a]carbazole featured bioactive and organic functional materials*

II.1.2. Preceding Reports of Synthesis of Benzo[*a*]Carbazole Fused NPAHs

Owing to the importance of benzo[*a*]carbazoles there has been a massive quest among researchers to synthesize them elegantly.[10] In 2005, Routier *et. al.* reported the synthesis of naphthocarbazolic PAHs via multi-steps Pd-catalyzed process.[7b] Various approaches towards the synthesis of benzo[*a*]carbazoles are classified as (a) using 2-phenylindoles under 4d-transition-metal catalysis (b) using diethynylarenes under 4d and 5d transition-metal catalysis (c) using 2-alkynylanilines under 4d and 5d transition-metal catalysis.

(a) Using 2-Phenylindoles Under 4d- Transition-Metal Catalysis: The 4d- transition-metals such as Rh and Pd have been employed to access fused benzo[*a*]carbazole motifs from 2-phenylindoles.[11]

In 2009, Jiao *et. al.* developed a Pd(II) catalyzed synthesis of benzo[*a*]carbazoles using 2-arylindoles and internal alkynes. The protocol utilizes molecular oxygen as the sole oxidant (Scheme II.1.2.1).[11a]

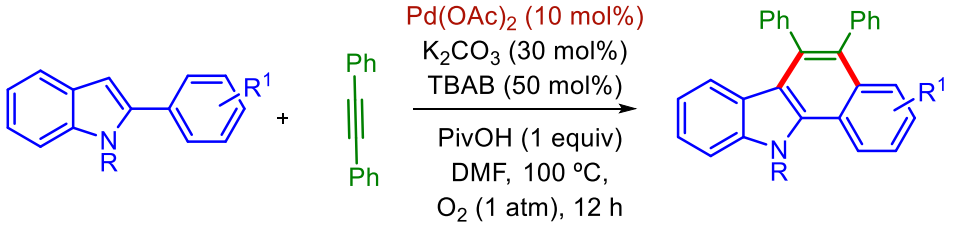

Scheme II.1.2.1. *Pd(II) catalyzed synthesis of benzo[a]carbazoles*

Benzo[*a*]carbazoles were synthesized by Zhang and Fan *et. al.* using 2-arylindoles and α-diazocarbonyl compounds under Rh(III) catalysis. The mechanism involves the formation of Rhodium-carbene intermediate, migratory insertion of the carbene into the Rh–C bond and protonolysis (Scheme II.1.2.2). [11b]

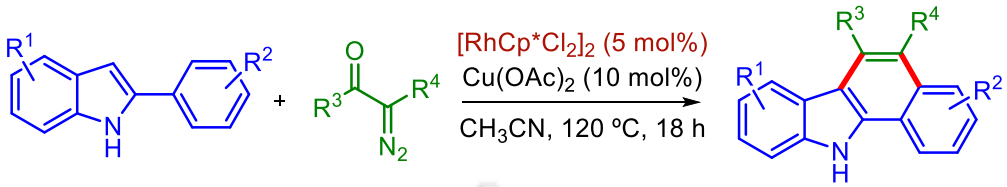

Scheme II.1.2.2. *Rh(III) catalyzed synthesis of benzo[a]carbazoles*

In 2019, Guo and Fan *et. al.* utilized benzoquinones as C2 synthon and synthesized 9H-dibenzo[*a*, *c*]carbazol-3-ols in a Rh(III) catalyzed system (Scheme II.1.2.3).[11d]

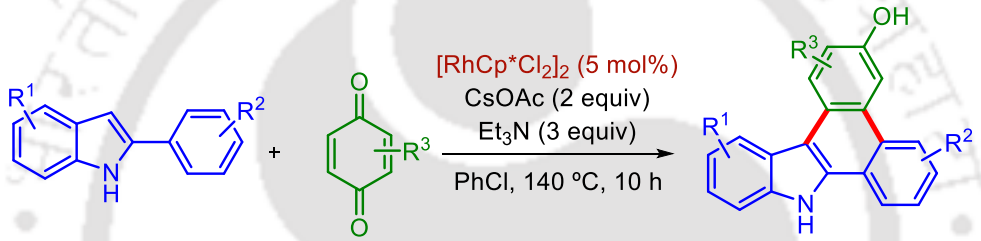

Scheme II.1.2.3. *Rh(III) catalyzed synthesis of benzo[a]carbazoles*

(b) Using Diethynylarenes Under 4d and 5d Transition-Metal Catalysis: The tandem oxidative annulation approach has gained much admiration due to its capability to access simultaneous ring cyclization in a single step.[12]

In 2010, Fuji and Ohno *et. al.* developed a gold(I)-catalyzed intramolecular cascade cyclization of diethynylarenes to benzo[*a*]carbazoles. The method delivers various alkyl chain and aryl substituted carbazoles (Scheme II.1.2.4).[12a]

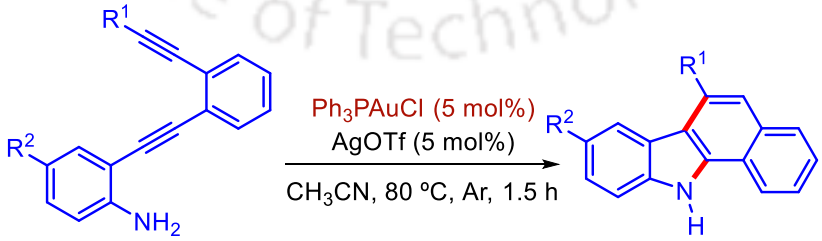

Scheme II.1.2.4. *Au(I) catalyzed synthesis of benzo[a]carbazoles*

In 2011, Ohno *et. al.* developed similar gold(I) catalyzed cascadic polycyclisation method for the synthesis of benzo[*a*]carbazolic derivatives from polyenynes. The protocol undergoes

hydroamination and consecutive hydroarylation of tri(poly)enyne anilines without any waste products. Thus, making the protocol a highly atom-economical one (Scheme II.1.2.5).[12c]

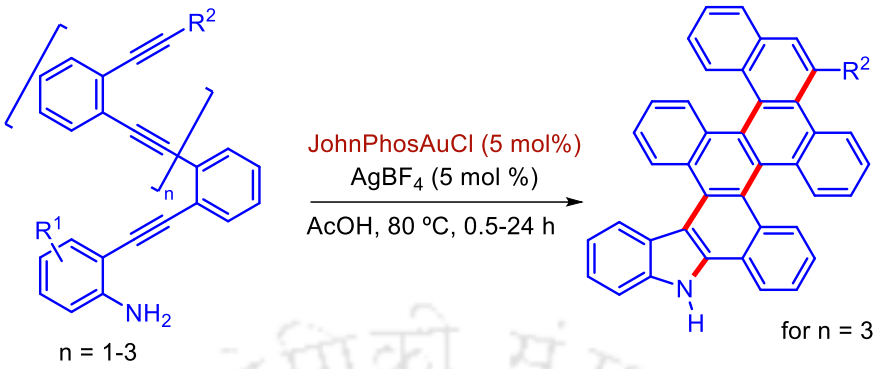

Scheme II.1.2.5. *Au(I) catalyzed synthesis of benzo[a]carbazoles*

In 2010, Wu *et. al.* developed a Pd(II) catalyzed cascadic path for the synthesis of benzo[*a*]carbazoles from enediynes. The mechanism involves the formation of 3-chlororindole from the initial cyclisation which is assisted by $CuCl_2$ followed by Pd(II) catalyzed activation of the second triple bond and annulation to deliver the benzo[*a*]carbazolic derivative (Scheme II.1.2.6).[12d]

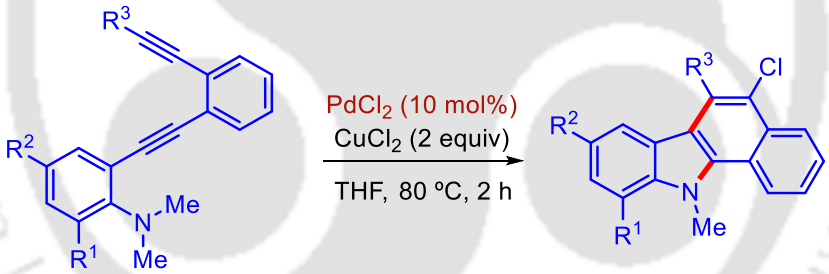

Scheme II.1.2.6. *Pd(II) catalyzed synthesis of benzo[a]carbazoles*

(c) Using 2-Alkynylanilines Under 4d and 5d Transition-Metal Catalysis: Various metals (Rh, Pd and Au) catalyzed intermolecular cyclization/oxidative annulation of *o*-alkynyl anilines with various coupling partners leading to benzo[*a*]carbazole have been conveyed.[13]

In 2016, Lin and Yao *et. al.* developed a one-pot Rh(III) catalyzed annulation for the synthesis of benzo[*a*]carbazoles using *o*-ethynylanilines and diazo compounds. The mechanism involves nucleophilic attack of the amine to the activated triple bond, aryl to aryl 1,4-rhodium migration, Rh-carbene intermediate formation to deliver the benzo[*a*]carbazolic product (Scheme II.1.2.7).[13a]

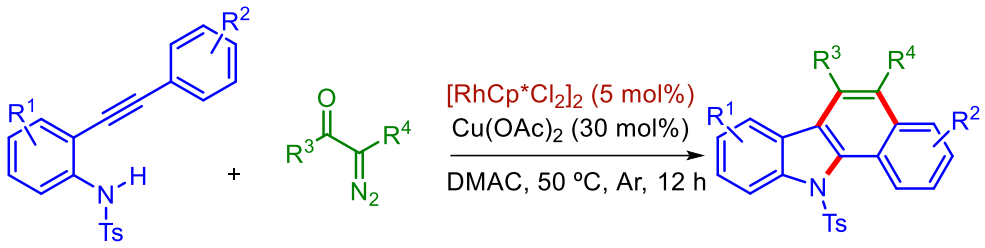

Scheme II.1.2.7. *Rh(III) catalyzed synthesis of benzo[a]carbazoles*

In 2012, Liang *et. al.* reported a Pd(II) catalyzed annulation reaction for the synthesis of benzo[*a*]carbazoles using *N*,*N*-dialkylaniline and internal alkynes. The mechanism involves molecular O_2 as the terminal oxidant (Scheme II.1.2.8).[13b]

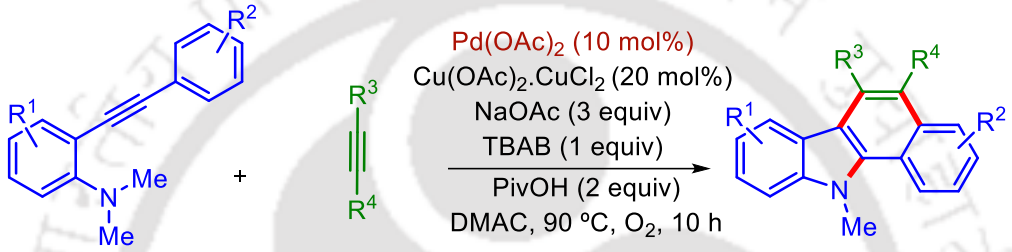

Scheme II.1.2.8. *Pd(II) catalyzed synthesis of benzo[a]carbazoles*

In 2016, Han, Zhang and gong *et. al.* synthesized benzo[*a*]carbazoles from aryl acetylene and 2-alkynyl arylazides in a Au(I) catalyzed pathway. The mechanism involves the formation of two gold carbene intermediate, cyclopropenation, Friedel-Crafts type reaction to deliver the final product (Scheme II.1.2.9).[13c]

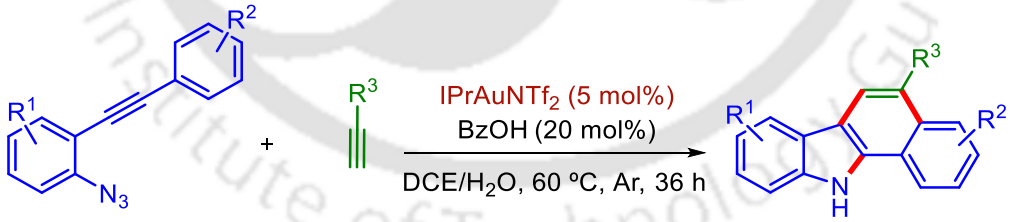

Scheme II.1.2.9. *Au(I) catalyzed synthesis of benzo[a]carbazoles*

However, all of these transformations are associated with the use of expensive transition metals. Thus, the usage of cheaper 3d metals to access highly functionalized benzo[*a*]carbazoles is mostly sought after. There are a few Cu-catalyzed dual C–C bond formations using maleimides, but the annulated products so obtained, invariably ended up having a reduced maleimide moiety and they proceed via a radical path.[14]

In 2015, Bissember *et. al.* utilized bis(1,10-phenanthroline)copper(I) complex in a

photochemical condition to activate the α C–H bonds of amines. The method exploited maleimide and *N,N*-dialkylaniline to synthesize octahydroisoquinolino[2,1-*a*]pyrrolo-[3,4-*c*]quinoline derivatives. The mechanism involves a crucial role of TFA in the oxidation of photoexcited Cu(I) to Cu(II) (Scheme II.1.2.10).[14a] The annulated products delivered, invariably ends up having a reduced maleimide moiety.

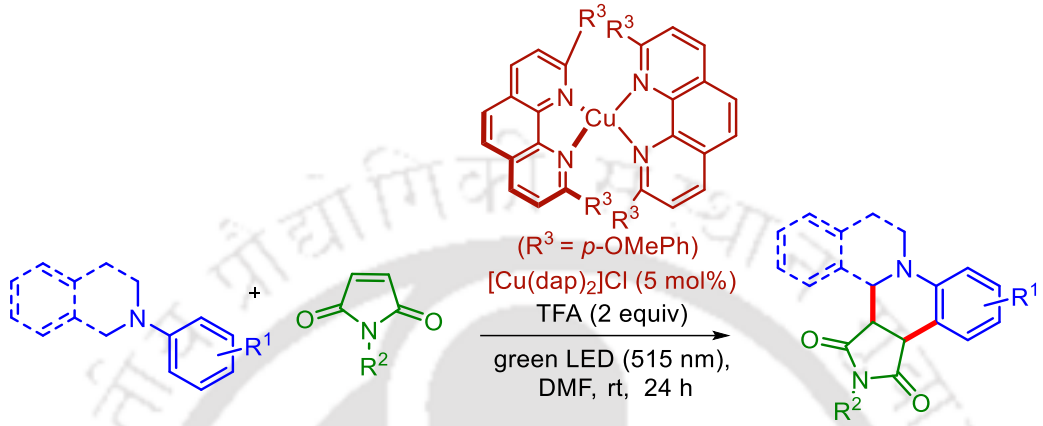

Scheme II.1.2.10. *Cu(I) catalyzed synthesis of octahydroisoquinolino[2,1-a]pyrrolo-[3,4-c]quinoline*

In 2011, Miura *et. al.* developed a Cu(II) catalyzed method or the synthesis of tetrahydroquinolines from *N,N*-dialkylaniline and maleimide/ benzylidene malononitriles via sp^3 sp^2 C–H bond activation (Scheme II.1.2.11).[14b] Here also, the annulated products delivered, invariably ends up having a reduced maleimide moiety.

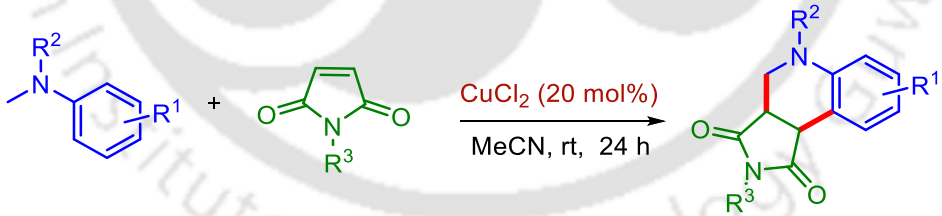

Scheme II.1.2.11. *Cu(II) catalyzed synthesis of tetrahydroquinolines*

II.1.3. Present Strategy for Synthesis of Benzo[*a*]carbazole Fused NPAHs

To the best of our knowledge, Cu catalyzed or mediated dual dehydrogenative C–H/C–H annulation leading to NPAHs is still unmet. There has been no report on dehydrogenative annulation of maleimide with an unprotected 2-alkanylaniline using copper salt to deliver benzo[*a*]carbazole. Thus, we aim at synthesizing benzo[*a*]carbazolic NPAHs from unprotected amines and maleimides using Cu(I) salt (Scheme II.1.3.1). Initially, 2-(phenylethynyl)aniline (**1a**) was reacted with N-ethylmaleimide (**2a**) in the presence of CuCl (1 equiv), Na_2CO_3 (1.5

equiv) and $AgNO_3$ (30 mol %) in dry DCE at 110 °C for 15 h under a nitrogen atmosphere to synthesize 2-Ethylbenzo[*a*]pyrrolo[3,4-*c*]carbazole-1,3(2*H*,8*H*)-dione (**3aa**).

Despite this anticipation, we had to overcome several challenges such as: i) homocoupling of 2-alkynylaniline as described by Fan and others;[15] ii) competitive C–H/N–H annulation from the N–H side; iii) stoppage of reaction at 2-phenylindole *via* protonation and reluctant to undergo subsequent annulation and, iv) overcoming the binding of the active Cu catalyst by the free amine employing $AgNO_3$ (which is trapped as a transient silver-amine complex).[16]

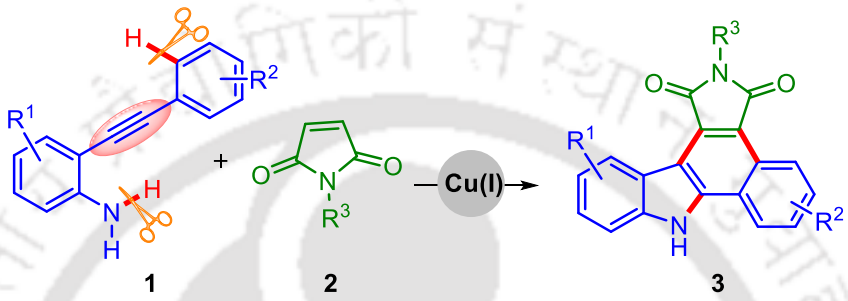

Scheme II.1.3.1. *Present strategy of Cu(I) mediated synthesis of benzo[a]carbazoles*

Herein, a Cu(I)-mediated C–H/C–H cascade-annulation is disclosed, where an intramolecular cyclization (C–N bond formation) is followed by an intermolecular oxidative annulation (two C–C bonds formation) of *o*-alkynylaniline (**1**) with maleimide (**2**) (*Scheme II.1.3.1*). The synthesis of benzo[*a*]pyrrolo[3,4-*c*]carbazole-1,3(2*H*,8*H*)-dione (**3**) is achieved under an inert atmosphere where copper acts both as a C–H activator as well as an oxidant in one-pot.

II.2. Optimization of Reaction Conditions

We initiated our synthetic planning taking 2-(phenylethynyl)aniline (**1a**) and *N*-ethylmaleimide (**2a**) as model substrates to achieve the optimal reaction condition. Initially, the reaction was carried out in the presence of CuCl (1 equiv), Na_2CO_3 (1.5 equiv) as the base and $AgNO_3$ (30 mol %) as an additive in dry DCE at 110 °C for 15 h under a nitrogen atmosphere (Table II.2.1., entry 1). As anticipated, the reaction ended up affording an annulated product **3aa**, but only in 18% yield along with the formation of a substantial amount of 2-phenylindole (**4a**, 60%). Encouraged by this result, various other copper salts *viz.* CuI, Cu_2O, $Cu(CH_3CN)_4BF_4$, $Cu(CH_3CN)_4PF_6$, $Cu(OAc)_2$ and $CuCl_2$ were screened (Table II.2.1., entries 2-7); among which, only $Cu(CH_3CN)_4BF_4$ was found to be most effective, delivering **3aa** in 45% yield (Table II.2.1., entry 4). Interestingly, on increasing the loading of copper salt from

1.0 to 1.5 equivalent, the yield improved up to 64%. This enhancement in the yield is due to the dual role of Cu serving partly as a catalyst and the rest as an oxidant (Table II.2.1., entry 8). The reaction in the absence of $AgNO_3$ gave a reduced yield (41%) (Table II.2.1., entry 9). Solvents screening revealed that the use of 2,2,2-trifluoroethanol (TFE), DMSO, and CH_3CN were unsuitable (Table II.2.1., entries 10-12), while DMF and toluene afforded product **3aa** in 10% and 47% yields respectively (Table II.2.1., entries 13 and 14). Thus, DCE turned out to be the ideal solvent. It was also observed that a base is essential for this transformation as in its absence the desired product was not obtained at all (Table II.2.1., entry 15). Keeping this in mind, several bases *viz*. Li_2CO_3, Cs_2CO_3, NaOAc, KOAc, Et_3N were investigated (Table II.2.1., entries 16-20) among which NaOAc standout yielding product **3aa** in 75% yield (Table II.2.1., entry 18). The reaction in the absence of copper salt (Table II.2.1., entry 21) or lower loading of $Cu(CH_3CN)_4BF_4$ (0.5 equiv) with additional terminal oxidants ($Cu(OAc)_2$ and O_2) was detrimental to product formation (Table II.2.1., entries 22 and 23). Further, it was observed that a reduced NaOAc (1 equiv) loading lowered the yield to 57% (Table II.2.1., entry 24). No improvement in the yield was observed by prolonging the reaction time to 24 h (Table II.2.1., entry 25) or lowering the reaction temperature to 90 °C (Table II.2.1., entry 26). The standard reaction in an open-air atmosphere performed poorly, providing product **3aa** in 33% yield (Table II.2.1., entry 27).

The best optimized condition is the use of **1a** (0.35 mmol), **2a** (0.53 mmol), $Cu(CH_3CN)_4BF_4$ (1.5 equiv), $AgNO_3$ (30 mol%), NaOAc (1.5 equiv), dry 1,2-DCE (1.5 mL), at 110 °C for 15 h under a nitrogen atmosphere.

Table II.2.1. *Optimization of Reaction Conditions*[a]

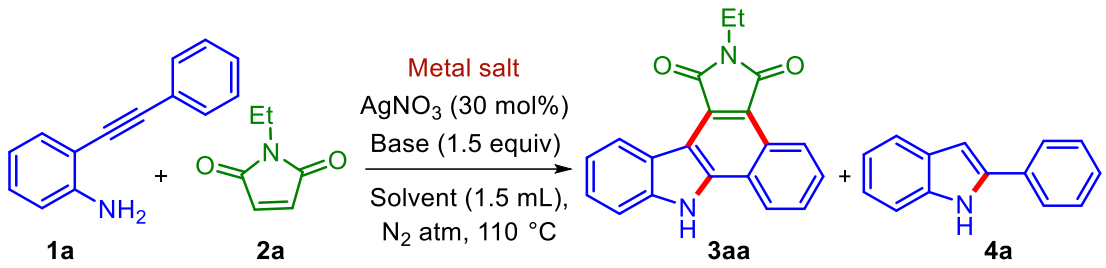

entry	metal salt (equiv)	base	solvent	yield of **3aa/4a** (%)[b]
1	CuCl (1.0)	Na_2CO_3	DCE	18/60
2	CuI (1.0)	Na_2CO_3	DCE	traces/63
3	Cu_2O (1.0)	Na_2CO_3	DCE	nd/57
4	$Cu(CH_3CN)_4BF_4$ (1.0)	Na_2CO_3	DCE	45/32
5	$Cu(CH_3CN)_4PF_6$ (1.0)	Na_2CO_3	DCE	nd/52
6	$Cu(OAc)_2$ (1.0)	Na_2CO_3	DCE	traces/61
7	$CuCl_2$ (1.0)	Na_2CO_3	DCE	traces/62
8	$Cu(CH_3CN)_4BF_4$ (1.5)	Na_2CO_3	DCE	64/21
9[c]	$Cu(CH_3CN)_4BF_4$ (1.5)	Na_2CO_3	DCE	41/19
10	$Cu(CH_3CN)_4BF_4$ (1.5)	Na_2CO_3	TFE	nd/49
11	$Cu(CH_3CN)_4BF_4$ (1.5)	Na_2CO_3	DMSO	nd/50
12	$Cu(CH_3CN)_4BF_4$ (1.5)	Na_2CO_3	CH_3CN	nd/54
13	$Cu(CH_3CN)_4BF_4$ (1.5)	Na_2CO_3	DMF	10/42
14	$Cu(CH_3CN)_4BF_4$ (1.5)	Na_2CO_3	toluene	47/36
15	$Cu(CH_3CN)_4BF_4$ (1.5)	--	DCE	traces/56
16	$Cu(CH_3CN)_4BF_4$ (1.5)	Li_2CO_3	DCE	51/14
17	$Cu(CH_3CN)_4BF_4$ (1.5)	Cs_2CO_3	DCE	53/17
18	**$Cu(CH_3CN)_4BF_4$ (1.5)**	**NaOAc**	**DCE**	**75/10**
19	$Cu(CH_3CN)_4BF_4$ (1.5)	KOAc	DCE	48/25
20	$Cu(CH_3CN)_4BF_4$ (1.5)	Et_3N	DCE	50/17
21	---	NaOAc	DCE	nd/12
22[d]	$Cu(CH_3CN)_4BF_4$ (0.5)	NaOAc	DCE	41/23
23[e]	$Cu(CH_3CN)_4BF_4$ (0.5)	NaOAc	DCE	35/30
24[f]	$Cu(CH_3CN)_4BF_4$ (1.5)	NaOAc	DCE	57/16
25[g]	$Cu(CH_3CN)_4BF_4$ (1.5)	NaOAc	DCE	77/9
26[h]	$Cu(CH_3CN)_4BF_4$ (1.5)	NaOAc	DCE	61/23
27[i]	$Cu(CH_3CN)_4BF_4$ (1.5)	NaOAc	DCE	33/48

[a]Reaction Conditions: **1a** (0.35 mmol), **2a** (0.53 mmol), metal salt, base (1.5 equiv), $AgNO_3$ (30 mol%), solvent (1.5 mL), 110 °C, N_2 atm. [b]Isolated yield. [c] No $AgNO_3$ used. [d]1 equiv. $Cu(OAc)_2$ used. [e]Under O_2 atmosphere. [f]1 equiv. base used. [g]24 h. [h]Reaction temperature 90 °C. [i]Open air atm. nd =not detected.

II.3. Substrate Scope of the Protocol

By executing the optimized reaction conditions (Table II.2.1., entry 18), we examined the generality and scope of the protocol using various *o*-alkynyl anilines and *N*-substituted and free N–H maleimides (Scheme II.3.1 and Scheme II.3.2). Firstly, the substrate scope of various *o*-alkynyl aniline was investigated with *N*-ethyl maleimide (**2a**) as the coupling partner and the results are tabulated in Scheme II.3.1. The substitution of electron-donating *p*-Me (**1b**), *p*-^{t}Bu (**1c**), *m*-Me (**1g**), and electron-withdrawing *p*-F (**1d**), *p*-Cl (**1e**), *p*-Br (**1f**), *m*-F (**1h**), *m*-Cl (**1i**) groups on the aryl ring of alkynyl fragment all reacted efficiently with *N*-ethyl maleimide (**2a**) to afford corresponding annulated products **3ba**-**3ia** in good to moderate yields (52%–75%). Notably, for the meta substituted *o*-alkynylanilines (**1g**, **1h** and **1i**), the annulation took place at the less hindered *ortho*-position of the aryl rings. To display the diversity and scope, hetero-aryl bearing 2-(thiophen-2-ylethynyl)aniline (**1j**) was tested under the identical conditions which provided the corresponding product **3ja** in 66 % yield. Similarly, the substitution of electron-donating -^{t}Bu (**1k**), -Me (**1l**) and electron-withdrawing -CF_3 (**1m**), -Cl (**1n**), -Br (**1o**) groups at the C4 position of the aniline, successfully underwent oxidative annulation with *N*-ethylmaleimide (**2a**) to construct annulated products **3ka**-**3oa** in decent yields (68%–74%). Next, maleimides possessing an *N*-benzyl group underwent successful annulation with 2-(phenylethynyl)aniline bearing various functional groups such as -Me (**1b**), -OMe (**1p**), -F (**1q**), -Cl (**1n** and **1r**), to yield products **3bb**-**3rb**, with yields ranging from 61% to 71%. The structure of **3rb** was confirmed by single-crystal X-ray analysis (Scheme II.3.1.). Interestingly, a N-methylated 4-chloro-*N*-methyl-2-(phenylethynyl)aniline (**1s**) also reacted successfully with *N*-ethyl maleimide **2a** to provide an annulated product **3sa** in 66% yield. To validate the feasibility of the strategy in large-scale synthesis, the reaction was performed on a 1 mmol scale under the standard condition, which provided **3aa** in 69% yield (Scheme II.3.1).

Then, we explored the scope of various *N*-substituted maleimides by taking 2-(phenylethynyl)aniline (**1a**) as the reacting partner (Scheme II.3.2). Various *N*-substituted maleimides *viz.* benzyl (**2b**), 4-methoxybenzyl (**2c**), methyl (**2d**), propyl (**2e**), isobutyl (**2f**), cyclohexyl (**2g**) all reacted competently with **1a** furnishing their anticipated annulated products **3ab**-**3ag** in good to moderate yields (60%–74%). Also, *N*-phenyl maleimides with *p*-OMe (**2h**), *p*-F (**2i**), *p*-CF_3 (**2j**), *m*-Cl (**2k**) substitutions, all reacted efficiently to afford products **3ah**-**3ak** in modest yields (53%–58%). Next, *N*-phenylmaleimide underwent successful oxidative annulation with a chloro substituted 2-(phenylethynyl)aniline (**1r**) to give **3rl** in 56% yield.

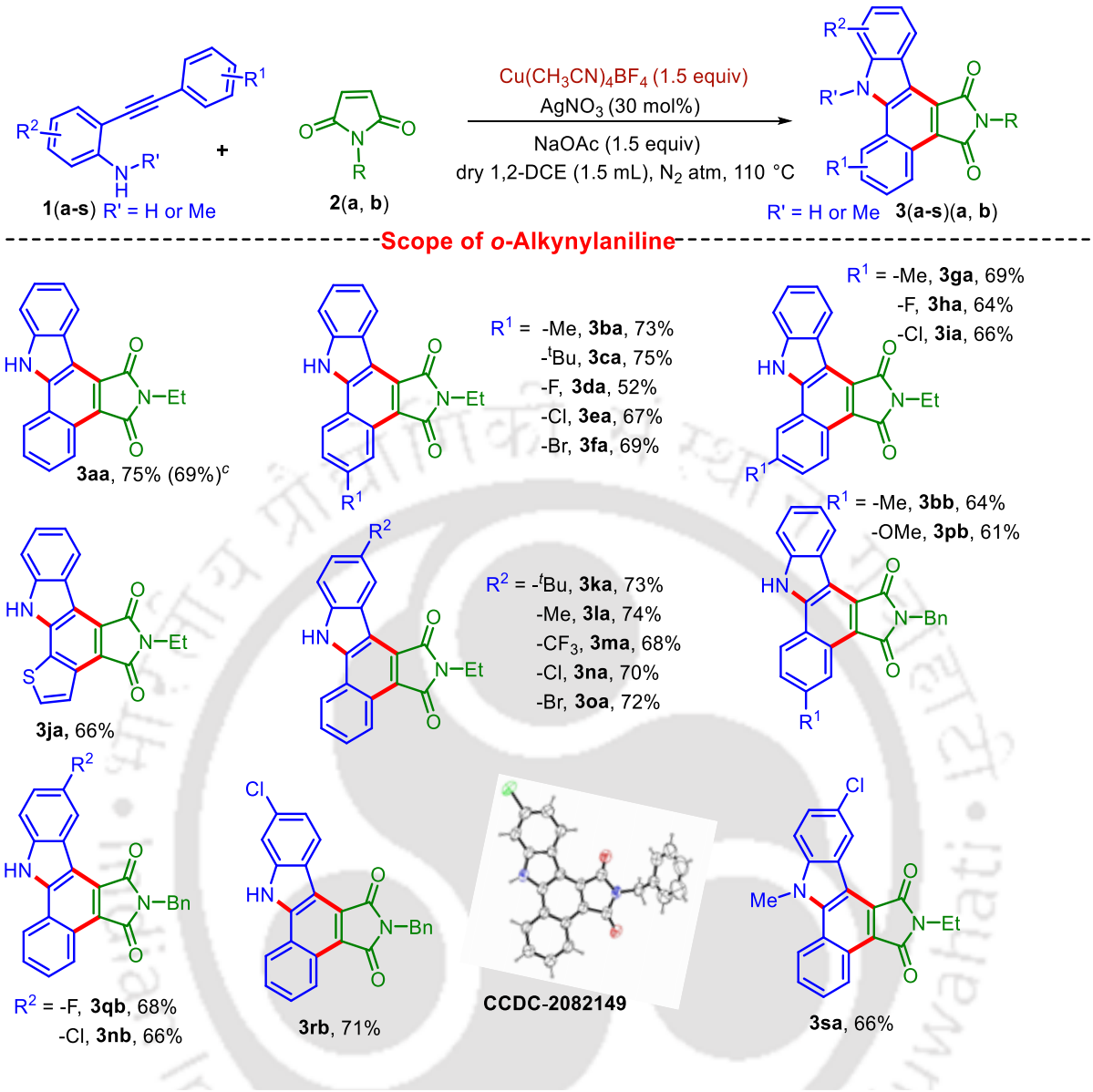

[a]Reaction conditions: **1** (0.35 mmol), **2** (0.53 mmol), $Cu(CH_3CN)_4BF_4$ (1.5 equiv), $AgNO_3$ (30 mol%), NaOAc (1.5 equiv), dry 1,2-DCE (1.5 mL) at 110 °C for 15 h under N_2 atmosphere. [b]Isolated yield. [c]Reaction performed at 1 mmol scale.

Scheme II.3.1. *Scope of o-Ethynylaniline* [a,b]

It was observed that *N*-substituted maleimides having long-chain alkyl groups such as *n*-hexyl (**2m**), *n*-heptyl (**2n**), and *n*-octyl (**2o**) offered higher yields of the products (**3am-3ao**, 74%–77%) compared to a shorter chain alkyl group. A chiral maleimide such as (S)-*N*-(1-phenylethyl) (**2p**) delivered **3ap** in 64% yield. Interestingly, maleimides having a free N–H group underwent successful annulation to give **3aq** in 50% yield thus opening further avenues for functionalization. On the other hand, benzoquinone (**2r**) reacted with 2-(phenylethynyl)aniline (**1a**) to give a C-3 olefinated product **3ar** in 73% yield. Nitrogen heterocycle bearing **1t** and **1u** and strongly electron-withdrawing bearing alkynyl aniline **1v**

failed to couple with maleimide **2a**. On the other hand, maleimide such as **2s** and internal olefins and alkynes *viz.* diethyl maleate **6a**, maleic anhydride **6b**, and diphenylacetylene (**6c**) failed to serve as the coupling partner with **1a** (Scheme II.3.2).

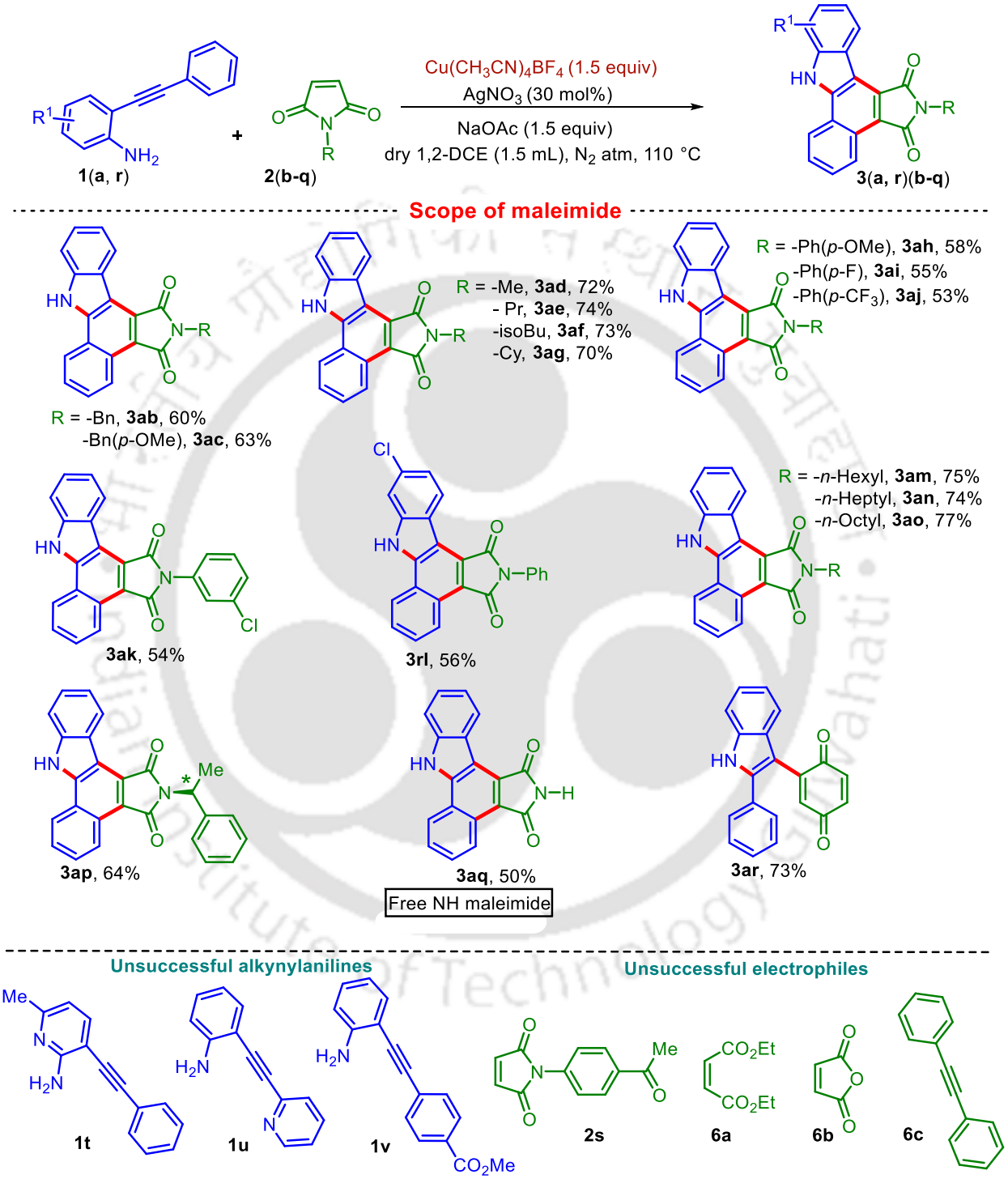

[a]Reaction conditions: **1** (0.35 mmol), **2** (0.53 mmol), $Cu(CH_3CN)_4BF_4$ (1.5 equiv), $AgNO_3$ (30 mol%), NaOAc (1.5 equiv), dry 1,2-DCE (1.5 mL) at 110 °C for 15 h under N_2 atmosphere. [b]Isolated yield.

Scheme II.3.2. *Scope of Maleimide and unsuccessful reagents*[a, b]

II.4. Study of Mechanistic Pathway

II.4.1. Control Experiments

To understand the nature of the reaction mechanism, a few control experiments were performed.

(a) Radical Scavenging Experiment

To eliminate the possibility of any radical path, 2-(phenylethynyl)aniline (**1a**) and *N*-ethylmaleimide (**2a**) were reacted in the presence of butylated hydroxytoluene (BHT) (2 equiv) and TEMPO (2 equiv) under the standard conditions. The yields of the product (**3aa**), 65% and 55% respectively was not significantly affected, thereby ruling out the likelihood of any radical pathway (Scheme II.4.1.1).

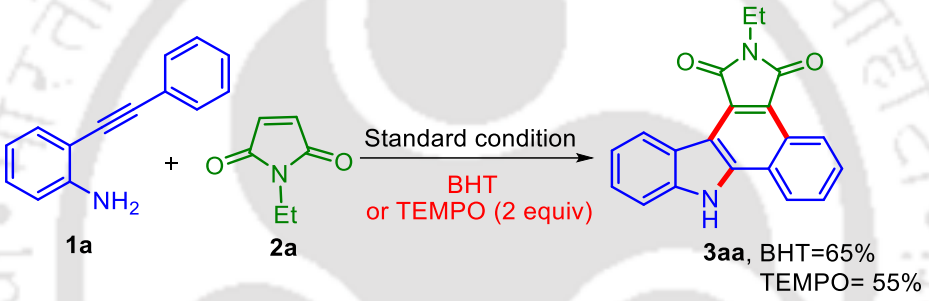

Scheme II.4.1.1. *Radical Scavenger Experiment*

(b) Reaction of *N*-ethylmaleimide with 2-Phenylindole

During the optimization of reaction conditions 2-phenylindole (**4a**) was obtained as a by-product (Table II.2.1). To ascertain whether it is an intermediate or a side product, a reaction of 2-phenylindole (**4a**) and *N*-ethylmaleimide (**2a**) under the standard conditions was carried out. The product (**3aa**) was obtained in 77% yield, thereby confirming its intermediacy (Scheme II.4.1.2).

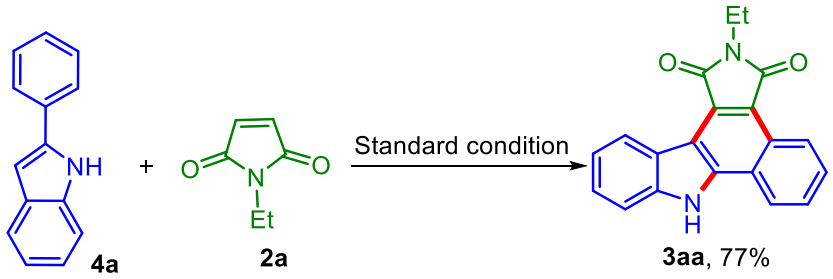

Scheme II.4.1.2. *Reaction of N-ethylmaleimide with 2-phenylindole*

(c) H/D Exchange Experiment

To confirm whether the C–H activation is reversible or not, 2-(phenylethynyl)aniline (**1a)** was treated with D_2O (5.0 equiv) under the standard reaction conditions but in the absence of *N*-ethylmaleimide (**2a**). It was observed that H/D exchange took place at the C-3 position of the *in situ* generated 2-phenylindole (**4a**) formed and 28% deuteration was observed (Scheme II.4.1.3). This confirms the C–H activation step to be reversible and the metallation takes place at the C3 position. We also performed the deuterium labelling experiment of **1a**, in the presence of **2a**. In this case, no deuteration took place on the unreacted *in situ* generated 2-phenylindole intermediate (**4a**). This is because when the C-3 position is activated the annulation is immediately initiated.

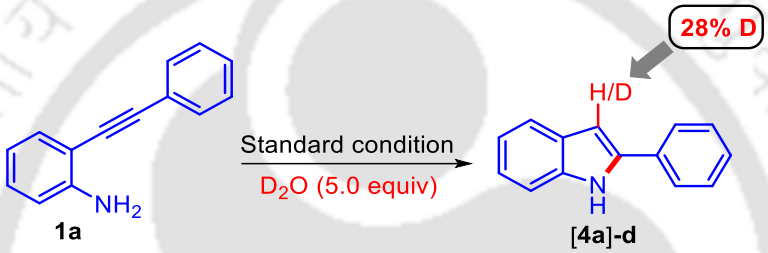

Scheme II.4.1.3. *H/D Exchange experiment*

(d) Reaction of *N*-ethylmaleimide with 2-(cyclohexylethynyl)aniline

Further, to check whether the C-3 position of indole is functionalized first or the *ortho*-position of C-2 phenyl ring of (**4a**), 2-(cyclohexylethynyl)aniline (**1w**) was reacted with (**2a**). The finding revealed that the alkylation took place at the C-3 position to afford **5wa** (57%) (Scheme II.4.1.4).

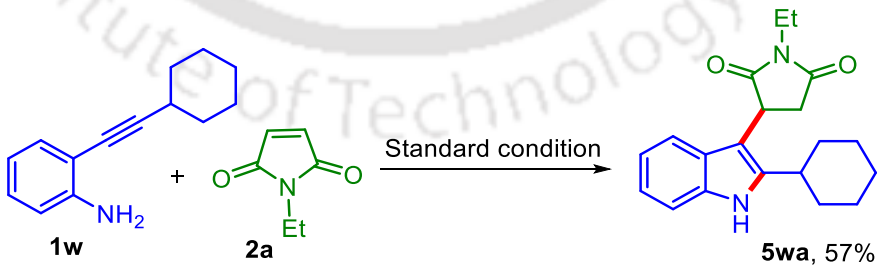

Scheme II.4.1.4. *Reaction of N-ethylmaleimide with 2-(cyclohexylethynyl)aniline*

(d) Detection of Intermediate in HRMS

In order to detect the intermediates, the crude reaction aliquot (5 h) of **3aa** was subjected to HRMS analysis. One of the intermediates **E** (Scheme II.4.2.1) was detected during the analysis (Figure II.4.1.1).

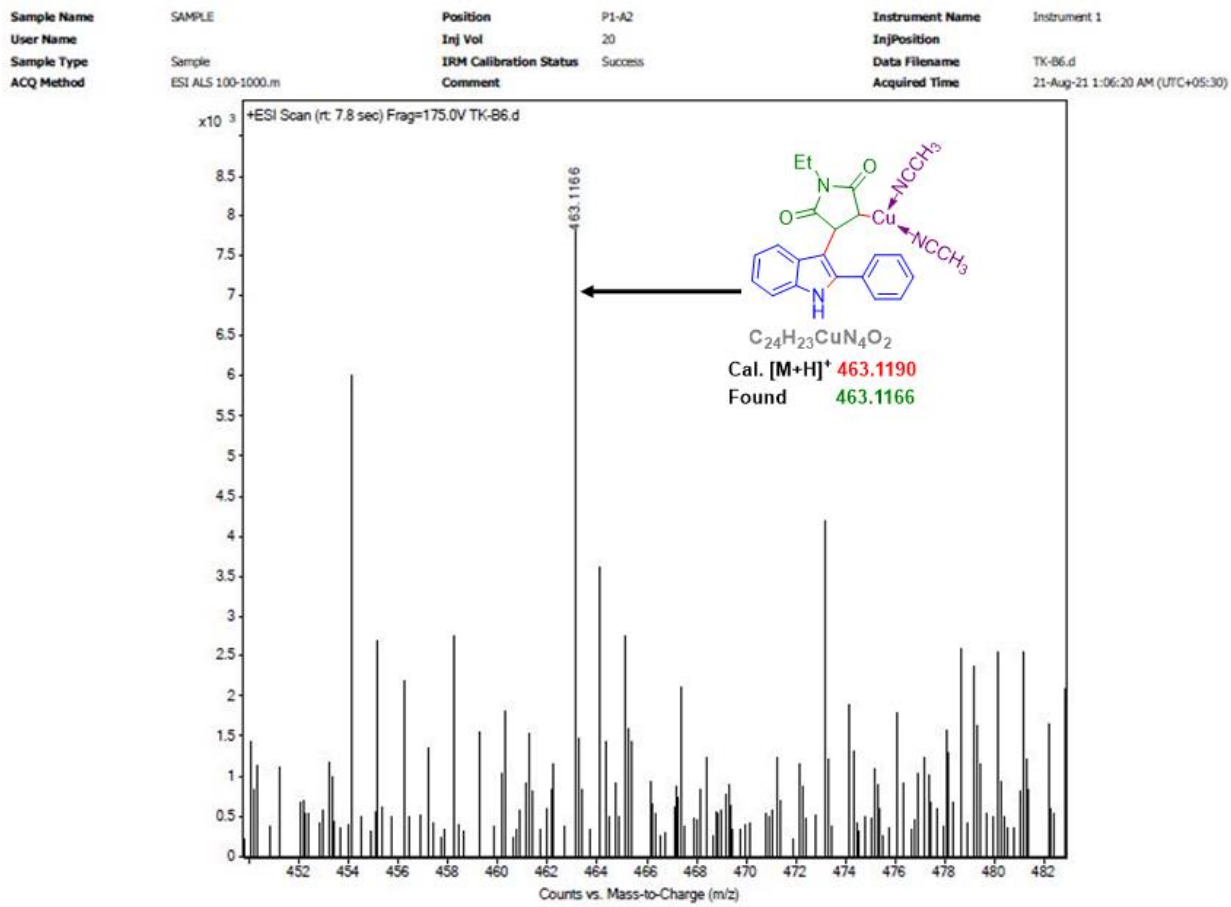

Figure II.4.1.1. *Detection of intermediate* ***E*** *in HRMS*

II.4.2. Mechanism

Based on the mechanistic studies in section II.4.1, HRMS analysis of reaction aliquots and earlier reports,[17] a plausible mechanism for this transformation is proposed in Scheme II.4.2.1. At first in the presence of silver salt, a transient silver-amine complex **I** is formed to prevent the transition metal poisoning from free –NH_2 of **1a**.[16] Then, the Cu/Ag salts polarizes the triple bond of 2-(phenylethynyl)aniline to promote a 5-endo dig cyclization followed by nucleophilic substitution of metal to provide an C3-cuprated indole species (**C**). The coordination of *N*-ethylmaleimide (**2a**) to intermediate **C** and subsequent migratory insertion into the reactive Cu–C bond give the intermediate **E** (detected by HRMS, Figure II.4.1.1). Further, the copper metal gets inserted into the *ortho*-C–H of the C-2 phenyl ring to deliver a seven-membered cupracycle **F**. Then the reductive elimination, followed by the oxidation of **G** affords the annulated product (**3aa**).

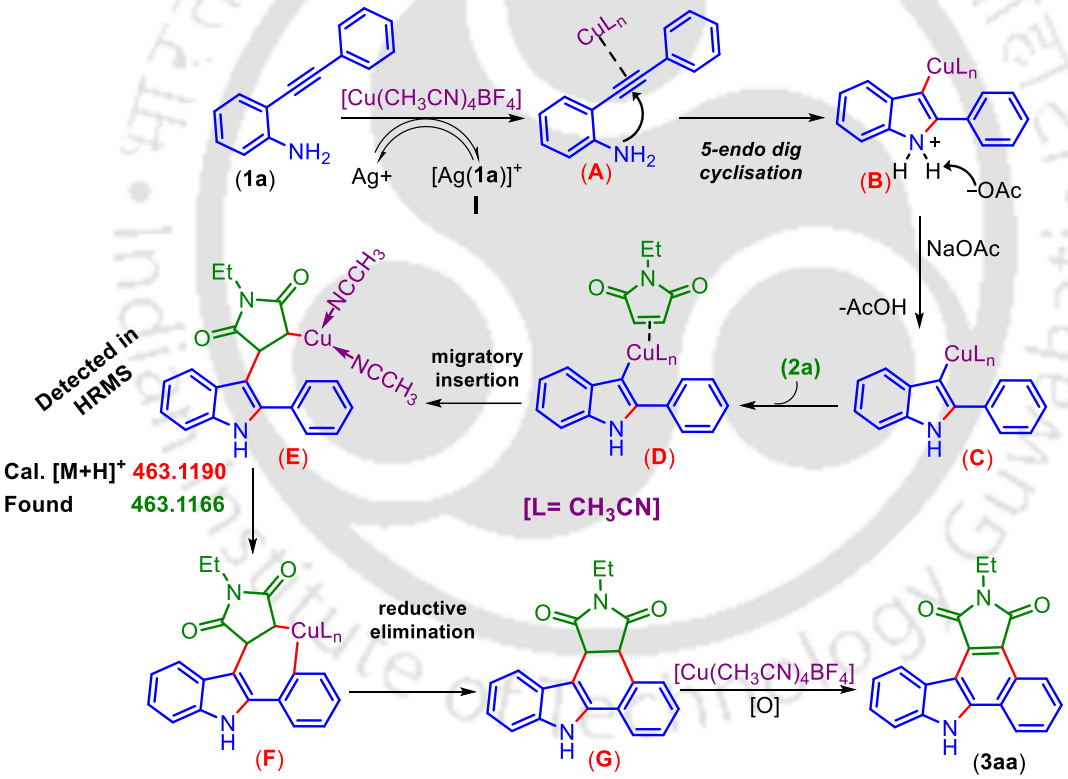

Scheme II.4.2.1. *A Plausible Mechanism for Cascade-Annulation*

II.5. Elucidation of Properties of the Synthesized Benzo[*a*]carbazoles

II.5.1 Theoretical study of the Frontier Orbitals

To gain insight into the electronic structure and the geometry of the annulated product (**3aa**), the density functional theory (DFT) calculation in its ground state was performed using B3LYP/6-31G+ (d, p) basis set level in DCM solvent modelled by polarizable continum model (CPCM) approach (Figure II.5.1.1.). The calculation reveals that the highest occupied molecular orbital (HOMO) of **3aa** is mainly localized over the carbazolic part whereas the lowest unoccupied molecular orbital (LUMO) is located mainly on the maleimide unit. The calculated energy level for HOMO is –5.94 eV and LUMO is –2.69 eV with an energy bandgap of 3.25 eV.

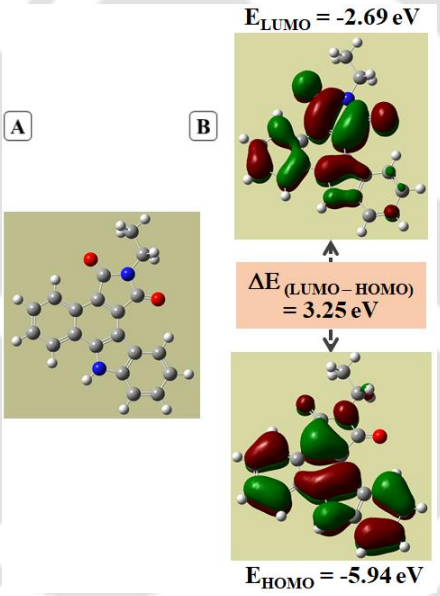

Figure II.5.1.1. *(A) Optimized ground state structure of* ***3aa*** *(B) Energies and shape of frontier orbitals (HOMO and LUMO) of* ***3aa*** *calculated at the B3LYP/6-31G+ (d, p) basis set level in DCM solvent modeled by the CPCM approach.*

II.5.2 Photophysical Study

Further, the photophysical properties of few representative compounds have been investigated. In DCM, they exhibit absorption $\boldsymbol{\lambda_{abs}^{max}}$ in the region of 412–425 nm with extinction coefficient (ε) in the range of 2.7× 10^3 – 9.1× 10^3 $M^{-1}cm^{-1}$ (Figure II.5.2.1.A) and the fluorescence emission $\boldsymbol{\lambda_{em}^{max}}$ ranging between 485–502 nm with a Stokes shift of 72 to 82 nm (Figure II.5.2.1.B)) (Table II.5.2.1.). Their excited state lifetime (τ) was found out to be in the range of 11.4–17.5 ns as obtained from time-resolved photoluminescence (TRPL) (Table

II.5.2.2.). It was also observed that there was a gradual bathochromic shift from 482 to 547 nm in the fluorescence emission of (**3aa**) upon varying the solvent polarity from nonpolar toluene to polar methanol with a decreased fluorescence intensity (Figure II.5.2.1.D), while its absorbance was unaffected (Figure II.5.2.1.C). Thus, this molecule possesses solvatochromic behavior (Table II.5.2.3.).

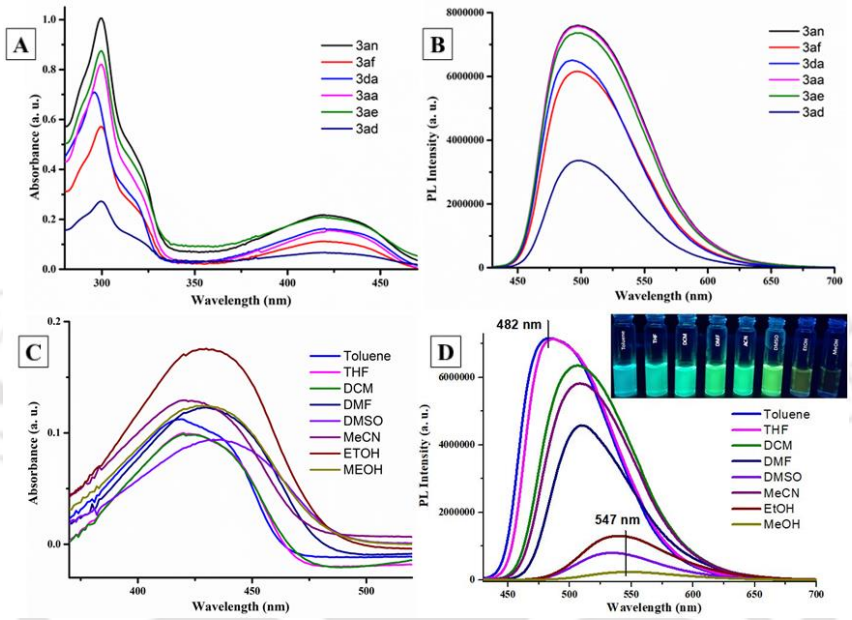

Figure II.5.2.1. *UV-visible (A) and photoluminescence (B) spectra of some selected annulated compounds in DCM at a concentration of 25 μM at room temperature. UV-visible (C) and Photoluminescence (D) spectra of* ***3aa*** *in different polarity solvents at a concentration of 20 μM at room temperature. excitation wavelength = 420 nm, slit = 2.*

Table II.5.2.1. *Photophysical properties of selected products*

Compound	$\lambda_{max,abs}$ (nm)[a]	ε ($M^{-1}cm^{-1}$)	$\lambda_{max,em}$ (nm)[b]	Stokes shift[c] (nm)	Life time (ns)[e] (τ)
3aa	425	6.2×10^3	497	72	15.8
3ba	420	9.1×10^3	500	80	14.6
3ca	420	3.7×10^3	502	82	15.3
3da	420	6.5×10^3	497	77	11.7
3ma	412	4.6×10^3	485	73	17.5
3rb	420	6.9×10^3	501	81	11.4
3ac	420	7.4×10^3	499	79	15.5
3ad	420	2.7×10^3	498	78	15.8
3ae	420	8.4×10^3	500	80	15.9
3af	420	4.5×10^3	497	77	16.0
3an	420	8.7×10^3	498	78	16.2

[a]Recorded at 25 µM in HPLC grade DCM at 25 °C. [b]Measured at 25 µM in HPLC grade DCM at 25 °C excited at 420 nm. [c]Stokes shift = $\lambda_{max,abs}$ - $\lambda_{max,em}$ (nm), $\lambda_{max,ab}$ are their π-π* absorption wavelengths. [e]405 nm laser used.

The results obtained in Time-Resolved Photoluminescence (TRPL) study are depicted below:

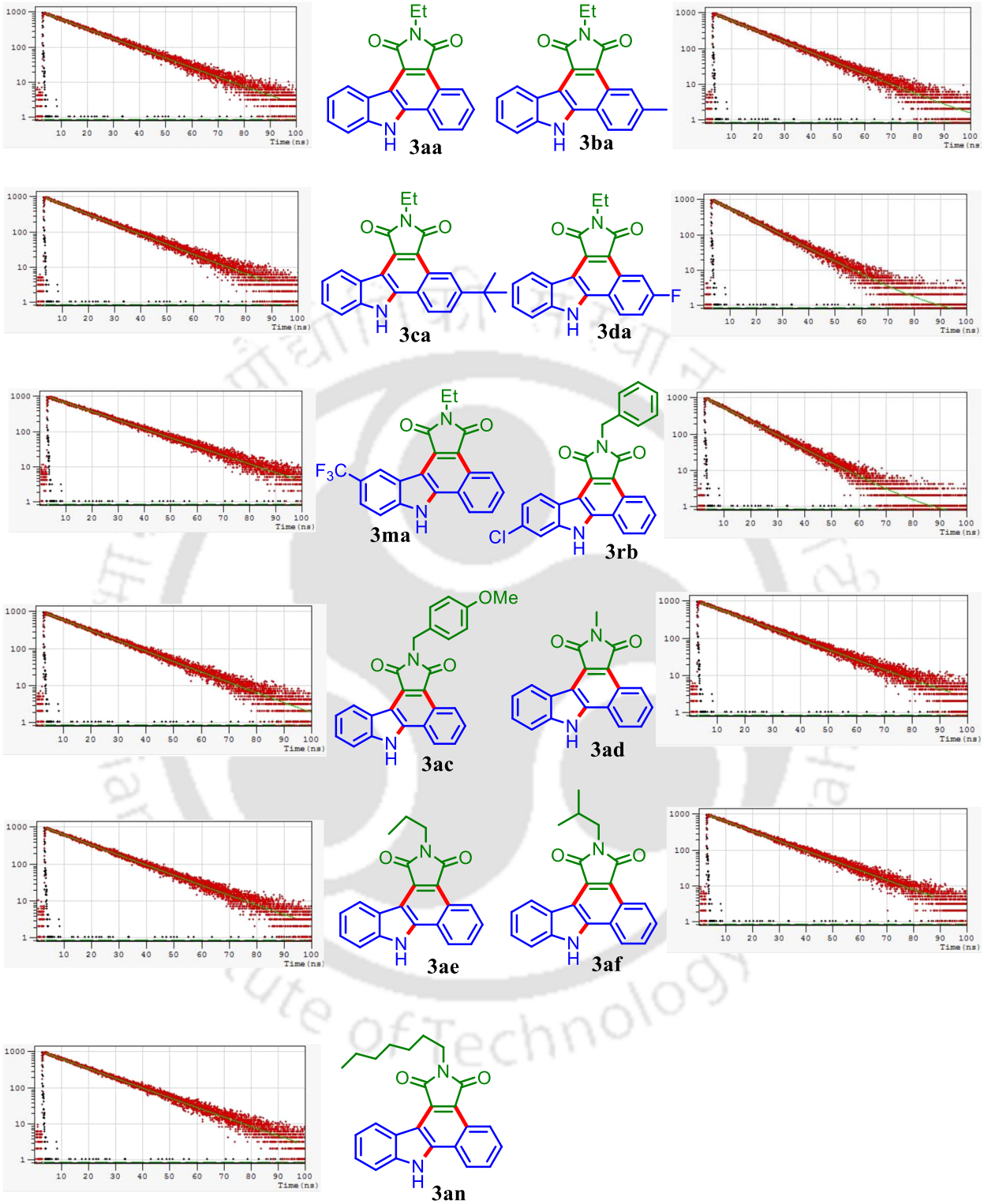

Figure II.5.2.2. *Time-resolved photoluminescence spectra.*

Table II.5.2.2. *Details of Time-Resolved Photoluminescence (TRPL) experiment*

Compound	Laser source (nm)	Emission (nm)	Fluorescence life time τ (ns)	$\chi 2$
3aa	405	497	15.8	1.089
3ba	405	500	14.6	1.072
3ca	405	502	15.3	1.097
3da	405	497	11.7	1.005
3ma	405	485	17.5	1.063
3rb	405	501	11.4	1.001
3ac	405	499	15.5	1.061
3ad	405	498	15.8	1.065
3ae	405	500	15.9	1.093
3af	405	497	16.0	1.097
3an	405	498	16.2	1.082

Table II.5.2.3. *Solvent effect on the photophysical properties of* ***3aa***

Solvent	$\lambda_{max,abs}$ (nm)[a]	$\lambda_{max,em}$ (nm)[b]
Toluene	418	482
THF	423	487
DCM	425	497
DMF	430	508
MeCN	422	508
DMSO	438	535
EtOH	430	539
MeOH	430	547

[a]Recorded at 20 µM in HPLC grade solvents at 25 °C. [b]Measured at 20 µM in HPLC grade solvents at 25 °C, excited at 420 nm.

The compounds also display aggregation-enhanced emission (AEE) phenomenon in the ethanol/hexane mixed solvent system (Figure II.5.2.3.A). The photoluminescence titration experiment shows that a gradual increase in the proportion of hexane to ethanol/hexane mixture causes an enhancement in fluorescence emission intensity with blue-shifted emission from 543 nm to 522 nm. At f_H 99.8%, the maximum fluorescence intensity of (**3aa**) was observed. Further, the morphology of the aggregates was investigated in field emission scanning electron microscope (FESEM) by drop-casting method, which reveals the formation of marigold flower-like aggregates at f_H 99.8% (Figure II.5.2.3.B).

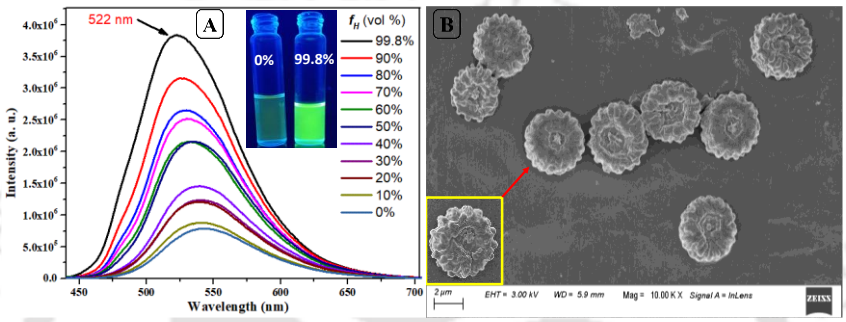

Figure II.5.2.3 *(A) Photoluminescence spectra of* ***3aa*** *in ethanol/hexane mixtures with different hexane fractions (f_H) with concentration = 20 μM, λ_{ex} = 425 nm, and slit = 2. The inset depicts fluorescence photographs of* ***3aa*** *in pure ethanol and ethanol/hexane mixture with 99.8% f_H taken under a 365 nm UV lamp. (B) Morphology of the* ***3aa*** *aggregates at 99.8% f_H in FESEM.*

II.5.3. Biological Study

Finally, the anti-cell proliferative effects of the compounds were evaluated. An alamarBlue-based cell viability assay was performed on HeLa cells treated with the synthesized compounds for an incubation duration of 48 h. As depicted in Figure II.5.3.1, no significant toxicity is observed from any of the four compounds namely **3ma**, **3an**, **3rb**, **3ae** for the concentrations up to 200 μM. So, this cell viability assay divulges that the compounds are non-cytotoxic and hence biocompatible. We then explored these fluorescent compounds for cellular imaging of HeLa cell lines. Confocal laser scanning microscope (CLSM) reveals bright luminescence of HeLa cells after treatment with representative compounds *viz.* **3ma**, **3an**, **3rb**, **3ae** over an incubation period of 30 mins (Figure II.5.3.2). Further, the Z-stack analysis of the treated cells indicates the uptake of these compounds into the cytoplasm of HeLa cells (Figure II.5.3.3). From CLSM images, it is apparent that the fluorescence signals are abundant in the cell cytoplasm. Thus, it is evident that these compounds can be used for bioimaging of various cell

types including cells of noncancerous origin since the compounds are highly fluorescent.

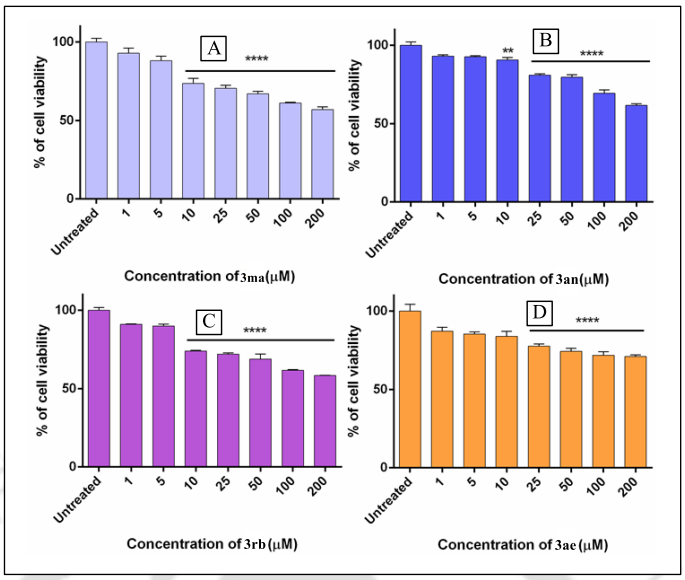

Figure II.5.3.1 *Effect of compounds* ***3ma*** *(A),* ***3an*** *(B),* ***3rb*** *(C),* ***3ae*** *(D) in terms of reduction in the percentage of viable cells as demonstrated by the alamarBlue assay. Statistical significance has been determined by one-way ANOVA, with *p < 0.05; **p < 0.01; ***p < 0.001; and ****p < 0.0001.*

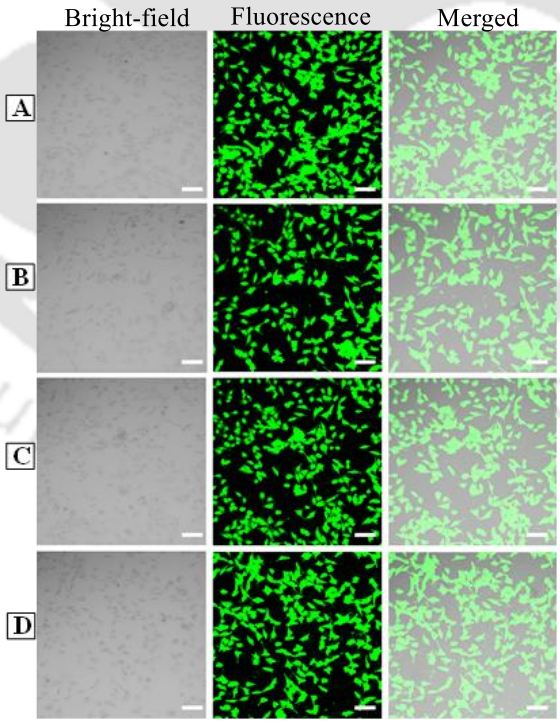

Figure II.5.3.2 *Confocal laser scanning microscopy images of HeLa cells stained with (A)* ***3ma****, (B)* ***3an*** *(C)* ***3rb****, (D)* ***3ae****. Cells were incubated with 50 μM for 30 min. Excitation: 405 nm. Emission range: 460−550 nm. Scale bar: 100 μm.*

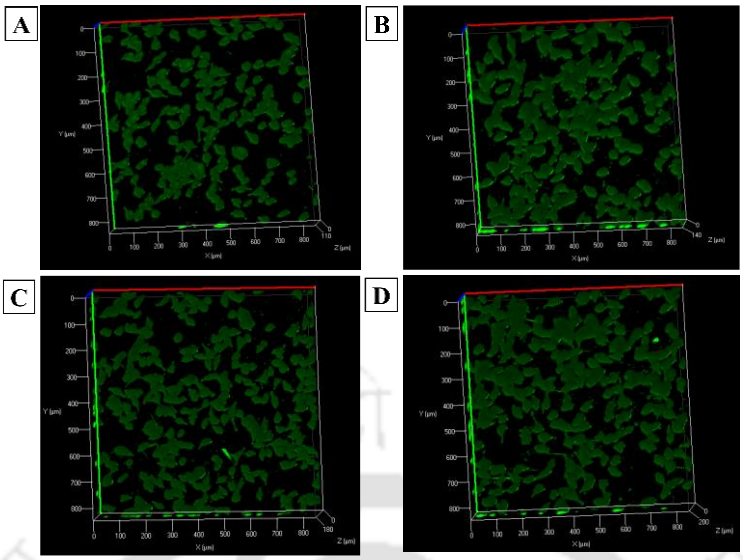

Figure II.5.3.3. *3D image of HeLa cells stained with (A)* ***3ma****, (B)* ***3an****, (C)* ***3rb****, (D)* ***3ae*** *obtained after Z-stacking in confocal laser scanning microscopy.*

II.6. Conclusion

In conclusion, an elegant and inexpensive copper(I) mediated dual annulation involving dual C–C bonds formation is reported. The tandem intramolecular and intermolecular C–H/C–H cyclization of *o*-alkynylanilines with maleimides leads to access a library of highly fluorescent benzo[*a*]carbazole fused products in good to moderate yield. This protocol efficiently offers two consecutive ring formations involving one new C–N and two C–C bonds formation in a single pot with excellent functional group diversity. The synthesized annulated products displayed strong emission in the green region 485–502 nm with a large Stokes shift and an excited-state lifetime of ~17 ns. The annulated compound (**3aa**) display AEE behavior in the ethanol/hexane solvent system and possess marigold flower-like morphology at the aggregated state. The compounds are biocompatible and convenient for the cellular imaging of HeLa cell lines.

II.7. Experimental Section

II.7.1. General Information and Instrumentation

All the chemicals were obtained from commercial sources and were used without further purification. The solvent 1,2-DCE was dried according to the standard method. The starting materials **1** and **2** were synthesized according to previously described methods.[18-19] Reactions

were monitored *via* TLC, prepared using silica gel 60 F_{254} (0.25mm) and was detected under UV light at 254 nm. Chromatography: Separation were carried out using 60-120 mesh sized silica gel. Ethyl acetate-hexane mixture was used as the eluent. NMR: ^{1}H-, ^{13}C-, ^{19}F- NMR spectra were recorded in 600, 500 and 400 MHz NMR in deuterated solvents and the chemical shifts (δ) are given in ppm. The ^{1}H spectra were referenced to the residual peaks of the solvents. For ^{1}H- $CDCl_3$ (7.26 ppm) and H_2O in DMSO-d_6 (3.3 ppm). For ^{13}C- $CDCl_3$(77.16 ppm) when both $CDCl_3$ and DMSO-d_6 are used; and DMSO-d_6 (39.5 ppm). IR spectra were recorded in neat using a FT-IR Spectrometer. HRMS were recorded using ESI (Q-TOF type mass analyser) in –ve and +ve modes. All UV-vis experiments were performed in a 1 mL quartz cuvettes of path length 1 cm. Photoluminescence was carried out on exciting at 420 nm in 1 mL quartz cuvettes. Fluorescence lifetime was measured in HPLC grade DCM solvent at a probe concentration of 25 µM by using 405 nm laser source. Morphology of the aggregate in the phenomenon of AEE was obtained at room temperature from a dried drop cast sample on an aluminium foil, using a field emission scanning electron microscope.

- **Materials for Biological Study**

Dulbecco's Modified Eagle's medium (DMEM), Phosphate Buffered Saline (PBS), Formaldehyde, Dimethyl sulfoxide (DMSO) was purchased from Sigma Aldrich (USA). Antibiotic-Antimycotic, Trypsin, Fetal Bovine Serum (FBS), alamarBlue™ were purchased from Thermo Fisher Scientific (USA). All the cell culture plastic wares were purchased from Eppendorf (Hamburg, Germany).

- **Cell Culture**

Human cervical cancer cell line (HeLa) was obtained from National Centre for Cell Sciences, Pune. Cells were maintained in Dulbecco's Modified Eagle's medium (DMEM) supplemented with 10% Fetal Bovine Serum (FBS) and 1% Antibiotic-Antimycotic solution. The culture was kept in a humidified atmosphere at 37 °C in a 5% carbon dioxide incubator. The media was changed at an interval of 3 days and sub-cultured upon reaching confluence.

- **Cell Viability Assay**

Cell Viability assay was done using alamarBlue™. Briefly, Hela cells were seeded in a 96 well plate at a density of 4000 cells/ well. Following attachment, cells were treated with varying concentrations of synthesized compounds for 48 h. After the treatment time, 10uL of 10X alamarBlue was added to each well of 96 well plates and incubated at 37 °C for 4

hours. Absorbance was measured at 570 nm with a reference wavelength of 600 nm. The experiments were done thrice independently and the treatments were done in triplicate. Cell viability was calculated using the following formula –

% of cell viability = {(A570-A600) sample / (A570-A600) Control} X 100

All the statistical analysis was performed using GraphPad Prism software.

- **Confocal Laser Scanning Microscopy**

Hela cells were seeded at a density of 0.5 x 10^6 cells on 35 mm confocal dishes. Following attachments, cells were treated with the compounds at a concentration of 50 µM for 30 minutes in complete media. After incubation, media was removed and cells were washed three times with PBS. To fix the cells, PBS was removed, and cells were incubated with 4% formaldehyde for 15 minutes. Following incubation, cells were washed three times with PBS. Untreated cells were used as control. Images were taken using a Confocal Laser Scanning Microscope and processed using Zen Blue software. Images were taken using an excitation laser of 405 nm and an emission filter range of 460–550 nm.

- **DFT Calculation**

The ground state DFT optimization of **3aa** was performed by using B3LYP hybrid functional[1] using 6-31G+ (d, p) basis set in DCM solvent modelled by Conductor-like Polarizable Continuum Model (CPCM) in Gaussian 09.[2]

(1) (a) Lee, C.; Yang, W.; Parr, R. G. *Phys. Rev. B.* **1988**, *37*, 785. (b) Becke, A. D. *J. Chem. Phys.* **1993**, *98*, 5648. (c) Stephens, P. J.; Devlin, F. J.; Chabalowski, C. F.; Frisch, M. J. *J. Phys. Chem.* **1994**, *98*, 11623.

(2) Gaussian 09, Revision D.01, Frisch, M. J.; Trucks, G. W.; Schlegel, H. B.; Scuseria, G. E.; Robb, M. A.; Cheeseman, J. R.; Scalmani, G.; Barone, V.; Mennucci, B.; Petersson, G. A.; Nakatsuji, H.; Caricato, M.; Li, X.; Hratchian, H. P.; Izmaylov, A. F.; Bloino, J.; Zheng, G.; Sonnenberg, J. L.; Hada, M.; Ehara, M.; Toyota, K.; Fukuda, R.; Hasegawa, J.; Ishida, M.; Nakajima, T.; Honda, Y.; Kitao, O.; Nakai, H.; Vreven, T.; Montgomery, J. A.; Jr.; Peralta, J. E.; Ogliaro, F.; Bearpark, M.; Heyd, J. J.; Brothers, E.; Kudin, K. N.; Staroverov, V. N.; Kobayashi, R.; Normand, J.; Raghavachari, K.; Rendell, A.; Burant, J. C.; Iyengar, S. S.; Tomasi, J.; Cossi, M.; Rega, N.; Millam, J. M.; Klene, M.; Knox, J. E.; Cross, J. B.; Bakken, V.; Adamo, C.; Jaramillo, J.; Gomperts, R.; Stratmann, R. E.; Yazyev, O.; Austin, A. J.; Cammi, R.; Pomelli, C.; Ochterski, J. W.; Martin, R. L.; Morokuma, K.; Zakrzewski, V. G.; Voth, G. A.; Salvador, P.; Dannenberg, J. J.; Dapprich, S.; Daniels, A. D.; Farkas,

Ö.; Foresman, J. B.; Ortiz, J. V.; Cioslowski, J.; Fox, D. J. Gaussian, Inc. Wallingford CT, **2009**.

II.7.2. Reaction Procedure

II.7.2.1. General Procedure for the Synthesis of *o*-Alkynylanilines (1)[18]

An oven-dried 25 mL round-bottom flask was charged with 2-iodoaniline derivatives (1 equiv, 2 mmol), $Pd(PPh_3)_2Cl_2$ (3 mol%, 0.06 mmol), CuI (4 mol%, 0.08 mmol) and a magnetic stir bar, which was stirred in Et_3N (7 mL) at room temperature for 5 minutes under N_2 atmosphere. Then phenylacetylene derivatives (1.2 equiv, 2.4 mmol) were added dropwise maintaining the inert atmosphere. The resulting mixture was stirred for 12 h. After completion of reaction, the reaction mixture was mixed with ethyl acetate (30 mL) and washed sequentially with cold 1N HCl (3 x 5 mL), water (1 x 10 mL) and saturated $NaHCO_3$ (1 × 5 mL). The organic layer was dried over anhydrous sodium sulfate and was evaporated under a reduced pressure. The residue so obtained was purified over column chromatography by eluting it with hexane:ethyl acetate (97:03) mixture to afford the desired products **1** in yield 66%–88%.

II.7.2.2. General Procedure for the Synthesis of Maleimides (2)

The maleimide derivatives were prepared by reported procedure.[19]

II.7.2.3. General Procedure for Synthesis of 3

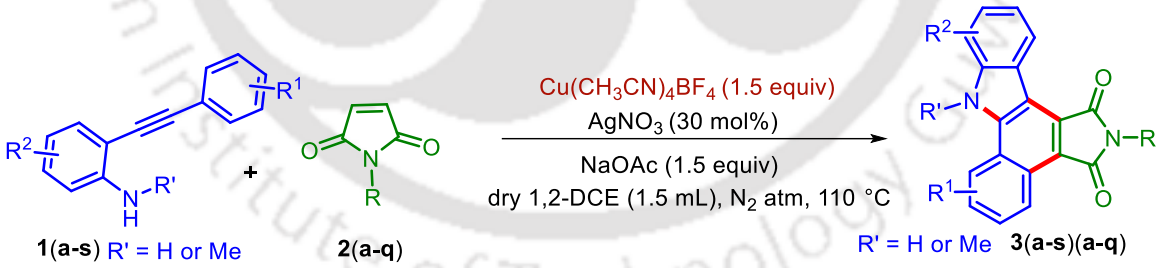

A 25 mL oven-dried double-necked round-bottom flask was charged with 2-alkynylaniline **1**(**a-s**) (0.35 mmol), maleimide **2**(**a-q**) (0.53 mmol), $Cu(CH_3CN)_4BF_4$ (1.5 equiv, 0.52 mmol), $AgNO_3$ (30 mol%, 0.10 mmol), NaOAc (1.5 equiv, 0.52 mmol) and a magnetic stir bar in dry 1,2-DCE (1.5 mL) under nitrogen atmosphere and was refluxed at 110 °C for 15 h. The progress of the reaction was monitored via TLC. After the completion of the reaction, the solvent was removed by rotary evaporation. The reaction mixture was then mixed with water (10 mL) and extracted with ethyl acetate (2 ×15 mL). The organic layer was dried over anhydrous sodium sulfate and was evaporated under reduced pressure. The residue so obtained was purified over

column chromatography by eluting it with hexane: ethyl acetate mixtures (~5-14% EtOAc in hexane) to afford the desired product **3**(**a-s**)(**a-q**) as a yellow solid in yield 50%–77%.

II.7.2.4. General Procedure for 1mmol Scale Synthesis of 3aa

A 25 mL oven-dried double-necked round-bottom flask was charged with 2-(phenylethynyl)aniline (**1a**) (1 mmol, 193 mg), *N*-ethyl maleimide (**2a**) (1.5 mmol, 188 mg), $Cu(CH_3CN)_4BF_4$ (1.5 equiv, 471 mg), $AgNO_3$ (30 mol%, 51 mg), NaOAc (1.5 equiv, 123 mg) and a magnetic stir bar in dry 1,2-DCE (2.0 mL) under nitrogen atmosphere and was refluxed at 110 °C for 15 h. The progress of the reaction was monitored via TLC. After the completion of the reaction, the solvent was removed by rotary evaporation. The reaction mixture was then mixed with water (10 mL) and extracted with ethyl acetate (2 ×15 mL). The organic layer was dried over anhydrous sodium sulfate and was evaporated under reduced pressure. The residue so obtained was purified over column chromatography by eluting it 7% EtOAc in hexane to afford the desired product **3aa** as a yellow solid in yield 69% (217 mg).

II.7.2.5. Procedure for Mechanistic Studies

(a) Procedure for Radical Scavenging Experiment

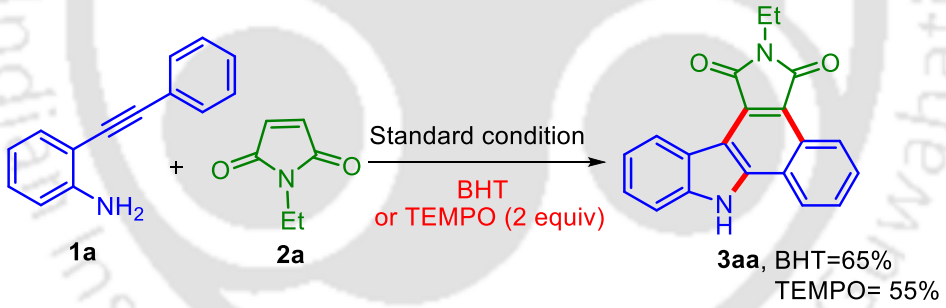

A 25 mL oven-dried double-necked round-bottom flask was charged with 2-alkynylaniline **1a** (0.35 mmol), maleimide **2a** (0.53 mmol), $Cu(CH_3CN)_4BF_4$ (1.5 equiv, 0.52 mmol), $AgNO_3$ (30 mol%, 0.10 mmol), NaOAc (1.5 equiv, 0.52 mmol), TEMPO (2 equiv, 0.7 mmol, 109 mg) or BHT (2 equiv, 0.7 mmol, 154 mg) and a magnetic stir bar in dry 1,2-DCE (1.5 mL) under nitrogen atmosphere and was refluxed at 110 °C for 15 h. The solvent was removed by rotary evaporation. The reaction mixture was then mixed with water (10 mL) and extracted with ethyl acetate (2 ×15 mL). The organic layer was dried over anhydrous sodium sulfate and was evaporated under reduced pressure. The residue so obtained was purified over column chromatography by eluting it with hexane: ethyl acetate mixture to afford the desired product **3aa** in 65% yield for BHT and in 55% yield for TEMPO.

(b) Procedure for Reaction of N-ethylmaleimide with 2-Phenylindole

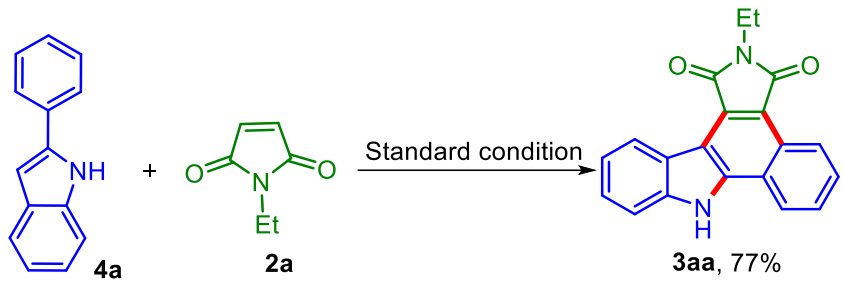

A 25 mL oven-dried double-necked round-bottom flask was charged with 2-phenylindole **4a** (0.35 mmol), maleimide **2a** (0.53 mmol), $Cu(CH_3CN)_4BF_4$ (1.5 equiv, 0.52 mmol), $AgNO_3$ (30 mol%, 0.10 mmol), NaOAc (1.5 equiv, 0.52 mmol) and a magnetic stir bar in dry 1,2-DCE (1.5 mL) under nitrogen atmosphere and was refluxed at 110 ºC for 15 h. The solvent was removed by rotary evaporation. The reaction mixture was then mixed with water (10 mL) and extracted with ethyl acetate (2 ×15 mL). The organic layer was dried over anhydrous sodium sulfate and was evaporated under reduced pressure. The residue so obtained was purified over column chromatography by eluting it with hexane: ethyl acetate mixture to afford **3aa** in 77% yield.

(c) Procedure for H/D Exchange Experiment

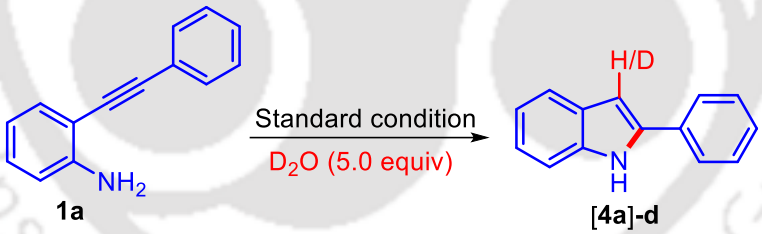

A 25 mL oven-dried double-necked round-bottom flask was charged with 2-alkynylaniline **1a** (0.35 mmol), $Cu(CH_3CN)_4BF_4$ (1.5 equiv, 0.52 mmol), $AgNO_3$ (30 mol%, 0.10 mmol), NaOAc (1.5 equiv, 0.52 mmol), D_2O (5equiv) and a magnetic stir bar in dry 1,2-DCE (1.5 mL) under nitrogen atmosphere and was refluxed at 110 ºC for 15 h. The solvent was removed by rotary evaporation. The residue so obtained was purified over column chromatography by eluting it with hexane: ethyl acetate mixture to afford **4a-d**.

(d) Procedure for Reaction of *N*-ethylmaleimide with 2-(cyclohexylethynyl)aniline

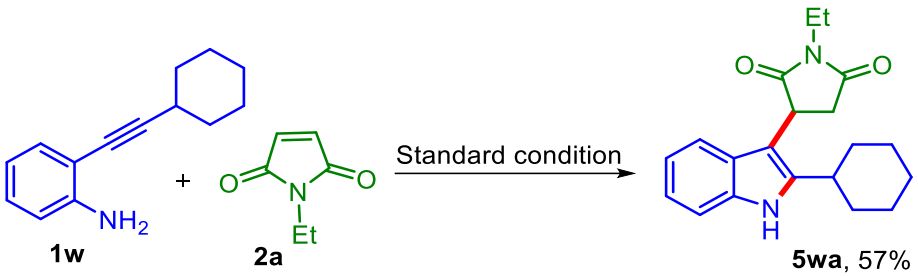

A 25 mL oven-dried double-necked round-bottom flask was charged with 2-(cyclohexylethynyl)aniline **1w** (0.35 mmol), maleimide **2a** (0.53 mmol), $Cu(CH_3CN)_4BF_4$ (1.5 equiv, 0.52 mmol), $AgNO_3$ (30 mol%, 0.10 mmol), NaOAc (1.5 equiv, 0.52 mmol) and a magnetic stir bar in dry 1,2-DCE (1.5 mL) under nitrogen atmosphere and was refluxed at 110 ^oC for 15 h. The progress of the reaction was monitored via TLC. The reaction mixture was then mixed with water (10 mL) and extracted with ethyl acetate (2 ×15 mL). The organic layer was dried over anhydrous sodium sulfate and was evaporated under reduced pressure. The residue so obtained was purified over column chromatography by eluting it with hexane: ethyl acetate mixture to afford **5wa** in 57% yield.

II.7.3. Crystallographic Description

Crystal data were collected with Bruker Smart Apex-II CCD diffractometer using graphite monochromated MoK_α radiation (λ = 0.71073 Å) at 298 K. Cell parameters were retrieved using SMART[a] software and refined with SAINT[a] on all observed reflections. Data reduction was performed with the SAINT software and corrected for Lorentz and polarization effects. Absorption corrections were applied with the program SADABS.[b] The structure was solved by direct methods implemented in SHELX-2014[c] program and refined by full-matrix least-squares methods on F2. All non-hydrogen atomic positions were located in difference Fourier maps and refined anisotropically. The hydrogen atoms were placed in their geometrically generated positions. For **3rb,** yellow crystals were isolated in needle shape from DCM at room temperature.

a. SMART V 4.043 Software for the CCD Detector System; Siemens Analytical Instruments Division: Madison, WI, 2008.

b. SAINT Plus (v 6.14) Bruker AXS Inc., Madison, WI, 2008.

c. Sheldrick, G. M. SHELXL-2014, Program for the Refinement of Crystal Structures; University of Göttingen: Göttingen (Germany), 1997.

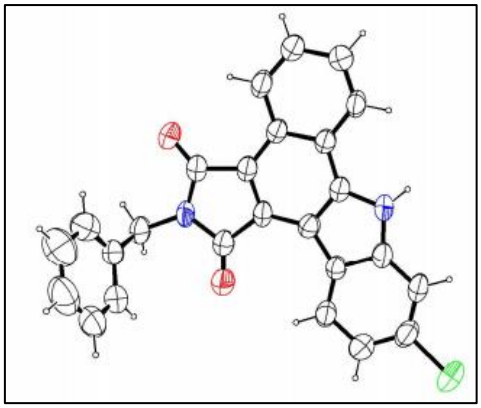

Figure II.6.3.1. *ORTEP diagram of* ***3rb*** *with ellipsoid probability 50%.*

Table II.6.3.1*. Crystal Data table for* ***3rb***

Empirical formula	$C_{25}H_{15}ClN_2O_2$
CCDC number	2082149
Formula weight	410.84
Temperature	296(2)
Wavelength	0.71073 Å
Crystal system	Monoclinic
Space group	P 21/c
Unit cell dimensions	a = 13.5395(18) Å, b = 17.218(2) Å, c = 8.4015(11) Å $\alpha = 90^o$, $\beta = 91.621(5)^o$, $\gamma = 90^o$
Volume	1957.8(4) $Å^3$
Z	4
Density (calculated)	1.394 g/cm^3
Absorption coefficient	0.220 mm^{-1}
F(000)	848
Crystal size	0.32 x 0.22 x 0.15
Theta range for data collection	1.505 to 24.999°
Index ranges	–16 < = h < = 16, –20 < = k < = 20, –9 < = l < = 9
Reflections collected	78946
Independent reflections	3432
Data completeness	1.00
Max. and min. transmission	0.876, 0.810
Refinement method	Full-matrix least-squares on F^2
Data / restraints / parameters	3432 / 0 / 275
Goodness-of-fit on F2	1.152
Final R indices [I>2sigma(I)]	R1 = 0.0809, wR2 = 0.1599
R indices (all data)	R1 = 0.1470, wR2 = 0.1938
Extinction coefficient	None
Largest diff. peak and hole	0.245 and –0.275

II.8. References

1. (a) Ito, H.; Ozaki, K.; Itami, K. *Angew. Chem., Int. Ed.* **2017**, *56*, 11144. (b) Yin, J.; Zhou, F.; Zhu, L.; Yang, M.; Lan, Yu.; You, J. *Chem. Sci.* **2018**, *9*, 5488. (c) Gońka, E.; Yang, L.; Steinbock, R.; Pesciaioli, F.; Kuniyil, R.; Ackermann, L. *Chem. Eur. J.* **2019**, *25*, 16246. (d) Ito, H.; Segawa, Y.; Murakami, K.; Itami, K. *J. Am. Chem. Soc.* **2019**, *141*, 3.
2. (a) Ackermann, L. *Acc. Chem. Res.* **2014**, *47*, 281. (b) Gulías, M.; Mascareñas, J. L. *Angew. Chem., Int. Ed.* **2016**, *55*, 11000. (c) Xu, F.; Kang, W. F.; Wang, Y.; Liu, C. S.; Tian, J. Y.; Zhao R. R.; Du, M. *Org. Lett.* **2018**, *20*, 3245.
3. (a) Guo, C.; Li, B.; Liu, H.; Zhang, X.; Zhang X.; Fan, X. *Org. Lett.* **2019**, *21*, 7189. (b) Peng, S.; Liu, S.; Zhang, S.; Cao, S.; Sun, J. *Org. Lett.* **2015**, *17*, 5032. (c) Kadam, V. D.; Feng, B.; Chen, X.; Liang, W.; Zhou, F.; Liu, Y.; Gao, G.; You, J. *Org. Lett*. **2018**, *20*, 7071. (d) Singam, M. K. R.; Babu, U. S.; Nagireddy, A.; Nanubolu, J. B.; Reddy, M. S. *J. Org. Chem*. **2021**, *86*, 8069. (e) Shinde, V. N.; Roy, T. K.; Jaspal, S.; Nipate, D. S.; Meena, N.; Rangan, K.; Kumar, D.; Kumar, A. *Adv. Synth. Catal*. **2020**, *362*, 5751. (f) Yang, X.; Li, Y.; Kong, L.; Li, X. *Org. Lett*. **2018**, *20*, 1957.
4. (a) Qi, S. L.; Li, Y.; Li, J. F.; Zhang, T.; Luan, Y. X.; Ye, M. *Org. Lett.* **2021**, *23*, 4034. (b) Gandeepan, P.; Müller, T.; Zell, D.; Cera, G.; Warratz, S.; Ackermann, L. *Chem. Rev.* **2019**, *119*, 2192. (c) Guo, X. -X.; Gu, D. -W.; Wu, Z.; Zhang, W. *Chem. Rev*. **2015**, *115*, 1622. (d) Gurram, R. K.; Rajesh, M.; Singam, M. K. R.; Nanubolu, J. B.; Reddy, M. S. *Org. Lett.* **2020**, *22*, 5326.
5. (a) Guo, X. -X.; Gu, D. -W.; Wu, Z.; Zhang, W. *Chem. Rev.* **2015**, *115*, 1622. (b) Aneeja, T.; Neetha, M.; Afsina, C. M. A.; Anilkumar, G. *RSC Adv.* **2020**, *10*, 34429. (c) Hu, M.; Song, R. -J.; Ouyang, X.-H.; Tan, F.-L.; Weia, W. -T.; Li, J.-H. *Chem. Commun*. **2016**, *52*, 3328.
6. (a) Knölker, H. J.; Reddy, K. R. *Chem. Rev.* **2002**, *102*, 4303. (b) Schmidt, A. W.; Reddy, K. R.; Knölker, H. -J. *Chem. Rev.* **2012**, *112*, 3193. (c) Ichikawa, S.; Tatebayashi, N.; Matsuda, A. *J. Org. Chem*. **2013**, *78*, 12065. (d) Tanious, F. A.; Ding, D.; Patrick, D. A.; Tidwell, R. R.; Wilson, W. D. *Biochemistry*. **1997**, *36*, 15315.
7. (a) Routier, S.; Me´rour, J. -Y.; Dias, N.; Lansiaux, A.; Bailly, C.; Lozach, O.; Meijer, L. *J. Med. Chem.* **2006**, *49*, 789. (b) Routier, S.; Peixoto, P.; Me´rour, J. -Y.; Coudert, G.; Dias, N.; Bailly, C.; Pierre, A.; Le´once, S.; Caignard, D. -H. *J. Med. Chem*. **2005**, *48*, 1401. (c) Peifer, C.; Stoiber, T.; Unger, E.; Totzke, F.; Schächtele, C.; Marmé, D.; Brenk, R.; Klebe, G.; Schollmeyer, D.; Dannhardt, G. *J. Med. Chem.* **2006**, *49*, 1271.

8. (a) Chen, C. H.; Wang, Y.; Michinobu, T.; Chang, S. -W.; Chiu, Y. C.; Ke, C.-Y.; Liou, G.-S. *ACS Appl. Mater. Interfaces* **2020**, *12*, 6144. (b) Qian, X.; Zhu, Y.-Z.; Chang, W. -Y.; Song, J.; Pan, B.; Lu, L.; Gao, H. -H.; Zheng, J.-Y. *ACS Appl. Mater. Interfaces*. **2015**, *7*, 9015. (c) Paramasivam, M.; Chitumalla, R. K.; Singh, S. P.; Islam, A.; Han, L.; Rao, V. J.; Bhanuprakash, K. *J. Phys. Chem. C.* **2015**, *119*, 17053.

9. (a) Mei, J.; Leung, N. L. C.; Kwok, R. T. K.; Lam, J. W. Y.; Tang, B. Z. *Chem. Rev.* **2015**, *115*, 11718. (b) Chang, Z.; Jiang, Y.; He, B.; Chen, J.; Yang, Z.; Lu, P.; Kwok, H. S.; Zhao, Z.; Qiua, H.; Tang, B. Z. *Chem. Commun.* **2013**, *49*, 594. (c) Ghosh, S.; Pal, S.; Rajamanickam, S.; Shome, R.; Mohanta, P. R.; Ghosh, S. S.; Patel, B. K. *ACS Omega.* **2019**, *4*, 5565.

10. (a) Gao, H.; Xu, Q. -L.; Yousufuddin, M.; Ess, D. H.; Kürti, L. *Angew. Chem., Int. Ed.* **2014**, *53*, 2701. (b) Fan, X.; Yu, L. -Z.; Wei, Y.; Shi, M. *Org. Lett.* **2017**, *19*, 4476. (c) Jash, M.; Das, B.; Chowdhury, C. *J. Org. Chem.* **2016**, *81*, 10987. (d) Mishra, U. K.; Yadav, S.; Ramasastry, S. S. V. *J. Org. Chem.* **2017**, *82*, 6729.

11. (a) Shi, Z.; Ding, S.; Cui, Y.; Jiao, N. *Angew. Chem., Int. Ed.* **2009**, *48*, 7895. (b) Bin, L.; Zhang, B.; Zhang, X.; Fan, X. *Chem. Commun.* **2017**, *53*, 1297. (c) Chen, G.; Zhang, X.; Jia, R.; Li, B.; Fan, X. *Adv. Synth. Catal.* **2018**, *360*, 3781. (d) Guo, S.; Liu, Y.; Zhao, L.; Zhang, X.; Fan, X. *Org. Lett.* **2019**, *21*, 6437. (e) Li, B.; Guo, C.; Shen, N.; Zhang, X.; Fan, X. *Org. Chem. Front.* **2020**, *7*, 3698. (f) Shinde, V. N.; Rangan, K.; Kumar, D.; Kumar, A. *J. Org. Chem.* **2021**, *86*, 2328. (g) Zhang, Q.; Li, Q.; Wang, C. *RSC Adv.* **2021**, *11*, 13030.

12. (a) Hirano, K.; Inaba, Y.; Watanabe, T.; Oishi, S.; Fujii, N.; Ohno, H. *Adv. Synth. Catal.* **2010**, *352*, 368. (b) Hirano, K.; Inaba, Y.; Takahashi, N.; Shimano, M.; Oishi, S.; Fujii, N.; Ohno, H. *J. Org. Chem.* **2011**, *76*, 1212. (c) Hirano, K.; Inaba, Y.; Takasu, K.; Oishi, S.; Takemoto, Y.; Fujii, N.; Ohno, H. *J. Org. Chem*. **2011**, *76*, 9068. (d) Chen, C. -C.; Chin, L. -Y.; Yang, S. -C.; Wu, M. -J. *Org. Lett.* **2010**, *12*, 5652.

13. (a) Guo, S.; Yuan, K.; Gu, M.; Lin, A.; Yao, H. *Org. Lett.* **2016**, *18*, 5236. (b) Xia, X. -F.; Wang, N.; Zhang, L. -L.; Song, X. -R.; Liu, X. -Y.; Liang, Y. -M. *J. Org. Chem.* **2012**, *77*, 9163. (c) Li, N.; Lian, X. -L.; Li, Y.-H.; Wang, T.-Y.; Han, Z.-Y.; Zhang, L.; Gong, L.-Z. *Org. Lett.* **2016**, *18*, 4178.

14. (a) Nicholls, T. P.; Constable, G. E.; Robertson, J. C.; Gardiner, M. G.; Bissember, A. C. *ACS Catal.* **2016**, *6*, 451. (b) Nishino, M.; Hirano, K.; Satoh, T.; Miura M. *J. Org. Chem.* **2011**, *76*, 6447.

15. (a) Jia, R.; Li, B.; Zhang, X.; Fan, X. *Org. Lett.* **2020**, *22*, 6810. (b) Jia, R.; Li, B.; Liang,

R.; Zhang, X.; Fan, X. *Org. Lett.* **2019**, *21*, 4996.

16. (a) Liang, Z.; Yao, J.; Wang, K.; Li, H.; Zhang, Y. *Chem. - Eur. J.* **2013**, *19*, 16825. (b) Cai, G.; Fu, Y.; Li, Y.; Wan, X.; Shi, Z. *J. Am. Chem. Soc.* **2007**, *129*, 7666.
17. (a) Sun, J.; Wang, K.; Wang, P.; Zheng, G.; Li, X. *Org. Lett.* **2019**, *21*, 4662. (b) Jillella, R.; Oh, D. h.; Oh, C. H. *New J. Chem*. **2018**, *42*, 16886. (c) Yu, J.; -Negrerie, D. Z.; Du, Y. *Org. Lett*. **2016**, *18*, 3322. (d) Hiroya, K.; Itoh, S.; Ozawa, M.; Kanamori, Y.; Sakamoto, T. *Tetrahedron Letters*. **2002**, *43*, 1277. (e) Jillella, R.; Oh, C. H. *RSC Adv.* **2018**, *8*, 22122. (f) Zhang, S.; Ma, H.; Ho, H. E.; Yamamoto, Y.; Bao, M.; Jin, T. *Org. Biomol. Chem*. **2018**, *16*, 5236.
18. (a) Hiroya, K.; Itoh, S.; Sakamoto, T. *J. Org. Chem.* **2004**, *69*, 1126. (b) Jillella, R.; Oh, D. H.; Oh, C. H. *New J. Chem*. **2018**, *42*, 16886.
19. (a) Mandal, R.; Emayavaramban, B.; Sundararaju, B. *Org. Lett.* **2018**, *20*, 2835. (b) Deshmukh, G. B.; Patil, N. S.; Gaikwada, V. B.; Bholay, A. D.; Patil, S. V. *J. Chem. Pharm. Res.* **2014**, *6*, 393.

II.9. Spectral Data

***2-(Phenylethynyl)aniline (1a)*:**

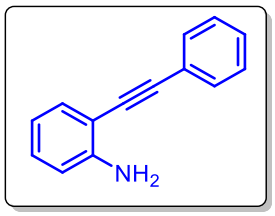

Light yellow solid (331 mg, 66% yield); ^{1}H NMR ($CDCl_3$, 600 MHz) δ 7.53 (dd, J = 7.7, 1.8 Hz, 2H), 7.37–7.33 (m, 4H), 7.15–7.13 (m, 1H), 6.72 (t, J = 7.6 Hz, 2H), 4.27 (s, 2H); ^{13}C{^{1}H} NMR (151 MHz, $CDCl_3$) δ 147.9, 132.3, 131.6, 129.9, 128.5, 128.3, 123.4, 118.1, 114.5, 108.1, 94.8, 86.0.

***2-(p-Tolylethynyl)aniline (1b)*:**

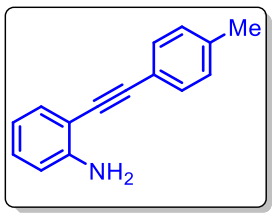

Light brown solid (351mg, 85% yield); ^{1}H NMR (400 MHz, $CDCl_3$) δ 7.42 (d, J = 8.1 Hz, 2H), 7.36 (d, J = 8 Hz, 1H), 7.16 (d, J = 7.6 Hz, 2H), 7.12 (d, J = 8 Hz, 1H), 6.72 (t, J = 7.7 Hz, 2H), 4.27 (s, 2H), 2.37 (s, 3H); ^{13}C{^{1}H} NMR (101 MHz, $CDCl_3$) δ 147.8, 138.5, 132.2, 131.5, 129.7, 129.3, 120.4, 118.1, 114.4, 108.3, 95.0, 85.3, 21.6.

***2-((4-(Tert-butyl)phenyl)ethynyl)aniline (1c)*:**

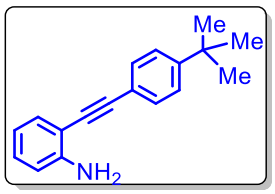

Brown solid (433 mg, 87% yield); ^{1}H NMR (600 MHz, $CDCl_3$) δ 7.46 (d, J = 8.4 Hz, 2H), 7.38–7.35 (m, 3H), 7.14–7.12 (m, 1H), 6.73–6.70 (m, 2H), 4.26 (s, 2H), 1.33 (s, 9H); ^{13}C{^{1}H} NMR (151 MHz, $CDCl_3$) δ 151.7, 147.8, 132.2, 131.3, 129.7, 125.5, 120.4, 118.1, 114.4, 108.4, 94.9, 85.3, 34.9, 31.3.

***2-((4-Fluorophenyl)ethynyl)aniline (1d)*:**

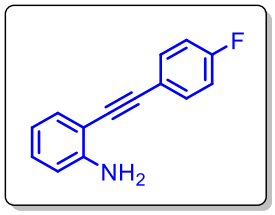

Light yellow solid (354 mg, 84% yield); ^{1}H NMR (600 MHz, $CDCl_3$) δ 7.51–7.49 (m, 2H), 7.35 (d, J = 7.2 Hz, 1H), 7.14 (td, J = 7.8, 1.2 Hz, 1H), 7.04 (t, J = 8.4 Hz, 2H), 6.72 (t, J = 7.2 Hz, 2H), 4.25 (s, 2H); ^{13}C{^{1}H} NMR (151 MHz, $CDCl_3$) δ 162.2 (d, J = 249.6 Hz), 147.9, 133.5 (d, J = 8.3 Hz), 132.3, 129.9, 119.5 (d, J = 3.5 Hz), 118.2, 115.8 (d, J = 22.0 Hz), 114.5, 107.9, 93.7, 85.7. ^{19}F NMR (565 MHz, $CDCl_3$) δ –111.1

***2-((4-Chlorophenyl)ethynyl)aniline (1e)*:**

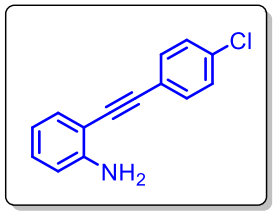

Light yellow solid (388 mg, 85% yield); ^{1}H NMR (500 MHz, $CDCl_3$) δ 7.44 (d, J = 8.6 Hz, 2H), 7.34 (d, J = 8.0 Hz, 1H), 7.32 (d, J = 8.6 Hz, 2H), 7.16 – 7.12 (m, 1H), 6.73 – 6.70 (m, 2H), 4.25 (s, 2H).; ^{13}C{^{1}H} NMR (126 MHz, $CDCl_3$) δ 147.96, 134.36, 132.79, 132.35, 130.12, 128.87, 122.01, 118.20, 114.56, 107.76, 93.69, 87.09.

***2-((4-Bromophenyl)ethynyl)aniline (1f)*:**

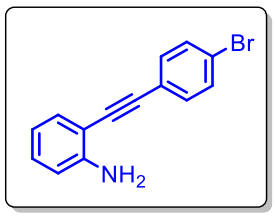

Light yellow solid (435 mg, 80% yield); ^{1}H NMR ($CDCl_3$, 500 MHz,) δ 7.47 (d, J = 8.5 Hz, 2H), 7.37 (d, J = 8.5 Hz, 2H), 7.35 (d, J = 8.4 Hz, 1H), 7.14 (td, J = 7.7, 1.6 Hz, 1H), 6.72-6.70 (m, 2H), 4.24 (s, 2H). ^{13}C{^{1}H} NMR (126 MHz, $CDCl_3$) δ 147.96, 132.99, 132.33, 131.79, 130.14, 122.53, 122.46, 118.20, 114.57, 107.72, 93.75, 87.28.

***2-(m-Tolylethynyl)aniline (1g)*:**

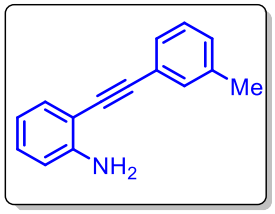

Brown solid (352 mg, 85% yield); ^{1}H NMR ($CDCl_3$, 600 MHz) ^{1}H NMR (400 MHz, CDCl3): δ 7.37–7.32 (m, 3H), 7.23 (d, J = 7.6 Hz, 1H), 7.14 (t, J = 7.6 Hz, 2H), 6.72 (t, J = 7.6 Hz, 2H), 4.27 (s, 2H), 2.36 (s, 3H); ^{13}C{^{1}H} NMR (101 MHz, $CDCl_3$) δ 147.9, 138.2, 132.3, 132.2, 129.8, 129.3, 128.7, 128.4, 123.2, 118.1, 114.4, 108.2, 95.0, 85.6, 21.4.

***2-((3-Fluorophenyl)ethynyl)aniline (1h)*:**

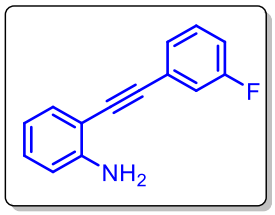

Brown solid (341 mg, 81% yield); ^{1}H NMR (400 MHz, $CDCl_3$) δ 7.36 (dd, J = 8.0, 1.2 Hz, 1H), 7.32–7.3 (m, 2H), 7.23–7.20 (m, 1H), 7.16 (td, J = 7.9, 1.5 Hz, 1H), 7.07–7.01 (m, 1H), 6.73 (d, J = 7.6 Hz, 2H), 4.27 (s, 2H); ^{13}C{^{1}H} NMR (101 MHz, $CDCl_3$) δ 162.5 (d, J = 247.3 Hz), 148.0, 132.4, 130.2, 130.1 (d, J = 8.8 Hz), 127.5 (d, J = 3.1 Hz), 125.3 (d, J = 9.5 Hz), 118.4, 118.2 (d, J = 3.4 Hz), 115.6 (d, J = 21.3 Hz), 114.6, 107.5, 93.5, 87.0; ^{19}F NMR (377 MHz, $CDCl_3$) δ –112.9.

***2-((3-Chlorophenyl)ethynyl)aniline (1i)*:**

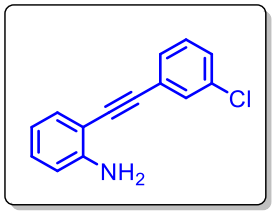

Brown solid (388 mg, 85% yield); ^{1}H NMR (500 MHz, $CDCl_3$) δ 7.50 (s, 1H), 7.39 (d, J = 7.3 Hz, 1H), 7.34 (d, J = 7.9 Hz, 1H), 7.31–7.28 (m, 1H), 7.27 (d, J = 7.6 Hz, 1H), 7.15 (td, J = 7.7, 1.6 Hz,1), 6.73–6.70 (m, 2H), 4.25 (s, 2H).; ^{13}C{^{1}H} NMR (126 MHz, $CDCl_3$) δ 148.1, 134.4, 132.4, 131.4, 130.3, 129.7, 129.6, 128.5, 125.2, 118.2, 114.6, 107.5, 93.4, 87.4.

***4-(Tert-butyl)-2-(phenylethynyl)aniline (1k)*:**

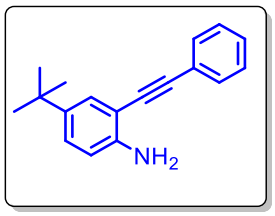

Light brown solid (438 mg, 88% yield); ^{1}H NMR (400 MHz, $CDCl_3$) δ 7.55–7.52 (m, 2H), 7.38 (d, J = 2 Hz, 1H), 7.34 (d, J = 6.4 Hz, 3H), 7.19 (dd, J = 8.4, 2.4 Hz, 1H), 6.69 (d, J = 8.4 Hz, 1H), 4.16 (s, 2H), 1.29 (s, 9H); ^{13}C{^{1}H} NMR (101 MHz, $CDCl_3$) δ 145.5, 141.0, 131.6, 128.8, 128.5, 128.3, 127.2, 123.6, 114.4, 107.6, 94.3, 86.6, 34.1, 31.5.

***4-Methyl-2-(phenylethynyl)aniline (1l)*:**

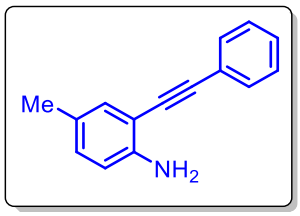

Brown solid (356mg, 86% yield); ^{1}H NMR (400 MHz, $CDCl_3$) δ 7.52 (dd, J = 7.5, 2.0 Hz, 2H), 7.35–7.33 (m, 3H), 7.19 (s, 1H), 6.96 (dd, J = 8.1, 1.6 Hz, 1H), 6.65 (d, J = 8.4 Hz, 1H), 4.14 (s, 2H), 2.23 (s, 3H); ^{13}C{^{1}H} NMR (101 MHz, $CDCl_3$) δ 145.6, 132.4, 131.6, 130.7, 128.5, 128.3, 127.4, 123.5, 114.7, 108.1, 94.5, 86.2, 20.4.

***2-(Phenylethynyl)-4-(trifluoromethyl)aniline (1m)*:**

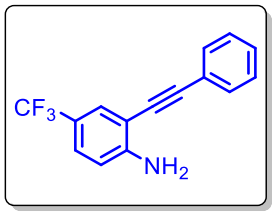

Light yellow solid (407 mg, 78% yield); ^{1}H NMR (600 MHz, $CDCl_3$) δ 7.63 (d, J = 1.1 Hz, 1H), 7.54–7.52 (m, 2H), 7.37–7.36 (m, 4H), 6.75 (d, J = 8.5 Hz, 1H), 4.58 (s, 2H); ^{13}C{^{1}H} NMR (151 MHz, $CDCl_3$) δ 150.3, 131.7, 129.7, 129.3, 128.8, 128.6, 126.7, 122.8, 113.8, 107.7, 95.8, 84.5; ^{19}F NMR (565 MHz, $CDCl_3$) δ –61.5.

***4-Chloro-2-(phenylethynyl)aniline (1n)*:**

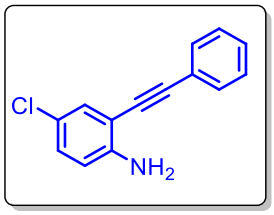

Light brown solid (345 mg, 76% yield); ^{1}H NMR (400 MHz, $CDCl_3$) δ 7.52 (q, J = 3.6 Hz, 2H), 7.37–7.33 (m, 4H), 7.09 (dd, J = 8.4, 2.4 Hz, 1H), 6.66 (d, J = 8.4 Hz, 1H), 4.28 (s, 2H); ^{13}C{^{1}H} NMR (101 MHz, $CDCl_3$) δ 146.5, 131.7, 131.5, 129.8, 128.7, 128.6, 122.9, 122.4, 115.6, 109.4, 95.7, 84.7.

***4-Bromo-2-(phenylethynyl)aniline (1o)*:**

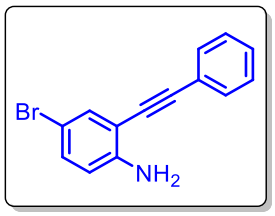

Light yellow solid (424 mg, 78% yield); ^{1}H NMR (400 MHz, $CDCl_3$) δ 7.53–7.5 (m, 2H), 7.48 (d, J = 2 Hz, 1H), 7.36–7.35 (m, 3H), 7.21 (dd, J = 8.8, 2.3 Hz, 1H), 6.61 (d, J = 8.7 Hz, 1H), 4.29 (s, 2H); ^{13}C{^{1}H} NMR (101 MHz, $CDCl_3$) δ 146.9, 134.3, 132.6, 131.6, 128.7, 128.6, 122.9, 115.9, 109.9, 109.1, 95.9, 84.6.

***4-Fluoro-2-(phenylethynyl)aniline (1q)*:**

Light yellow solid (333 mg, 79% yield); ^{1}H NMR (400 MHz, $CDCl_3$) δ 7.54–7.51 (m, 2H), 7.36–7.35 (m, 3H), 7.07 (dd, J = 9.2,

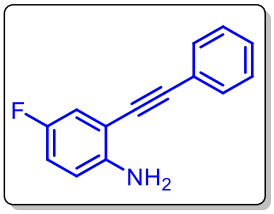

2.9 Hz, 1H), 6.88 (td, J = 8.5, 2.8 Hz, 1H), 6.66 (dd, J = 8.8, 4.8 Hz, 1H), 4.14 (s, 2H); $^{13}C\{^1H\}$ NMR (101 MHz, $CDCl_3$) δ 155.4 (d, J = 236.8 Hz), 144.3 (d, J = 1.9 Hz), 131.7, 128.7, 128.6, 125.3, 122.9, 117.9 (d, J = 23.6 Hz), 117.0 (d, J = 22.9 Hz), 115.4 (d, J = 8.1 Hz), 108.9 (d, J = 9.39 Hz), 85.1 (d, J = 3.14 Hz); ^{19}F NMR (377 MHz, $CDCl_3$) δ –126.9.

***5-Chloro-2-(phenylethynyl)aniline (1r)*:**

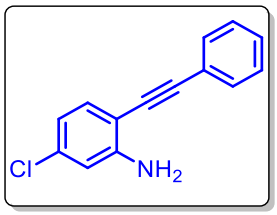

Light yellow solid (364 mg, 80% yield); ^1H NMR (400 MHz, $CDCl_3$) δ 7.53–7.50 (m, 2H), 7.35 (dd, J = 5.0, 1.9 Hz, 3H), 7.26 (d, J = 1.9 Hz, 1H), 6.72 (d, J = 1.9 Hz, 1H), 6.69 (dd, J = 8.6, 2.0 Hz, 1H), 4.34 (s, 2H); $^{13}C\{^1H\}$ NMR (151 MHz, $CDCl_3$) δ 148.8, 135.4, 133.2, 131.6, 128.6, 123.1, 118.3, 114.2, 106.6, 95.5, 85.0.

***4-Chloro-N-methyl-2-(phenylethynyl)aniline (1s)*:**

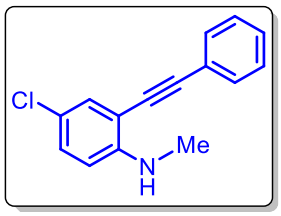

Orange liquid (392 mg, 81% yield); ^1H NMR (500 MHz, $CDCl_3$) δ 7.52–7.48 (m, 2H), 7.35–7.34 (m, 3H), 7.33–7.32 (m, 1H), 7.17 (d, J = 8.5 Hz, 1H), 6.51 (d, J = 8.8 Hz, 1H), 4.65 (s, 1H), 2.90 (d, J = 4.4 Hz, 3H); $^{13}C\{^1H\}$ NMR (126 MHz, $CDCl_3$) δ 148.6, 131.7, 131.5, 130.0, 128.6, 128.5, 123.0, 120.7, 110.2, 108.8, 95.9, 84.9, 30.6.

***2-Ethylbenzo[a]pyrrolo[3,4-c]carbazole-1,3(2H,8H)-dione (3aa)*:**

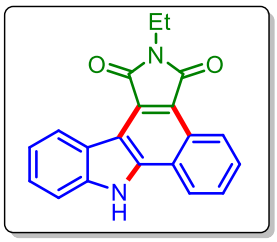

Yellow solid (83 mg, 75% yield); purified over column of silica gel (7% EtOAc in hexane); ^1H NMR (400 MHz, $CDCl_3$+DMSO-d_6 (4:1)) δ 12.56 (s, 1H), 9.22 (dd, J = 6.1, 3.2 Hz, 1H), 9.15 (d, J = 7.9 Hz, 1H), 8.76 (dd, J = 6.3, 3.2 Hz, 1H), 7.88–7.85 (m, 3H), 7.68 (t, J = 7.6 Hz, 1H), 7.52 (t, J = 7.5 Hz, 1H), 3.97 (q, J = 7.1 Hz, 2H), 1.52 (t, J = 7 Hz, 3H); $^{13}C\{^1H\}$ NMR (151 MHz, $CDCl_3$+DMSO-d_6 (4:1)) δ 169.4, 168.5, 139.9, 139.3, 127.0, 126.9, 126.4, 125.6, 125.5, 124.5, 123.6, 121.9, 121.8, 120.8, 119.8, 117.0, 111.6, 110.7, 31.5, 13.4; IR (neat, cm^{-1}) 3291, 1748, 1673, 1596, 1460, 1339, 1247, 1016, 815, 744; HRMS (–ESI) $[M–H]^-$ calcd for $C_{20}H_{13}N_2O_2^-$ 313.0983, found 313.0984.

***2-Ethyl-5-methylbenzo[a]pyrrolo[3,4-c]carbazole-1,3(2H,8H)-dione (3ba)*:**

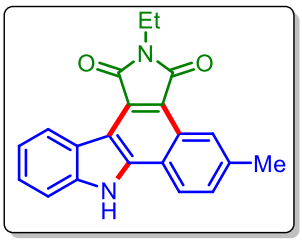

Yellow solid (82 mg, 73% yield); purified over column of silica gel (7% EtOAc in hexane); ^{1}H NMR (600 MHz, $CDCl_3$+DMSO-d_6 (4:1)) δ 12.37 (s, 1H), 9.04 (d, J = 7.8 Hz, 1H), 8.88 (s, 1H), 8.53 (d, J = 8.4 Hz, 1H), 7.74 (d, J = 7.8 Hz, 1H), 7.60–7.57 (m, 2H), 7.43 (t, J = 7.2 Hz, 1H), 3.88 (q, J = 7.2 Hz, 2H), 2.69 (s, 3H), 1.44 (t, J = 7.2 Hz, 3H); ^{13}C{^{1}H} NMR (151 MHz, $CDCl_3$+DMSO-d_6 (4:1)) δ 169.6, 168.7, 140.2, 139.3, 137.1, 128.6, 127.1, 125.9, 125.4, 123.60, 123.59, 121.7, 121.0, 120.2, 119.8, 116.5, 111.4, 110.7, 31.6, 21.2, 13.5; IR (neat, cm^{-1}) 3375, 2935, 1745, 1672, 1602, 1569, 1375, 1248, 810, 737; HRMS (–ESI) [M–H]$^-$ calcd for $C_{21}H_{15}N_2O_2^-$ 327.1139, found 327.1139.

***5-(Tert-butyl)-2-ethylbenzo[a]pyrrolo[3,4-c]carbazole-1,3(2H,8H)-dione (3ca)*:**

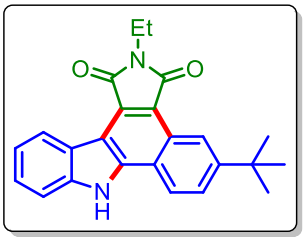

Yellow solid (97 mg, 75% yield); purified over column of silica gel (8% EtOAc in hexane); ^{1}H NMR (600 MHz, $CDCl_3$+DMSO-d_6 (4:1)) δ 12.52 (s, 1H), 9.25 (s, 1H), 9.14 (d, J = 7.9 Hz, 1H), 8.71 (d, J = 9 Hz, 1H), 7.97 (d, J = 8.4 Hz, 1H), 7.82 (d, J = 8.4 Hz, 1H), 7.67–7.64 (m, 1H), 7.51–7.48 (m, 1H), 3.97 (q, J =7.2, 2H), 1.64 (s, 9H), 1.51 (t, J = 7.2 Hz, 3H); ^{13}C{^{1}H} NMR (151 MHz, $CDCl_3$+DMSO-d_6 (4:1)) δ 169.9, 168.8, 150.2, 140.1, 139.4, 127.0, 126.0, 125.5, 125.4, 123.6, 121.7, 121.0, 120.2, 119.9, 119.7, 117.1, 111.5, 110.8, 34.4, 31.6, 30.4, 13.5; IR (neat, cm^{-1}) 3468, 2958, 1752, 1689, 1602, 1456, 1368, 1250, 1014, 821, 746; HRMS (–ESI) [M–H]$^-$ calcd for $C_{24}H_{21}N_2O_2^-$ 369.1609, found 369.1626.

***2-Ethyl-5-fluorobenzo[a]pyrrolo[3,4-c]carbazole-1,3(2H,8H)-dione (3da)*:**

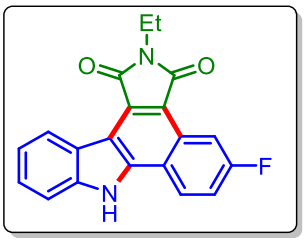

Yellow solid (60 mg, 52% yield); purified over column of silica gel (12% EtOAc in hexane); ^{1}H NMR (600 MHz, DMSO-d_6) δ 12.62 (s, 1H), 8.61 (d, J = 7.9 Hz, 1H), 8.38 (dd, J = 9.1, 6 Hz, 1H), 8.20 (dd, J = 10.2, 2.4 Hz, 1H), 7.52 (d, J = 7.8 Hz, 1H), 7.47 (td, J = 8.4, 2.4 Hz, 1H), 7.45–7.41 (m, 1H), 7.23 (t, J = 7.8 Hz, 1H), 3.45 (q, J = 7.2 Hz, 2H), 1.12 (t, J = 7.2 Hz, 3H); ^{13}C{^{1}H} NMR (101 MHz, DMSO-d_6) δ 169.3, 168.3, 161.3 (d, J = 247.4 Hz), 140.3, 139.8, 128.2, 126.6,

125.6 (d, J = 9.5 Hz), 123.9, 120.9, 120.8, 119.2, 117.2 (d, J = 25.6 Hz), 116.4 (d, J = 5.4 Hz) 111.7, 111.6, 108.2 (d, J = 22.9 Hz), 32.1, 13.9; ^{19}F NMR (565 MHz, DMSO-d$_6$) δ –110.6; IR (neat, cm^{-1}) 3607, 3365, 1745, 1678, 1604, 1563, 1459, 1343, 1197, 814, 743; HRMS (–ESI) [M–H]$^-$ calcd for $C_{20}H_{12}FN_2O_2^-$ 331.0888, found 331.0889.

***5-Chloro-2-ethylbenzo[a]pyrrolo[3,4-c]carbazole-1,3(2H,8H)-dione (3ea)*:**

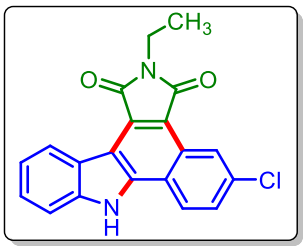

Yellow solid (82 mg, 67% yield); purified over column of silica gel (7% EtOAc in hexane); ^{1}H NMR (500 MHz, DMSO-d$_6$) δ 12.79 (s, 1H), 8.74 (d, J = 8.0 Hz, 1H), 8.72–8.71 (m, 1H), 8.48 (d, J = 9.0 Hz, 1H), 7.69 (d, J = 9.0 Hz, 1H), 7.63 (d, J = 8.0 Hz, 1H), 7.52 (t, J = 7.6 Hz, 1H), 7.32 (t, J = 7.5 Hz, 1H), 3.58 (q, J = 7.2 Hz, 2H), 1.20 (t, J = 7.2 Hz, 3H). ^{13}C{^{1}H} NMR (126 MHz, DMSO-d$_6$) δ 169.2, 168.3, 140.0, 139.9, 133.0, 128.3, 127.7, 126.8, 126.2, 124.7, 123.9, 123.2, 120.9, 120.4, 116.2, 112.2, 111.8, 32.1, 13.8. IR (neat, cm^{-1}) 3611, 2939, 1745, 1675, 1455, 1372, 1223, 1029, 826, 745. HRMS (–ESI) [M–H]$^-$ calcd for $C_{20}H_{12}ClN_2O_2^-$ 347.0593, found 347.0584.

***5-Bromo-2-ethylbenzo[a]pyrrolo[3,4-c]carbazole-1,3(2H,8H)-dione (3fa)*:**

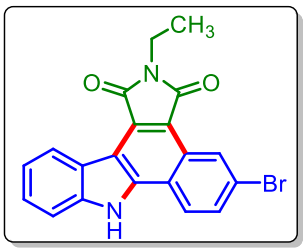

Yellow solid (95 mg, 69% yield); purified over column of silica gel (7% EtOAc in hexane); ^{1}H NMR (500 MHz, DMSO-d$_6$) δ 12.95 (s, 1H), 9.04 (d, J = 2.0 Hz, 1H), 8.85 (d, J = 8.0 Hz, 1H), 8.55 (d, J = 9.0 Hz, 1H), 7.92 (dd, J = 9.0, 2.0 Hz, 1H), 7.71 (d, J = 8.0 Hz, 1H), 7.57 (t, J = 7.7 Hz, 1H), 7.38 (t, J = 7.5 Hz, 1H), 3.67 (q, J = 7.2 Hz, 2H), 1.25 (t, J = 7.0 Hz, 3H). ^{13}C{^{1}H} NMR (151 MHz, DMSO-d$_6$) δ 169.4, 168.5, 140.2, 140, 130.4, 128.4, 126.9, 126.7, 126.6, 124.9, 124.0, 121.9, 121.0, 120.9, 120.8, 116.3, 112.3, 111.9, 30.7, 13.9. IR (neat, cm^{-1}) 3319, 1741, 1688, 1451, 1378, 1149, 1015, 779. HRMS (–ESI) [M–H]$^-$ calcd for $C_{20}H_{12}BrN_2O_2^-$ 391.0088, found 391.0097.

***2-Ethyl-6-methylbenzo[a]pyrrolo[3,4-c]carbazole-1,3(2H,8H)-dione (3ga)*:**

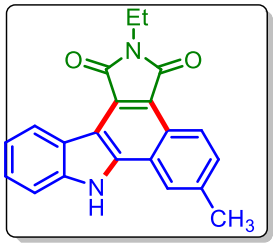

Yellow solid (79 mg, 69% yield); purified over column of silica gel (8% EtOAc in hexane); ^{1}H NMR (400 MHz, DMSO-d$_6$) δ 12.81 (s, 1H), 8.82 (t, J = 8.8 Hz, 2H), 8.40 (s, 1H), 7.67 (d, J = 8.4 Hz, 1H), 7.60 (d, J = 8.5 Hz, 1H), 7.49 (t, J = 7.6 Hz, 1H), 7.31 (t, J = 7.5 Hz,

1H), 3.64 (q, J = 6.9 Hz, 2H), 2.55 (s, 3H), 1.20 (t, J = 7.2 Hz, 3H); $^{13}C\{^1H\}$ NMR (151 MHz, $CDCl_3$+DMSO-d_6 (4:1)) δ 170.6, 169.6, 140.3, 139.9, 137.3, 129.8, 127.0, 126.1, 124.6, 124.5, 123.0, 121.8, 121.6, 120.6, 120.4, 118.2, 112.7, 111.2, 32.3, 22.1, 14.1; IR (neat, cm^{-1}) 3369, 1741, 1673, 1603, 1446, 1374, 1240, 821, 740. HRMS (–ESI) $[M–H]^-$ calcd for $C_{21}H_{15}N_2O_2^-$ 327.1139, found 327.1159.

***2-Ethyl-6-fluorobenzo[a]pyrrolo[3,4-c]carbazole-1,3(2H,8H)-dione (3ha)*:**

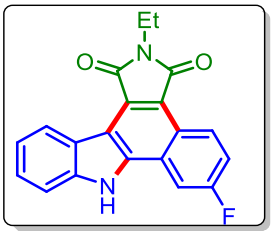

Yellow solid (74 mg, 64% yield); purified over column of silica gel (13% EtOAc in hexane); ^1H NMR (400 MHz, $CDCl_3$+DMSO-d_6 (4:1)) δ 12.64 (s, 1H), 9.61–9.57 (m, 1H), 9.49 (d, J = 7.9 Hz, 1H), 8.8–8.77 (m, 1H), 8.14 (d, J = 8.5 Hz, 1H), 8.03 (d, J = 8.0 Hz, 1H), 7.96–7.92 (m, 1H), 7.87 (t, J = 7.5 Hz, 1H), 4.32 (q, J =7.2 Hz, 2H), 1.87 (t, J = 7.0 Hz, 3H); $^{13}C\{^1H\}$ NMR (151 MHz, $CDCl_3$+DMSO-d_6 (4:1)) δ 170.1, 169.2, 161.1 (d, J = 249.1 Hz), 139.94, 139.91, 128.1, 126.9, 126.3, 124.5, 123.9, 123.1, 121.4, 120.6, 118.0, 117.3 (d, J = 24.5 Hz),112.9, 111.2, 106.8 (d, J = 22.5 Hz), 32.3, 14.0; ^{19}F NMR (377 MHz, $CDCl_3$+DMSO-d_6 (4:1)) δ –110.6; IR (neat, cm^{-1}) 3166, 3422, 1750, 1693, 1464, 1347, 1204, 1004, 824, 739. HRMS (–ESI) $[M–H]^-$ calcd for $C_{20}H_{12}FN_2O_2^-$ 331.0888, found 331.0889.

***6-Chloro-2-ethylbenzo[a]pyrrolo[3,4-c]carbazole-1,3(2H,8H)-dione (3ia)*:**

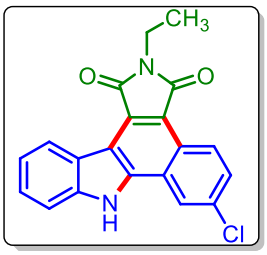

Yellow solid (81 mg, 66% yield); purified over column of silica gel (7% EtOAc in hexane); ^1H NMR (500 MHz, DMSO-d_6) δ 12.76 (s, 1H), 8.80 (d, J = 9.0 Hz, 1H), 8.77 (d, J = 8.0 Hz, 1H), 8.60 (s, 1H), 7.70 (dd, J = 9.0, 2.0 Hz, 1H), 7.63 (d, J = 8.0 Hz, 1H), 7.52 (t, J = 7.5 Hz, 1H), 7.33 (t, J = 7.5 Hz, 1H), 3.61 (q, J = 7.3 Hz, 2H), 1.22 (t, J = 7.2 Hz, 3H). $^{13}C\{^1H\}$ NMR (126 MHz, DMSO-d_6) δ 169.3, 168.5, 139.8, 139.1, 132.4, 128.4, 127.6, 126.8, 126.7, 123.9, 123.9, 123.0, 121.8, 120.8, 117.3, 112.5, 111.8, 32.1, 13.9. IR (neat, cm^{-1}) 3609, 2951, 1750, 1688, 1466, 1379, 1230, 1025, 828, 758. HRMS (–ESI) $[M–H]^-$ calcd for $C_{20}H_{12}ClN_2O_2^-$ 347.0593, found 347.0588.

***5-Ethylpyrrolo[3,4-c]thieno[2,3-a]carbazole-4,6(5H,11H)-dione (3ja)*:**

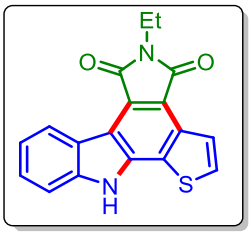

Yellow solid (73 mg, 66% yield); purified over column of silica gel (9% EtOAc in hexane); ^{1}H NMR (600 MHz, DMSO-d_6) δ 12.44 (s, 1H), 8.70–8.65 (m, 1H), 7.98–7.93 (m, 1H), 7.83–7.77 (m, 1H), 7.48–7.45 (m, 1H), 7.41–7.38 (m, 1H), 7.19–7.17 (m, 1H), 3.50 (q, J = 7.2 Hz, 2H), 1.11 (t, J = 7.0 Hz, 3H); ^{13}C{^{1}H} NMR (151 MHz, DMSO-d_6) δ 168.9, 168.6, 140.6, 138.2, 132.5, 131.3, 127.1, 126.9, 124.4, 124.2, 121.6, 120.8, 120.5, 116.9, 113.2, 111.6, 32.1, 14.0; IR (neat, cm^{-1}) 3604, 2949, 1741, 1685, 1456, 1370, 1225, 1021, 820, 755. HRMS (–ESI) [M–H]$^-$ calcd for $C_{18}H_{11}N_2O_2S^-$ 319.0547, found 319.0551.

***11-(Tert-butyl)-2-ethylbenzo[a]pyrrolo[3,4-c]carbazole-1,3(2H,8H)-dione (3ka)*:**

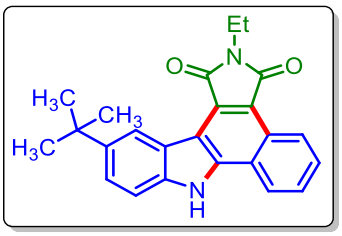

Yellow solid (95 mg, 73% yield); purified over column of silica gel (7% EtOAc in hexane); ^{1}H NMR (600 MHz, $CDCl_3$+DMSO-d_6 (4:1)) δ 12.50 (s, 1H), 9.72–9.65 (m, 2H), 9.11 (s, 1H), 8.25–8.24 (m, 2H), 8.20–8.18 (m, 2H), 4.4 (q, J = 7.2 Hz, 2H), 2.09 (s, 9H), 1.93 (t, J = 7.8 Hz, 3H); ^{13}C{^{1}H} NMR (151 MHz, $CDCl_3$+DMSO-d_6 (4:1)) δ 170.5, 169.6, 143.8, 141.0, 138.1, 127.9, 127.5, 127.0, 126.4, 125.4, 124.3, 122.7, 122.3, 121.6, 120.5, 117.7, 113.0, 110.7, 34.7, 32.3, 31.8, 14.2; IR (neat, cm^{-1}) 3341, 1743, 1679, 1592, 1372, 1295, 1147, 1020, 815, 773. HRMS (–ESI) [M–H]$^-$ calcd for $C_{24}H_{21}N_2O_2^-$ 369.1609, found 369.1610.

***2-Ethyl-11-methylbenzo[a]pyrrolo[3,4-c]carbazole-1,3(2H,8H)-dione (3la)*:**

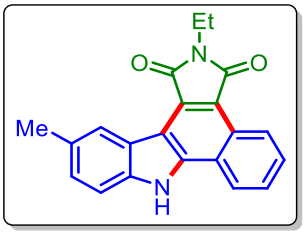

Yellow solid (85 mg, 68%); purified over column of silica gel (7% EtOAc in hexane); ^{1}H NMR (600 MHz, DMSO-d_6) δ 12.69 (s, 1H), 8.83 (dd, J = 7.0, 2.2 Hz, 1H), 8.55 (s, 1H), 8.51–8.49 (m, 1H), 7.69–7.67 (m, 2H), 7.49 (d, J = 8.4 Hz, 1H), 7.27 (d, J = 7.8 Hz, 1H), 3.58 (q, J = 7.1 Hz, 2H), 2.43 (s, 3H), 1.16 (t, J = 7.2 Hz, 3H); ^{13}C{^{1}H} NMR (151 MHz, DMSO-d_6) δ 169.8, 168.9, 140.5, 138.2, 129.6, 128.2, 128.0, 127.6, 125.9, 124.8, 123.6, 122.8, 122.4, 121.4, 117.2, 111.7, 111.5, 32.1, 21.4, 14.0; IR (neat, cm^{-1}) 3328, 2922, 1745, 1674,

1596, 1376, 1178, 939, 773; HRMS (–ESI) $[M–H]^-$ calcd for $C_{21}H_{15}N_2O_2^-$ 327.1139, found 327.1140.

***2-Ethyl-11-(trifluoromethyl)benzo[a]pyrrolo[3,4-c]carbazole-1,3(2H,8H)-dione (3ma)*:**

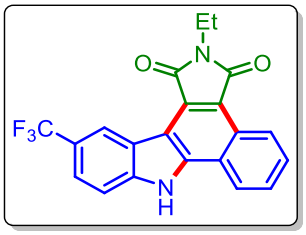

Yellow solid (90 mg, 68% yield); purified over column of silica gel (14% EtOAc in hexane); ^{1}H NMR (600 MHz, DMSO-d_6) δ 13.00 (s, 1H), 8.94 (s, 1H), 8.71–8.69 (m, 1H), 8.40–8.37 (m, 1H), 7.68–7.66 (m, 4H), 3.53 (q, J = 7.2 Hz, 2H), 1.16 (t, J = 7.2 Hz, 3H); ^{13}C{^{1}H} NMR (151 MHz, DMSO-d_6) δ 169.4, 168.6, 141.4, 141.0, 128.6, 127.9, 127.2, 126.1, 125.9, 124.7, 124.4, 122.7, 122.6, 122.4, 121.2, 121.1 (dd, J = 10.7, 6.1 Hz) , 120.5, 118.4, 112.5, 111.2, 32.2, 13.9; ^{19}F NMR (565 MHz, DMSO-d_6) δ –58.7; IR (neat, cm^{-1}) 3362, 2922, 1755, 1676, 1597, 1332, 1283, 1104, 1059, 921, 645, 566; HRMS (–ESI) $[M–H]^-$ calcd for $C_{21}H_{12}F_3N_2O_2^-$ 381.0856, found 381.0855.

***11-Chloro-2-ethylbenzo[a]pyrrolo[3,4-c]carbazole-1,3(2H,8H)-dione (3na)*:**

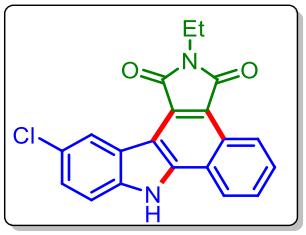

Yellow solid (85 mg, 70% yield); purified over column of silica gel (10% EtOAc in hexane); ^{1}H NMR (400 MHz, $CDCl_3$+DMSO-d_6 (4:1)) δ 12.55 (s, 1H), 9.26 (d, J = 7.6 Hz, 1H), 9.14 (s, 1H), 8.73 (d, J = 7.2 Hz, 1H), 7.97–7.96 (m, 2H), 7.85–7.79 (m, 1H), 7.68 (d, J = 8.5 Hz, 1H), 4.04 (q, J = 6.8 Hz, 2H), 1.63 (t, J = 6.7 Hz, 3H); ^{13}C{^{1}H} NMR (101 MHz, $CDCl_3$+DMSO-d_6 (4:1)) δ 169.6, 168.7, 140.7, 137.9, 127.5, 127.2, 126.9, 126.0, 125.7, 125.2, 124.9, 123.2, 122.3, 122.2, 122.1, 117.8, 112.0, 111.1, 31.9, 13.7; IR (neat, cm^{-1}) 3321, 2283, 1682, 1456, 1282, 1075, 773; HRMS (–ESI) $[M–H]^-$ calcd for $C_{20}H_{12}ClN_2O_2^-$ 347.0593, found 347.0576.

***11-Bromo-2-ethylbenzo[a]pyrrolo[3,4-c]carbazole-1,3(2H,8H)-dione (3oa)*:**

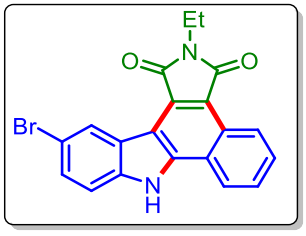

Yellow solid (99 mg, 72% yield); purified over column of silica gel (8% EtOAc in hexane); ^{1}H NMR (600 MHz, DMSO-d_6) δ 12.85 (s, 1H), 8.78 (s, 1H), 8.75 (d, J = 6.0 Hz, 1H), 8.42 (d, J = 4.7 Hz, 1H), 7.69–7.67 (m, 2H), 7.52 (q, J = 8.0 Hz, 2H), 3.54 (q, J = 7.0 Hz, 2H), 1.15 (t, J = 7.2 Hz, 3H); ^{13}C{^{1}H} NMR (151 MHz, DMSO-d_6) δ 169.5, 168.8, 140.7, 138.5, 128.87, 128.86, 128.6, 127.95, 127.93, 126.02, 126.01, 125.9, 124.8, 122.8, 122.4, 113.8, 112.8, 110.7, 32.2,

13.9; IR (neat, cm^{-1}) 3313, 1747, 1681, 1453, 1374, 1141, 1018, 773; HRMS (–ESI) $[M–H]^-$ calcd for $C_{20}H_{12}BrN_2O_2^-$ 391.0088, found 391.0104.

***2-Benzyl-5-methylbenzo[a]pyrrolo[3,4-c]carbazole-1,3(2H,8H)-dione (3bb)*:**

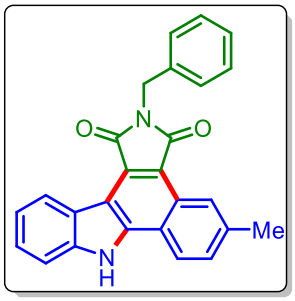

Yellow solid (88 mg, 64% yield); purified over column of silica gel (7% EtOAc in hexane); ^1H NMR (600 MHz, DMSO-d_6): δ 12.80 (s, 1H), 8.78 (d, J = 7.9 Hz, 1H), 8.64 (s, 1H), 8.45 (d, J = 8.5 Hz, 1H), 7.64 (d, J = 7.8 Hz, 1H), 7.56–7.55 (m, 1H), 7.48 (t, J = 7.6 Hz, 1H), 7.32 (d, J = 7.8 Hz, 2H), 7.28 (q, J = 7.6 Hz, 3H), 7.20 (t, J = 7.3 Hz, 1H), 4.75 (s, 2H), 2.48 (s, 3H); $^{13}C\{^1H\}$ NMR (151 MHz, $CDCl_3$+DMSO-d_6 (4:1)) δ 169.6, 168.6, 140.5, 139.5, 137.3, 136.6, 128.8, 127.9, 127.5, 127.4, 127.0, 126.8, 126.2, 125.6, 123.8, 121.8, 121.1, 120.3, 120.0, 116.5, 111.6, 110.8, 40.4, 21.4; IR (neat, cm^{-1}) 3490, 1698, 1431, 1342, 1241, 1062, 750, 703, 627; HRMS (–ESI) $[M–H]^-$ calcd for $C_{26}H_{17}N_2O_2^-$ 389.1296, found 389.1296.

***2-Benzyl-5-methoxybenzo[a]pyrrolo[3,4-c]carbazole-1,3(2H,8H)-dione (3pb)*:**

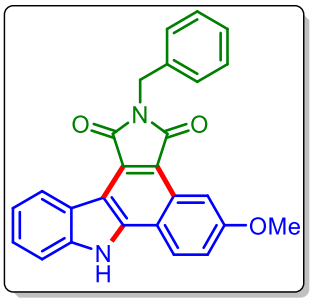

Yellow solid (87 mg, 61% yield); purified over column of silica gel (14% EtOAc in hexane); ^1H NMR (500 MHz, DMSO-d_6) δ 12.77 (s, 1H), 8.83 (d, J = 7.9 Hz, 1H), 8.56 (d, J = 9.2 Hz, 1H), 8.32 (s, 1H), 7.68 (d, J = 8.1 Hz, 1H), 7.52 (t, J = 7.6 Hz, 1H), 7.45 (dd, J = 9.2, 2.7 Hz, 1H), 7.39 (d, J = 7.7 Hz, 2H), 7.33 (t, J = 7.5 Hz, 2H), 7.30–7.23 (m, 2H), 4.83 (s, 2H), 3.94 (s, 3H); $^{13}C\{^1H\}$ NMR (151 MHz, DMSO-d_6) δ 169.8, 168.8, 159.3, 141.2, 140.1, 137.3, 128.6, 128.3, 127.9, 127.5, 127.4, 126.5, 124.6, 123.8, 121.2, 120.7, 119.8, 117.5, 115.9, 111.7, 111.2, 103.6, 55.3, 40.6; IR (neat, cm^{-1}) 3427, 1744, 1684, 1624, 1432, 1340, 1217, 915, 816, 736; HRMS (–ESI) $[M–H]^-$ calcd for $C_{26}H_{17}N_2O_3^-$ 405.1245, found 405.1259.

***2-Benzyl-11-fluorobenzo[a]pyrrolo[3,4-c]carbazole-1,3(2H,8H)-dione (3qb)*:**

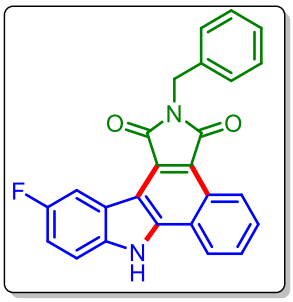

Yellow solid (94 mg, 68% yield); purified over column of silica gel (10% EtOAc in hexane); ^{1}H NMR (600 MHz, DMSO-d$_6$) δ 12.79 (s, 1H), 8.78–8.77 (m, 1H), 8.45–8.44 (m, 1H), 8.34 (dd, J = 9.6, 3 Hz, 1H), 7.68 (dd, J = 6.4, 3.3 Hz, 2H), 7.57 (dd, J = 9, 4.2 Hz, 1H), 7.33 (d, J = 7.2 Hz, 2H), 7.3 (d, J = 7.2 Hz, 2H) , 7.28 (s, 1H), 7.21 (t, J = 7.2 Hz, 1H), 4.72 (s, 2H); ^{13}C{^{1}H} NMR (151 MHz, DMSO-d$_6$) δ 169.4, 168.7, 157.2 (d, J = 234.4 Hz), 141.3, 137.1, 136.3, 128.6, 128.4, 127.8, 127.4, 127.3, 127.3, 125.9, 124.7, 122.6 (d, J = 31.3 Hz), 121.3 (d, J = 8.7 Hz), 117.3, 114.5 (d, J = 25.7 Hz), 112.9 (d, J = 9.4 Hz), 111.4 (d, J = 4.1 Hz), 108.6 (d, J = 25.1 Hz), 40.6; ^{19}F NMR (565 MHz, DMSO-d$_6$) δ –122.1; IR (neat, cm^{-1}) 3449, 2960, 1749, 1692, 1630, 1382, 1172, 929, 754, 694; HRMS (–ESI) [M–H]$^-$ calcd for $C_{25}H_{14}FN_2O_2^-$ 393.1045, found 393.1041.

***2-Benzyl-11-chlorobenzo[a]pyrrolo[3,4-c]carbazole-1,3(2H,8H)-dione (3nb)*:**

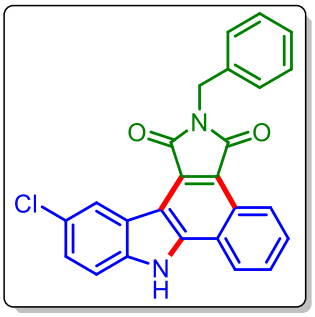

Yellow solid (95 mg, 66% yield); purified over column of silica gel (9% EtOAc in hexane); ^{1}H NMR (600 MHz, DMSO-d$_6$) δ 12.96 (s, 1H), 8.83–8.80 (m, 1H), 8.68 (s, 1H), 8.50–8.48 (m, 1H), 7.73 –7.71 (m, 2H), 7.61 (d, J = 9.0 Hz, 1H), 7.45 (dd, J = 8.4, 1.8 Hz, 1H), 7.32 (d, J = 7.2 Hz, 2H), 7.27 (t, J = 7.6 Hz, 2H), 7.20 (t, J = 7.3 Hz, 1H), 4.74 (s, 2H); ^{13}C{^{1}H} NMR (151 MHz, DMSO-d$_6$) δ 169.5, 168.8, 141.1, 138.3, 137.2, 137.1, 128.7, 128.6, 128.1, 127.5, 127.4, 126.4, 126.1, 124.9, 124.8, 122.8, 122.6, 122.2, 117.9, 113.5, 110.9, 40.7; IR (neat, cm^{-1}) 3400, 1752, 1692, 1597, 1459, 1376, 1283, 1059, 756, 699; HRMS (–ESI) [M–H]$^-$ calcd for $C_{25}H_{14}ClN_2O_2^-$ 409.0749, found 409.0741.

***2-Benzyl-10-chlorobenzo[a]pyrrolo[3,4-c]carbazole-1,3(2H,8H)-dione (3rb)*:**

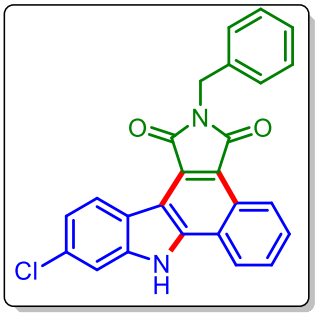

Yellow solid (102 mg, 71% yield); purified over column of silica gel (9% EtOAc in hexane); ^{1}H NMR (600 MHz, DMSO-d_6) δ 12.78 (s, 1H), 8.77 (s, 1H), 8.61 (d, J = 8.4 Hz, 1H), 8.40 (d, J = 7.8 Hz, 1H), 7.68–7.66 (m, 2H), 7.52–7.50 (m, 1H), 7.33 (d, J = 7.2 Hz, 2H), 7.29 (t, J = 7.8 Hz, 2H), 7.25–7.20 (m, 2H), 4.72 (s, 2H); ^{13}C{^{1}H} NMR (151 MHz, DMSO-d_6) δ 169.3, 168.5, 140.7, 140.3, 137.1, 130.9, 128.6, 128.4, 127.8, 127.5, 127.3, 126.9, 125.8, 124.9, 124.7, 122.6, 122.3, 120.9, 119.8, 117.8, 111.3, 111.2, 40.6; IR (neat, cm^{-1}) 3411, 1748, 1685, 1561, 1377, 1224, 1061, 757, 627; HRMS (–ESI) [M–H]$^{-}$ calcd for $C_{25}H_{14}ClN_2O_2^{-}$ 409.0749, found 409.0752.

***11-Chloro-2-ethyl-8-methylbenzo[a]pyrrolo[3,4-c]carbazole-1,3(2H,8H)-dione (3sa)*:**

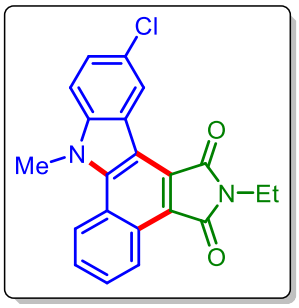

Yellow solid (84 mg, 66% yield); purified over column of silica gel (6% EtOAc in hexane); ^{1}H NMR (500 MHz, $CDCl_3$) δ 9.25 (d, J = 8 Hz, 1H), 9.19 (s, 1H), 8.70 (d, J = 8 Hz, 1H), 7.77–7.70 (m, 2H), 7.54 (dd, J = 8.8, 2.2 Hz, 1H), 7.45 (d, J = 8.5 Hz, 1H), 4.36 (s, 4H), 3.82 (q, J = 7.2 Hz, 2H), 1.37 (t, J = 7.2 Hz, 4H); ^{13}C{^{1}H} NMR (126 MHz, $CDCl_3$) δ 170.2, 169.3, 140.7, 140.3, 128.2, 127.9, 127.8, 127.6, 127.2, 126.9, 126.5, 124.8, 124.1, 122.8, 122.2, 119.5, 113.2, 110.3, 34.9, 32.9, 14.4. IR (neat, cm^{-1}) 2987, 1754, 1696, 1473, 1450, 1407, 1374, 1352, 1284, 885, 776; HRMS (+ESI) [M+H]$^{+}$ calcd for $C_{21}H_{16}ClN_2O_2^{+}$ 363.0895, found 363.0886.

***2-Benzylbenzo[a]pyrrolo[3,4-c]carbazole-1,3(2H,8H)-dione (3ab)*:**

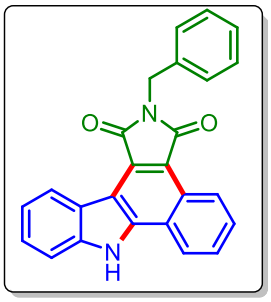

Yellow solid (78 mg, 60% yield); purified over column of silica gel (7% EtOAc in hexane); ^{1}H NMR (400 MHz, DMSO-d_6) δ 12.94 (s, 1H), 8.92 (dd, J = 6.5, 2.8 Hz, 1H), 8.84 (d, J = 7.9 Hz, 1H), 8.64–8.61 (m, 1H), 7.79–7.76 (m, 2H), 7.69 (d, J = 8.1 Hz, 1H), 7.52 (t, J = 7.6 Hz, 1H), 7.36 (d, J = 7.6 Hz, 2H), 7.33–7.27 (m, 3H), 7.23 (d, J = 7.2 Hz, 1H), 4.81 (s, 2H); ^{13}C{^{1}H} NMR (151 MHz, DMSO-d_6) δ 169.7, 168.9, 140.6, 139.9, 137.2, 128.6, 128.4, 127.9, 127.5, 127.4, 127.4, 126.7, 125.9, 124.8, 123.9, 122.8, 122.5, 121.2, 120.8, 117.4, 111.9, 111.9, 40.7; IR (neat, cm^{-1}) 3335, 2925, 1747, 1680, 1598, 1461,

1429, 1378, 1341, 1243, 933, 740; HRMS (–ESI) $[M–H]^-$ calcd for $C_{25}H_{15}N_2O_2^-$ 375.1139, found 375.1159.

***2-(4-Methoxybenzyl)benzo[a]pyrrolo[3,4-c]carbazole-1,3(2H,8H)-dione (3ac)*:**

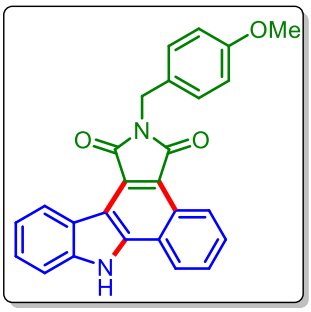

Yellow solid (89 mg, 63% yield); purified over column of silica gel (13% EtOAc in hexane); ^{1}H NMR (600 MHz, DMSO-d_6) δ 12.82 (s, 1H), 8.83 (dd, J = 6.3, 2.1 Hz, 1H), 8.76 (d, J = 7.9 Hz, 1H), 8.53–8.51 (m, 1H), 7.69–7.67 (m, 2H), 7.62 (d, J = 7.8 Hz, 1H), 7.46 (t, J = 7.6 Hz, 1H), 7.28 (t, J = 7.5 Hz, 1H), 7.25 (d, J = 8.4 Hz, 2H), 6.81 (d, J = 9.0 Hz, 2H), 4.65 (s, 2H), 3.61 (s, 3H); ^{13}C{^{1}H} NMR (151 MHz, DMSO-d_6) δ 169.6, 168.8, 158.6, 140.5, 139.9, 129.2, 129.1, 128.3, 127.8, 127.5, 126.6, 125.9, 124.8, 123.9, 122.8, 122.5, 121.1, 120.8, 117.3, 113.9, 111.9, 111.8, 55.1, 40.1; IR (neat, cm^{-1}) 3338, 2859, 1747, 1688, 1599, 1462, 1237, 1022, 743, 623; HRMS (–ESI) $[M–H]^-$ calcd for $C_{26}H_{17}N_2O_3^-$ 405.1245, found 405.1262.

***2-Methylbenzo[a]pyrrolo[3,4-c]carbazole-1,3(2H,8H)-dione (3ad)*:**

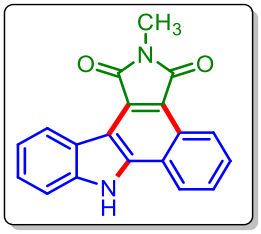

Yellow solid (76 mg, 72% yield); purified over column of silica gel (7% EtOAc in hexane); ^{1}H NMR (500 MHz, DMSO-d_6) δ 12.78 (s, 1H), 8.84 (d, J = 7.6 Hz, 1H), 8.78 (d, J = 8.0 Hz, 1H), 8.53 (d, J = 7.6 Hz, 1H), 7.71–7.69 (m, 2H), 7.65 (d, J = 8.1 Hz, 1H), 7.49 (t, J = 7.8 Hz, 1H), 7.30 (t, J = 7.6 Hz, 1H), 3.02 (s, 3H); ^{13}C{^{1}H} NMR (151 MHz, $CDCl_3$+DMSO-d_6 (4:1)) δ 169.2, 168.3, 139.6, 139.0, 126.73, 126.70, 126.2, 125.2, 124.1, 124.0, 123.2, 121.6, 120.5, 119.6, 116.8, 111.3, 110.5, 110.4, 22.4; IR (neat, cm^{-1}) 3324, 1749, 1685, 1597, 1433, 1374, 1147, 985, 836, 734; HRMS (–ESI) $[M–H]^-$ calcd for $C_{19}H_{11}N_2O_2^-$ 299.0826, found 299.0827.

***2-Propylbenzo[a]pyrrolo[3,4-c]carbazole-1,3(2H,8H)-dione (3ae)*:**

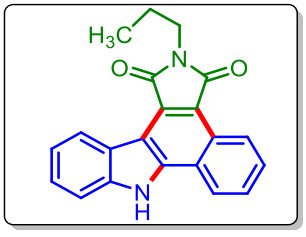

Yellow solid (85 mg, 74% yield); purified over column of silica gel (7% EtOAc in hexane); ^{1}H NMR (400 MHz, DMSO-d_6) δ 12.87 (s, 1H), 8.89 (dd, J = 6.2, 3 Hz, 1H), 8.82 (d, J = 7.9 Hz, 1H), 8.58 (dd, J = 6.2, 3.0 Hz, 1H), 7.75–7.72 (m, 2H), 7.66 (d, J = 8.1 Hz, 1H),

7.49 (t, J = 7.6 Hz, 1H), 7.31 (t, J = 7.5 Hz, 1H), 3.55 (t, J = 7.0 Hz, 2H), 1.63 (m, 2H), 0.86 (t, J = 7.4 Hz, 3H); $^{13}C\{^1H\}$ NMR (151 MHz, $CDCl_3$+DMSO-d_6 (4:1)) δ 169.8, 168.9, 140.1, 139.4, 127.0, 126.9, 126.5, 125.7, 125.6, 124.6, 123.7, 122.1, 121.9, 120.9, 119.9, 117.0, 111.8, 110.8, 38.4, 21.3, 10.7; IR (neat, cm^{-1}) 3327, 1752, 1673, 1370, 749, 596; HRMS (–ESI) $[M–H]^-$ calcd for $C_{21}H_{15}N_2O_2^-$ 327.1139, found 327.1136.

***2-Isobutylbenzo[a]pyrrolo[3,4-c]carbazole-1,3(2H,8H)-dione (3af)*:**

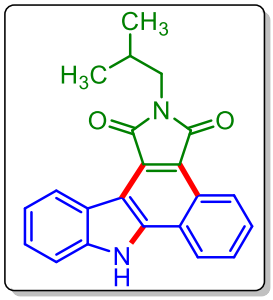

Yellow solid (88 mg, 73% yield); purified over column of silica gel (7% EtOAc in hexane); ^1H NMR (400 MHz, DMSO-d_6) δ 12.73 (s, 1H), 8.75 (d, J = 6.8 Hz, 1H), 8.70 (d, J = 8.0 Hz, 1H), 8.44 (d, J = 8.7 Hz, 1H), 7.62–7.60 (m, 2H), 7.59–7.55 (m, 1H), 7.41 (t, J = 7.5 Hz, 1H), 7.21 (t, J = 7.3 Hz, 1H), 3.29 (2H, merged with moisture peak of DMSO-d_6), 1.96–1.91 (m, 1H), 0.79 (d, J = 6.1 Hz, 6H); ^{13}C $\{^1H\}$ NMR (151 MHz, DMSO-d_6) δ 170.2, 169.3, 140.4, 139.9, 128.2, 127.7, 127.4, 126.6, 125.9, 124.8, 124.0, 122.8, 122.5, 121.2, 120.8, 117.2, 111.9, 111.9, 44.6, 27.7, 20.1; IR (neat, cm^{-1}) 3604, 3215, 2957, 1746, 1680, 1461, 1382, 1339, 1247, 1044, 744, 627; HRMS (–ESI) $[M–H]^-$ calcd for $C_{22}H_{17}N_2O_2^-$ 341.1296, found 341.1313.

***2-Cyclohexylbenzo[a]pyrrolo[3,4-c]carbazole-1,3(2H,8H)-dione (3ag)*:**

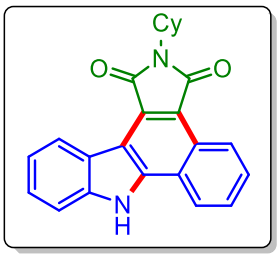

Yellow solid (90 mg, 70% yield); purified over column of silica gel (7% EtOAc in hexane); ^1H NMR (600 MHz, $CDCl_3$+DMSO-d_6 (4:1)) δ 12.54 (s, 1H), 9.20–9.19 (m, 1H), 9.12 (d, J = 7.9 Hz, 1H), 8.73–8.72 (m, 1H), 7.83–7.82 (m, 2H), 7.80 (d, J = 7.8 Hz, 1H), 7.62 (t, J = 7.5 Hz, 1H), 7.46 (t, J = 7.4 Hz, 1H), 4.32–4.28 (m, 1H), 2.44 (q, J = 12.4 Hz, 2H), 2.04 (d, J = 12.6 Hz, 2H), 1.96 (d, J = 11.9 Hz, 2H), 1.86 (d, J = 12.7 Hz, 1H), 1.54 (q, J = 12.9 Hz, 2H), 1.44 (t, J = 13.0 Hz, 1H); $^{13}C\{^1H\}$ NMR (151 MHz, $CDCl_3$+DMSO-d_6 (4:1)) δ 169.9, 169.1, 140.2, 139.5, 127.2, 127.1, 126.6, 125.8, 125.6, 124.7, 123.9, 122.3, 122.0, 121.1, 120.0, 116.9, 111.8, 110.8, 49.6, 29.5, 25.4, 24.5; IR (neat, cm^{-1}) 3327, 2921, 1750, 1671, 1600, 1462, 1360, 1245, 1014,

739, 625; HRMS (–ESI) $[M–H]^-$ calcd for $C_{24}H_{19}N_2O_2^-$ 367.1452, found 367.1467.

***2-(4-Methoxyphenyl)benzo[a]pyrrolo[3,4-c]carbazole-1,3(2H,8H)-dione (3ah)*:**

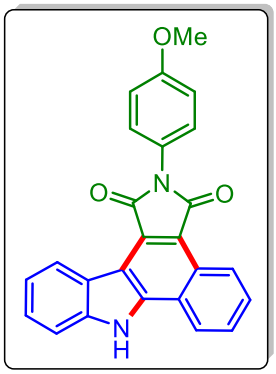

Yellow solid (79 mg, 58% yield); purified over column of silica gel (14% EtOAc in hexane); ^{1}H NMR (400 MHz, DMSO-d_6) δ 12.89 (s, 1H), 8.93–8.90 (m, 1H), 8.81 (d, J = 7.9 Hz, 1H), 8.61–8.58 (m, 1H), 7.76–7.72 (m, 2H), 7.65 (d, J = 8 Hz, 1H), 7.48 (t, J = 7.2 Hz, 1H), 7.39 (d, J = 8.9 Hz, 2H), 7.29 (t, J = 7.5 Hz, 1H), 7.03 (d, J = 8.9 Hz, 2H), 3.76 (s, 3H); ^{13}C{^{1}H} NMR (151 MHz, DMSO-d_6) δ 169.3, 168.4, 158.7, 140.6, 139.9, 129.0, 128.4, 127.9, 127.6, 126.7, 126.1, 124.9, 124.8, 124.0, 122.9, 122.6, 121.2, 120.9, 117.3, 114.1, 111.95, 111.93, 55.4; IR (neat, cm^{-1}) 3411, 1747, 1692, 1600, 1515, 1378, 1248, 1029, 739; HRMS (–ESI) $[M–H]^-$ calcd for $C_{25}H_{15}N_2O_3^-$ 391.1088, found 391.1090.

***2-(4-Fluorophenyl)benzo[a]pyrrolo[3,4-c]carbazole-1,3(2H,8H)-dione (3ai)*:**

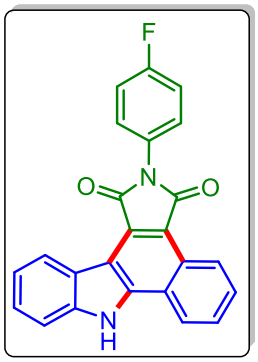

Yellow solid (73 mg, 55% yield); purified over column of silica gel (13% EtOAc in hexane); ^{1}H NMR (400 MHz, DMSO-d_6) δ 12.86 (s, 1H), 8.87 (dd, J = 6.7, 2.6 Hz, 1H), 8.77 (d, J = 8.0 Hz, 1H), 8.56 (dd, J = 6.7, 2.5 Hz, 1H), 7.73–7.69 (m, 2H), 7.63 (d, J = 8.1 Hz, 1H), 7.53 (dd, J = 8.9, 5.1 Hz, 2H), 7.49–7.44 (m, 1H), 7.33 (t, J = 9.0 Hz, 2H), 7.27 (t, J = 7.5 Hz, 1H); ^{13}C{^{1}H} NMR (151 MHz, DMSO-d_6) δ 168.9, 168.0, 161.2 (d, J = 244.9 Hz), 140.6, 139.9, 129.7 (d, J = 8.7 Hz), 128.5 (d, J = 2.9 Hz), 128.4, 127.9, 127.5, 126.7, 126.0, 124.9, 123.9, 122.8, 122.6, 121.2, 120.9, 117.2, 115.8, 115.6, 111.9; ^{19}F NMR (377 MHz, DMSO-d_6) δ –114.0; IR (neat, cm^{-1}) 3387, 1758, 1692, 1507, 1378, 1223, 1100, 747, 627; HRMS (–ESI) $[M–H]^-$ calcd for $C_{24}H_{12}FN_2O_2^-$ 379.0888, found 379.0869.

***2-(4-(Trifluoromethyl)phenyl)benzo[a]pyrrolo[3,4-c]carbazole-1,3(2H,8H)-dione (3aj)*:**

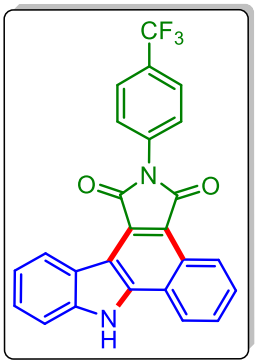

Yellow solid (79 mg, 53% yield); purified over column of silica gel (13% EtOAc in hexane); ^{1}H NMR (400 MHz, DMSO-d$_6$) δ 12.95 (s, 1H), 8.92–8.89 (m, 1H), 8.79 (d, J = 7.6 Hz, 1H), 8.60–8.57 (m, 1H), 7.85 (d, J = 8.5 Hz, 2H), 7.76–7.72 (m, 3H), 7.64 (d, J = 8.0 Hz, 1H), 7.48–7.44 (m, 2H), 7.30–7.25 (m, 1H); ^{13}C{^{1}H} NMR (151 MHz, DMSO-d$_6$) δ 168.5, 167.8, 140.8, 140.1, 135.9, 129.9, 128.7, 128.2, 127.8, 127.6, 126.8, 126.1, 125.9 (d, J = 3.6 Hz), 125.1, 125.0, 124.0, 122.9, 122.8, 121.2, 121.0, 117.3, 112.0 (d, J = 6.2 Hz); ^{19}F NMR (377 MHz, DMSO-d$_6$) δ –60.8; IR (neat, cm^{-1}) 3389, 1754, 1702, 1461, 1377, 1325, 1022, 995, 823, 744, 624; HRMS (–ESI) [M–H]$^-$ calcd for $C_{25}H_{12}F_3N_2O_2^-$ 429.0856, found 429.0879.

***2-(3-Chlorophenyl)benzo[a]pyrrolo[3,4-c]carbazole-1,3(2H,8H)-dione (3ak)*:**

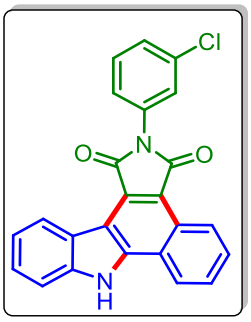

Yellow solid (74 mg, 54% yield); purified over column of silica gel (10% EtOAc in hexane); ^{1}H NMR (600 MHz, DMSO-d$_6$) δ 13.00 (s, 1H), 8.96 (d, J = 7.2 Hz, 1H), 8.84 (d, J = 7.8 Hz, 1H), 8.65 (d, J = 7.8 Hz, 1H), 7.82–7.77 (m, 2H), 7.69 (d, J = 8.4 Hz, 1H), 7.58–7.53 (m, 4H), 7.50 (t, J = 7.8 Hz, 1H), 7.31 (t, J = 7.2 Hz, 1H); ^{13}C{^{1}H} NMR (151 MHz, DMSO-d$_6$) δ 168.8, 167.9, 140.8, 140.1, 132.2, 131.1, 129.3, 128.9, 128.6, 128.2, 128.1, 127.7, 126.8, 126.1, 125.0, 124.0, 122.9, 122.8, 121.2, 121.0, 117.4, 112.0; IR (neat, cm^{-1}) 3416, 2922, 1753, 1693, 1498, 1377, 1168, 1091, 738, 625; HRMS (–ESI) [M–H]$^-$ calcd for $C_{24}H_{12}ClN_2O_2^-$ 395.0593, found 395.0591.

***10-Chloro-2-phenylbenzo[a]pyrrolo[3,4-c]carbazole-1,3(2H,8H)-dione (3rl)*:**

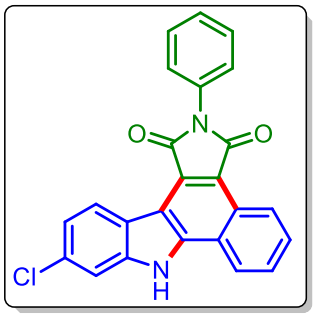

Yellow solid (78 mg, 56% yield); purified over column of silica gel (9% EtOAc in hexane); ^{1}H NMR (400 MHz, DMSO-d$_6$) δ 13.09 (s, 1H), 8.96 (dd, J = 6.4, 3.1 Hz, 1H), 8.80 (d, J = 8.8 Hz, 1H), 8.62 (dd, J = 6.3, 2.4Hz, 1H), 7.83–7.81 (m, 2H), 7.68 (d, J = 1.2 Hz, 1H), 7.52 (d, J = 4.1 Hz, 4H), 7.44 – 7.40 (m , 1H), 7.35 (dd, J = 8.8, 1.6 Hz, 1H); ^{13}C{^{1}H} NMR (101 MHz, DMSO-d$_6$) δ 168.9, 168.1, 141.1, 140.5, 132.1, 131.1, 128.8, 128.7, 128.3, 127.8, 127.6, 127.4, 126.2, 125.2, 125.1, 122.9, 122.8, 121.2, 120.1, 118.0, 111.6, 111.4; IR (neat,

cm^{-1}) 3230, 2945, 1742, 1599, 1588, 1320. 1230, 820, 799; HRMS (–ESI) [M–H]$^-$ calcd for $C_{24}H_{12}ClN_2O_2^-$ 395.0593, found 395.0591.

***2-Hexylbenzo[a]pyrrolo[3,4-c]carbazole-1,3(2H,8H)-dione (3am)*:**

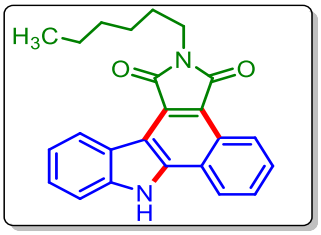

Yellow solid (97 mg, 75% yield); purified over column of silica gel (7% EtOAc in hexane); ^{1}H NMR (600 MHz, DMSO-d$_6$) δ 12.57 (s, 1H), 8.59 (dd, J = 15.3, 7.8 Hz, 2H), 8.30 (d, J = 7.8 Hz, 1H), 7.52–7.45 (m, 3H), 7.32 (t, J = 7.5 Hz, 1H), 7.13 (t, J = 7.2 Hz, 1H), 2.34–2.32 (m, 1H), 1.42–1.39 (m, 2H), 1.15–1.00 (m, 7H), 0.64–0.63 (m, 3H); ^{13}C{^{1}H} NMR (151 MHz, DMSO-d$_6$) δ 169.8, 168.9, 140.3, 1399, 128.1, 127.5, 127.3, 126.5, 125.8, 124.7, 123.9, 122.7, 122.3, 121.2, 120.7, 117.2, 111.8, 111.7, 37.1, 30.9, 28.2, 26.1, 22.0, 13.9; IR (neat, cm^{-1}) 3346, 2923, 1746, 1673, 1598, 1459, 1366, 1153, 744, 627; HRMS (–ESI) [M–H]$^-$ calcd for $C_{24}H_{21}N_2O_2^-$ 369.1609, found 369.1628.

***2-Heptylbenzo[a]pyrrolo[3,4-c]carbazole-1,3(2H,8H)-dione (3an)*:**

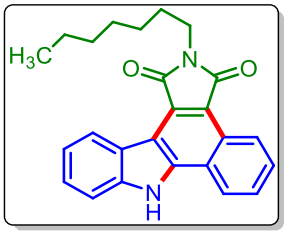

Yellow solid (99 mg, 74% yield); purified over column of silica gel (7% EtOAc in hexane); ^{1}H NMR (400 MHz, DMSO-d$_6$) δ 12.71 (s, 1H), 8.76–8.74 (m, 1H), 8.71 (d, J = 7.9 Hz, 1H), 8.46–8.43 (m, 1H), 7.64–7.60 (m, 2H), 7.57 (d, J = 8.1 Hz, 1H), 7.42 (t, J = 7.6 Hz, 1H), 7.23 (t, J = 7.5 Hz, 1H), 3.44 (t, J = 7.1 Hz, 2H), 1.53–1.49 (m, 2H), 1.20–1.14 (m, 4H), 1.12–1.07 (m, 4H), 0.70 (t, J = 6.8 Hz, 3H); ^{13}C{^{1}H} NMR (151 MHz, DMSO-d$_6$) δ 169.9, 169.0, 140.3, 139.9, 128.1, 127.6, 127.4, 126.5, 125.8, 124.7, 123.9, 122.7, 122.4, 121.2, 120.7, 117.3, 111.8, 111.8, 37.1, 31.2, 28.3, 28.2, 26.3, 22.0, 13.9; IR (neat, cm^{-1}) 3350, 2925, 2856, 1745, 1672, 1598, 1368, 1244, 1015, 745; HRMS (–ESI) [M–H]$^-$ calcd for $C_{25}H_{23}N_2O_2^-$ 383.1765, found 383.1786.

***2-Octylbenzo[a]pyrrolo[3,4-c]carbazole-1,3(2H,8H)-dione (3ao)*:**

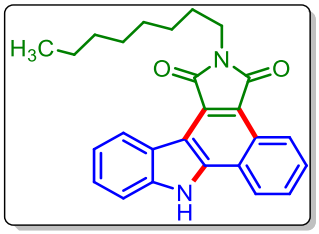

Yellow solid (107 mg, 77% yield); purified over column of silica gel (7% EtOAc in hexane); ^{1}H NMR (600 MHz, DMSO-d$_6$) δ 12.79 (s, 1H), 8.82 (d, J = 7.2 Hz, 1H), 8.77 (d, J = 7.9 Hz, 1H), 8.52 (d, J = 8.4 Hz, 1H), 7.71–7.66 (m, 2H), 7.62 (d, J = 8.4 Hz, 1H), 7.47 (t, J = 7.6 Hz, 1H), 7.28 (t, J = 7.5 Hz, 1H), 3.51 (t, J = 7.1 Hz, 2H), 1.58–1.53 (m, 2H), 1.24–1.19 (m, 4H), 1.15–1.12 (m, 6H), 0.72 (t, J = 6.9 Hz, 3H); ^{13}C{^{1}H} NMR (151 MHz, DMSO-d$_6$) δ 169.9, 169.0, 140.4, 139.9, 128.1, 127.6, 127.4, 126.5, 125.8, 124.7, 123.9, 122.7, 122.4, 121.1, 120.7, 117.3, 111.8, 111.8, 37.1, 31.2, 28.6, 28.2, 26.3, 22.1, 13.9; IR (neat, cm^{-1}) 3326, 2925, 2853, 1749, 1673, 1598, 1365, 1246, 1014, 744, 626; HRMS (–ESI) [M–H]$^-$ calcd for $C_{26}H_{25}N_2O_2^-$ 397.1922, found 397.1922.

***2-(1-Phenylethyl)benzo[a]pyrrolo[3,4-c]carbazole-1,3(2H,8H)-dione (3ap)*:**

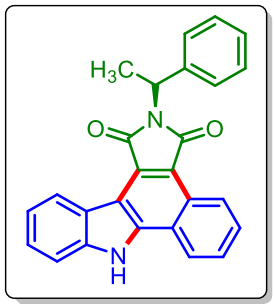

Yellow solid (87 mg, 64% yield); purified over column of silica gel (8% EtOAc in hexane); ^{1}H NMR (500 MHz, DMSO-d$_6$) δ 12.87 (s, 1H), 8.93–8.91 (m, 1H), 8.82 (d, J = 7.5 Hz, 1H), 8.61–8.59 (m, 1H), 7.75–7.74 (m, 2H), 7.66 (d, J = 7.5 Hz, 1H), 7.49 (t, J = 7.8 Hz, 1H), 7.44 (d, J = 7.5 Hz, 2H), 7.32–7.28 (m, 3H), 7.20 (t, J = 7.3 Hz, 1H), 5.53 (q, J = 7.5 Hz, 1H), 1.89 (d, J = 7.0 Hz, 3H); ^{13}C{^{1}H} NMR (151 MHz, DMSO-d$_6$) δ 169.8, 169.0, 141.2, 140.6, 139.9, 128.5, 128.3, 127.8, 127.5, 127.2, 126.7, 126.6, 125.9, 124.8, 124.0, 122.8, 122.6, 121.1, 120.8, 117.1, 111.9, 111.8, 48.5, 17.8; IR (neat, cm^{-1}) 3422, 2930, 1750, 1692, 1460, 1347, 1022, 747, 697; HRMS (–ESI) [M–H]$^-$ calcd for $C_{26}H_{17}N_2O_2^-$ 389.1296, found 389.1291.

***Benzo[a]pyrrolo[3,4-c]carbazole-1,3(2H,8H)-dione (3aq)*:**

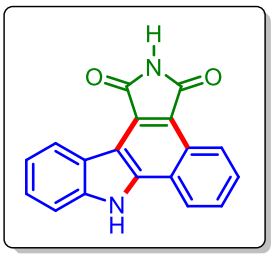

Yellow solid (50 mg, 50% yield); purified over column of silica gel (9% EtOAc in hexane); ^{1}H NMR (500 MHz, DMSO-d$_6$) δ 12.92 (s, 1H), 11.11 (s, 1H), 8.99 (d, J = 8.0 Hz, 1H), 8.90 (d, J = 8.0 Hz, 1H), 8.68 (d, J = 8.0 Hz, 1H), 7.86–7.77 (m, 2H), 7.73 (d, J = 8 Hz, 1H), 7.55 (t, J = 7.5 Hz, 1H), 7.37 (t, J = 7.5 Hz, 1H); ^{13}C{^{1}H} NMR (126 MHz, DMSO-d$_6$) δ 171.5, 170.5, 140.4, 139.9, 128.6, 128.2, 127.8,

126.5, 126.0, 124.9, 124.0, 122.7, 122.6, 121.3, 120.7, 118.5, 111.8, 111.7; IR (neat, cm^{-1}) 3425, 3411, 2830, 1740, 1682, 1457, 1351, 1012, 750, 680; HRMS (–ESI) $[M–H]^-$ calcd for $C_{18}H_9N_2O_2^-$ 285.0670, found 285.0660.

***2-(2-Phenyl-1H-indol-3-yl)cyclohexa-2,5-diene-1,4-dione (3ar)*:**

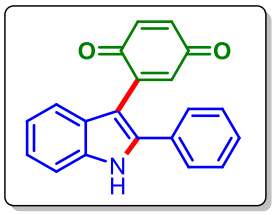

Yellow solid (76 mg, 73% yield); purified over column of silica gel (5% EtOAc in hexane); ^1H NMR (500 MHz, $CDCl_3$) δ 8.56 (s, 1H), 7.57 (d, J = 8.0 Hz, 1H), 7.45–7.42 (m, 3H), 7.4 (s, 1H), 7.40–7.35 (m, 2H), 7.27 (d, J = 7.5 Hz, 1H), 7.21 (t, J = 7.8 Hz, 1H), 6.98 (d, J = 2.5 Hz, 1H), 6.82–6.79 (m, 1H), 6.75 (d, J = 10.0 Hz, 1H).; $^{13}C\{^1H\}$ NMR (126 MHz, $CDCl_3$) δ 187.7, 186.1, 143.0, 139.4, 137.1, 136.7, 136.3, 133.7, 132.7, 129.21, 128.8, 128.3, 128.2, 123.5, 121.6, 119.6, 111.5, 106.6; IR (neat, cm^{-1}) 3427, 3421, 2839, 1744, 1672, 1455, 1356, 1013, 751, 685; HRMS (+ESI) $[M+H]^+$ calcd for $C_{20}H_{14}NO_2^+$ 300.1019, found 300.1032.

***3-(2-Cyclohexyl-1H-indol-3-yl)-1-ethylpyrrolidine-2,5-dione (5wa)*:**

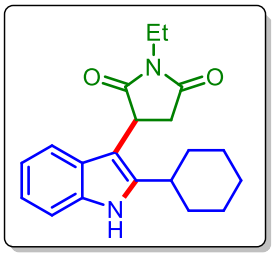

Brown solid (64 mg, 57% yield); purified over column of silica gel (10% EtOAc in hexane); ^1H NMR (600 MHz, $CDCl_3$) δ 8.08 (s, 1H), 7.30 (d, J = 7.8 Hz, 1H), 7.12 (t, J = 7.6 Hz, 1H), 7.09 (d, J = 7.8 Hz, 1H), 7.03 (t, J = 7.6 Hz, 1H), 4.23 (dd, J = 9.8, 4.8 Hz, 1H), 3.72 (q, J = 7.2 Hz, 2H), 3.16 (dd, J = 18.6, 9.7 Hz, 1H), 2.96 (dd, J = 18.6, 4.8 Hz, 1H), 2.80 (tt, J = 11.4, 2.9 Hz, 1H), 2.05 (d, J = 12.5 Hz, 1H), 1.91–1.86 (m, 3H), 1.79 (d, J = 12.6 Hz, 1H), 1.50 (qd, J = 12.5, 3.0 Hz, 2H), 1.44–1.36 (m, 2H), 1.28 (t, J = 7.2 Hz, 3H), 1.25 (s, 1H). ^{13}C $\{^1H\}$ NMR (151 MHz, $CDCl_3$) δ 178.6, 176.9, 142.5, 135.4, 126.1, 121.8, 120.1, 117.6, 111.3, 105.8, 37.7, 36.6, 36.1, 34.3, 33.6, 33.4, 26.8, 26.8, 26.2, 13.3; HRMS (+ESI) $[M+H]^+$ calcd for $C_{20}H_{25}N_2O_2^+$ 325.1911, found 325.1890.

II.10. NMR Spectra

2-Ethylbenzo[*a*]pyrrolo[3,4-*c*]carbazole-1,3(2*H*,8*H*)-dione (3aa): ^{1}H NMR ($CDCl_3$ + DMSO-d_6 (4:1), 400 MHz)

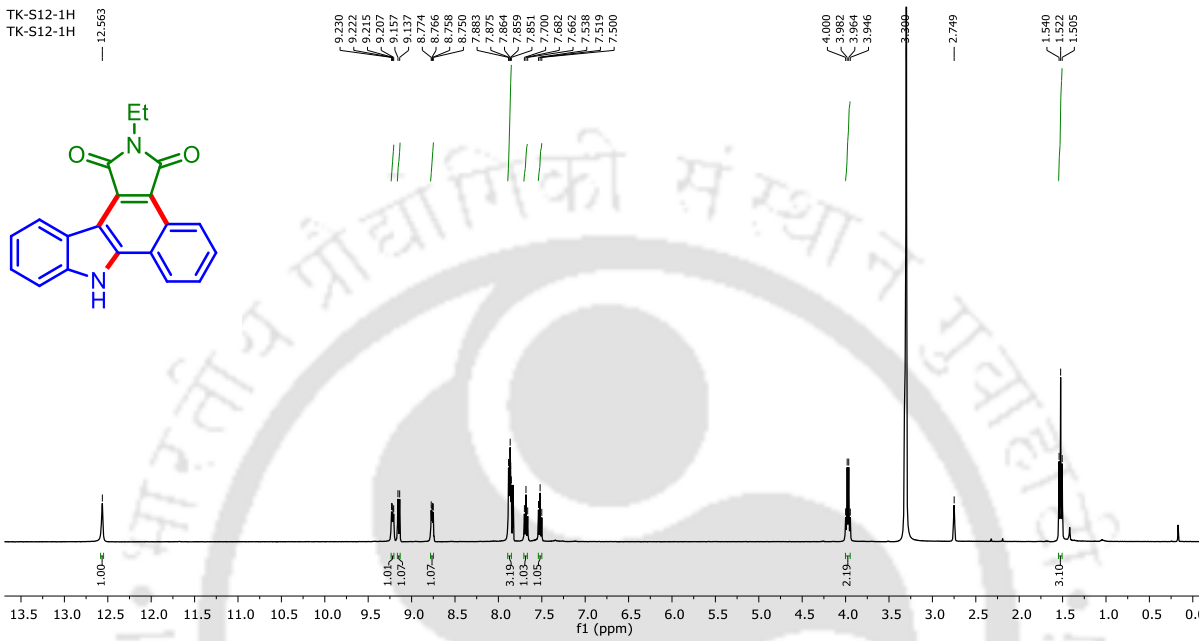

2-Ethylbenzo[*a*]pyrrolo[3,4-*c*]carbazole-1,3(2*H*,8*H*)-dione (3aa): ^{13}C{^{1}H} NMR ($CDCl_3$ + DMSO-d_6 (4:1), 151 MHz)

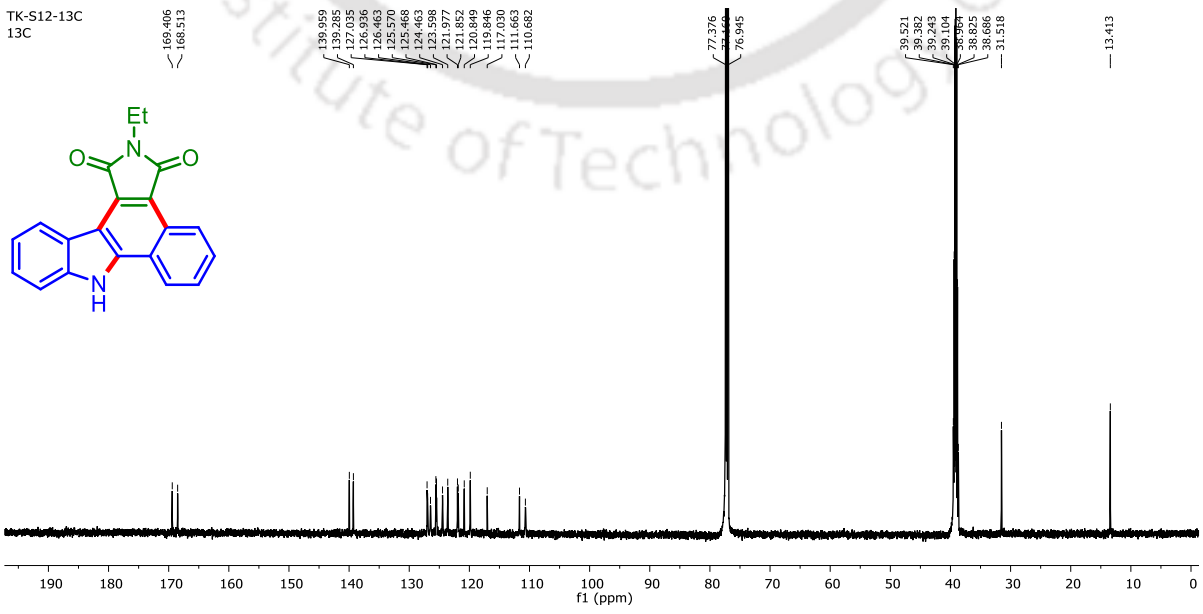

2-Ethyl-5-methylbenzo[*a*]pyrrolo[3,4-*c*]carbazole-1,3(2*H*,8*H*)-dione. (3ba): ^{1}H NMR ($CDCl_3$ + DMSO-d_6 (4:1), 600 MHz)

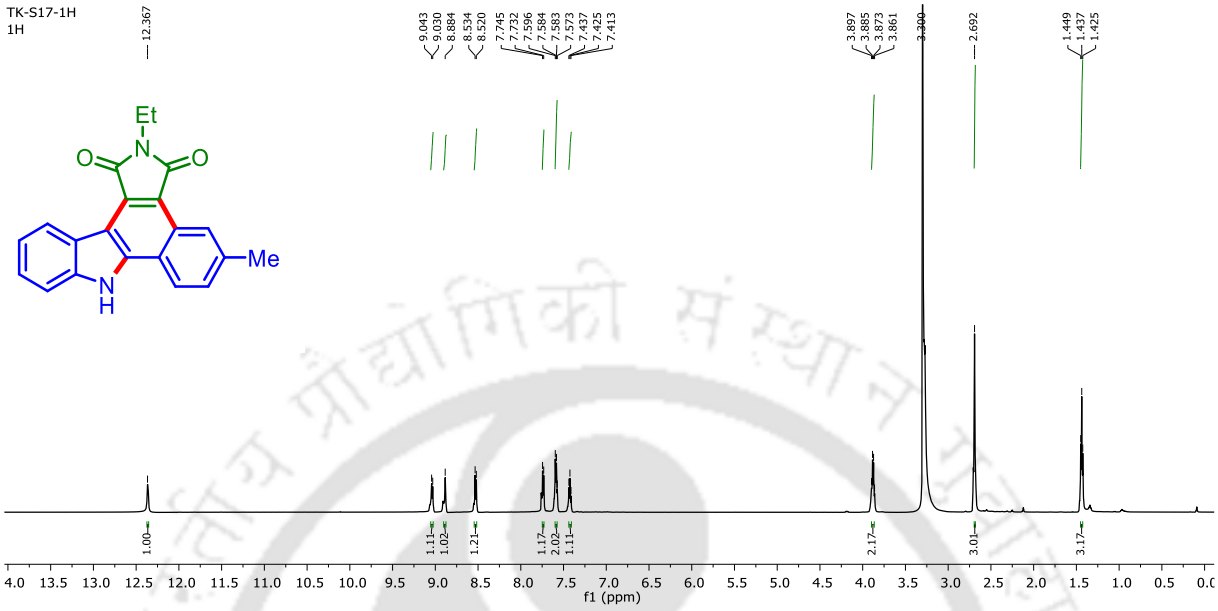

2-Ethyl-5-methylbenzo[*a*]pyrrolo[3,4-*c*]carbazole-1,3(2*H*,8*H*)-dione (3ba): ^{13}C{^{1}H} NMR ($CDCl_3$ + DMSO-d_6 (4:1), 151 MHz)

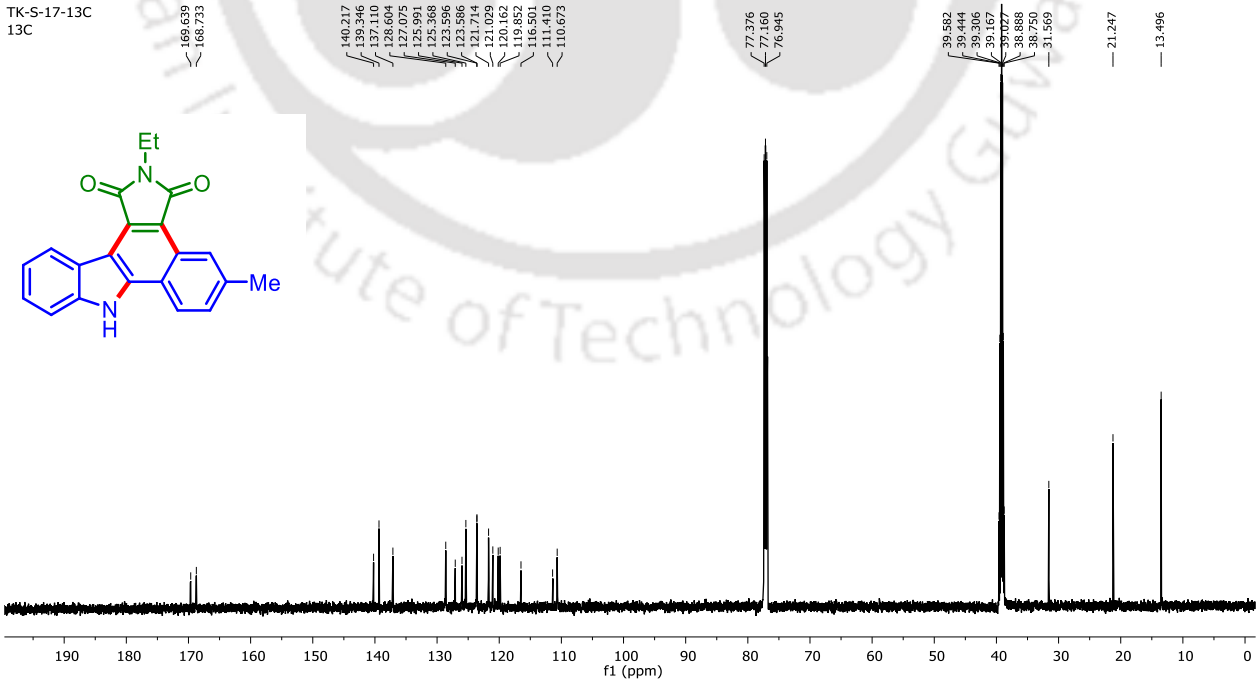

5-Chloro-2-ethylbenzo[*a*]pyrrolo[3,4-*c*]carbazole-1,3(2*H*,8*H*)-dione (3ea): ^{1}H NMR (DMSO-d$_6$, 500 MHz)

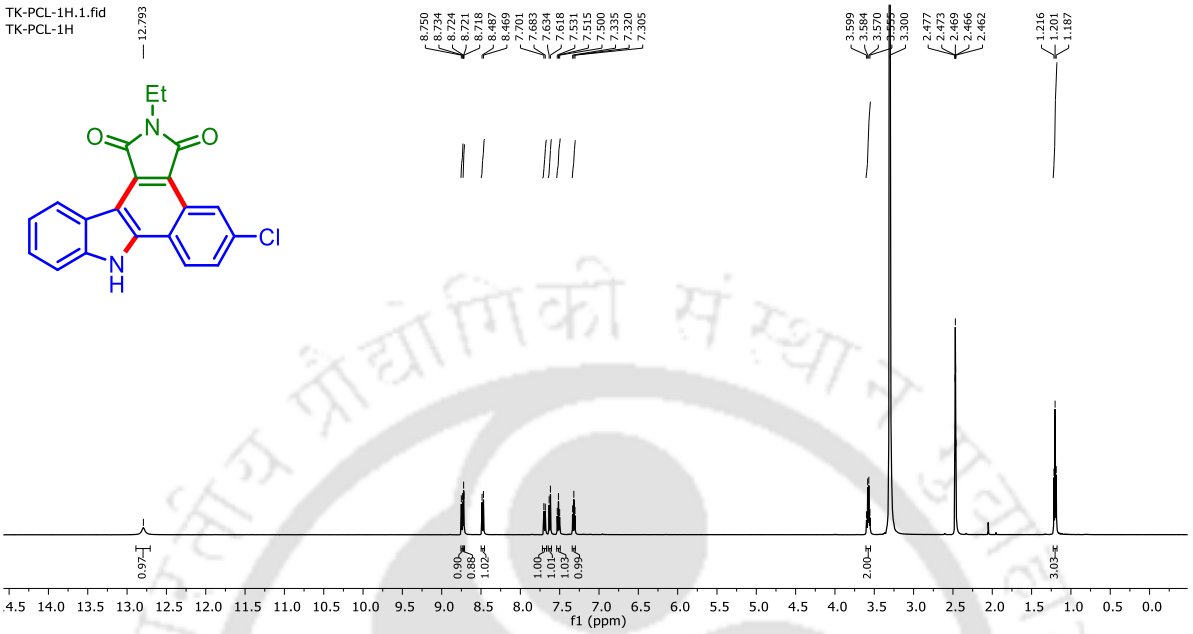

5-Chloro-2-ethylbenzo[*a*]pyrrolo[3,4-*c*]carbazole-1,3(2*H*,8*H*)-dione (3ea): ^{13}C{^{1}H} NMR (DMSO-d$_6$, 126 MHz)

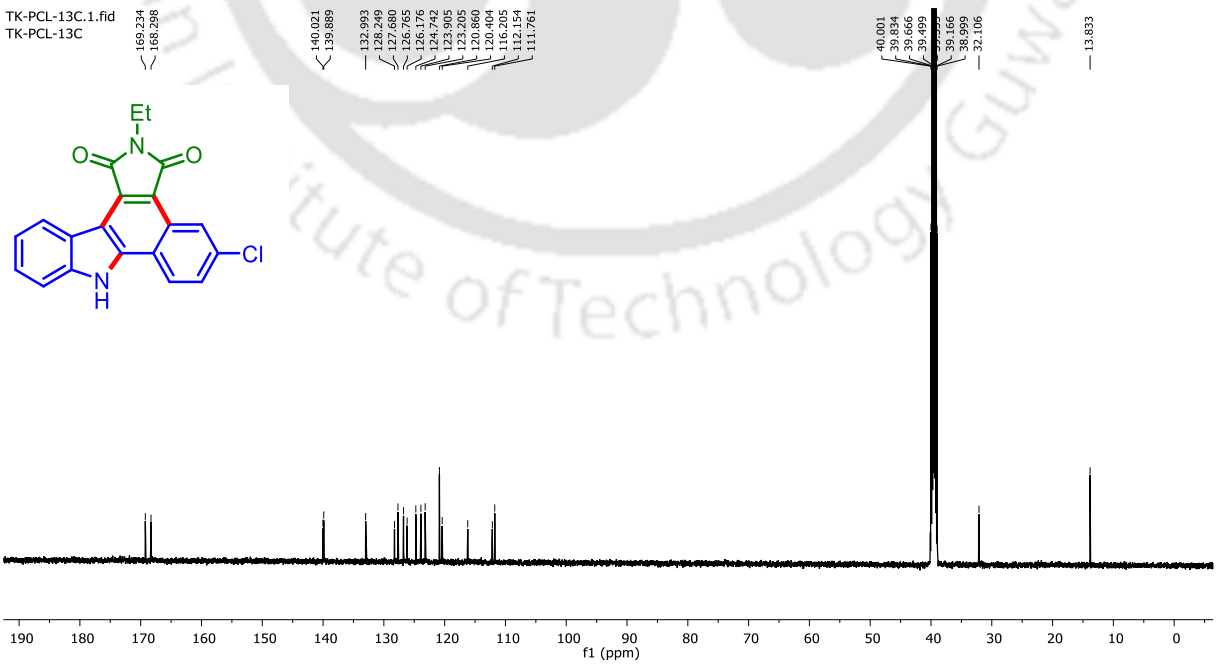

6-Chloro-2-ethylbenzo[*a*]pyrrolo[3,4-*c*]carbazole-1,3(2*H*,8*H*)-dione (3ia): ^{1}H NMR (DMSO-d$_6$, 500 MHz)

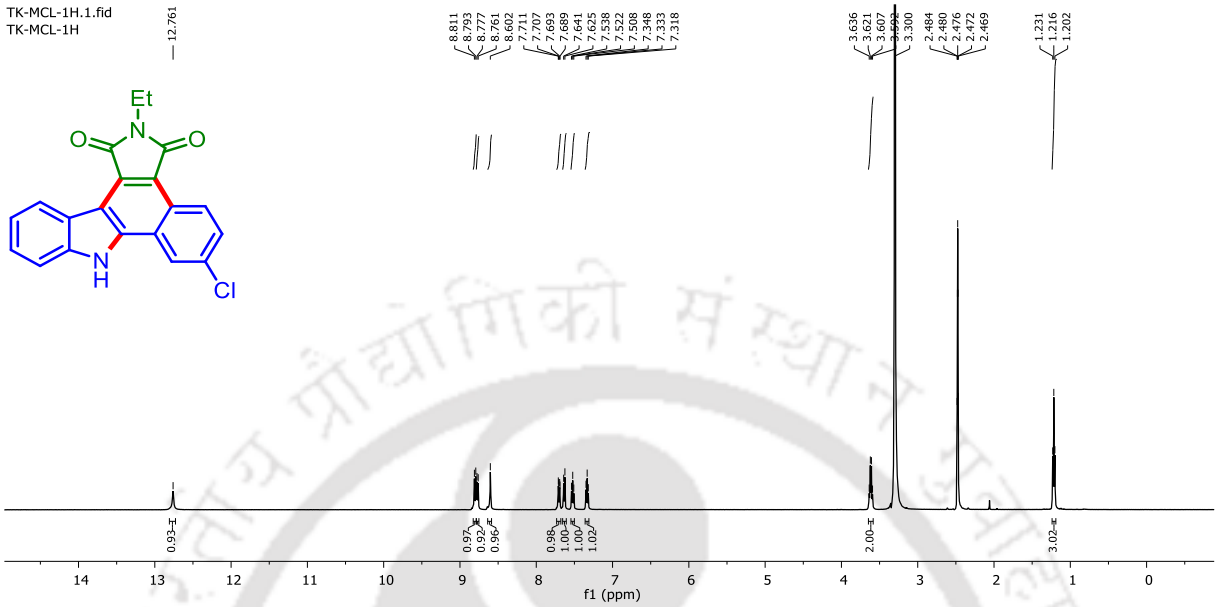

6-Chloro-2-ethylbenzo[*a*]pyrrolo[3,4-*c*]carbazole-1,3(2*H*,8*H*)-dione (3ia): ^{13}C{^{1}H} NMR (DMSO-d$_6$, 126 MHz)

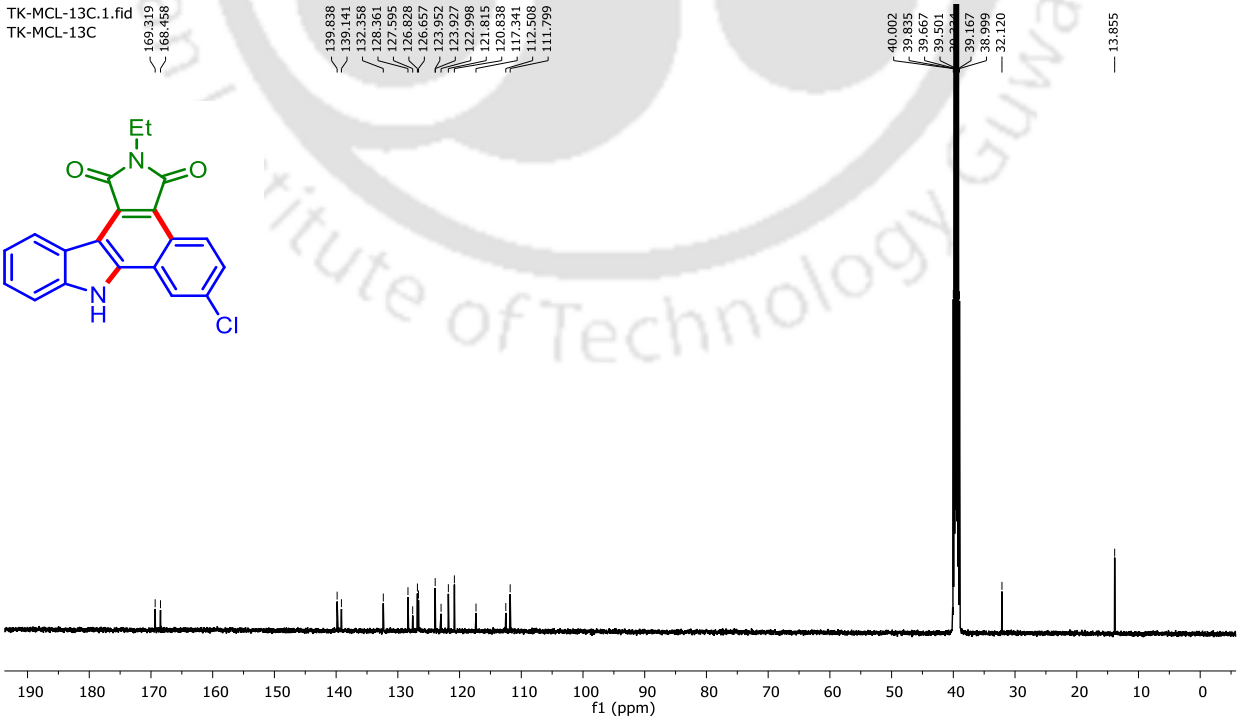

5-Ethylpyrrolo[3,4-*c*]thieno[2,3-*a*]carbazole-4,6(5*H*,11*H*)-dione (3ja): ^{1}H NMR (DMSO-d$_6$, 600 MHz)

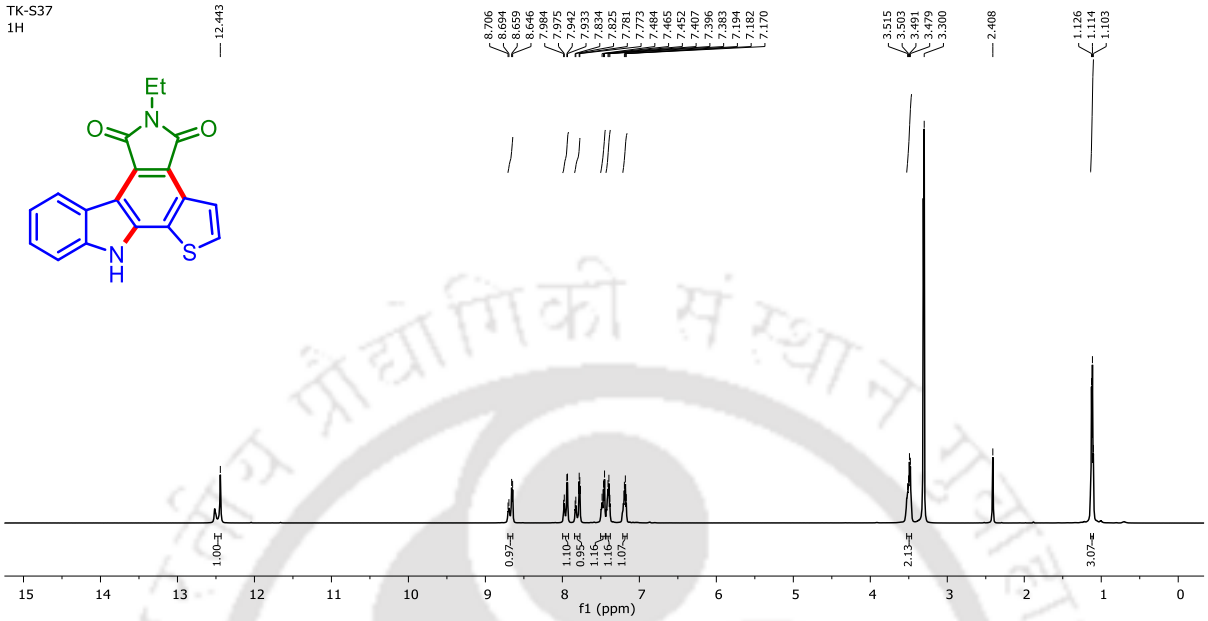

5-Ethylpyrrolo[3,4-*c*]thieno[2,3-*a*]carbazole-4,6(5*H*,11*H*)-dione (3ja): ^{13}C{^{1}H} NMR (DMSO-d$_6$, 151 MHz)

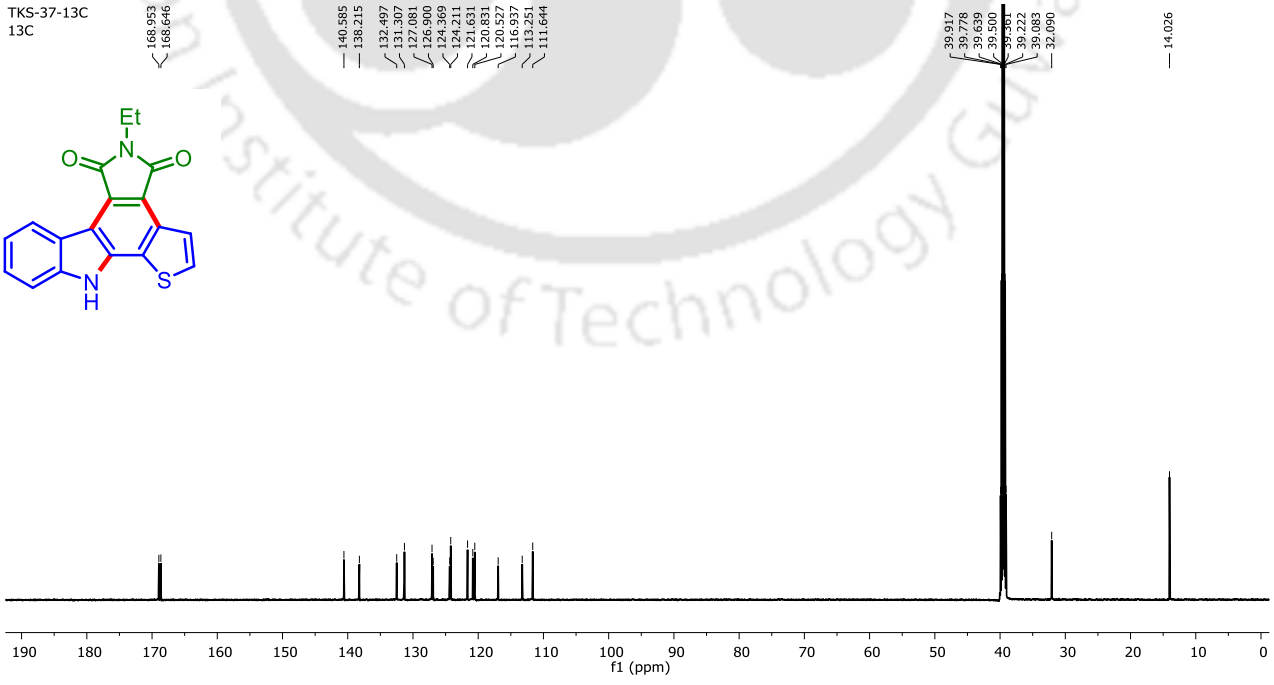

2-Ethyl-11-(trifluoromethyl)benzo[*a*]pyrrolo[3,4-*c*]carbazole-1,3(2*H*,8*H*)-dione (3ma): ^{1}H NMR (DMSO-d$_6$, 600 MHz)

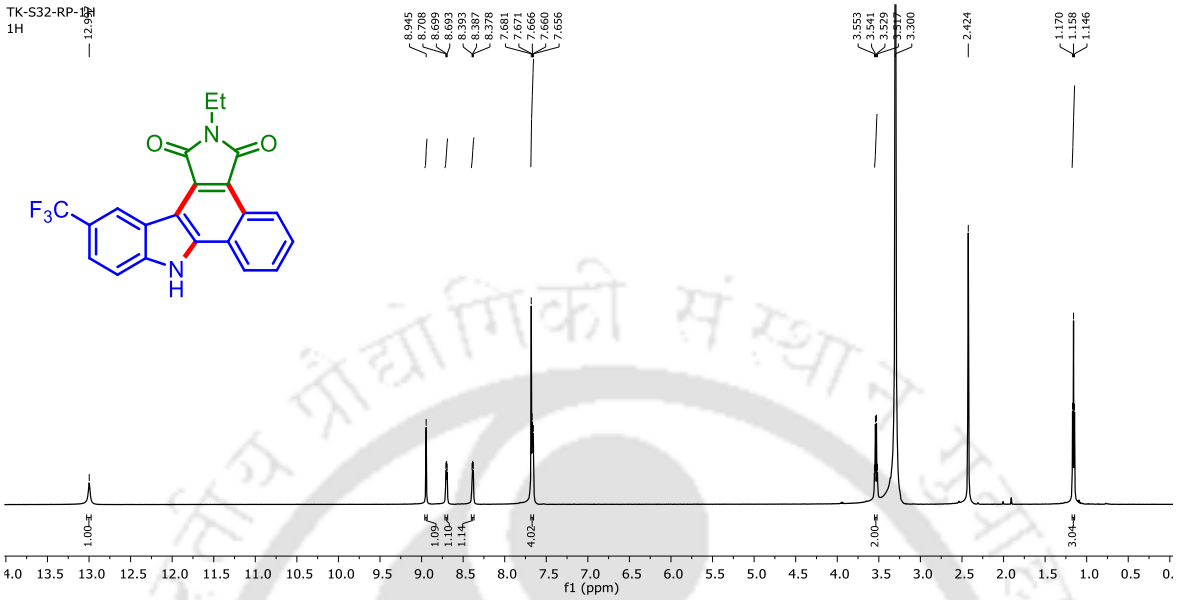

2-Ethyl-11-(rifluoromethyl)benzo[*a*]pyrrolo[3,4-*c*]carbazole-1,3(2*H*,8*H*)-dione (3ma): ^{13}C{^{1}H} NMR (DMSO-d$_6$, 151 MHz)

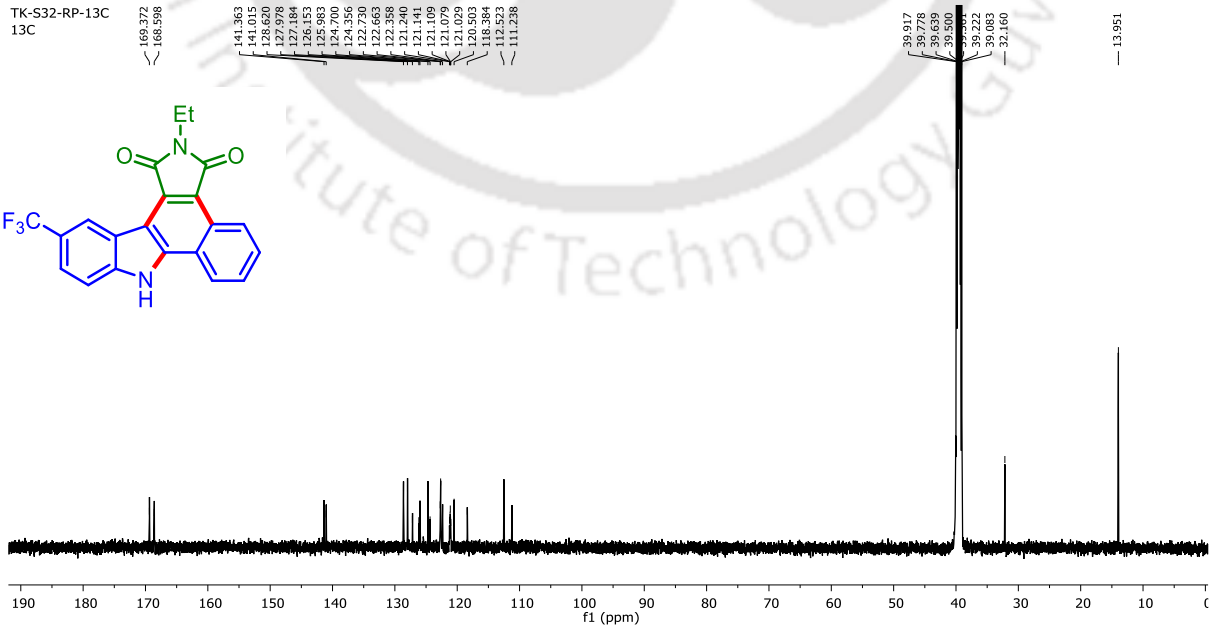

2-Ethyl-11-(trifluoromethyl)benzo[*a*]pyrrolo[3,4-*c*]carbazole-1,3(2*H*,8*H*)-dione (3ma): ^{19}F NMR (DMSO-d$_6$, 565 MHz)

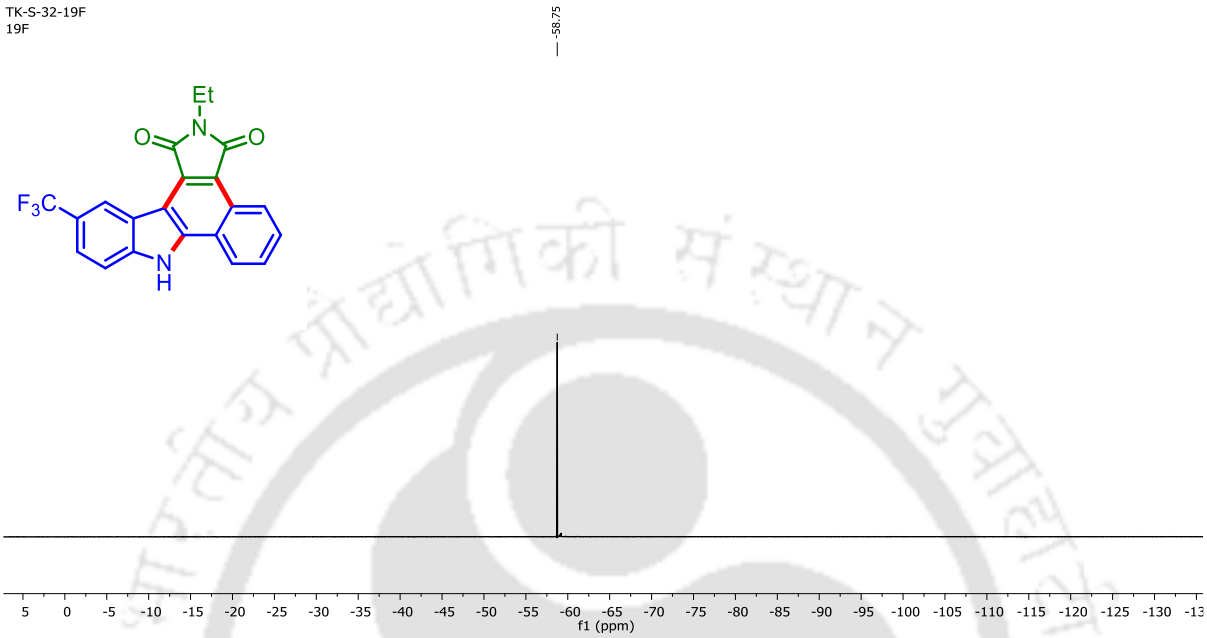

2-Benzyl-10-chlorobenzo[*a*]pyrrolo[3,4-*c*]carbazole-1,3(2*H*,8*H*)-dione (3rb): ^{1}H NMR (DMSO-d$_6$, 600 MHz)

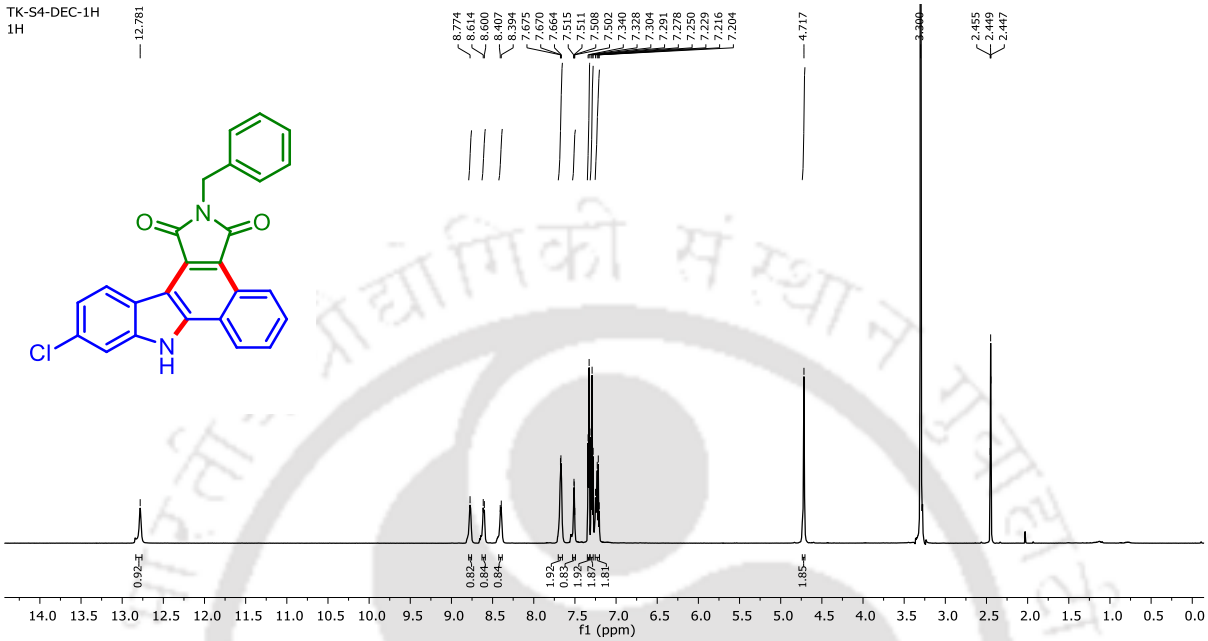

2-Benzyl-10-chlorobenzo[*a*]pyrrolo[3,4-*c*]carbazole-1,3(2*H*,8*H*)-dione (3rb): ^{13}C{^{1}H} NMR (DMSO-d$_6$, 151 MHz)

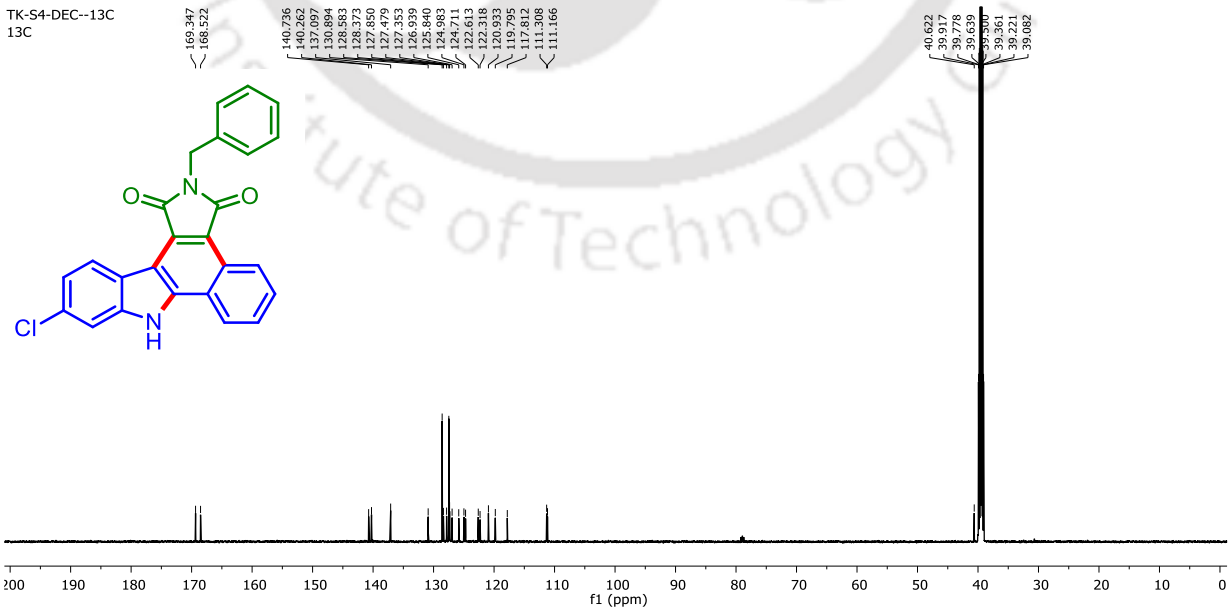

11-Chloro-2-ethyl-8-methylbenzo[*a*]pyrrolo[3,4-*c*]carbazole-1,3(2*H*,8*H*)-dione (3sa): ^{1}H NMR ($CDCl_3$, 500 MHz)

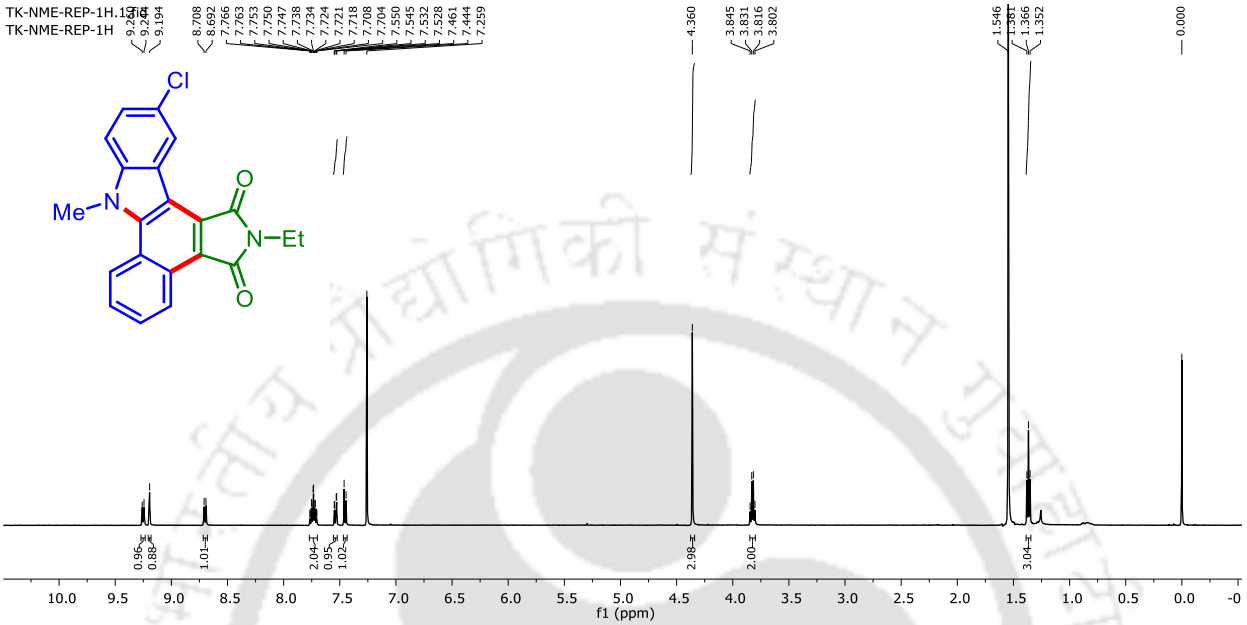

11-Chloro-2-ethyl-8-methylbenzo[*a*]pyrrolo[3,4-*c*]carbazole-1,3(2*H*,8*H*)-dione (3sa): ^{13}C{^{1}H} NMR ($CDCl_3$, 126 MHz)

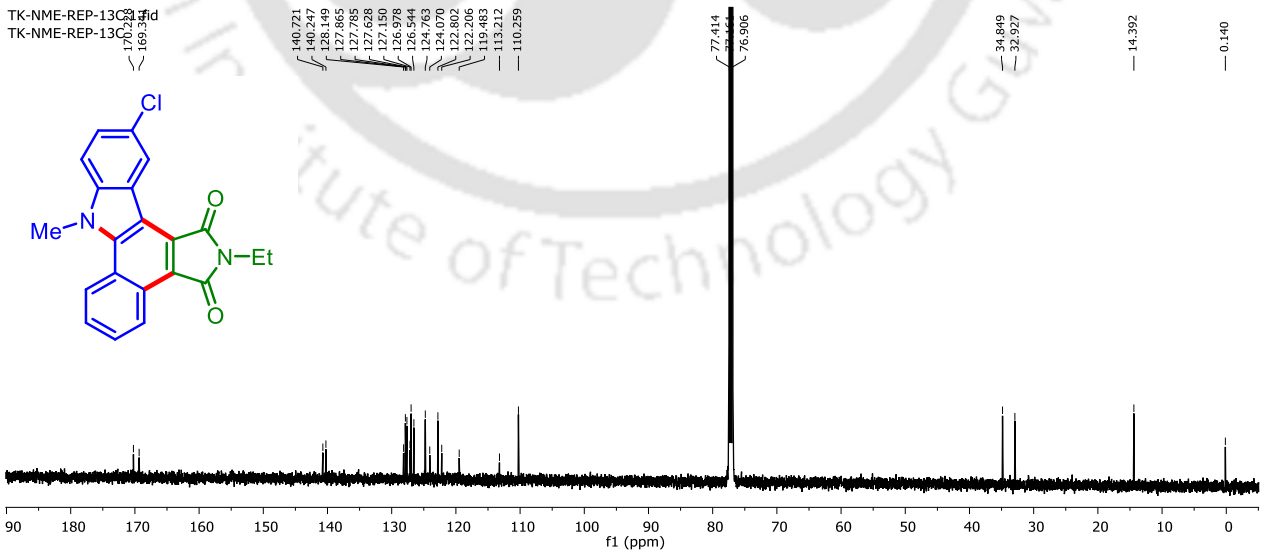

2-Methylbenzo[*a*]pyrrolo[3,4-*c*]carbazole-1,3(2*H*,8*H*)-dione (3ad): ^{1}H NMR (DMSO-d$_6$, 500 MHz)

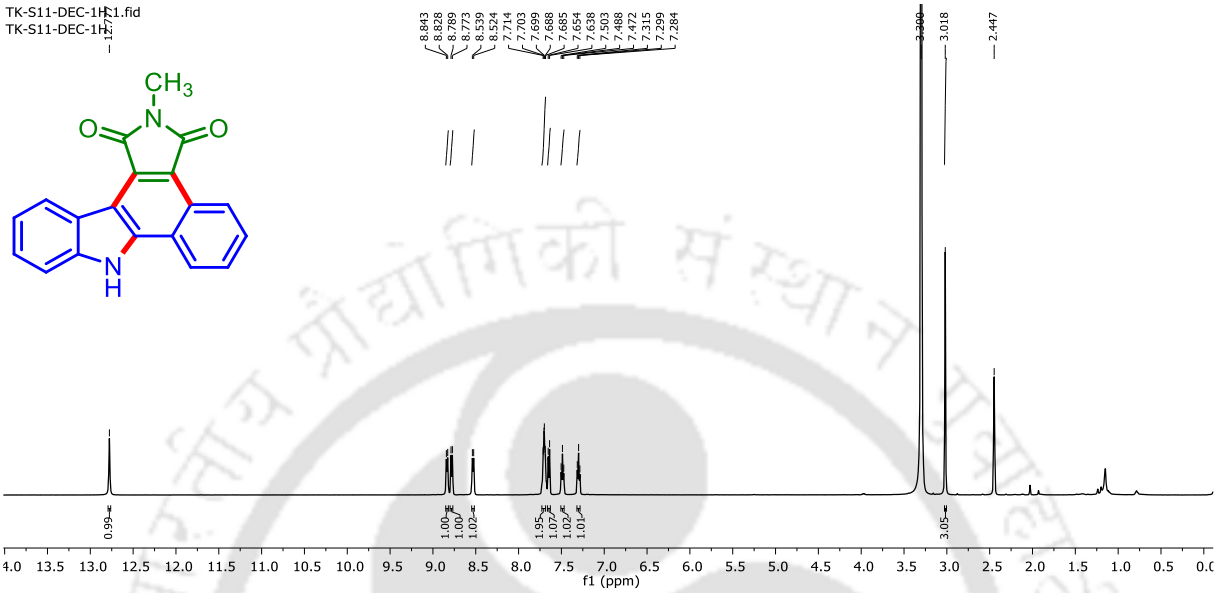

2-Methylbenzo[*a*]pyrrolo[3,4-*c*]carbazole-1,3(2*H*,8*H*)-dione (3ad): ^{13}C{^{1}H} NMR (CDCl$_3$ + DMSO-d$_6$ (4:1), 151 MHz)

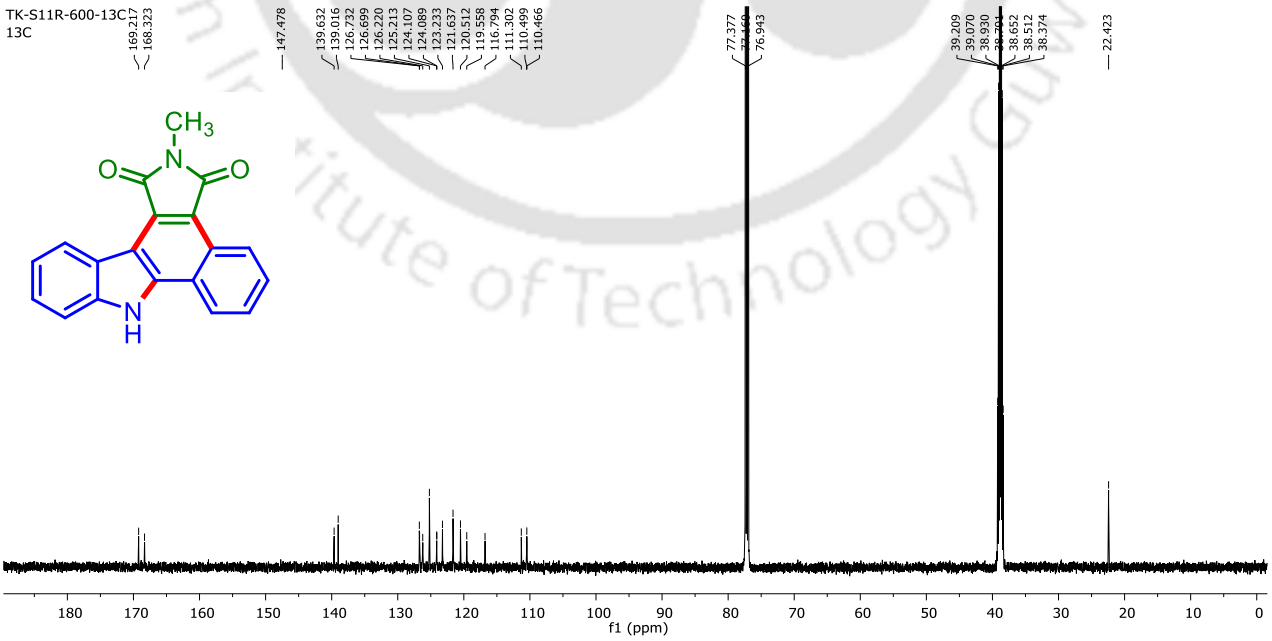

2-Heptylbenzo[*a*]pyrrolo[3,4-*c*]carbazole-1,3(2*H*,8*H*)-dione (3an): ^{1}H NMR (DMSO-d$_6$, 400 MHz)

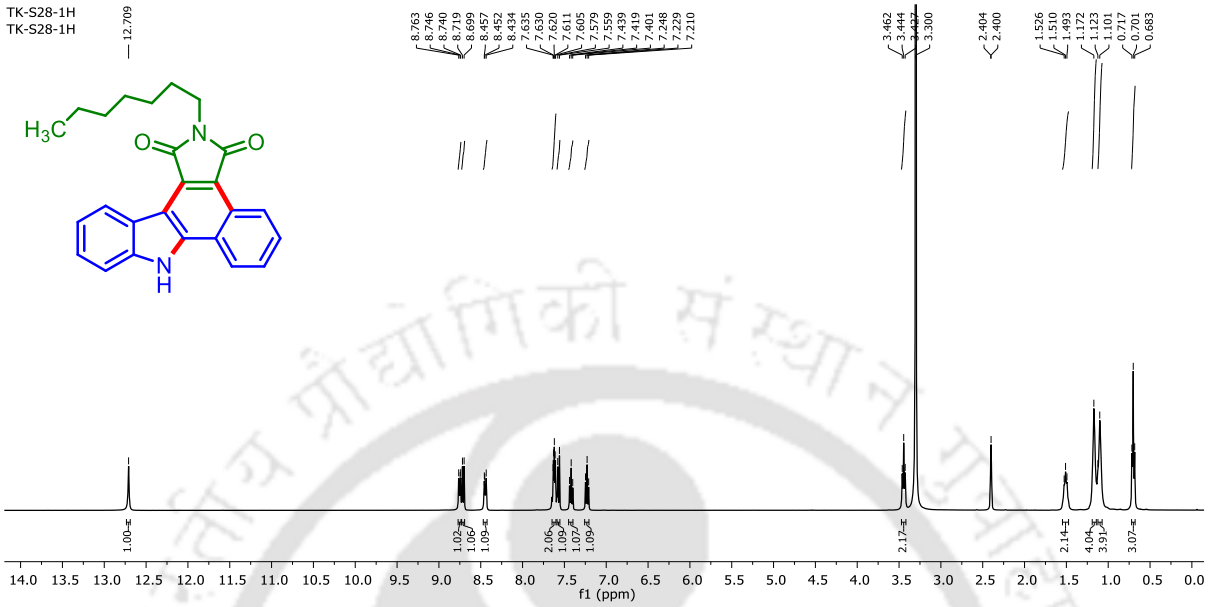

2-Heptylbenzo[*a*]pyrrolo[3,4-*c*]carbazole-1,3(2*H*,8*H*)-dione (3an): ^{13}C{^{1}H} NMR (DMSO-d$_6$, 151 MHz)

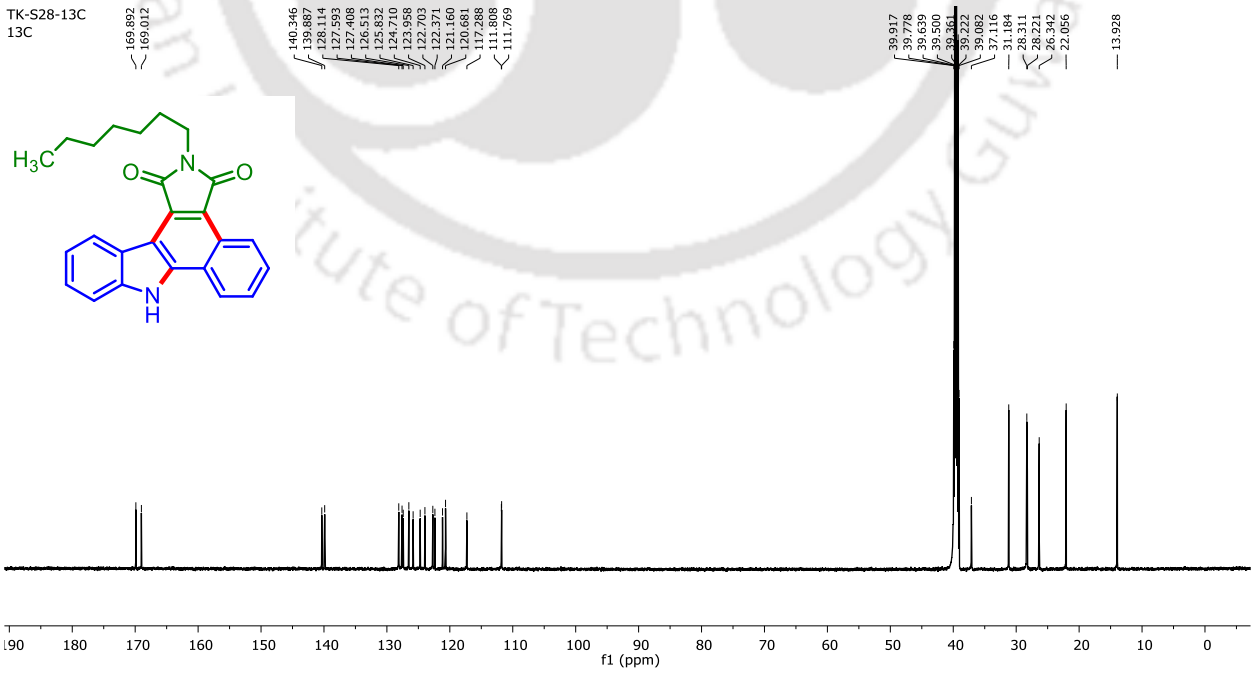

Benzo[*a*]pyrrolo[3,4-*c*]carbazole-1,3(2*H*,8*H*)-dione (3aq): ^{1}H NMR (DMSO-d$_6$, 500 MHz)

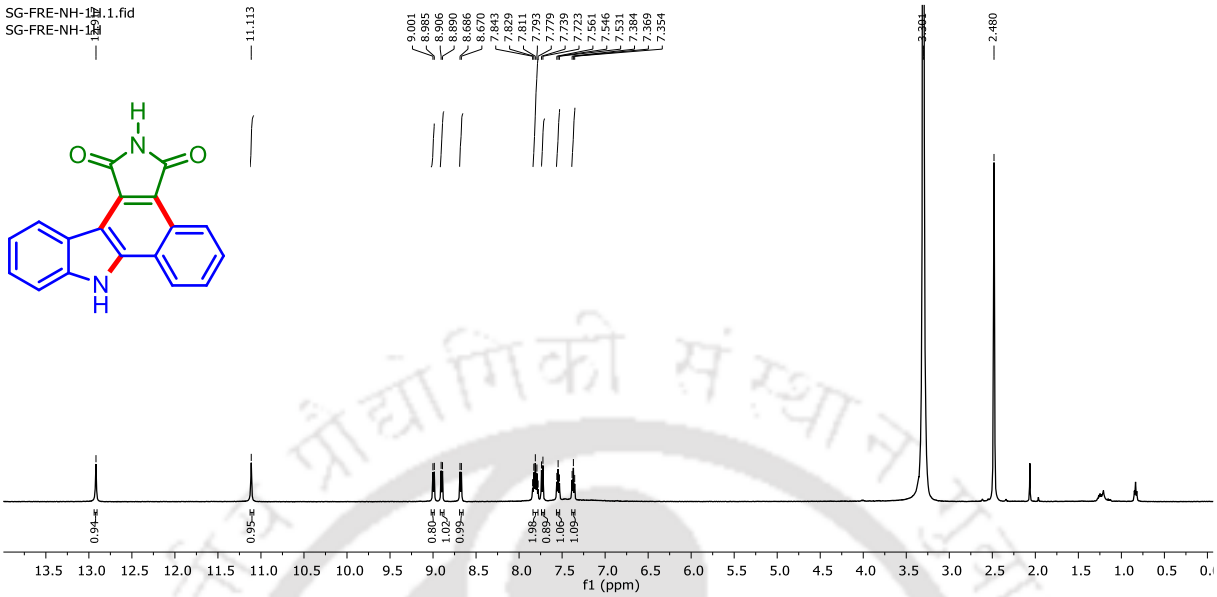

Benzo[*a*]pyrrolo[3,4-*c*]carbazole-1,3(2*H*,8*H*)-dione (3aq): ^{13}C{^{1}H} NMR (DMSO-d$_6$, 126 MHz)

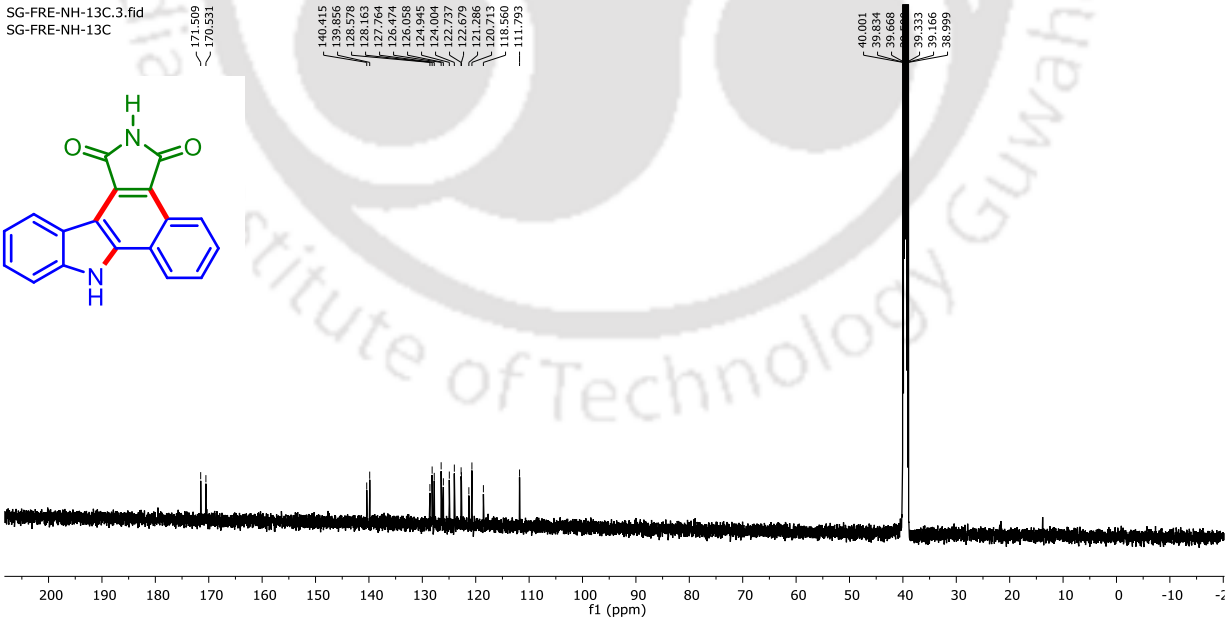

2-(2-Phenyl-1*H*-indol-3-yl)cyclohexa-2,5-diene-1,4-dione (3ar): ^{1}H NMR ($CDCl_3$, 500 MHz)

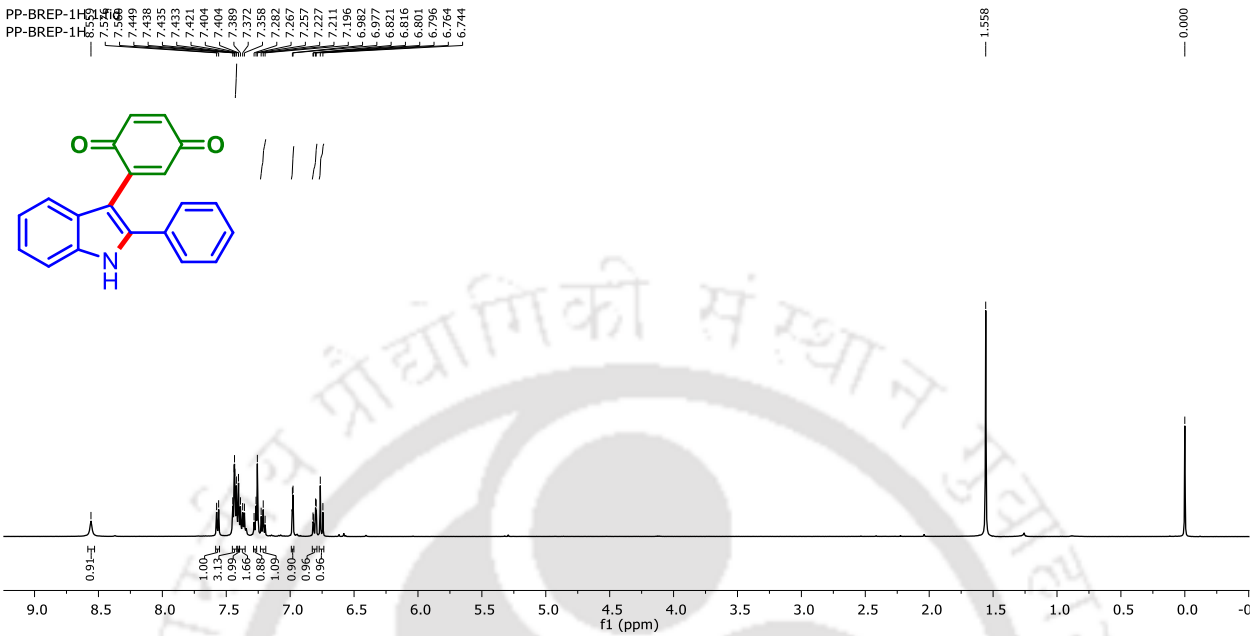

2-(2-Phenyl-1*H*-indol-3-yl)cyclohexa-2,5-diene-1,4-dione (3ar): ^{13}C{^{1}H} NMR ($CDCl_3$, 126 MHz)

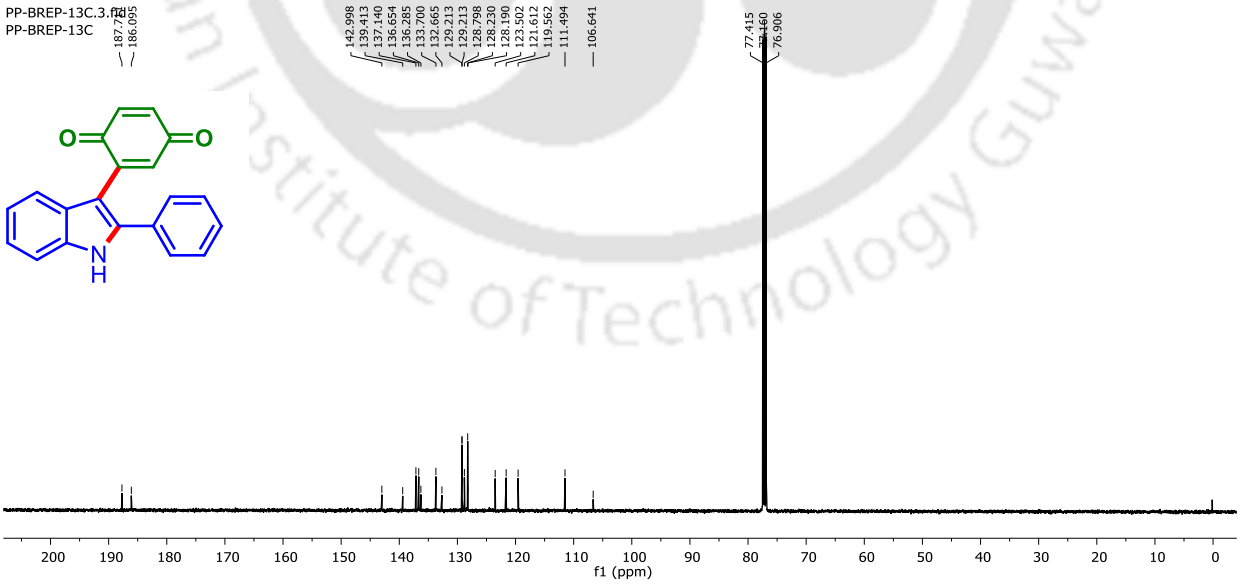

Dearomative Bis-Functionalization of Quinoxalines and Bis-*N*-Arylation of (Benz)imidazoles via Cu(II) Mediated Addition of Boronic Acids

III

Chapter

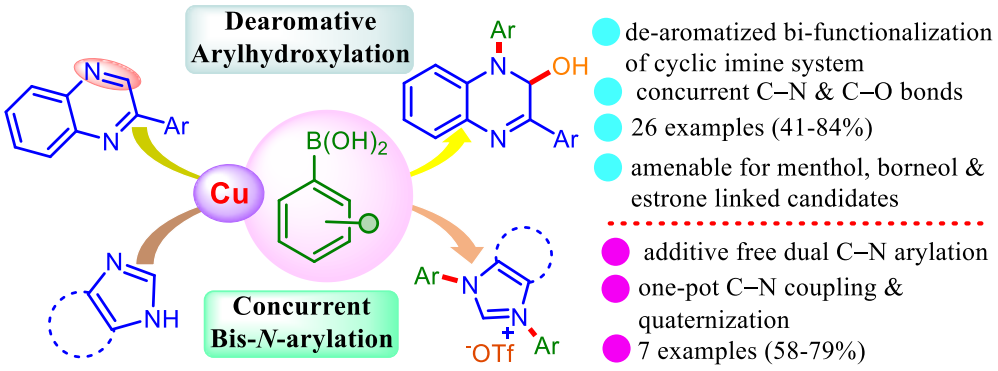

ABSTRACT

A $Cu(OTf)_2$ mediated regioselective de-aromatized aryl-hydroxylation across $C(sp^2)$=N bond of 2-aryl quinoxalines and bis-N-arylation of (benz)imidazoles is developed using aryl boronic acids. For dearomative aryl-hydroxylation, the C-center should be electrophilic (ca. 0.08), N-center nucleophilic (ca. –0.50), and the $C(sp^2)$=N bond should be polarized (Δe = 0.609).

Reference:

Khandelia, T.; Ghosh, S.; Patel, B. K. *Chem. Commun*. **2023**, *59*, 2118.

III.1. Introduction

The concurrent installation of two functional groups across C–C unsaturated bonds has emerged as a straightforward approach to enhance molecular complexity.[1] Significant effort has been devoted to crafting bi-functionalization employing transition metal or photocatalytic approaches.[2] On the other hand a similar bis-functionalization across C(sp^2)=N bond in an aromatic heterocyclic system is far less explored as the addition leads to dearomatization and thus the approach requires sophisticated reaction protocols.[3] In this context, regioselective de-aromatized bis-functionalization of the C(sp^2)=N bond under mild conditions is a challenging and demanding task for synthetic chemists.

The C–C bonds containing compounds are mostly inert and have fewer synthetic values, nevertheless, their utility is boosted through the incorporation of heteroatoms. Among all carbon-heteroatom bond forming reactions, the construction of C–N and C–O bonds have gained much attention due to their prevalence in the structural core of numerous natural products, pharmaceuticals, and polymeric materials.[4]

III.1.1. Importance of Hydroxy Group Containing N-Heterocycles

The hydroxy group containing N-heterocycles are prevalent in numerous biologically important structures. Some of the examples are anti-malarial drug quinine, antifungal and antiviral drugs such as fluconazole and zidovudine, inhibitor of adenosine deaminase, inhibitor of gastric acid secretion, muscarinic antagonist, etc. (Figure III.1.1.1.).

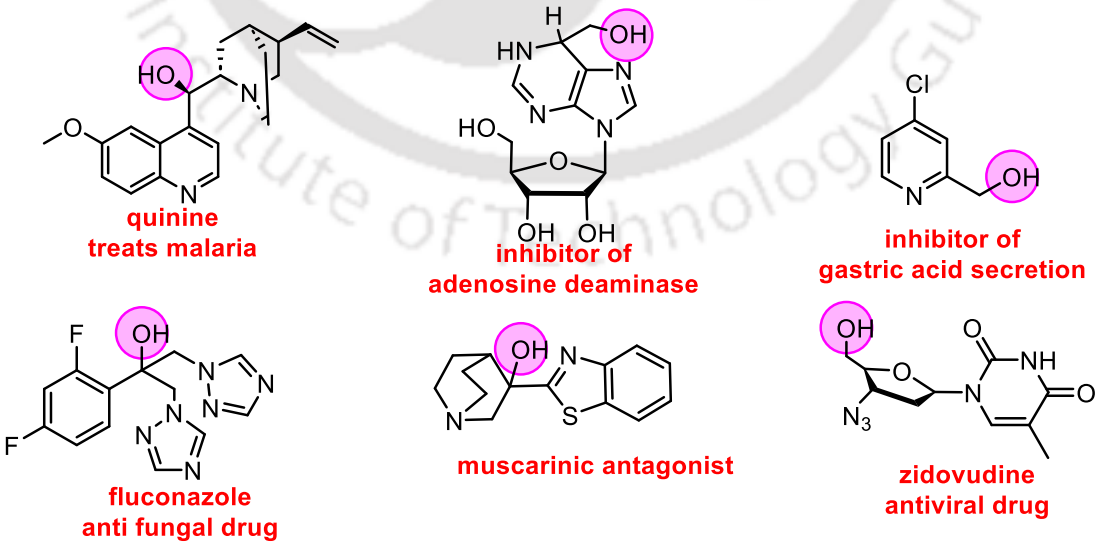

Figure III.1.1.1. *Hydroxy group containing bio-pharmaceuticals*

III.1.2. Preceding Reports of C–N Bond Formation and Reactivity of Boronic Acid

The C–N bonds are constructed via nucleophilic substitutions and transition metal catalyzed cross-coupling reactions.[5] In this context, the transition-metal catalyzed C–N cross-couplings such as Buchwald-Hartwig, Ullmann, and Chan-Evans-Lam (CEL) are well established (Scheme III.1.2.1).[6] But on the downside, to forge such C–N cross-couplings, a free N–H group is inevitable along with the usage of suitable ligands, base and transition metals.

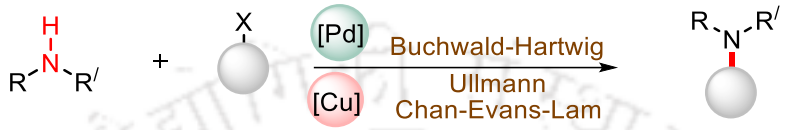

Scheme III.1.2.1. *Conventional C–N coupling reactions*

III.1.2.1. Quaternization of N-Heterocycles Using Boronic Acid

The regioselective C(aryl)–N bond formation across the C(sp^2)=N bond of heteroarenes is an alternative avenue to classical C–N bond forming reactions. In this context, You[7] and Watson[8] *et. al.* independently obtained *N*-arylated (benz)imidazoles and *N*-arylated pyridines respectively, using arylboronic acid under metal-catalyzed conditions, both of which provided quaternized salts without losing their aromaticity (Scheme III.1.2.1.1).

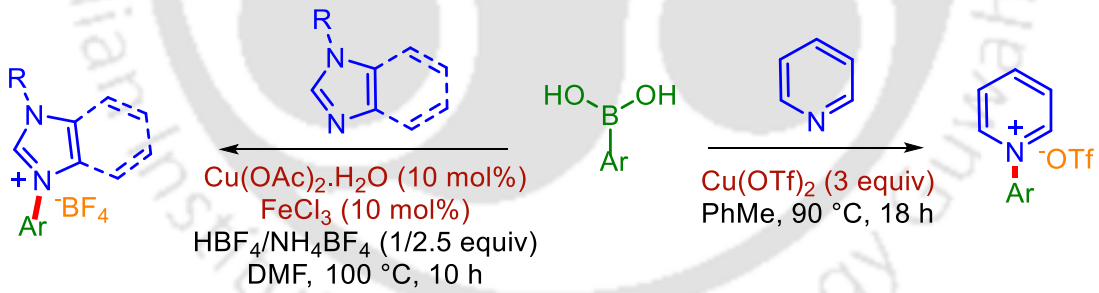

Scheme III.1.2.1.1. *Addition of boronic acid to heteroarenes (N center)*

III.1.2.2. Arylation of N-Heterocycles Using Boronic Acid

N-containing heteroarenes such as quinoline and 2-phenylpyridine upon reaction with arylboronic acids underwent *α*-arylation[9] and *ortho*-arylation[10] through *α*-activation or chelation-assisted strategies using metal catalysts.

In 2010, Baran *et. al.* developed a method for arylation of N-heteroarenes using boronic acids with the usage of $AgNO_3$ and $K_2S_2O_8$ oxidant at room temperature (Scheme III.1.2.2.1).[9b]

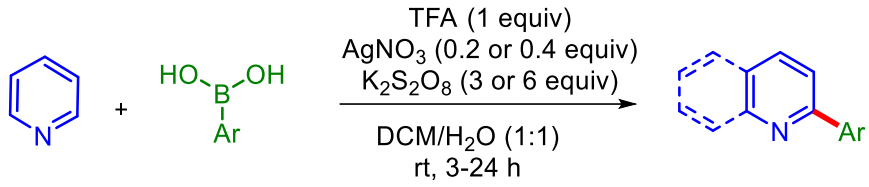

Scheme III.1.2.2.1. *Addition of boronic acid to C center of heteroarenes*

In 2021, Zhang *et. al.* developed a method for α-arylation of N-heteroarenes using (hetero)arylboronic acids under iridium catalysis (Scheme III.1.2.2.2). The process is mediated by H_2O.[9a]

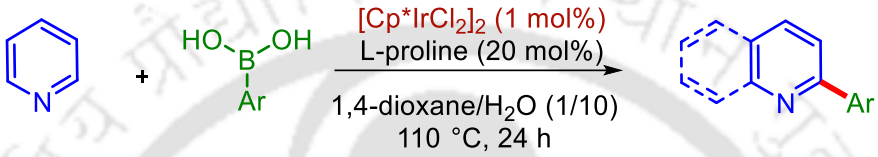

Scheme III.1.2.2.2. *Addition of boronic acid to C center of heteroarenes*

In 2011, Wan *et. al.* reported an oxidatively coupled *ortho* arylation of arenes using boronic acid under Ru(II) catalysis. The process is mediated by molecular O_2 (Scheme III.1.2.2.3).[10a]

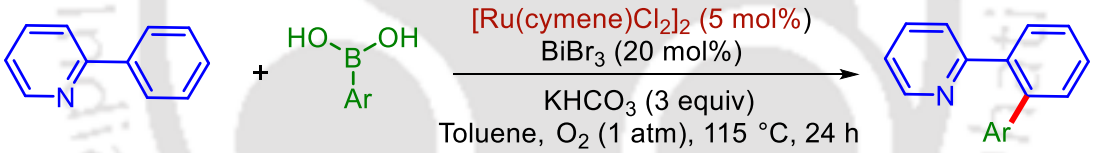

Scheme III.1.2.2.3. *Ortho arylation of arenes using boronic acid*

In 2015, Maheswaran *et. al.* reported *ortho* arylation of 2-phenylpyridine using boronic acid under Ru(II) catalysis. The process was mediated by $PhI(OCOCF_3)_2$ (Scheme III.1.2.2.4).[10b]

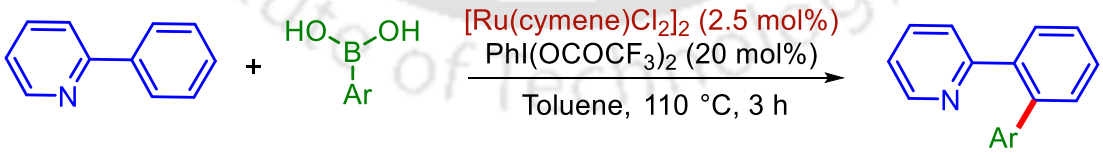

Scheme III.1.2.2.4. *Ortho arylation of 2-phenylpyridine using boronic acid*

III.1.3. Present Strategy for C–N Bond Formation Using Boronic Acid

Quinoxaline is a privileged class of N-containing heterocycles, found in many natural products, pharmaceuticals, and materially relevant functional motifs.[11] Furthermore, N-containing heterocycles have been widely functionalized using 3d–transition metals.[12] Among these, copper-catalyzed or mediated reactions are more sought after due to their low cost and easy availability.[13] Thus, for a substituted quinoxaline (**1**) having two types of C(sp^2)=N bonds, a query arose, which C(sp^2)=N bond will react with boronic acid? Whether it will give N–arylated quaternized salt or add across the C(sp^2)=N bond to provide a bis-functionalized product? With this quest in mind, 2-phenyl quinoxaline (**1a**) was reacted with phenylboronic acid (**2a**) in the presence of 20 mol% $Cu(OTf)_2$ in toluene at 90 °C for 15 h. Unlike imidazole[7] and pyridine[8] the product was not a quarternary salt but a dearomatized aryl-hydroxylated product *viz.* 1,3-diphenyl-1,2-dihydroquinoxalin-2-ol (**3aa**) (Scheme III.1.3.1). When (benz)imidazole **9** was subjected to the standard conditions with boronic acid, bis-arylated quaternized (benz)imidazole **10** was obtained (Scheme III.1.3.1).

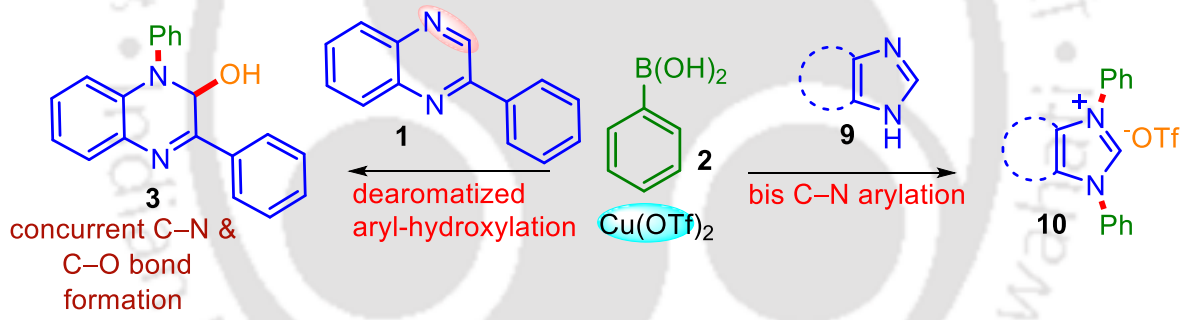

Scheme III.1.3.1. *Present strategy of Cu(II) mediated aryl-hydroxylation across C(sp^2)=N bond of 2-aryl quinoxalines and bis-N-arylation of (benz)imidazoles*

III.2 Optimization of Reaction Conditions

After confirming the structure of **3aa** (by ^1H, ^{13}C NMR, and X-ray crystallographic techniques) and to arrive at the optimal reaction conditions, various reaction parameters were tuned keeping **1a** and **2a** as the model coupling partners (Table III.2.1). At first a series of copper salts *viz.* CuF_2, $CuCl_2$, $Cu(acac)_2$, $CuBr_2$, and $Cu(OAc)_2$ were screened, but none could enhance the yield of **3aa** (Table III.2.1, entries 2-6). A sequential enhancement in $Cu(OTf)_2$ loading from 0.2 to 1.2 equiv, improved the yield of **3aa** from 21% to 84% (Table III.2.1, entries 7-9). However, a further enhancement in $Cu(OTf)_2$ loading to 1.5 and 2 equivalents did

not improve the yield of **3aa** significantly (Table III.2.1, entry 10-11). The use of other solvents *viz.* *o*-xylene, *m*-xylene, 1,2-dichloroethane (DCE), chlorobenzene, 1,2-dichlorobenzene (DCB), tetrahydrofuran (THF), 2,2,2-trifluoroethanol (TFE), and DMSO were all found inferior to toluene (Table III.2.1, entries 12-19). A control reaction in the absence of $Cu(OTf)_2$ yielded no trace of **3aa**, suggesting the crucial role of $Cu(OTf)_2$ in this protocol (Table III.2.1., entry 20). Further, the reaction performed at a higher temperature (100 °C) failed to improve the yield (Table III.2.1, entry 21), while there was no reaction at room temperature (Table III.2.1, entry 22). No noticeable enhancement in the yield was observed by prolonging the reaction time to 20 h (Table III.2.1, entry 23).

The best optimized condition is the use of **1a** (0.35 mmol), **2a** (0.56 mmol), $Cu(OTf)_2$ (1.2 equiv), toluene (1.5 mL), at 90 °C for 15 h.

Table III.2.1. *Optimization of reaction conditions*[a]

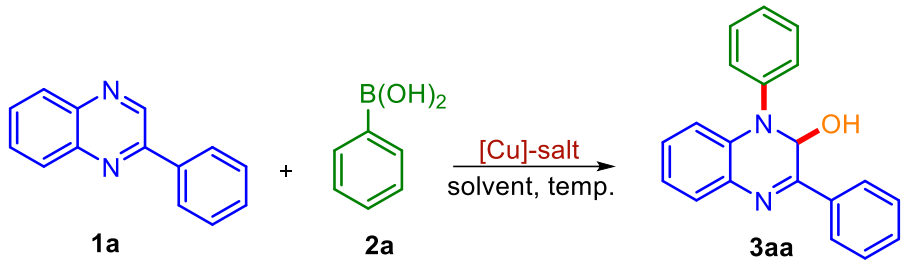

Entry	Cu salt (equiv)	Solvent	Yield of **3aa** (%)[b]
1	$Cu(OTf)_2$ (0.2)	Toluene	21
2	CuF_2 (0.2)	Toluene	13
3	$CuCl_2$ (0.2)	Toluene	nd
4	$Cu(acac)_2$ (0.2)	Toluene	nd
5	$CuBr_2$ (0.2)	Toluene	nd
6	$Cu(OAc)_2$ (0.2)	Toluene	nd
7	$Cu(OTf)_2$ (0.5)	Toluene	35
8	$Cu(OTf)_2$ (1.0)	Toluene	77
9	**$Cu(OTf)_2$ (1.2)**	**Toluene**	**84**
10	$Cu(OTf)_2$ (1.5)	Toluene	86
11	$Cu(OTf)_2$ (2)	Toluene	87
12	$Cu(OTf)_2$ (1.2)	*o*–Xylene	71
13	$Cu(OTf)_2$ (1.2)	*m*–Xylene	70
14	$Cu(OTf)_2$ (1.2)	1,2-DCE	57
15	$Cu(OTf)_2$ (1.2)	PhCl	61
16	$Cu(OTf)_2$ (1.2)	1,2-DCB	64
17	$Cu(OTf)_2$ (1.2)	THF	nd
18	$Cu(OTf)_2$ (1.2)	TFE	nd
19	$Cu(OTf)_2$ (1.2)	DMSO	nd
20	--	Toluene	nd
21[c]	$Cu(OTf)_2$ (1.2)	Toluene	84
22[d]	$Cu(OTf)_2$ (1.2)	Toluene	nd
23[e]	$Cu(OTf)_2$ (1.2)	Toluene	85

[a]Reaction Conditions: **1a** (0.35 mmol), **2a** (0.56 mmol), copper salt, solvent (1.5 mL), 90 °C, 15h. [b]Isolated yield. [c]Reaction carried out at 100 °C. [d]Reaction carried out at rt. [e]20 h. nd = not detected.

III.3. Substrate Scope of the Protocol

III.3.1. 2-Aryl Quinoxaline and Boronic Acid Derivatives

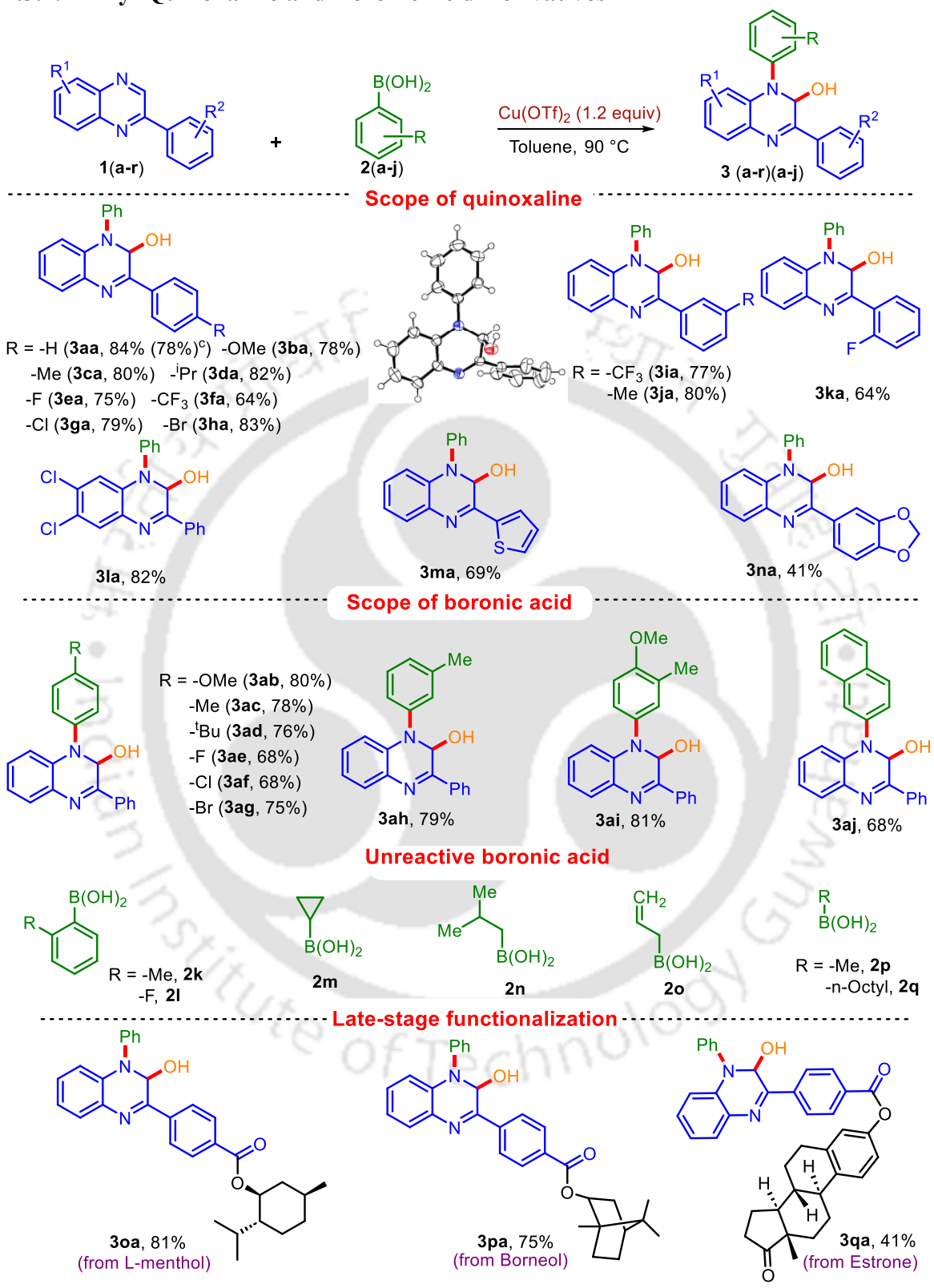

[a]Reaction conditions: **1** (0.35 mmol), **2** (0.56 mmol), $Cu(OTf)_2$ (1.2 equiv), toluene (1.5 mL) at 90 °C for 15 h. [b]Isolated yield. [c]Reaction performed on a 1 mmol scale.

Scheme III.3.1.1. *Substrate scope of 2-aryl quinoxaline and boronic acid*[a, b]

After arriving at the optimized reaction conditions, the scope and generality of this protocol towards various 2-(hetero)arylquinoxalines (**1**) and arylboronic acids (**2**) were examined and the results are summarized in Scheme III.3.1.1. An array of electronically diverse substituents having electron-donating *p*-OMe (**1b**), *p*-Me (**1c**), *p*-^{i}Pr (**1d**), *m*-Me (**1j**), and withdrawing *p*-F (**1e**), *p*-CF_3 (**1f**), *p*-Cl (**1g**), *p*-Br (**1h**), *m*-CF_3 (**1i**), *o*-F (**1k**) on the aryl ring of 2-aryl quinoxalines and 6,7-dichloro (**1l**) on the quinoxaline, all reacted well with phenylboronic acid (**2a**) to furnish the corresponding bis-adducts **3ba-3la** in good to moderate yields (64–84%) (Scheme III.3.1.1). The 2-thiophenyl (**1m**) and 2-benzodioxolyl (**1n**) containing quinoxalines successfully reacted with phenylboronic acid (**2a**) to give the addition product **3ma** (69%) and **3na** (41%) respectively in moderate yields. Interestingly, 2-phenylquinoxalines having natural product pendants *viz.* L-menthol (**1o**), borneol (**1p**) and estrone (**1q**) also underwent successful aryl-hydroxylation giving products **3oa** (81%), **3pa** (75%) and **3qa** (41%) respectively. A one mmol scale synthesis of **3aa** in 78% isolated yield demonstrates the scalability of the protocol (Scheme III.3.1.1).

Next, the scope of various phenylboronic acids was examined. An array of electronically varied substituents *p*-OMe (**2b**), *p*-Me (**2c**), *p*-^{t}Bu (**2d**), *p*-F (**2e**), *p*-Cl (**2f**), *p*-Br (**2g**), *m*-Me (**2h**), and di-substituted *p*-OMe, *m*-Me (**2i**) on the aryl ring of phenylboronic acids, all reacted competently under the reaction protocol to deliver aryl-hydroxylated products (**3ab-3ai**) in good yields (68–81%) (Scheme III.3.1.1). Further, the reaction of 2-naphthaleneboronic acid (**2j**) with (**1a**) delivered the corresponding adduct **3aj** in moderate yield (68%). However, *o*-substituted boronic acids viz. *o*-Me (**2k**) and *o*-F (**2l**) were found to be unreactive, this may be due to steric hindrance. In this protocol, aliphatic boronic acids (**2m-2q**) also failed to respond.

III.3.2. Quinoxaline Analogues and Phenylboronic Acid

Thereafter, a query arises whether a similar addition across C(sp^2)=N bonds having a diverse steric and electronic environment in quinoxaline analogues, 2-phenylquinazoline (**4**), quinoxaline (**5**), 2-methylquinoxaline (**6**) (Scheme III.3.2.1) will occur?

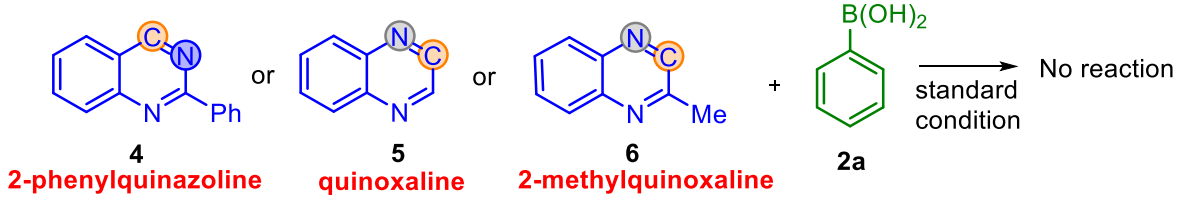

Scheme III.3.2.1. *Reaction of quinoxaline analogues*

Under the standard reaction conditions, 2-phenylquinazoline (**4**), quinoxaline (**5**), 2-methylquinoxaline (**6**), neither gave any addition nor any quaternized product (Scheme III.3.2.1).

III.3.2.1 Atomic Charge Distribution Calculations of 2-Phenylquinoxaline and Quinoxaline Analogues

To find out the reason for the failure, atomic charge distribution calculations (6-31G+ (d, p) basis set) on substrates **1a** and (**4** to **6**) were carried out (Scheme III.3.2.1.1). From the atomic charge distribution pattern of **1a**, the sterically less hindered C(sp^2)=N bond has a Mulliken charge of –0.528 and 0.081 respectively at the N and C atoms, with a charge difference of 0.609 (Scheme III.3.2.1.1).

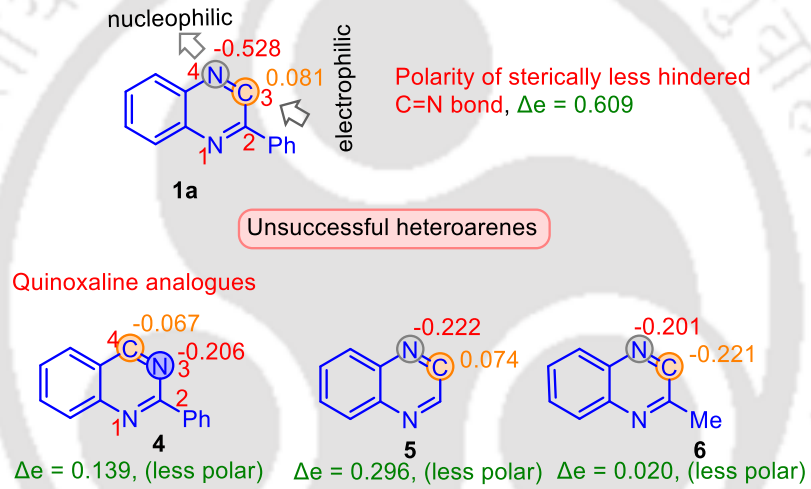

Scheme III.3.2.1.1 *Atomic charge distribution over 2-phenylquinoxaline (**1a**) and other heteroarenes.*

Thus, the essential requirement is, the C-center should be electrophilic (*ca.* 0.08), N-center nucleophilic (*ca.* –0.50), and the C(sp^2)=N bond should be sufficiently polarized (Δe = 0.609) which is not the case with substrates (**4**–**6**). For 2-phenylquinazoline (**4**), the N3–C4 double bond is found to be less polar (Δe = 0.139), with N3 being less nucleophilic (–0.206) and C4-center not so electrophilic (–0.067) as seen from their calculated Mulliken charge. Also, the C2 phenyl ring prevents the N-atom from binding to the metal (steric hindrance). Similarly, for quinoxaline (**5**) and 2-methylquinoxaline (**6**), the designated C(sp^2)=N bond is less polar (Δe = 0.296 and Δe = 0.020 respectively) and is electronically not favourable (Scheme III.3.2.1.1).

III.3.3. Isoquinoline, Quinoline and Phenylboronic Acid

Under the optimized protocol, isoquinoline (**7**) gave a quaternized product **7'** (81%), while quinoline (**8**) provided a C–2 phenylated product **8'** (66%) on reaction with phenylboronic acid (**2a**) (Scheme III.3.3.1). The pyridine is known to quaternize under similar conditions (Scheme III.3.3.1).[8]

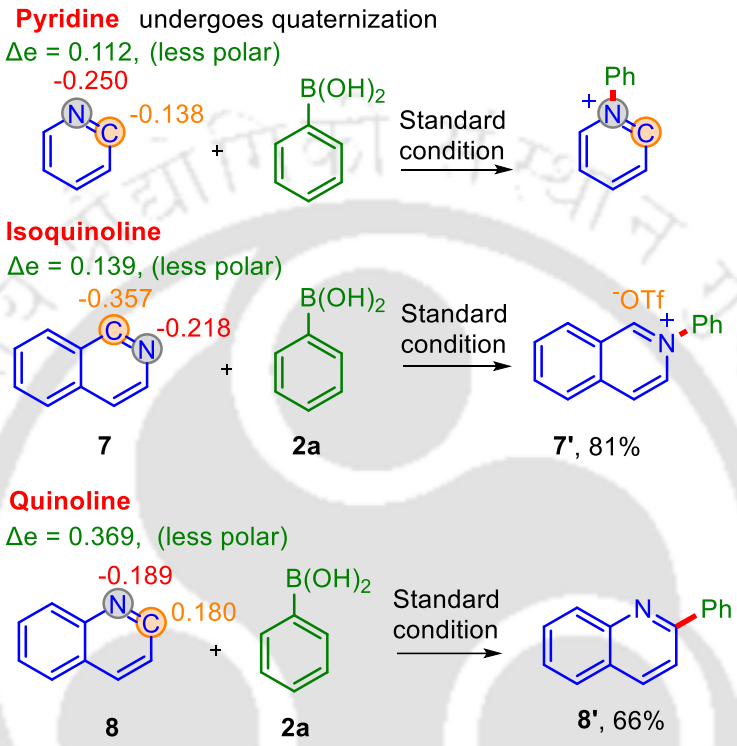

Scheme III.3.3.1. *Atomic charge distribution and reactivity of pyridine, isoquinoline and quinoline*

III.3.3.1 Atomic Charge Distribution Calculations of Pyridine, Isoquinoline and Quinoline

The electronic environment of pyridine (Δe = 0.112, Mulliken charge of –0.250 at N and –0.138 at C) (Scheme III.3.3.1.1) is very similar to isoquinoline (**7**) (Δe = 0.139, Mulliken charge of –0.218 at N and –0.357 at C). While quinoline **8** has a highly electrophilic C center (0.180) for undergoing quaternization and a less polar C(sp^2)=N bond (Δe = 0.369) compared to **1a** to undergo bis-functionalization (Scheme III.3.3.1).

After these calulations we have a reasonable understanding of the failure to undergo addition across C(sp^2)=N bond in other six or fused six-membered mono or di-aza heterocycles (**4**–**8**).

III.3.4. (Benz)imidazole and Phenylboronic Acid Derivatives

Next, the query arises whether five-membered di-aza heterocycles *viz.* benzimidazole and imidazole systems (**9a-d**) would undergo addition, mono-arylation or bis-arylated quaternization? When benzimidazole (**9a-b**) and imidazole (**9c-d**) were subjected to the present conditions all provided bis-arylated quaternized products **10**(**a-d**)(**a-j**) (Scheme III.3.4.2.1).

III.3.4.1 Atomic Charge Distribution Calculations of Benzimidazole and Imidazole

The electronic charge distribution indicates the possibility of aryl-hydroxylation, but the effective delocalization of the adjacent N-atom lone pair makes the system more stable because of resonance (Scheme III.3.4.1.1).

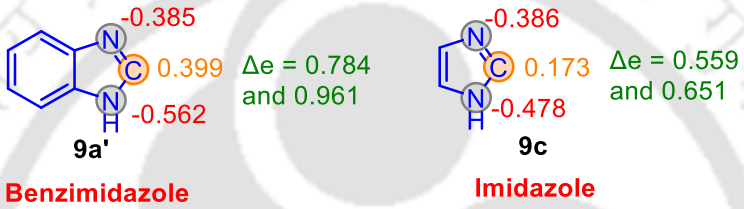

Scheme III.3.4.1.1. *Atomic charge distribution of benzimidazole and imidazole*

III.3.4.2 Substrate Scope of (Benz)Imidazole and Phenylboronic Acid

The bis-arylated product was obtained even when 1 equivalent of phenylboronic acid (**2a**) was used without giving any mono-arylated product. Theoretically, a minimum of two equivalents of **2a** is needed, therefore 2.5 equivalent was used for subsequent reactions. The scope was further extended to benzimidazoles having 5-Me (**9a**) and 5-Cl (**9b**) substituents, both of which reacted with **2a** to deliver the diarylated adducts **10aa** and **10ba** in 64% and 58% yields respectively (Scheme III.3.4.2.1). The structure of the product **10aa** has been confirmed by XRD analysis (Scheme III.3.4.2.1). Further, when imidazole (**9c**) was reacted with **2a**, it afforded di arylated product **10ca** (68% yield). When the free N–H site of the imidazole was protected as an N-vinyl derivative (**9d**), a mono N-arylated product was obtained to provide quaternized adduct **10da** in 79% yield. When imidazole was reacted with other boronic acids such as 2-naphthaleneboronic acid (**2j**), *p*-OMe (**2b**) and *p*-Cl (**2f**) phenylboronic acids, all provided diarylated C–N adducts **10cj** (68%), **10cb** (66%) and **10cf** (68%) respectively. This reaction is also easily scalable to one mmol for the synthesis of **10ca** giving 67% of the isolated yield (Scheme III.3.4.2.1).

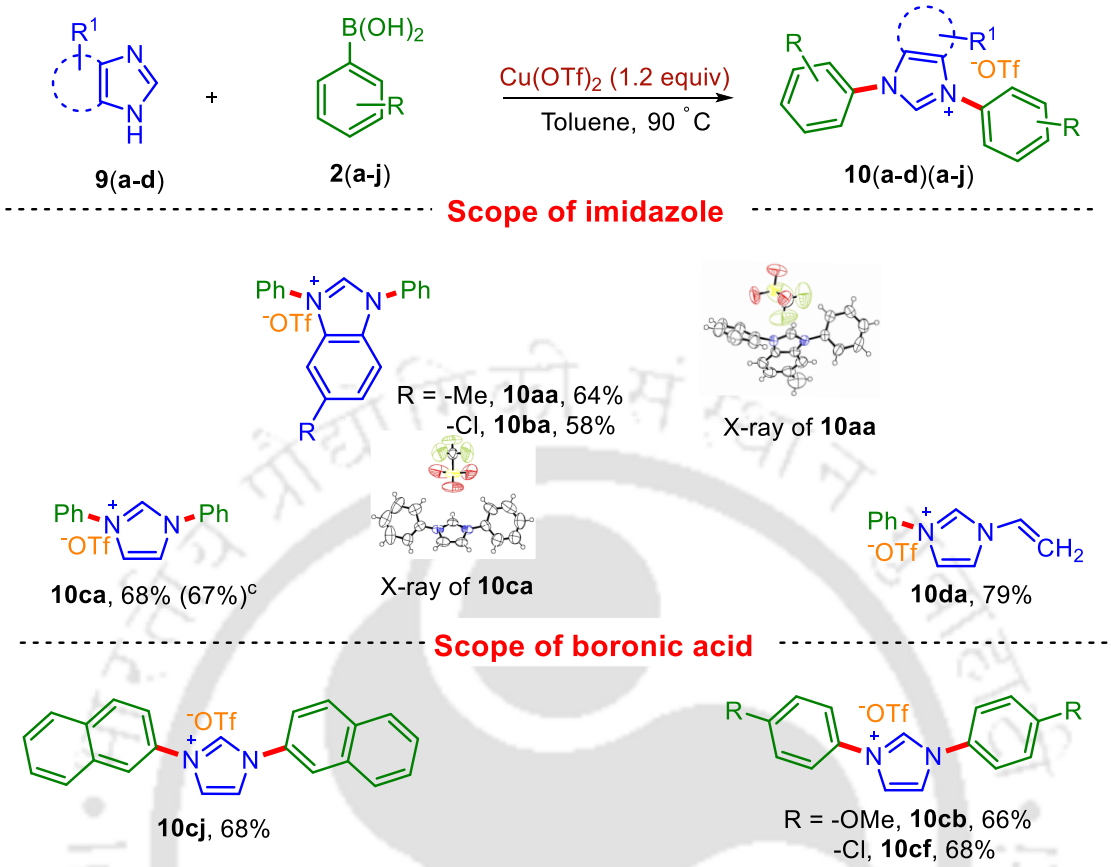

[a]Reaction conditions: **9** (0.35 mmol), **2** (0.88 mmol), $Cu(OTf)_2$ (1.2 equiv), toluene (1.5 mL) at 90 °C for 15 h. [b]Isolated yield. [c]Reaction performed on a 1 mmol scale.

Scheme III.3.4.2.1. *Substrate scope of (benz)imidazole and phenylboronic acid*[a, b]

III.4. Study of Mechanistic pathway

III.4.1. Control Experiments for Aryl-hydroxylation

To understand the nature of the reaction mechanism, a few control experiments were performed.

(a) Radical Scavenging Experiment

A standard reaction (between **1a** and **2a**) in the presence of radical scavengers TEMPO, BHT and DPE (2 equiv) did not affect the yield of product **3aa**, thereby ruling out any possibilities of a radical path (Scheme III.4.1.1)

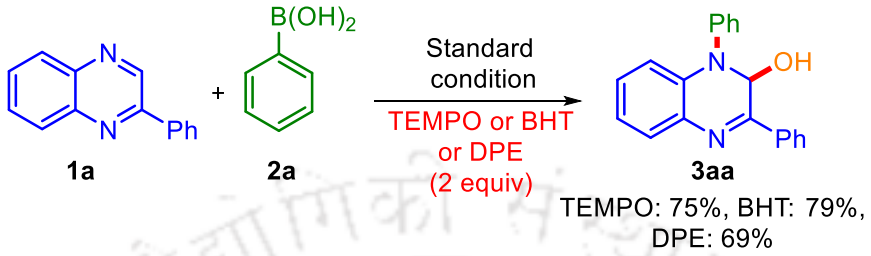

Scheme III.4.1.1. *Radical Scavenging Experiment*

(b) H/D Exchange Experiment

No deuterium exchange was observed at the C3 position of **1a** under the standard condition in the presence of D_2O (5 equiv) and toluene-d_8 (5 equiv), with and without phenylboronic acid (**2a**). This suggests the non-involvement of C3–H bond in the initial activation step; and suggests the possibility of a concerted path (Scheme III.4.1.2).

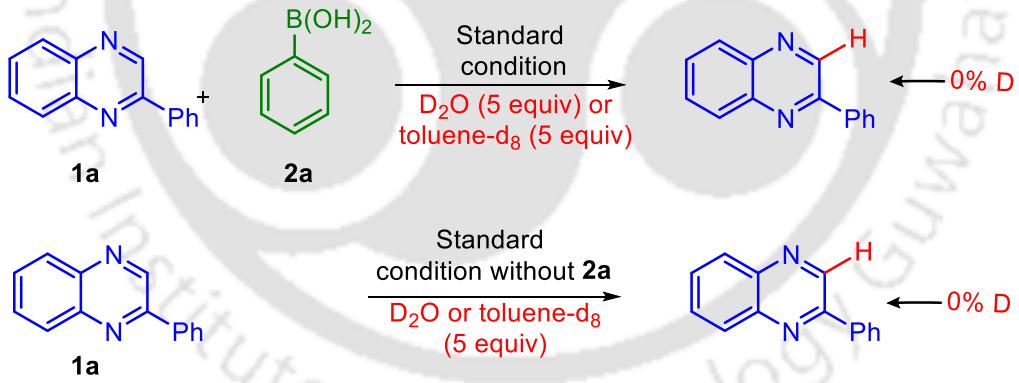

Scheme III.4.1.2. *H/D Exchange experiment*

(c) Experiment for Investigation of the Source of Hydroxyl Oxygen

- **Study of Effect of Addition of External Water**

The addition of external water was found to have a deteriorating effect (Scheme III.4.1.3).

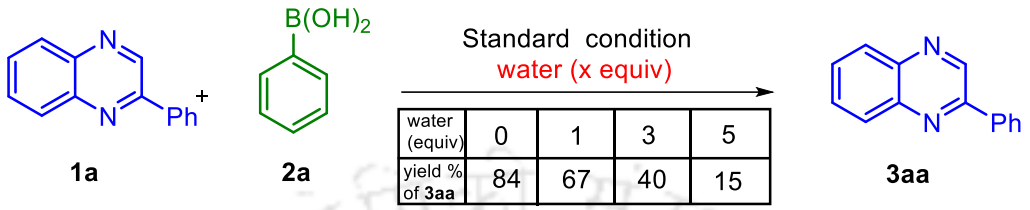

water (equiv)	0	1	3	5
yield % of **3aa**	84	67	40	15

Scheme III.4.1.3. *Study of effect of addition of external water*

- **Reaction Under Dry Conditions**

The reaction was unaffected using purified boronic acid and anhydrous toluene under an argon atmosphere (Scheme III.4.1.4).

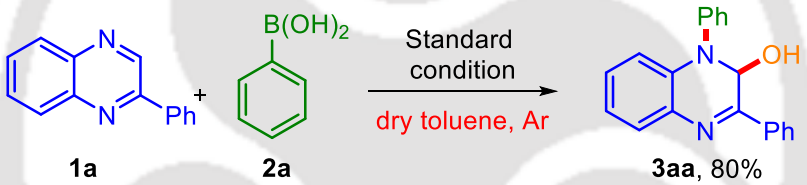

Scheme III.4.1.4. *Reaction under dry conditions*

Thus, moisture from the solvent and oxygen or moisture from the atmosphere is not the source of hydroxyl oxygen.

- **Reaction with Phenyltrifluoroborate**

Three equivalents of H_2O are released upon trimerization of boronic acid (**2a**) when heated in toluene which may be the source of –OH group.[14] However, in place of phenylboronic acid (**2a**) when phenyltrifluoroborate (**2a'**) was used (which does not trimerize and release water), it reacted giving a hydroxyarylated product (**3aa**) in a similar yield in an anhydrous condition and under an inert atmosphere (Scheme III.4.1.5). Thus, the hydroxyl group is not originating from phenylboronic acid, but from some other source.

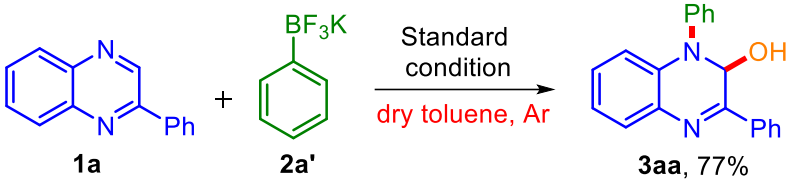

Scheme III.4.1.5. *Reaction with phenyltrifluoroborate*

➢ **Thermogravimetric Analysis (TGA)**

The only other possible source of –OH group might be from Cu–bound H_2O. The thermogravimetric analysis (TGA) of the humid air-exposed $Cu(OTf)_2$ showed the presence of H_2O in the metal salt (Figure III.4.1.1) which is the source of –OH group.

The thermogravimetric analysis (TGA) of the air exposed $Cu(OTf)_2$ salt was conducted from 29 ° to 400 °C to ensure the presence of absorbed H_2O molecules in the metal salt (Figure III.4.1.1). The TGA curve displays a single weight loss of 9% from 80 °C to 143 °C. This weight loss suggests the presence of two molecules of water per formula unit of $Cu(OTf)_2$.

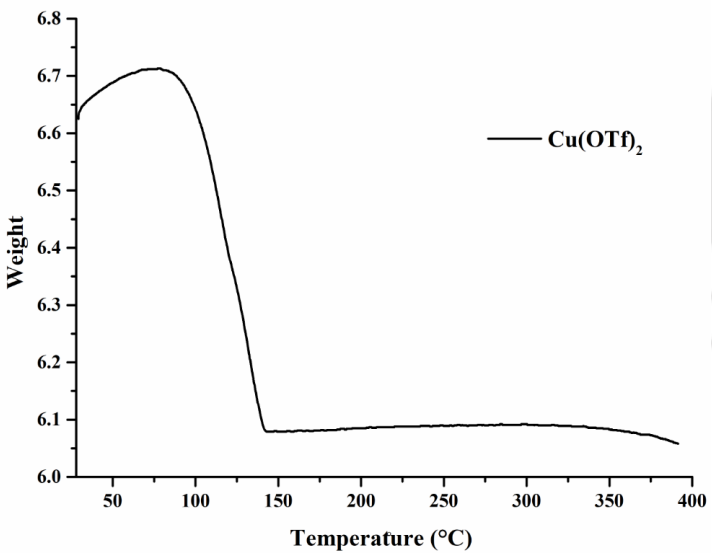

Figure *III.4.1.1.* TGA curve of $Cu(OTf)_2$

(d) Detection of Intermediate in HRMS

In order to detect the intermediates, the crude reaction aliquot (2 h) of **3aa** was subjected to HRMS analysis. Two of the intermediates **A** and **B** (Scheme III.4.2.1) was detected during the analysis (Figure III.4.1.2 and Figure III.4.1.3).

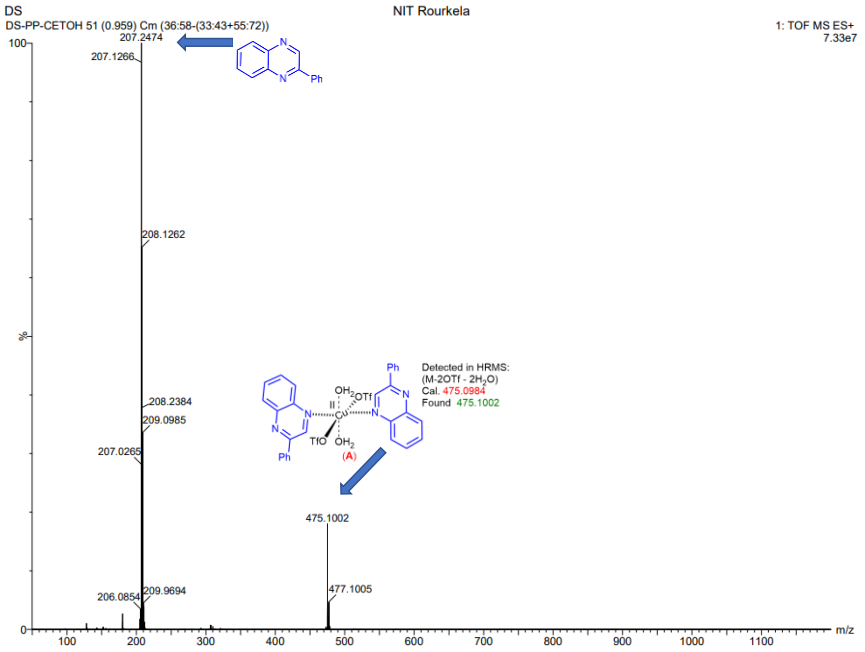

Figure III.4.1.2. *Detection of complex* ***A*** *in HRMS*

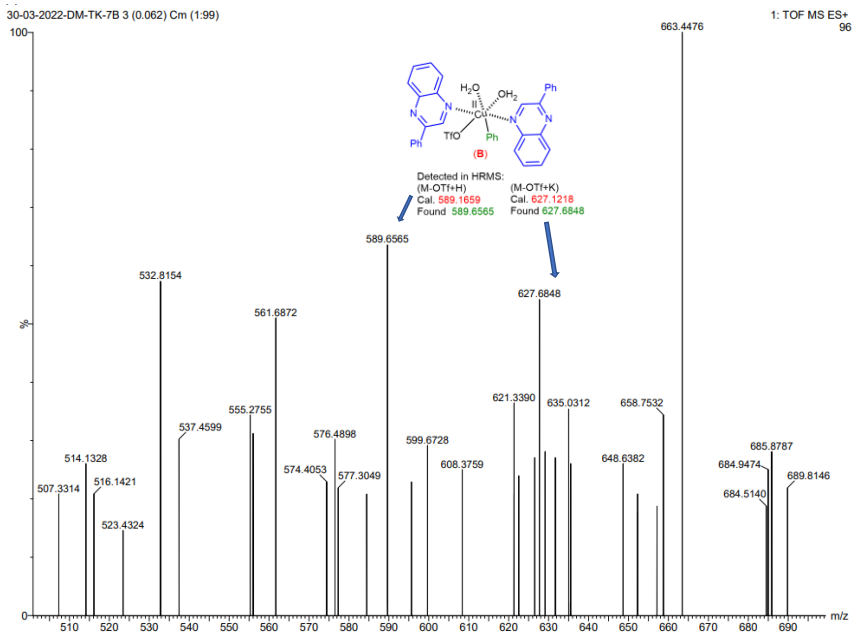

Figure III.4.1.3. *Detection of complex* ***B*** *in HRMS*

III.4.2. Mechanism of Aryl-hydroxylation

Based on previous reports,[15] results obtained from the control reactions in section III.4.1 and high-resolution mass spectrometry (HRMS) analysis of the reaction aliquots, a plausible mechanism is proposed (Scheme III.4.2.1). Initially, $Cu(OTf)_2$ forms a complex **A** with 2-phenylquinoxaline (detected by HRMS). Trans-metallation of the phenyl ring of the boronic acid with **A** resulted in another intermediate (**B**) (detected by HRMS). The Cu(II) complex (**B**) is oxidized to Cu(III) by $Cu(OTf)_2$ via disproportionation reaction to give **C**. This is followed by migration of the Cu bound –OH group to the C3 position of **1a** with the formation of the Cu–N bond to give **D**. Next, reductive elimination of **D** offers the final product **3aa** with the release of reduced species **E**.

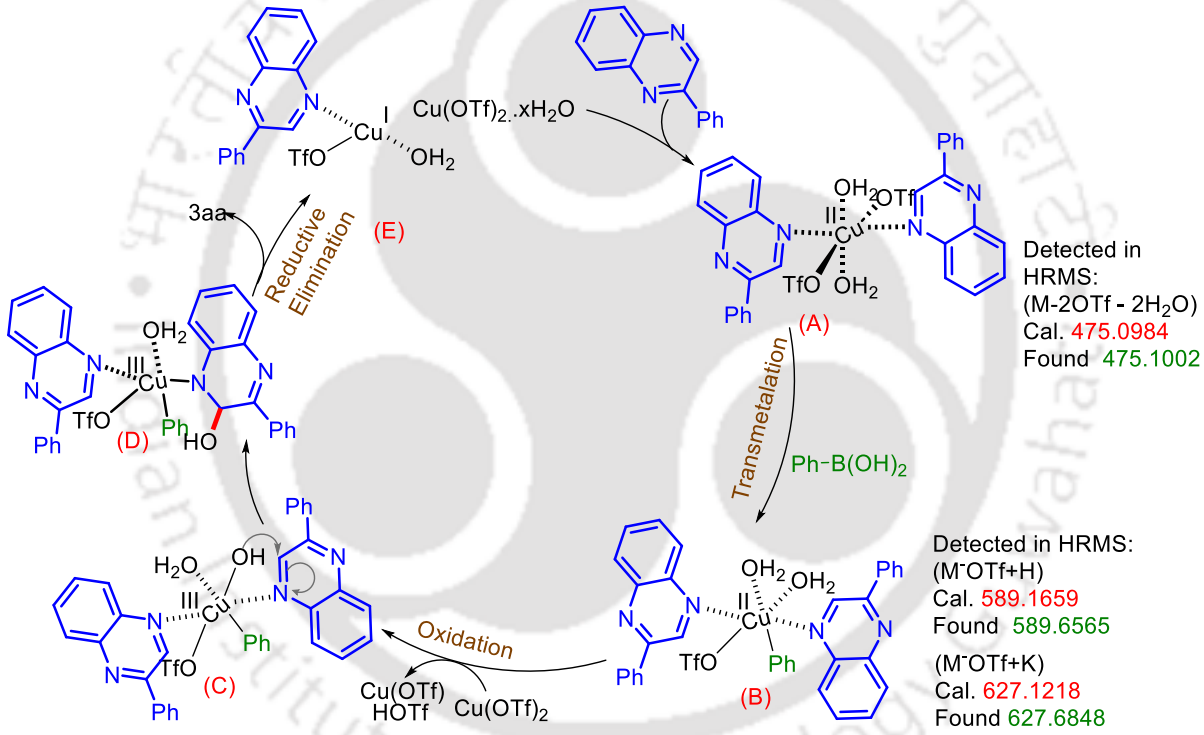

Scheme III.4.2.1. *plausible mechanism of aryl-hydroxylation*

III.4.3. Mechanism of Bis-*N*-Arylation of (Benz)imidazoles

The mechanism for the formation of **10** is explained which involves transmetallation, coordination, oxidation and reductive elimination where Chan-Evans-Lam (CEL) reaction delivers the N-arylated (benz)imidazole (Scheme III.4.3.1).

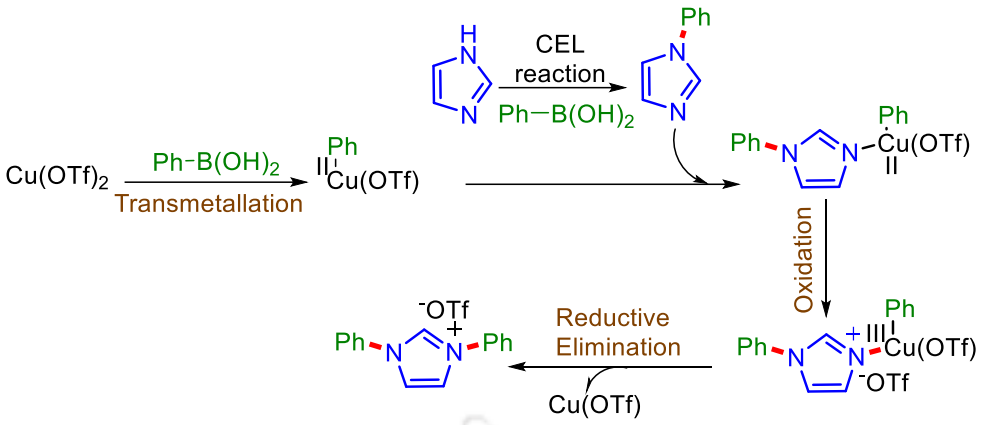

Scheme III.4.3.1. *plausible mechanism of bis-N-arylation of (benz)imidazoles*

III.5. Post-synthetic Modification

The synthetic utility of the protocol was demonstrated by subjecting **3aa** and **10ca** to further reactions. The C–OH group of **3aa** can be oxidized using $AgNO_3$/ $K_2S_2O_8$ to deliver amide **11** in good yield (79%) (Scheme III.5.1).[16] Also, modification of **10ca** upon treatment with diphenylacetylene under ruthenium catalysis offered a dual C–H/C–H annulated product **12** (89%) (Scheme III.5.1).[17]

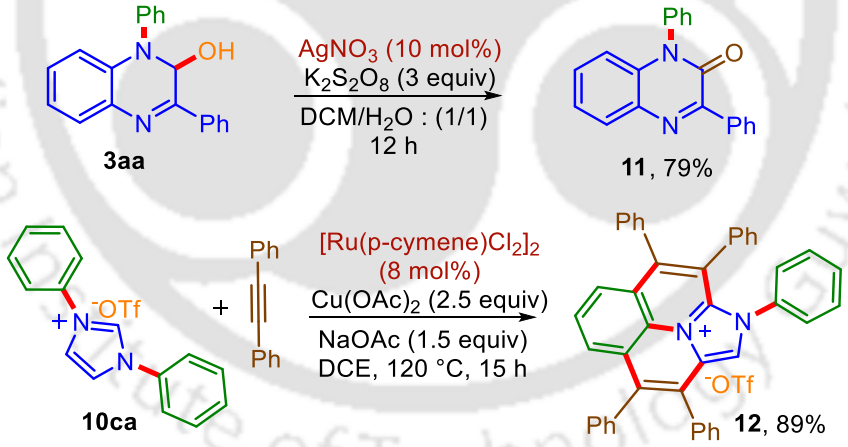

Scheme III.5.1. *Post-synthetic modification. Yield refers to the isolated product.*

III.6. Conclusion

In conclusion, this work presents a $Cu(OTf)_2$ mediated addition of phenylboronic acid to C(sp^2)=N bond embedded in 2-aryl quinoxaline to deliver dearomatized bifunctionalized (hydroxyarylated) quinoxalines. The essential requirement for aryl-hydroxylation is that the C(sp^2)=N bond should be sufficiently polarized (Δe = 0.609) (C-center electrophilic (*ca.* 0.08),

N-center nucleophilic (*ca.* −0.50) and sterically unhindered. Under similar conditions, (benz)imidazole undergo *bis*-N-arylation. Mechanistic investigation indicates copper bound aryl and –OH group addition to the selective C=N bond.

III.7. Experimental Section

III.7.1. General Information and Instrumentation

All chemicals were obtained from commercial sources and were used without further purification. The starting material **1** was synthesized according to previously described methods.[18] Reactions were monitored via TLC, prepared using silica gel 60 F_{254} (0.25 mm), and were detected under UV light at 254 nm. For chromatography, separation was carried out using 60−120 mesh-sized silica gel. Ethyl acetate/ hexane and methanol/ DCM mixtures were used as the eluent. ^{1}H, ^{13}C, and ^{19}F NMR spectra were recorded in 600, 500, and 400 MHz NMR in deuterated solvents, and the chemical shifts (δ) are given in ppm. The ^{1}H spectra were referenced to TMS (0 ppm) for $CDCl_3$ and H_2O in DMSO-d_6 (3.3 ppm) for DMSO-d_6; for ^{13}C $CDCl_3$ (77.16 ppm) and for DMSO-d_6 (39.5 ppm). IR spectra were recorded neat using an FT-IR spectrometer. HRMS was recorded using ESI (Q-TOF type mass analyzer) in positive modes.

III.7.2. General Procedure

III.7.2.1. General Procedure for the Synthesis of 3aa

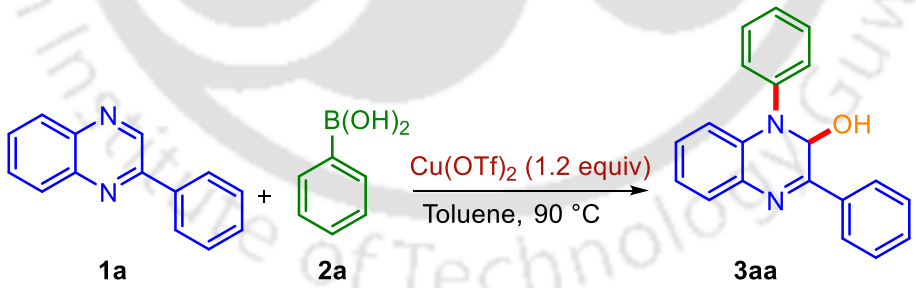

An oven-dried 5 mL round-bottom flask was charged with 2-phenylquinoxaline (**1a)** (0.35 mmol, 72 mg), phenylboronic acid **2a** (0.56 mmol, 68 mg), $Cu(OTf)_2$ (1.2 equiv, 0.42 mmol, 152 mg), a magnetic stir bar in toluene (1.5 mL) and was heated at 90 °C for 15 h. The progress of the reaction was monitored via TLC. After completion of the reaction, the solvent was removed by rotary evaporation. The reaction mixture was then mixed with water (10 mL) and extracted with ethyl acetate (2 × 15 mL). The organic layer was dried over anhydrous sodium

sulfate and was evaporated under reduced pressure. The residue so obtained was purified over column chromatography by eluting with hexane: ethyl acetate (96:4) mixture to afford the desired product **3aa** as yellow solids in 84% yields (88 mg).

III.7.2.2. Procedure for the Synthesis of 3aa in 1mmol Scale

An oven-dried 10 mL round-bottom flask was charged with 2-phenylquinoxaline (**1a)** (1 mmol, 206 mg), phenylboronic acid **2a** (1.6 mmol, 193.6 mg), $Cu(OTf)_2$ (1.2 equiv, 1.2 mmol, 434 mg), a magnetic stir bar in toluene (2 mL) and was heated at 90 °C for 15 h. The progress of the reaction was monitored via TLC. After completion of the reaction, the solvent was removed by rotary evaporation. The reaction mixture was then mixed with water (10 mL) and extracted with ethyl acetate (2 × 15 mL). The organic layer was dried over anhydrous sodium sulfate and was evaporated under reduced pressure. The residue so obtained was purified over column chromatography by eluting with hexane: ethyl acetate (96:4) mixture to afford the desired product **3aa** as yellow solids in 78% yields (234 mg).

III.7.2.3. Procedure for the Synthesis of 7'

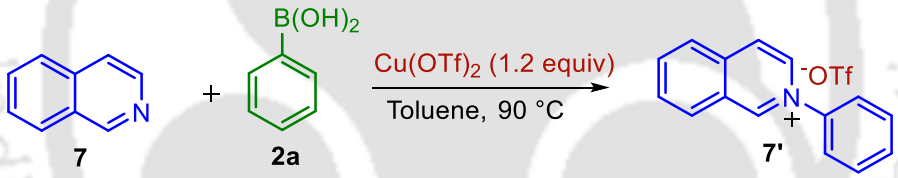

An oven-dried 5 mL round-bottom flask was charged with isoquinoline (**7**) (0.35 mmol, 45 mg), phenylboronic acid **2a** (0.88 mmol, 68 mg), $Cu(OTf)_2$ (1.2 equiv, 0.42 mmol, 152 mg), and a magnetic stir bar in toluene (1.5 mL) and was heated at 90 °C for 15 h. The progress of the reaction was monitored via TLC. After completion of the reaction, the solvent was removed by rotary evaporation. The reaction mixture was then purified over column chromatography by eluting with DCM: Methanol (95: 5) mixtures to afford the product **7'** as brown gummy solid in 81% yield.

III.7.2.4. Procedure for the Synthesis of 8'

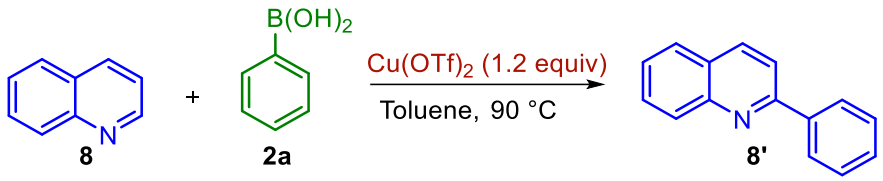

An oven-dried 5 mL round-bottom flask was charged with quinoline (**8**) (1.05 mmol, 135 mg), phenylboronic acid **2a** (0.56 mmol, 68 mg), $Cu(OTf)_2$ (1.2 equiv, 0.42 mmol, 152 mg), and a magnetic stir bar in toluene (1.5 mL) and was heated at 90 °C for 15 h. The progress of the reaction was monitored via TLC. After completion of the reaction, the solvent was removed by rotary evaporation. The reaction mixture was then mixed with water (10 mL) and extracted with ethyl acetate (2 × 15 mL). The organic layer was dried over anhydrous sodium sulfate and was evaporated under reduced pressure. The residue so obtained was purified over column chromatography by eluting with hexane: ethyl acetate (97:3) mixture to afford the product **8'** as white solid in 66% yield.

III.7.2.5. General Procedure for the Synthesis of 10

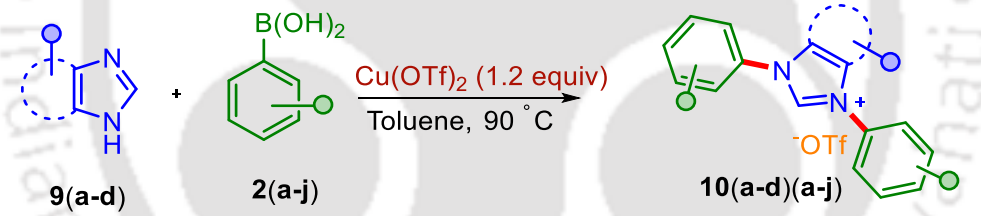

An oven-dried 5 mL round-bottom flask was charged with benzimidazole **9 a–b** (0.35 mmol) or imidazole **9 c–d** (0.35 mmol), phenylboronic acid **2a–j** (0.88 mmol), $Cu(OTf)_2$ (1.2 equiv, 0.42 mmol), and a magnetic stir bar in toluene (1.5 mL) and was heated at 90 °C for 15 h. The progress of the reaction was monitored via TLC. After completion of the reaction, the solvent was removed by rotary evaporation. The reaction mixture was then purified over column chromatography by eluting with DCM: Methanol (95: 5) mixtures to afford the desired products [**10(a–d)(a–j)**] as white and light brown solids in 58%–79% yields.

III.7.2.6. Procedure for the Synthesis of 10ca in 1 mmol Scale

An oven-dried 10 mL round-bottom flask was charged with imidazole **9c** (1 mmol, 68 mg) phenylboronic acid **2a** (2.5 mmol, 303 mg), $Cu(OTf)_2$ (1.2 equiv, 1.2 mmol, 434 mg), and a magnetic stir bar in toluene (2 mL) and was heated at 90 °C for 15 h. The progress of the

reaction was monitored via TLC. After completion of the reaction, the solvent was removed by rotary evaporation. The reaction mixture was then purified over column chromatography by eluting with DCM: Methanol (95: 5) mixture to afford the desired product **10ca** as white solid in 67% yield (248 mg).

III.7.2.7. Procedure for the Synthesis of 11

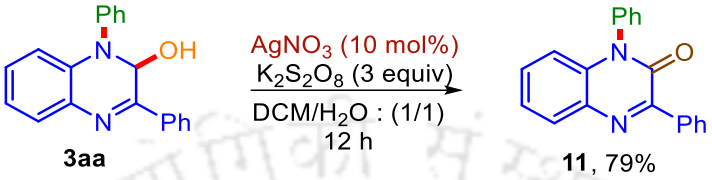

An oven-dried 5 mL round-bottom flask was charged with **3aa** (0.2 mmol, 60 mg), $AgNO_3$ (10 mol%, 3 mg), $K_2S_2O_8$ (3 equiv, 162 mg) and a magnetic stir bar in DCM/H_2O (1:1) (1.5 mL) and was stirred at rt for 12 h. The progress of the reaction was monitored via TLC. After completion of the reaction, the solvent was removed by rotary evaporation. The reaction mixture was then mixed with water (10 mL) and extracted with ethyl acetate (2 × 15 mL). The organic layer was dried over anhydrous sodium sulfate and was evaporated under reduced pressure. The residue so obtained was purified over column chromatography by eluting with hexane: ethyl acetate (98:2) mixture to afford the product **11** as white solid in 79% yield (47 mg).

III.7.2.8. Procedure for the Synthesis of 12

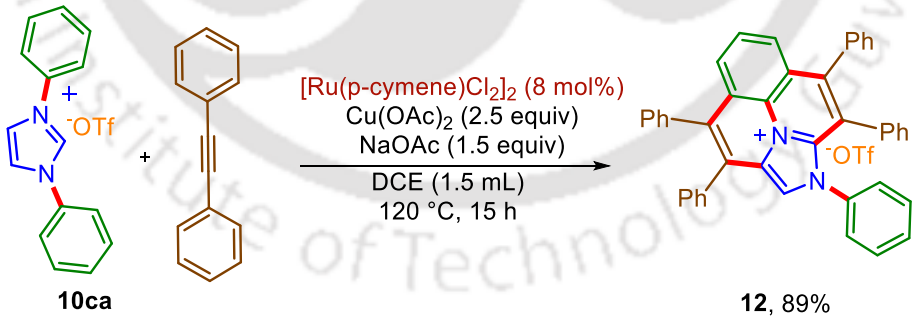

An oven-dried 5 mL round-bottom flask was charged with **10ca** (0.2 mmol, 74 mg), diphenylacetylene (0.4 mmol, 71 mg), $[Ru(p\text{-cymene})Cl_2]_2$ (8 mol%, 10 mg), $Cu(OAc)_2$ (2.5 equiv, 90 mg), NaOAc (1.5 equiv, 24 mg) and a magnetic stir bar in DCE (1.5 mL) and was refluxed at 120 °C for 15 h. The progress of the reaction was monitored via TLC. After completion of the reaction, the solvent was removed by rotary evaporation. The reaction

mixture was then purified over column chromatography by eluting with DCM: Methanol (95: 5) mixtures to afford the product **12** as dark brown gummy solid in 89% yields (128 mg).

III.7.2.9. Procedure for Mechanistic Studies

(a) Procedure for Radical Scavenging Experiment

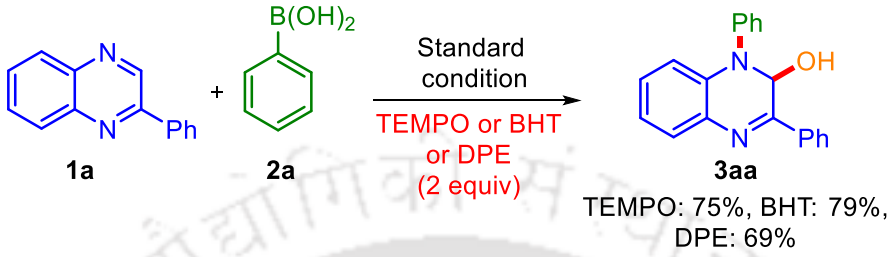

A 5 mL oven-dried round-bottom flask was charged with 2-phenylquinoxaline **1a** (0.35 mmol, 72 mg), phenylboronic acid **2a** (0.56 mmol, 68 mg), $Cu(OTf)_2$ (1.2 equiv, 0.42 mmol, 151 mg), TEMPO (2 equiv, 0.7 mmol, 109 mg) or BHT (2 equiv, 0.7 mmol, 154 mg) or 1,1-diphenylethylene (DPE) (2 equiv, 0.7 mmol, 126 mg) and a magnetic stir bar in toluene (1.5 mL) and was heated at 90 °C for 15 h. The solvent was removed by rotary evaporation. The reaction mixture was then mixed with water (10 mL) and extracted with ethyl acetate (2 × 15 mL). The organic layer was dried over anhydrous sodium sulfate and was evaporated under reduced pressure. The residue so obtained was purified over column chromatography by eluting with hexane: ethyl acetate (96:4) mixture to afford the desired product **3aa** as yellow solid in 78 mg (75% yield) for TEMPO, 83 mg (79% yield) for BHT and 72 mg (69% yield) for DPE. This observation suggests non-involvement of any radical path.

(b) Procedure for H/D Exchange Experiment

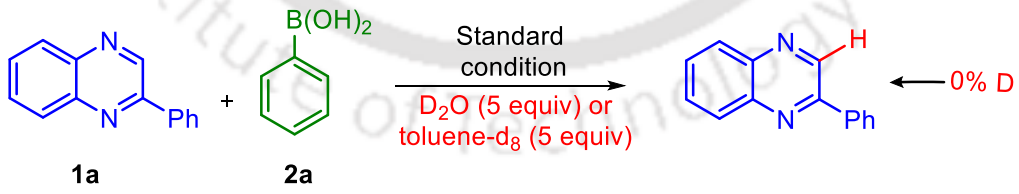

A 5 mL oven-dried round-bottom flask was charged with 2-phenylquinoxaline **1a** (0.35 mmol, 72 mg), phenylboronic acid **2a** (0.56 mmol, 68 mg), $Cu(OTf)_2$ (1.2 equiv, 0.42 mmol, 152 mg), D_2O (5 equiv) or toluene-d_8 (5 equiv) and a magnetic stir bar in toluene (1.5 mL) and was heated at 90 °C for 15 h. The solvent was removed by rotary evaporation. The reaction mixture was then mixed with water (10 mL) and extracted with ethyl acetate (2 × 15 mL). The

organic layer was dried over anhydrous sodium sulfate and was evaporated under reduced pressure. The residue so obtained was purified over column chromatography by eluting with hexane: ethyl acetate (96: 4) mixture to afford an orange product. The extent of deuteration was determined by comparing the ^{1}H NMR of **1a'** to that of un-deuterated 2-phenylquinoxaline **1a**. Upon comparison, no deuteration was observed.

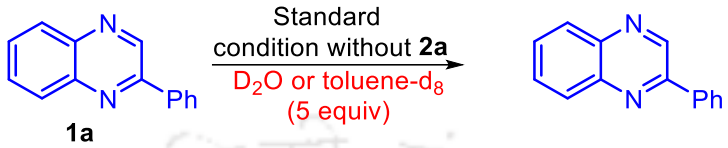

A 5 mL oven-dried round-bottom flask was charged with 2-phenylquinoxaline **1a** (0.35 mmol, 72 mg), $Cu(OTf)_2$ (1.2 equiv, 0.42 mmol, 152 mg), D_2O (5 equiv) or toluene-d_8 (5 equiv) and a magnetic stir bar in toluene (1.5 mL) and was heated at 90 °C for 15 h. The solvent was removed by rotary evaporation. The reaction mixture was then mixed with water (10 mL) and extracted with ethyl acetate (2 × 15 mL). The organic layer was dried over anhydrous sodium sulfate and was evaporated under reduced pressure. The residue so obtained was purified over column chromatography by eluting with hexane: ethyl acetate (96: 4) mixture to afford an orange product. The extent of deuteration was determined by comparing the ^{1}H NMR **1a''** to that of un-deuterated 2-phenylquinoxaline **1a**. Upon comparison, no deuteration was observed.

(c) Procedure for Investigation of the Source of Hydroxyl Oxygen

- **Study of Effect of Addition of External Water**

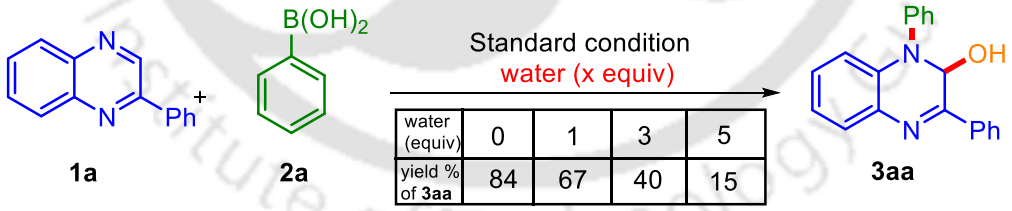

water (equiv)	0	1	3	5
yield % of **3aa**	84	67	40	15

Four 5 mL oven-dried round-bottom flasks were charged with 2-phenylquinoxaline **1a** (0.35 mmol, 72 mg), phenylboronic acid **2a** (0.56 mmol, 68 mg), $Cu(OTf)_2$ (1.2 equiv, 0.42 mmol, 152 mg), H_2O (0/ 1/ 3/ 5 equiv respectively) and a magnetic stir bar in toluene (1.5 mL) and was heated at 90 °C for 15 h. Solvents were removed by rotary evaporation. The reaction mixtures were then mixed with water (10 mL) and extracted with ethyl acetate (2 × 15 mL). The organic layers were dried over anhydrous sodium sulfate and evaporated under reduced pressure. The residue so obtained was purified over column chromatography by eluting with hexane: ethyl acetate (96: 4) mixtures to afford the

product **3aa** as yellow solids in 84% (88 mg), 67% (70 mg), 40% (42 mg), 15% (16 mg) yields respectively for 0, 1, 3, 5 equiv of H_2O added.

➢ **Reaction Under Dry Condition**

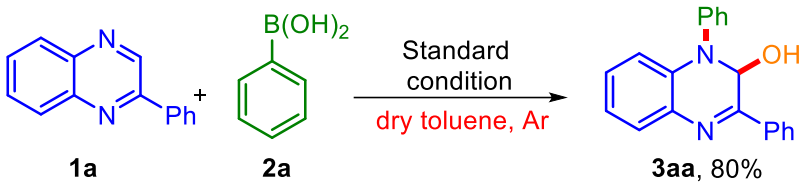

A 5 mL oven-dried round-bottom flask was charged with 2-phenylquinoxaline **1a** (0.35 mmol, 72 mg), purified phenylboronic acid **2a** (0.56 mmol, 68 mg), $Cu(OTf)_2$ (1.2 equiv, 0.42 mmol, 152 mg), and a magnetic stir bar in anhydrous toluene (1.5 mL) under an argon atmosphere and was heated at 90 °C for 15 h. The solvent was removed by rotary evaporation. The reaction mixture was then mixed with water (10 mL) and extracted with ethyl acetate (2 × 15 mL). The organic layer was dried over anhydrous sodium sulfate and was evaporated under reduced pressure. The residue so obtained was purified over column chromatography by eluting with hexane:ethyl acetate (96:4) mixture to afford the product **3aa** as yellow solids in 80% yield (84 mg).

➢ **Reaction with Phenyltrifluoroborate**

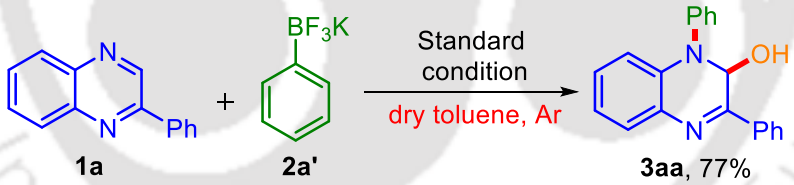

A 5 mL oven-dried round-bottom flask was charged with 2-phenylquinoxaline **1a** (0.35 mmol, 72 mg), potassium phenyltrifluoroborate (**2a'**) (0.56 mmol, 103 mg), $Cu(OTf)_2$ (1.2 equiv, 0.42 mmol, 152 mg) and a magnetic stir bar in anhydrous toluene (1.5 mL) under an argon atmosphere and was heated at 90 °C for 15 h. The solvent was removed by rotary evaporation. The reaction mixture was then mixed with water (10 mL) and extracted with ethyl acetate (2 × 15 mL). The organic layer was dried over anhydrous sodium sulfate and was evaporated under reduced pressure. The residue so obtained was purified over column chromatography by eluting with hexane: ethyl acetate (96: 4) mixture to afford the product **3aa** as yellow solid in 77% yield (81 mg).

III.7.3. Crystallographic Description

Crystal data were collected with Bruker Smart Apex-II CCD diffractometer using graphite monochromated MoK$_\alpha$ radiation (λ = 0.71073 Å) at 298 K for **10aa** and **10ca**. While **3aa** was collected with a XtaLAB Pro II AFC12 (RINC): Kappa single diffractometer. Cell parameters were retrieved using SMART[a] software and refined with SAINT[a] on all observed reflections. Data reduction was performed with the SAINT software and corrected for Lorentz and polarization effects. Absorption corrections were applied with the program SADABS.[b] The structure was solved by direct methods implemented in SHELX-2014[c] program and refined by full-matrix least-squares methods on F2. All non-hydrogen atomic positions were located in difference Fourier maps and refined anisotropically. The hydrogen atoms were placed in their geometrically generated positions.

a. SMART V 4.043 Software for the CCD Detector System; Siemens Analytical Instruments Division: Madison, WI, 2008.
b. SAINT Plus (v 6.14) Bruker AXS Inc., Madison, WI, 2008.
c. Sheldrick, G. M. SHELXL-2014, Program for the Refinement of Crystal Structures; University of Göttingen: Göttingen (Germany), 1997.

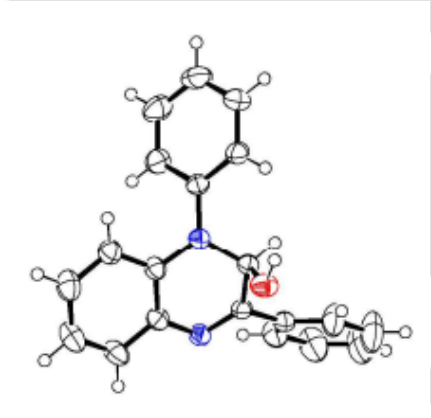

Figure III.7.3.1. *ORTEP diagram of* ***3aa*** *with ellipsoid probability 50%*

Table III.7.3.1. *Crystal Data table for* ***3aa***

Empirical formula	$C_{20}H_{16}N_2O$
CCDC number	2215417
Formula weight	300.36
Temperature	298(2)
Wavelength	0.71073 Å
Crystal system	orthorhombic
Space group	Pbca

Unit cell dimensions	a = 9.0540(7) Å, b = 11.6026(5) Å, c = 29.7549(17) Å α = 90°, β = 90°, γ = 90°
Volume	3125.8 (3) $Å^3$
Z	8
Density (calculated)	1.276 g/cm^{-3}
Absorption coefficient	0.080
F(000)	1264
Theta range for data collection	2.614 to 26.521°
Index ranges	–7 < = h < = 10, –10 < = k < = 13, –31< = l < = 35
Reflections collected	11732
Independent reflections	4877
Data completeness	1.00
Max. and min. transmission	0.975, 0.972
Refinement method	Full-matrix least-squares on F2
Data / restraints / parameters	2761/ 0/ 212
Goodness-of-fit on F2	1.020
Final R indices [I>2sigma(I)]	0.0568, wR2 = 0.1140
R indices (all data)	0.0740, wR2 = 0.1215

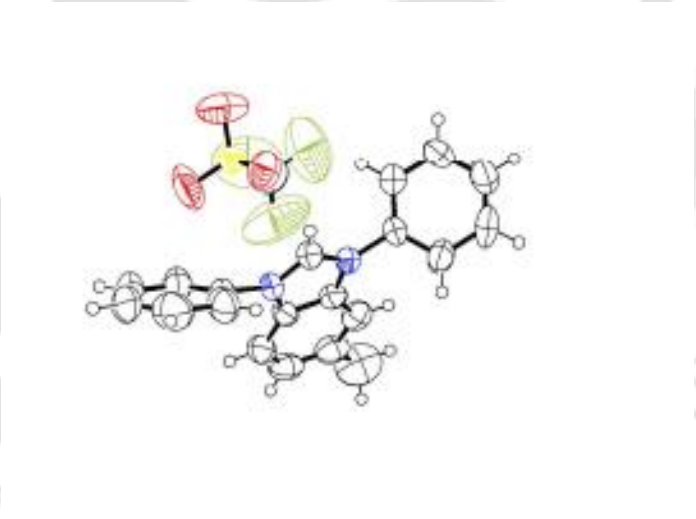

Figure III.7.3.2. *ORTEP diagram of* ***10aa*** *with ellipsoid probability 50%.*

Table III.7.3.2. *Crystal Data table for* ***10aa***

Empirical formula	$C_{21}H_{17}F_3O_3N_2S$
CCDC number	2215422
Formula weight	434.42
Temperature	298
Wavelength	0.71073 Å
Crystal system	monoclinic
Space group	P 21/n

Unit cell dimensions	a = 11.7342(7) Å, b = 10.5428(6) Å, c = 16.8353(10) Å α = 90°, β = 90.689 (2)°, γ = 90°
Volume	2082.6 (2) $Å^3$
Z	4
Density (calculated)	1.386 g/cm^{-3}
Absorption coefficient	0.207
F(000)	896
Theta range for data collection	2.60 to 20.84°
Index ranges	–11 < = h < = 11, –10 < = k < = 10, –16 < = l < = 16
Reflections collected	38013
Independent reflections	9900
Data completeness	1
Max. and min. transmission	0.7446, 0.6005
Refinement method	Full-matrix least-squares on F2
Data / restraints / parameters	2195/ 0/ 272
Goodness-of-fit on F2	1.027
Final R indices [I>2sigma(I)]	0.0963, wR2 = 0.1720
R indices (all data)	0.1158, wR2 = 0.1846

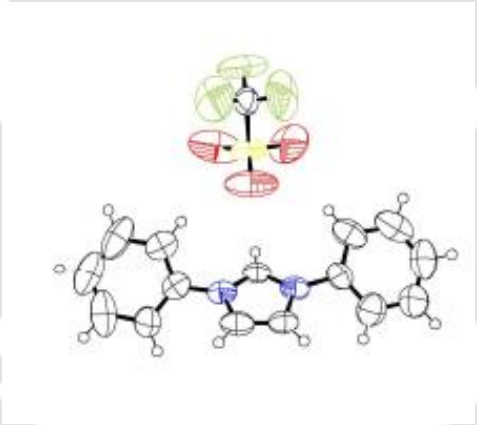

Figure III.7.3.3. *ORTEP diagram of* ***10ca*** *with ellipsoid probability 50%.*

Table III.7.3.3. *Crystal Data table for* ***10ca***

Empirical formula	$C_{16}H_{13}F_3O_3N_2S$
CCDC number	2215420
Formula weight	370.34
Temperature	298
Wavelength	0.71073 Å
Crystal system	orthorhombic
Space group	Pnma
Unit cell dimensions	a = 10.1440 (5) Å, b = 17.4540 (9) Å, c = 9.2908 (5) Å α = 90° , β = 90° , γ = 90°

Volume	1644.97 (15) $Å^3$
Z	4
Density (calculated)	1.495 g/cm^{-3}
Absorption coefficient	0.247
F(000)	760
Theta range for data collection	2.97 to 26.10°
Index ranges	–12 < = h < = 12, –20 < = k < = 20, –11 < = l < = 11
Reflections collected	41668
Independent reflections	9788
Data completeness	1
Max. and min. transmission	0.7454, 0.5754
Refinement method	Full-matrix least-squares on F2
Data / restraints / parameters	1499 / 0 / 121
Goodness-of-fit on F2	1.098
Final R indices [I>2sigma(I)]	0.0747, wR2 = 0.1379
R indices (all data)	0.0883, wR2 = 0. 1477

III.8. References

1. (a) Wolfe, J. P. *Angew. Chem., Int. Ed*. **2012**, *51*, 10224. (b) Li, Z. L.; G. Fang, C.; Gu, Q. S.; Liu, X. Y. *Chem. Soc. Rev*., **2020**, *49*, 32. (c) Zhong, L. J.; Xiong, Z. Q.; Ouyang, X. H.; Li, Y.; Song, R. J.; Sun, Q.; Lu, X.; Li, J. H.; *J. Am. Chem. Soc*. **2022**, *144*, 339.

2. (a) Dhungana, R. K.; KC, S.; Basnet, P.; Giri, R. *Chem. Rec*. **2018**, *18*, 1314. (b) Dorn, S. K.; Brown, M. K. *ACS Catal*. **2022**, *12*, 2058. (c) Koike, T.; Akita, M. *Org. Chem. Front*. **2016**, *3*, 1345.

3. (a) Fernandez-Ibanez, M. A.; Macia, B.; Pizzuti, M. G.; Minnaard, A. J.; Feringa, B. L.; *Angew. Chem., Int. Ed*. **2009**, *48*, 9339. (b) Lutz, J. P.; Chau, S. T.; Doyle, A. G. *Chem. Sci*., **2016**, *7*, 4105. (c) Ahamed, M.; Todd, M. H. *Eur. J. Org. Chem*. **2010**, 5935. (d) Grigolo, T. A.; Subhit, A. R.; Smith, J. M. *Org. Lett*. **2021**, *23*, 6703.

4. (a) Cho, S. H.; Kim, J. Y.; Kwak, J.; Chang, S. *Chem. Soc. Rev*., **2011**, *40*, 5068. (b) Evano, G.; Wang, J.; Nitelet, A. *Org. Chem. Front*. **2017**, *4*, 2480. (c) Titarenko, Z.; Vasilevich, N.; Zernov, V.; Kirpichenok, M.; Genis, D. *J Comput Aided Mol Des*. **2013**, *27*, 125. (d) Niu, L.; Liu, J.; Liang, X. A.; Wang, S.; Lei, A. *Nat Commun* **2019**, *10*, 467. (e) Kong, Y.; Xu, W.; Liu, X.; Weng, J. *Chinese Chemical Letters* **2020**, *31*, 3245.

5. (a) Hartwig, J. F. Nature, **2008**, *455*, 314. (b) Monnier, F.; Taillefer, M. *Angew. Chem., Int. Ed*. **2009**, *48*, 6954.

6. (a) Bariwal. J.; Eycken, E. V. d. *Chem. Soc. Rev.,* **2013**, *42*, 9283. (b) Sambiagio, C.; Marsden, S. P.; Blacker, A. J.; McGowan, P. C. *Chem. Soc. Rev*., **2014**, *43*, 3525. (c) Chan, D. M. T.; Monaco, K. L.; Wang, R. P.; Winters, M. P. *Tetrahedron Lett*. **1998**, *39*, 2933. (d) Evans, D. A.; Katz, J. L.; West, T. R. *Tetrahedron Lett*. **1998**, *39*, 2937. (e) Lam, P. Y. S.; Clark, C. G.; Saubern, S.; Adams, J.; Winters, M. P.; Chan, D. M. T.; Combs, A. *Tetrahedron Lett.* **1998**, *39*, 2941.

7. Li, S.; Yang, F.; Lv, T.; Lan, J.; Gao, G.; You, J. *Chem. Commun.* **2014**, *50*, 3941.

8. Bell, N. L.; Xu, C.; Fyfe, J. W. B.; Vantourout, J. C.; Brals, J.; Chabbra, S.; Bode, B. E.; Cordes, D. B.; Slawin, A. M. Z.; McGuire, T. M.; Watson, A. J. B. *Angew. Chem., Int. Ed.* **2021**, *60*, 7935.

9. (a) Cao, L.; Zhao, H.; Guan, R.; Jiang, H.; Dixneuf, P. H.; Zhang, M. *Nat Commun.* **2021**,*12*, 4206. (b) Seiple, I. B.; Su, S.; Rodriguez, R. A.; Gianatassio, R.; Fujiwara, Y.; Sobel, A. L.; Baran, P. S. *J. Am. Chem. Soc.* **2010**, *132*, 13194.

10. (a) Li, H.; Wei, W.; Xu, Y.; Zhanga, C.; Wan, X. *Chem. Commun*., **2011**, *47*, 1497. (b) Reddy, G. M.; Rao, N. S. S.; Satyanarayana, P.; Maheswaran, H. *RSC Adv.,* **2015**, *5*, 105347.

11. (a) Yashwantrao, G.; Saha, S. *Org. Chem. Front.,* **2021**, *8*, 2820. (b) Ghosh, S.; Pal, S.; Rajamanickam, S.; Shome, R.; Mohanta, P. R.; Ghosh, S. S.; Patel, B. K. *ACS Omega*, **2019**, *4*, 5565.

12. (a) Gandeepan, P.; Müller, T.; Zell, D.; Cera, G.; Warratz, S.; Ackermann, L. *Chem. Rev*. **2019**, *119*, 2192. (b) Chandra, D.; Kumar, N.; Sumit, Parmar, D.; Gupta, P.; Sharma, U. *Chem. Commun*., **2021**, *57*, 11613. (c) Ghosh, S.; Khandelia, T.; Patel, B. K. *Org. Lett.* **2021**, *23*, 7370. (d) Trammel, G. L.; Kuniyil, R.; Crook, P. F.; Liu, P.; Brown, M. K. *J. Am. Chem. Soc*. **2021**, *143*, 16502.

13. (a) Guo, X. X.; Gu, D. W.; Wu, Z.; Zhang, W. *Chem. Rev*. **2015**, *115*, 1622. (b) Khandelia, T.; Ghosh, S.; Panigrahi, P.; Shome, R.; Ghosh, S. S.; Patel, B. K. *J. Org. Chem*. **2021**, *86*, 16948. (c) Kumar, M.; Verma, S.; Mishra, V.; Reiser, O.; Verma, A. K. *J. Org. Chem*.

2022, *87*, 6263. (d) Park, J.; Han, S. H.; Sharma, S.; Han, S.; Shin, Y.; Mishra, N. K.; Kwak, J. H.; Lee, C. H.; Lee, J.; Kim, I. S. *J. Org. Chem*. **2014**, *79*, 4735.

14. Antoft-Finch, A.; Blackburn, T.; Snieckus, V. *J. Am. Chem. Soc*. **2009**, *131*, 17750.

15. (a) Vantourout, J. C.; Miras, H. N.; Llobet, A. I.; Sproules, S.; Watson, A. J. B. *J. Am. Chem. Soc.* **2017**, *139*, 4769 (b) West, M. J.; Fyfe, J. W. B.; Vantourout, J. C.; Watson, A. J. B. *Chem. Rev.* **2019**, *119*, 12491.

16. Yu, J.; Zhao, H.; Liang, S.; Bao, X.; Zhu, C. *Org. Biomol. Chem.,* **2015**, *13*, 7924.

17. Ge, Q.; Li, B.; Song, H.; Wang, B. *Org. Biomol. Chem*. **2015**, *13*, 7695. (b) Thenarukandiyil, R.; Gupta, S. K.; Choudhury, J. *ACS Catal.* **2016**, *6*, 5132.

18. Kumar, K.; Mudshinge, S. R.; Goyal, S.; Gangar, M.; Nair, V. A. *Tetrahedron Letters.* **2015**, *56*, 1266.

III.9. Spectral Data

***1,3-Diphenyl-1,2-dihydroquinoxalin-2-ol (3aa)*:**

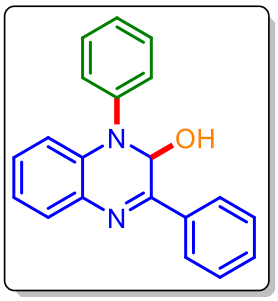

Yellow solid (88 mg, 84% yield), m.p. 150–153 °C. ^{1}H NMR (500 MHz, $CDCl_3$) δ 8.11–8.09 (m, 2H), 7.63 (d, J = 8 Hz, 1H), 7.55 (d, J = 7.5 Hz, 2H), 7.45–7.42 (m, 5H), 7.28 (t, J = 7.5 Hz, 1H), 7.14 (t, J = 7.5 Hz, 1H), 7.02–6.97 (m, 2H), 6.06 (s, 1H), 3.03 (s, 1H).; ^{13}C{^{1}H} NMR (101 MHz, $CDCl_3$) δ 153.6, 143.4, 136.1, 133.7, 132.4, 130.7, 129.7, 128.9, 128.6, 128.4, 127.5, 126.2, 125.3, 120.7, 115.8, 76.1. IR (neat, cm^{-1}) 3153, 3064, 1591, 1482, 1451, 1325, 1253, 1048, 750, 692. HRMS (ESI) $[M - OH]^+$ calcd for $C_{20}H_{15}N_2^+$ 283.1235, found 283.1237.

***3-(4-Methoxyphenyl)-1-phenyl-1,2-dihydroquinoxalin-2-ol (3ba)*:**

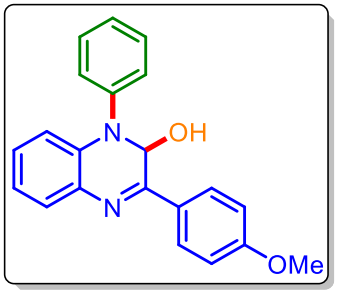

Yellow solid (90 mg, 78% yield); m.p. 145–150 °C. ^{1}H NMR (500 MHz, $CDCl_3$) δ 8.06 (d, J = 9 Hz, 2H), 7.59 (d, J = 8 Hz, 1H), 7.55 (d, J = 8 Hz, 2H), 7.43 (t, J = 7.7 Hz, 2H), 7.28 (d, J = 7.5 Hz, 1H), 7.11 (t, J = 7.5 Hz, 1H), 7.00 (d, J = 8 Hz, 1H), 6.96 (t, J = 7.8 Hz, 3H), 6.04 (s, 1H), 3.86 (s, 3H), 3.02 (s, 1H).; ^{13}C{^{1}H} NMR (101 MHz, $CDCl_3$) δ 161.8, 153.3, 143.6, 133.9, 132.2, 129.7, 129.2,

128.8, 128.3, 127.9, 126.0, 125.2, 120.7, 115.8, 114.2, 76.0, 55.6. IR (neat, cm^{-1}) 3319, 1601, 1486, 1306, 1250, 1023, 956, 834, 746. HRMS (ESI) $[M - OH]^+$ calcd for $C_{21}H_{17}N_2O^+$ 313.1341, found 313.1339.

***1-Phenyl-3-(p-tolyl)-1,2-dihydroquinoxalin-2-ol (3ca)*:**

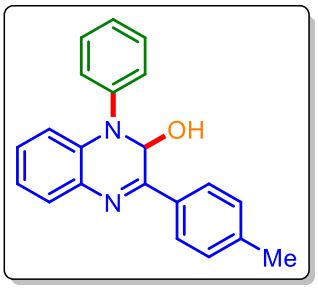

Yellow solid (88 mg, 80% yield); m.p. 190–192 °C. ^1H NMR (500 MHz, $CDCl_3$) δ 7.95 (d, J = 8.0 Hz, 2H), 7.54 (d, J = 8 Hz, 3H), 7.42 (t, J = 7.8 Hz, 2H), 7.27 (d, J = 7.5 Hz, 1H), 7.21 (d, J = 7.5 Hz, 2H), 7.09 (t, J = 7.7 Hz, 1H), 6.98 (d, J = 8 Hz, 1H), 6.92 (t, J = 7.5 Hz, 1H), 6.02 (s, 1H), 3.32 (s, 1H), 2.39 (s, 3H).; $^{13}C\{^1H\}$ NMR (126 MHz, $CDCl_3$) δ 153.6, 143.5, 141.0, 133.8, 133.3, 132.3, 129.7, 129.5, 128.4, 128.2, 127.5, 126.1, 125.3, 120.6, 115.7, 76.1, 21.6. IR (neat, cm^{-1}) 3127, 1591, 1484, 1327, 1288, 1255, 1046, 1023, 750, 693, 473. HRMS (ESI) $[M - OH]^+$ calcd for $C_{21}H_{17}N_2^+$ 297.1392, found 297.1393.

***3-(4-Isopropylphenyl)-1-phenyl-1,2-dihydroquinoxalin-2-ol (3da)*:**

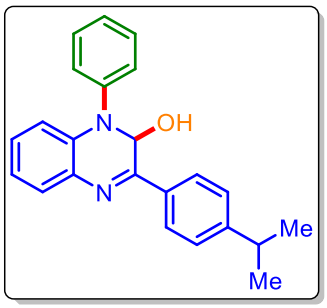

Yellow solid (98 mg, 82% yield); m.p. 154–158 °C. ^1H NMR (500 MHz, $CDCl_3$) δ 8.05 (d, J = 8.0 Hz, 2H), 7.65 (d, J = 8 Hz, 1H), 7.55 (d, J = 8 Hz, 2H), 7.44 (t, J = 7.7 Hz, 2H), 7.33–7.29 (m, 3H), 7.14 (t, J = 7.3 Hz, 1H), 7.03–7.00 (m, 2H), 6.06 (d, J = 8.5 Hz, 1H), 2.99–2.92 (m, 1H), 2.78 (d, J = 10.5 Hz, 1H), 1.27 (d, J = 7.0 Hz, 6H).; $^{13}C\{^1H\}$ NMR (151 MHz, $CDCl_3$) δ 153.7, 152.0, 143.5, 133.9, 133.8, 132.4, 129.7, 128.6, 128.2, 127.6, 127.0, 126.1, 125.3, 120.7, 115.9, 76.1, 34.3, 24.0, 23.9. IR (neat, cm^{-1}) 3335, 2960, 1667, 1595, 1491, 1329, 1017, 838, 750, 697. HRMS (ESI) $[M - OH]^+$ calcd for $C_{23}H_{21}N_2^+$ 325.1705, found 325.1712.

***3-(4-Fluorophenyl)-1-phenyl-1,2-dihydroquinoxalin-2-ol (3ea)*:**

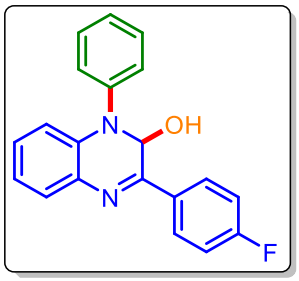

Yellow solid (84 mg, 75% yield); m.p. 127–130 °C. ^{1}H NMR (500 MHz, $CDCl_3$) δ 8.11–8.08 (m, 2H), 7.59 (d, J = 7.5 Hz, 1H), 7.55 (d, J = 7.5 Hz, 2H), 7.44 (t, J = 7.8 Hz, 2H), 7.29 (t, J = 7.5 Hz, 1H), 7.16–7.10 (m, 3H), 7.01–6.96 (m, 2H), 6.01 (d, J = 10.5 Hz, 1H), 3.04 (d, J = 10.5 Hz, 1H).; ^{13}C{^{1}H} NMR (126 MHz, $CDCl_3$) δ 165.4, 163.4, 152.5, 143.4, 133.6, 132.4 (d, J = 3.2 Hz), 132.3, 129.8, 129.7 (d, J = 8.7 Hz), 128.5 (d, J = 8.8 Hz), 126.3, 125.3, 120.8, 116.0, 115.8 (d, J = 6.3 Hz), 76.1. ^{19}F NMR (471 MHz, $CDCl_3$) δ –109.68. IR (neat, cm^{-1}) 3194, 1592, 1490, 1318, 1225, 1155, 973, 831, 745, 697. HRMS (ESI) [M – OH]$^{+}$ calcd for $C_{20}H_{14}FN_2^{+}$ 301.1141, found 301.1142.

***1-Phenyl-3-(4-(trifluoromethyl)phenyl)-1,2-dihydroquinoxalin-2-ol (3fa)*:**

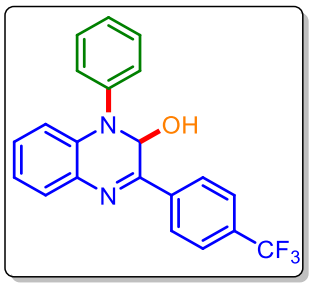

Yellow solid (82 mg, 64% yield); m.p. 70–72 °C. ^{1}H NMR (400 MHz, $CDCl_3$) δ 8.18 (d, J = 8 Hz, 2H), 7.67 (d, J = 8.4 Hz, 2H), 7.59–7.55 (m, 3H), 7.45 (t, J = 7.8 Hz, 2H), 7.31 (t, J = 7.2 Hz, 1H), 7.15 (t, J = 7.7 Hz, 1H), 6.99 (d, J = 8.4 Hz, 1H), 6.96 (t, J = 7.7 Hz, 1H), 6.02 (s, 1H), 3.38 (s, 1H).; ^{13}C{^{1}H} NMR (126 MHz, $CDCl_3$) δ 151.8, 143.2, 139.3, 133.4, 132.5, 132.0 (d, J = 32 Hz), 129.8, 129.2, 128.8, 127.8, 127.5, 126.5, 125.7 (q, J = 3.9 Hz), 125.5, 120.8, 115.9, 76.0. IR (neat, cm^{-1}) 3288, 1590, 1487, 1409, 1318, 1164, 1115, 1066, 1014, 747. HRMS (ESI) [M – OH]$^{+}$ calcd for $C_{21}H_{14}F_3N_2^{+}$ 351.1109, found. 351.1125.

***3-(4-Chlorophenyl)-1-phenyl-1,2-dihydroquinoxalin-2-ol (3ga)*:**

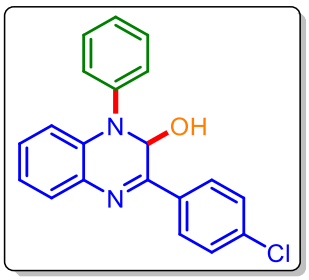

Yellow solid (93 mg, 79% yield); m.p. 147–148 °C. ^{1}H NMR (500 MHz, $CDCl_3$) δ 8.05 (d, J = 8.5 Hz, 2H), 7.61 (d, J = 8 Hz, 1H), 7.55 (d, J = 7.5 Hz, 2H), 7.46–7.41 (m, 4H), 7.30 (d, J = 7.5 Hz, 1H), 7.15 (t, J = 7.5 Hz, 1H), 7.02–6.98 (m, 2H), 6.01 (d, J = 9.5 Hz, 1H), 2.98 (d, J = 10 Hz, 1H).; ^{13}C{^{1}H} NMR (126 MHz, $CDCl_3$) δ 152.4, 143.3, 136.8, 134.6, 133.6, 132.4, 129.8, 129.1, 128.8, 128.7, 126.3, 125.4, 120.8, 115.9, 76.0. IR (neat, cm^{-1})

3066, 1588, 1489, 1333, 1166, 1011, 865, 677. HRMS (ESI) [M – OH]$^+$ calcd for $C_{20}H_{14}ClN_2^+$ 317.0846, found 317.0923.

***3-(4-Bromophenyl)-1-phenyl-1,2-dihydroquinoxalin-2-ol (3ha)*:**

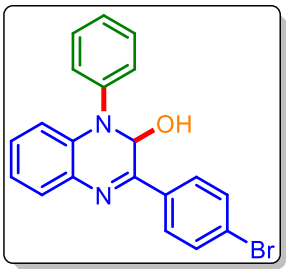

Yellow solid (110 mg, 83% yield); m.p. 155–163 °C. ^{1}H NMR (500 MHz, $CDCl_3$) δ 7.84 (d, J = 8.5 Hz, 2H), 7.54 (d, J = 7.5 Hz, 2H), 7.49 (d, J = 8.5 Hz, 2H), 7.42 (q, J = 8.0 Hz, 3H), 7.28 (t, J = 7.5 Hz, 1H), 7.07 (t, J = 7.3 Hz, 1H), 6.94 (d, J = 8 Hz, 1H), 6.81 (t, J = 7.5 Hz, 1H), 5.93 (d, J = 10.5 Hz, 1H), 3.89 (d, J = 10.5 Hz, 1H).; ^{13}C{^{1}H} NMR (126 MHz, $CDCl_3$) δ 152.1, 143.3, 134.7, 133.4, 132.3, 131.9, 129.7, 129.0, 128.7, 128.3, 126.3, 125.4, 125.4, 120.7, 115.6, 76.0. IR (neat, cm^{-1}) 3189, 1586, 1488, 1393, 1318, 1248, 1071, 1005, 827, 748. HRMS (ESI) [M – OH]$^+$ calcd for $C_{20}H_{14}BrN_2^+$ 361.0340, found 361.0342.

***1-Phenyl-3-(3-(trifluoromethyl)phenyl)-1,2-dihydroquinoxalin-2-ol (3ia)*:**

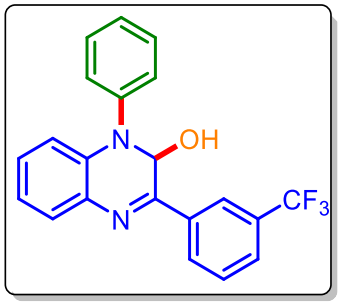

Yellow solid (99 mg, 77% yield); m.p. 127–130 °C. ^{1}H NMR (500 MHz, $CDCl_3$) δ 8.38 (s, 1H), 8.28 (d, J = 8 Hz, 1H), 7.69 (d, J = 8 Hz, 1H), 7.65 (d, J = 7 Hz, 1H), 7.59–7.55 (m, 3H), 7.46 (t, J = 7.7 Hz, 2H), 7.31 (t, J = 7.3 Hz, 1H), 7.17 (t, J = 7.6 Hz, 1H), 7.01 (t, J = 7.5 Hz, 2H), 6.04 (d, J = 10.5 Hz, 1H), 2.99 (d, J = 10.6 Hz, 1H).; ^{13}C{^{1}H} NMR (126 MHz, $CDCl_3$) δ 151.8, 143.2, 136.9, 133.4, 132.5, 131.5, 131.3, 130.6, 129.8, 129.3, 129.1, 128.9, 127.0 (q, J = 3.7 Hz), 126.5, 125.5, 124.4 (q, J = 3.8 Hz), 120.9, 115.9, 76.0. ^{19}F NMR (471 MHz, $CDCl_3$) δ –62.62. IR (neat, cm^{-1}) 3075, 1590, 1486, 1396, 1304, 1165, 1119, 978, 917, 799, 750, 694. HRMS (ESI) [M – OH]$^+$ calcd for $C_{21}H_{14}F_3N_2^+$ 351.1109, found 351.1106.

***1-Phenyl-3-(m-tolyl)-1,2-dihydroquinoxalin-2-ol (3ja)*:**

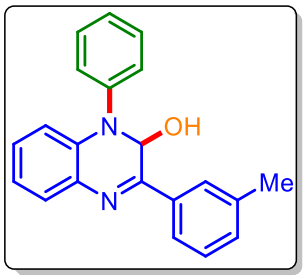

Yellow solid (88 mg, 80% yield); m.p. 90–93 °C. ^{1}H NMR (500 MHz, $CDCl_3$) δ 7.84–7.82 (m, 2H), 7.54–7.50 (m, 3H), 7.41 (t, J = 7.7 Hz, 2H), 7.29–7.24 (m, 2H), 7.20 (d, J = 7.5 Hz, 1H), 7.06 (t, J = 7.5 Hz, 1H), 6.94 (d, J = 8 Hz, 1H), 6.89–6.85 (m, 1H), 6.00 (s, 1H), 3.67 (s, 1H), 2.36 (s, 3H).; ^{13}C{^{1}H} NMR (126 MHz, $CDCl_3$) δ 153.7, 143.5, 138.3, 136.0, 133.8, 132.4, 131.4, 129.6, 128.6, 128.3, 128.2, 128.1, 126.0, 125.3, 124.8, 120.6, 115.7, 76.1, 21.6. IR (neat, cm^{-1}) 3064, 2957, 1666, 1588, 1483, 1270, 1015, 954, 744, 693. HRMS (ESI) [M – OH]$^{+}$ calcd for $C_{21}H_{17}N_2^{+}$ 297.1392, found 297.1390.

***3-(2-Fluorophenyl)-1-phenyl-1,2-dihydroquinoxalin-2-ol (3ka)*:**

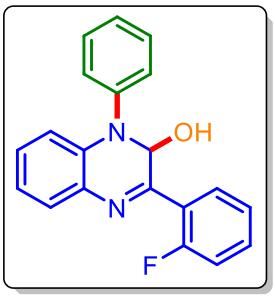

Yellow solid (73 mg, 64% yield); m.p. 140–145 °C. ^{1}H NMR (500 MHz, $CDCl_3$) δ 8.12 (t, J = 7.5 Hz, 1H), 7.67 (d, J = 7.5 Hz, 1H), 7.54 (d, J = 8 Hz, 2H), 7.44 (t, J = 8 Hz, 3H), 7.30–7.26 (m, 2H), 7.19–7.11 (m, 2H), 7.03 (t, J = 7.5 Hz, 2H), 6.06 (d, J = 5 Hz, 1H), 2.81 (d, J = 6.5 Hz, 1H).; ^{13}C{^{1}H} NMR (101 MHz, $CDCl_3$) δ 162.5, 160.0, 151.0 (d, J = 3.2 Hz), 143.2, 133.8, 132.8, 132.1 (d, J = 8.9 Hz), 131.4 (d, J = 2.9 Hz), 129.7, 128.7, 128.7, 126.2, 125.3, 124.9 (d, J = 3.2 Hz), 120.7, 116.6 (d, J = 23.4 Hz), 115.8, 76.7. ^{19}F NMR (376 MHz, $CDCl_3$) δ -113.47. IR (neat, cm^{-1}) 3129, 1587, 1486, 1447, 1332, 1227, 1097, 976, 744, 696. HRMS (ESI) [M + H]$^{+}$ calcd for $C_{20}H_{16}FON_2^{+}$ 319.1241, found 319.1242.

***6,7-Dichloro-1,3-diphenyl-1,2-dihydroquinoxalin-2-ol (3la)*:**

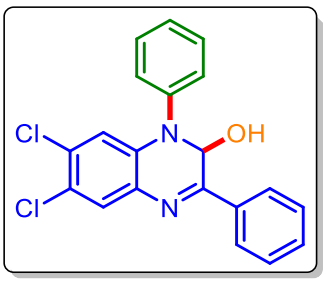

Yellow solid (106 mg, 82% yield); m.p. 175–185 °C. ^{1}H NMR (400 MHz, $CDCl_3$) δ 7.92–7.90 (m, 2H), 7.54–7.46 (m, 5H), 7.40–7.30 (m, 4H), 6.97 (s, 1H), 5.97 (d, J = 10.4 Hz, 1H), 4.18 (d, J = 10.0 Hz, 1H).; ^{13}C{^{1}H} NMR (101 MHz, $CDCl_3$) δ 154.6, 142.6, 135.0, 132.7, 132.2, 132.0, 131.2, 130.1, 129.0, 128.9, 127.7, 127.1, 125.8, 123.3, 116.5, 75.8. IR (neat, cm^{-1}) 3138, 1591, 1472,

1389, 1337, 1102, 975, 895, 701. HRMS (ESI) $[M - OH]^+$ calcd for $C_{20}H_{13}Cl_2N_2^+$ 351.0456, found. 351.0446

***1-Phenyl-3-(thiophen-2-yl)-1,2-dihydroquinoxalin-2-ol (3ma)*:**

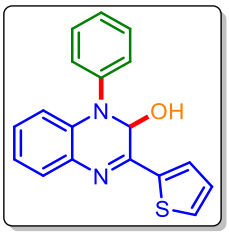

Yellow solid (74 mg, 69% yield); m.p. 140–143 °C. ^{1}H NMR (400 MHz, $CDCl_3$) δ 7.62–7.60 (m, 2H), 7.57–7.54 (m, 2H), 7.49 (d, J = 5.0 Hz, 1H), 7.45 (t, J = 7.9 Hz, 2H), 7.31 (d, J = 7.6 Hz, 1H), 7.15–7.10 (m, 2H), 7.03–6.98 (m, 2H), 6.06 (s, 1H), 2.79 (s, 1H).; ^{13}C{^{1}H} NMR (126 MHz, $CDCl_3$) δ 149.4, 143.4, 142.9, 133.6, 132.6, 130.4, 129.8, 128.4, 128.3, 128.2, 128.1, 126.3, 125.4, 120.9, 115.9, 76.4. IR (neat, cm^{-1}) 3065, 1661, 1588, 1486, 1422, 1281, 1003, 938, 852, 742. HRMS (ESI) $[M - OH]^+$ calcd for $C_{18}H_{13}N_2S^+$ 289.0799, found 289.0789 .

***3-(Benzo[d][1,3]dioxol-5-yl)-1-phenyl-1,2-dihydroquinoxalin-2-ol (3na)*:**

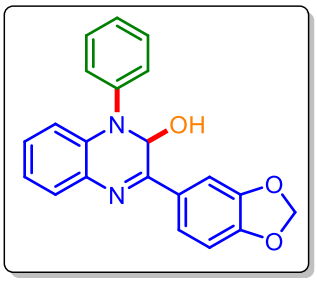

Yellow solid (49 mg, 41% yield); m.p. 138–141 °C. ^{1}H NMR (500 MHz, $CDCl_3$) δ 7.71 (s, 1H), 7.63–7.60 (m, 2H), 7.55 (d, J = 7.5 Hz, 2H), 7.44 (t, J = 7.7 Hz, 2H), 7.29 (d, J = 7.5 Hz, 1H), 7.14 (t, J = 7.7 Hz, 1H), 7.02 (d, J = 7.5 Hz, 2H), 6.87 (d, J = 8.5 Hz, 1H), 6.03 (d, J = 2.5 Hz, 2H), 5.99 (d, J = 17 Hz, 1H), 2.76 (d, J = 10.5 Hz, 1H).; ^{13}C{^{1}H} NMR (101 MHz, $CDCl_3$) δ 153.0, 150.0, 148.4, 143.5, 133.7, 132.2, 130.7, 129.7, 128.3, 128.1, 126.1, 125.2, 122.5, 120.8, 115.8, 108.3, 107.6, 101.7, 76.1. IR (neat, cm^{-1}) 3067, 1591, 1485, 1444, 1236, 1097, 1034, 933, 746, 696. HRMS (ESI) $[M - OH]^+$ calcd for $C_{21}H_{15}N_2O_2^+$ 327.1134, found 327.1128.

***1-(4-Methoxyphenyl)-3-phenyl-1,2-dihydroquinoxalin-2-ol (3ab)*:**

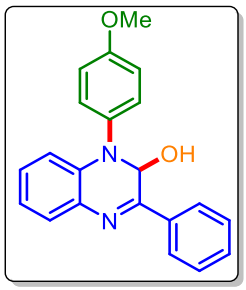

Yellow solid (93mg, 80% yield); m.p. 169–172 °C. ^{1}H NMR (500 MHz, $CDCl_3$) δ 8.13–8.11 (m, 2H), 7.65 (d, J = 8 Hz, 1H), 7.47-7.45 (m, 5H), 7.14 (t, J = 7.5 Hz, 1H), 7.00–6.97 (m, 3H), 6.85 (d, J = 8.5 Hz, 1H), 6.02 (d, J = 6 Hz, 1H), 3.86 (s, 3H), 2.78 (d, J = 9.5 Hz, 1H).; ^{13}C{^{1}H} NMR (126 MHz, $CDCl_3$) δ 158.3, 153.2, 136.3, 136.2, 133.4, 133.3, 130.6, 128.9, 128.8, 128.5, 127.7,

127.5, 120.2, 115.4, 115.0, 76.3, 55.7. IR (neat, cm^{-1}) 3118, 2935, 1590, 1483, 1326, 1253, 1048, 1024, 1000, 751, 693. HRMS (ESI) $[M - OH]^+$ calcd for $C_{21}H_{17}N_2O^+$ 313.1341, found 313.1340.

***3-Phenyl-1-(p-tolyl)-1,2-dihydroquinoxalin-2-ol (3ac)*:**

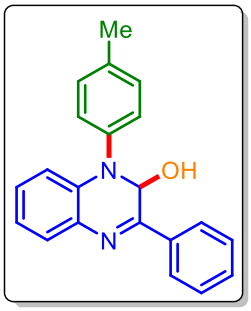

Yellow solid (86 mg, 78% yield); m.p. 150–155 °C. ^1H NMR (400 MHz, $CDCl_3$) δ 8.02–8.00 (m, 2H), 7.50 (dd, J = 9.7, 1.7 Hz, 1H), 7.43–7.35 (m, 5H), 7.22 (d, J = 10 Hz, 2H), 7.09–7.04 (m, 1H), 6.90 (dd, J = 10.5, 1.5 Hz, 1H), 6.88–6.84 (m, 1H), 5.98 (d, J = 9 Hz, 1H), 3.54 (d, J = 10 Hz, 1H), 2.38 (s, 3H).; $^{13}C\{^1H\}$ NMR (101 MHz, $CDCl_3$) δ 153.1, 140.8, 136.1, 136.0, 133.5, 132.7, 130.5, 130.2, 128.7, 128.4, 128.3, 127.5, 125.5, 120.3, 115.5, 76.2, 21.2. IR (neat, cm^{-1}) 3122, 1606, 1510, 1483, 1340, 1283, 1019, 970, 824, 750, 690. HRMS (ESI) $[M - OH]^+$ calcd for $C_{21}H_{17}N_2^+$ 297.1392, found 297.1396.

***1-(4-(Tert-butyl)phenyl)-3-phenyl-1,2-dihydroquinoxalin-2-ol (3ad)*:**

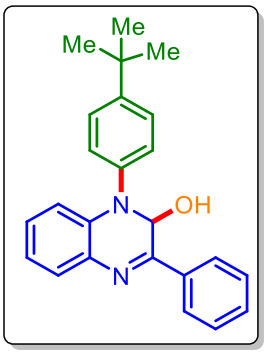

Yellow solid (95 mg, 76% yield); m.p. 70–75 °C. ^1H NMR (500 MHz, $CDCl_3$) δ 8.02–8.00 (m, 2H), 7.52 (d, J = 7.9 Hz, 1H), 7.43 (q, J = 8.5 Hz, 5H), 7.39–7.35 (m, 2H), 7.07 (t, J = 7.5 Hz, 1H), 6.96 (d, J = 8 Hz, 1H), 6.86 (t, J = 7.5 Hz, 1H), 6.00 (s, 1H), 3.59 (s, 1H), 1.35 (s, 9H).; $^{13}C\{^1H\}$ NMR (101 MHz, $CDCl_3$) δ 153.2, 149.2, 140.7, 136.0, 133.5, 132.6, 130.5, 128.7, 128.33, 128.31, 127.5, 126.5, 125.0, 120.3, 115.7, 76.1, 34.7, 31.5. IR (neat, cm^{-1}) 3517, 2955, 1602, 1510, 1479, 1371, 1265, 954, 748, 691. HRMS (ESI) $[M - OH]^+$ calcd for $C_{24}H_{23}N_2^+$ 339.1861 , found 339.1863.

***1-(4-Fluorophenyl)-3-phenyl-1,2-dihydroquinoxalin-2-ol (3ae)*:**

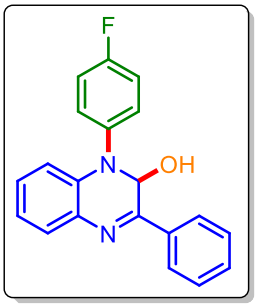

Yellow solid (76 mg, 68% yield); m.p. 153–155 °C. ^1H NMR (500 MHz, $CDCl_3$) δ 8.09-8.07 (m, 2H), 7.60 (d, J = 7.5 Hz, 1H), 7.53-7.51 (m, 2H), 7.45–7.43 (m, 3H), 7.13 (t, J = 8.25 Hz, 3H), 6.97 (t, J = 7.5 Hz, 1H), 6.86 (d, J = 8 Hz, 1H), 5.98 (d, J = 10.5 Hz, 1H), 3.09 (d, J = 10.5 Hz, 1H).; $^{13}C\{^1H\}$ NMR (126 MHz, $CDCl_3$) δ 162.0, 160.1, 153.5, 139.4 (d, J = 3.0 Hz), 136.0, 133.5, 132.7,

130.7, 128.9, 128.7 (d, J = 14.6 Hz), 127.7 (d, J = 8.3 Hz), 127.5, 120.7, 116.6 (d, J = 22.6 Hz),115.3, 76.2. ^{19}F NMR (471 MHz, $CDCl_3$) δ –120.20. IR (neat, cm^{-1}) 3074, 1611, 1502, 1338, 1288, 1158, 1104, 974, 836, 750, 695. HRMS (ESI) $[M - OH]^+$ calcd for $C_{20}H_{14}FN_2^+$ 301.1141, found 301.1144.

***1-(4-Chlorophenyl)-3-phenyl-1,2-dihydroquinoxalin-2-ol (3af)*:**

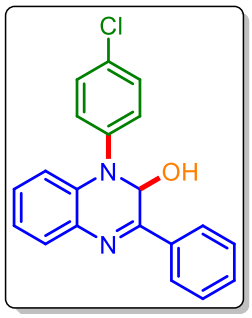

Yellow solid (79 mg, 68% yield); m.p. 160–162 °C. ^{1}H NMR (400 MHz, $CDCl_3$) δ 8.13–8.11 (m, 2H), 7.66 (dd, J = 7.6, 1.6 Hz, 1H), 7.50 (d, J = 8.8 Hz, 2H), 7.48–7.46 (m, 3H), 7.40 (d, J = 8.8 Hz, 2H), 7.19–7.14 (m, 1H), 7.04 (td, J = 7.5, 1.3 Hz, 1H), 7.00–6.98 (dd, J = 8.2, 1.2 Hz, 1H), 6.00 (d, J = 10 Hz, 1H), 2.88 (d, J = 10.8 Hz, 1H).; ^{13}C{^{1}H} NMR (126 MHz, $CDCl_3$) δ 153.8, 142.0, 136.0, 133.8, 132.1, 131.6, 130.8, 129.9, 128.9, 128.8, 128.6, 127.5, 126.5, 121.1, 115.7, 75.9. IR (neat, cm^{-1}) 3065, 1589, 1486, 1091, 1017, 976, 831, 749, 692. HRMS (ESI) $[M - OH]^+$ calcd for $C_{20}H_{14}ClN_2^+$ 317.0846 , found 317.0844.

***1-(4-Bromophenyl)-3-phenyl-1,2-dihydroquinoxalin-2-ol (3ag)*:**

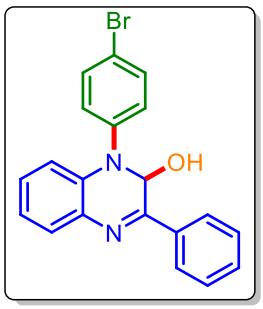

Yellow solid (99 mg, 75% yield); m.p. 145–47 °C. ^{1}H NMR (500 MHz, $CDCl_3$) δ 8.12-8.10 (m, 2H), 7.65 (d, J = 7.5 Hz, 1H), 7.55 (d, J = 8.5 Hz, 2H), 7.47–7.44 (m, 5H), 7.16 (t, J = 7.5 Hz, 1H), 7.03 (t, J = 7.5 Hz, 1H), 7.00 (d, J = 8 Hz, 1H), 6.00 (d, J = 10.5 Hz, 1H), 2.89 (d, J = 10.5 Hz, 1H).; ^{13}C{^{1}H} NMR (126 MHz, $CDCl_3$) δ 153.8, 142.5, 136.0, 133.9, 132.8, 131.9, 130.8, 128.9, 128.8, 128.6, 127.5, 126.8, 121.2, 119.3, 115.7, 75.9. IR (neat, cm^{-1}) 3063, 1611, 1489, 1338, 1283, 1075, 977, 828, 749. HRMS (ESI) $[M - OH]^+$ calcd for $C_{20}H_{14}BrN_2^+$ 361.0340, found 361.0343.

***3-Phenyl-1-(m-tolyl)-1,2-dihydroquinoxalin-2-ol (3ah)*:**

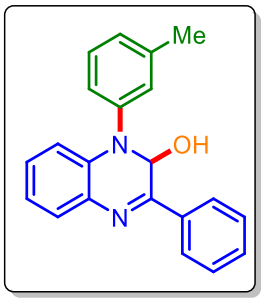

Yellow solid (87 mg, 79% yield); m.p. 90–95 °C. ^{1}H NMR (500 MHz, $CDCl_3$) δ 8.11–8.10 (m, 2H), 7.63 (dd, J = 8, 1.5 Hz, 1H), 7.45–7.43 (m, 3H), 7.38 (s, 1H), 7.35–7.29 (m, 2H), 7.14 (t, J = 7.5 Hz, 1H), 7.09 (d, J = 7.0 Hz, 1H), 7.03–6.97 (m, 2H), 6.05 (d, J = 10 Hz, 1H), 2.98 (d, J = 10.5 Hz, 1H), 2.39 (s, 3H).; ^{13}C{^{1}H} NMR (126 MHz, $CDCl_3$) δ 153.5, 143.4, 139.8, 136.2, 133.7, 132.5, 130.6, 129.5, 128.8, 128.6, 128.4, 127.5, 127.0, 125.9, 122.4, 120.6, 116.0, 76.1, 21.6. IR (neat, cm^{-1}) 3056, 1596, 1482, 1330, 1177, 1018, 965, 692. HRMS (ESI) [M – OH]$^{+}$ calcd for $C_{21}H_{17}N_2^{+}$ 297.1392 , found 297.1393.

***1-(4-Methoxy-3-methylphenyl)-3-phenyl-1,2-dihydroquinoxalin-2-ol (3ai)*:**

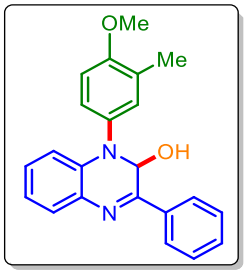

Yellow solid (98 mg, 81% yield); m.p. 152–156 °C. ^{1}H NMR (500 MHz, $CDCl_3$) δ 8.12–8.10 (m, 2H), 7.63 (d, J = 7.5 Hz, 1H), 7.46–7.44 (m, 3H), 7.34–7.31 (m, 2H), 7.13 (t, J = 7.5 Hz, 1H), 6.96 (t, J = 7.3 Hz, 1H), 6.87 (t, J = 8 Hz, 2H), 6.02 (d, J = 9 Hz, 1H), 3.87 (s, 3H), 2.88 (d, J = 10.0 Hz, 1H), 2.25 (s, 3H).; ^{13}C{^{1}H} NMR (101 MHz, $CDCl_3$) δ 156.5, 153.0, 136.2, 135.7, 133.4, 133.2, 130.5, 128.8, 128.6, 128.5, 128.1, 127.5, 124.8, 120.0, 115.4, 110.7, 76.4, 55.7, 16.5. IR (neat, cm^{-1}) 3341, 2922, 1605, 1498, 1459, 1231, 1101, 1022, 940, 749. HRMS (ESI) [M – OH]$^{+}$ calcd for $C_{22}H_{19}N_2O^{+}$ 327.1497, found 327.1488.

***1-(Naphthalen-2-yl)-3-phenyl-1,2-dihydroquinoxalin-2-ol (3aj)*:**

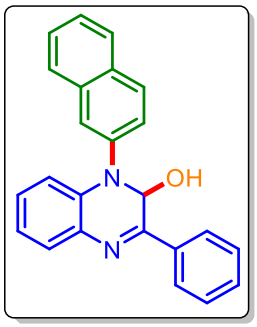

Yellow solid (83 mg, 68% yield); m.p. 148–151 °C. ^{1}H NMR (500 MHz, $CDCl_3$) δ 8.18–8.16 (m, 2H), 8.11 (s, 1H), 7.87 (t, J = 8 Hz, 3H), 7.70 (d, J = 7.5 Hz, 1H), 7.57 (d, J = 8.5 Hz, 1H), 7.53 (t, J = 7 Hz, 1H), 7.51–7.46 (m, 4H), 7.17 (t, J = 7.5 Hz, 1H), 7.09–7.05 (m, 2H), 6.20 (d, J = 10 Hz, 1H), 2.92 (d, J = 10.5 Hz, 1H).; ^{13}C{^{1}H} NMR (126 MHz, $CDCl_3$) δ 153.8, 141.1, 136.1, 134.4, 134.0, 132.2, 131.7, 130.7, 129.2, 128.9, 128.8, 128.5, 127.9, 127.5, 126.9, 126.0, 124.3, 122.2, 121.1, 116.1, 76.4. IR (neat,

cm^{-1}) 3072, 1576, 1451, 1319, 1168, 1027, 958, 638. HRMS (ESI) [M – OH]$^+$ calcd for $C_{24}H_{17}N_2^+$ 333.1392, found 333.1390.

***(1S,2R,5S)-2-Isopropyl-5-methylcyclohexyl 4-((S)-3-hydroxy-4-phenyl-3,4-dihydroquinoxalin-2-yl)benzoate (3oa)*:**

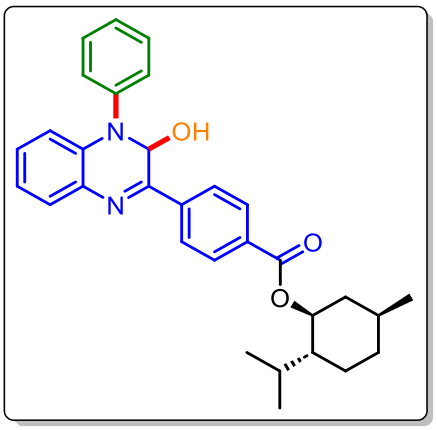

Yellow solid (137 mg, 81% yield); m.p. 156–158 °C. ^{1}H NMR (500 MHz, $CDCl_3$) δ 8.11 (t, J = 8.5 Hz, 2H), 8.05 (t, J = 8.0 Hz, 2H), 7.58–7.52 (m, 3H), 7.42 (t, J = 7.0 Hz, 2H), 7.28 (t, J = 7.7 Hz, 1H), 7.13–7.08 (m, 1H), 6.96–6.90 (m, 2H), 6.0–6.00 (m, 1H), 4.97–4.91 (m, 1H), 3.75–3.50 (m, 1H), 2.16–2.13 (m, 1H), 1.98–1.92 (m, 1H), 1.80–1.71 (m, 3H), 1.60–1.55 (m, 2H), 1.18– 1.09 (m, 2H), 0.93 (t, J = 7.2 Hz, 6H), 0.80 (dd, J = 7.2, 3.7 Hz, 3H).; ^{13}C{^{1}H} NMR (126 MHz, $CDCl_3$) δ 165.9, 165.8, 152.4, 152.3, 143.25, 139.82, 139.77, 133.5, 132.61, 132.55, 132.22, 132.19, 129.92, 129.91, 129.7, 128.9, 128.8, 128.7, 127.39, 127.38, 126.3, 125.4, 120.7, 115.81, 115.77, 75.97, 75.90, 75.37, 75.35, 47.39, 41.06, 34.4, 31.6, 26.8, 26.7, 23.94, 23.85, 22.2, 20.87, 20.84, 16.82, 16.73. IR (neat, cm^{-1}) 3339, 2912, 1655, 1478, 1454, 1222, 1214, 1007, 950, 782. HRMS (ESI) [M – OH]$^+$ calcd for $C_{31}H_{33}N_2O_2^+$ 465.2542, found 465.2471.

***(4R)-1,7,7-Trimethylbicyclo[2.2.1]heptan-2-yl 4-((S)-3-hydroxy-4-phenyl-3,4-dihydroquinoxalin-2-yl)benzoate (3pa)*:**

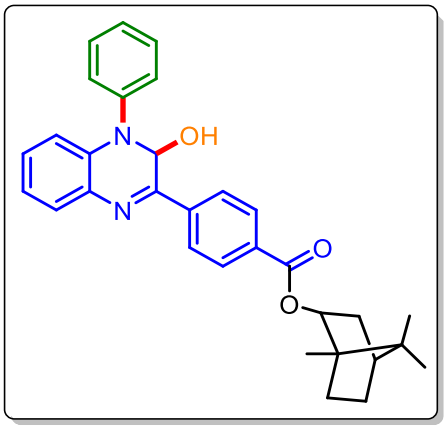

Yellow solid (126 mg, 75% yield); m.p. 154–158 °C. ^{1}H NMR (500 MHz, $CDCl_3$) δ 8.15–8.12 (m, 2H), 8.08–8.06 (m, 2H), 7.60–7.57 (m, 1H), 7.55 (d, J = 8 Hz, 2H), 7.44 (t, J = 7.8 Hz, 2H), 7.28 (t, J = 7.3 Hz, 1H), 7.13 (t, J = 7.5 Hz, 1H), 6.98–6.94 (m, 2H), 6.03 (d, J = 8 Hz, 1H), 5.14–5.10 (m, 1H), 3.47 (s, 1H), 2.51–2.45 (m, 1H), 2.16– .10 (m, 1H), 1.85–1.78 (m, 1H), 1.75 (t, J = 4.5 Hz, 1H), 1.46–1.39 (m, 1H), 1.36–1.31 (m, 1H), 1.14 (dd, J = 13.5, 3.5 Hz, 1H), 0.97 (s, 3H), 0.92 (s, 6H).; ^{13}C{^{1}H} NMR (126 MHz, $CDCl_3$) δ 166.6, 152.36, 152.32, 143.3, 139.89, 139.87, 133.6, 132.59, 132.58, 132.29, 132.26, 129.88, 129.75, 128.97, 128.83, 127.4, 126.3, 125.4, 120.8, 115.8, 81.0, 75.97, 75.96, 49.3, 48.0, 45.2, 37.0, 37.0, 28.2, 27.6, 19.9, 19.1, 13.8. IR (neat, cm^{-1}) 3439, 2913, 1675, 1454, 1426, 1208, 1157, 1009, 850, 672. HRMS (ESI) $[M - OH]^+$ calcd for $C_{31}H_{31}N_2O_2^+$ 463.2386 , found 463.2390.

***(8R,9S,13S,14S)-13-Methyl-17-oxo-7,8,9,11,12,13,14,15,16,17-decahydro-6H-cyclopenta[a]phenanthren-3-yl 4-((S)-3-hydroxy-4-phenyl-3,4-dihydroquinoxalin-2-yl)benzoate (3qa)*:**

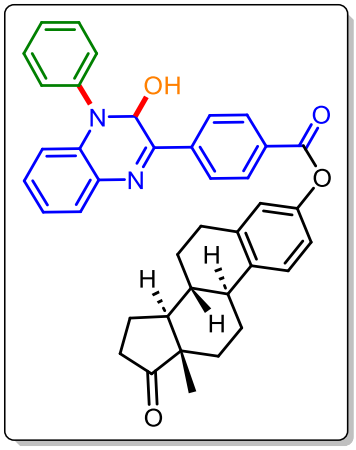

Yellow solid (86 mg, 41% yield); m.p. 140–146 °C. ^{1}H NMR (500 MHz, $CDCl_3$) δ 8.59 (d, J = 8 Hz, 1H), 8.40–8.35 (m, 2H), 8.27 (d, J = 8 Hz, 1H), 8.19 (dd, J = 19.5, 8.0 Hz, 1H), 8.12 (d, J = 8.0 Hz, 1H), 7.85–7.98 (m, 1H), 7.72 (d, J = 8 Hz, 1H), 7.66 (t, J = 7.5 Hz, 1H), 7.54 (d, J = 7.5 Hz, 1H), 7.40–7.31 (m, 6H), 6.99 (d, J = 10.5 Hz, 1H), 4.16 (d, J = 5.5 Hz, 1H), 2.98– 2.93 (m, 3H), 2.36–2.29 (m, 3H), 2.08–1.98 (m, 6H), 1.26 (s, 3H), 0.94 (d, J = 3 Hz, 1H), 0.88 (t, J = 6.5 Hz, 2H).; ^{13}C{^{1}H} NMR (126 MHz, $CDCl_3$) δ 143.3, 131.1, 130.8, 130.6, 130.4, 130.3, 130.2, 129.98, 129.91, 129.7, 129.4, 129.1, 128.4, 127.8, 127.6, 126.7, 121.8, 120.3, 119.0, 115.7, 110.8, 77.4, 50.7, 48.1, 44.4, 38.2, 36.0, 29.8, 26.5, 25.96, 22.8, 21.8, 14.3, 14.0. IR (neat, cm^{-1}) 3349, 2930, 1657, 1480, 1447, 1209, 1201, 1021, 869, 632. HRMS (ESI) $[M - OH]^+$ calcd for $C_{39}H_{35}N_2O_3^+$ 579.2648, found 579.2664.

***2-Phenylisoquinolin-2-ium trifluoromethanesulfonate (7l)*:**

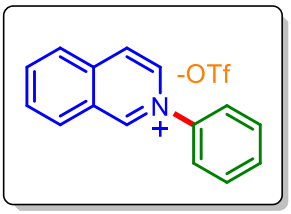

brown gummy solid (100 mg, 81% yield); ^{1}H NMR (400 MHz, DMSO-d_6) δ 10.30 (s, 1H), 8.97 (dd, J = 6.8, 1.6 Hz, 1H), 8.65 (d, J = 6.8 Hz, 1H), 8.54 (d, J = 8.8 Hz, 1H), 8.37 (d, J = 8.4 Hz, 1H), 8.29–8.24 (m, 1H), 8.09– .05 (m, 1H), 7.93–7.90 (m, 2H), 7.74–7.68 (m, 3H).; ^{13}C{^{1}H} NMR (101 MHz, DMSO-d_6) δ 150.5, 143.0, 137.7, 137.3, 135.0, 131.5, 131.2, 131.1, 130.3, 127.4, 127.3, 125.8, 125.0. ^{19}F NMR (471 MHz, DMSO) δ –78.10. IR (neat, cm^{-1}) 3229, 2940, 1690, 1468, 1432, 1278, 1211, 1001, 859,

659. HRMS (ESI) $[M - OTf]^+$ calcd for $C_{15}H_{12}N^+$ 206.0964, found 206.1009.

***2-Phenylquinoline (8′)*:**

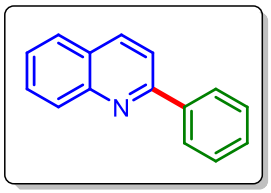

White solid (47 mg, 66% yield); m.p. 120–125 °C. ^{1}H NMR (600 MHz, $CDCl_3$) δ 8.23 (d, J = 8.4 Hz, 1H), 8.19–8.16 (m, 3H), 7.88 (d, J = 9 Hz, 1H), 7.83 (d, J = 8.4 Hz, 1H), 7.73 (t, J = 7.8 Hz, 1H), 7.55–7.52 (m, 3H), 7.47 (t, J = 7.6 Hz, 1H).; ^{13}C{^{1}H} NMR (151 MHz, $CDCl_3$) δ 157.5, 148.4, 139.9, 136.9, 129.9, 129.8, 129.5, 129.0, 127.7, 127.6, 127.3, 126.4, 119.2. IR (neat, cm^{-1}) 3269, 2953, 1645, 1459, 1427, 1269, 1219, 1091, 779, 619. HRMS (ESI) $[M + H]^+$ calcd for $C_{15}H_{12}N^+$ 206.0964, found 206.1009.

***5-Methyl-1,3-diphenyl-1H-benzo[d]imidazol-3-ium trifluoromethanesulfonate (10aa)*:**

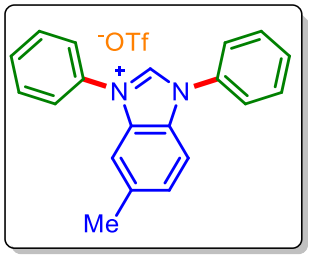

White solid (97 mg, 64% yield); m.p. 151–155 °C. ^{1}H NMR (500 MHz, DMSO-d_6) δ 10.38 (s, 1H), 7.85–7.82 (m, 4H), 7.73 (d, J = 8.5 Hz, 1H), 7.72–7.68 (m, 4H), 7.66–7.64 (m, 2H), 7.52 (d, J = 9.5 Hz, 1H), 6.46 (s, 1H), 2.44 (s, 3H).; ^{13}C{^{1}H} NMR (126 MHz, DMSO-d_6) δ 142.3, 138.4, 133.13, 133.08, 131.5, 130.7, 130.459, 130.456, 129.4, 129.2, 125.5, 125.3, 113.4, 113.2, 21.1. ^{19}F NMR (471 MHz, DMSO-d_6) δ –78.20. IR (neat, cm^{-1}) 3139, 1570, 1289, 1219, 1119, 1104, 1021, 1001, 858, 720. HRMS (ESI) $[M - OTf]^+$ calcd for $C_{20}H_{17}N_2^+$ 285.1392, found 285.1389.

***5-Chloro-1,3-diphenyl-1H-benzo[d]imidazol-3-ium trifluoromethanesulfonate (10ba)*:**

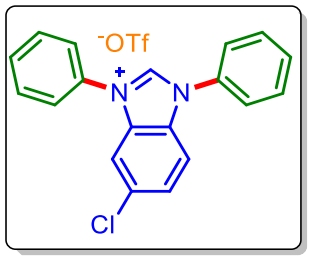

White solid (92 mg, 58% yield); m.p. 149–156 °C. ^{1}H NMR (500 MHz, DMSO-d_6) δ 10.56 (s, 1H), 8.02 (d, J = 1.5 Hz, 1H), 7.92 (d, J = 9.0 Hz, 1H), 7.90–7.86 (m, 3H), 7.78–7.70 (m, 7H), 6.47 (s, 1H).; ^{13}C{^{1}H} NMR (126 MHz, DMSO-d_6) δ 143.9, 132.72, 132.66, 132.4, 132.0, 130.9, 130.8, 130.5, 130.2, 128.2, 125.4, 125.3, 115.5, 113.7. ^{19}F NMR (471 MHz, DMSO-d_6) δ –72.99. IR (neat, cm^{-1}) 3138, 1579, 1248, 1211, 1169, 1144, 1023, 1007, 813,

758. HRMS (ESI) $[M - OTf]^+$ calcd for $C_{19}H_{14}ClN_2^+$ 305.0846, found 305.0869.

***1,3-Diphenyl-1H-imidazol-3-ium trifluoromethanesulfonate (10ca)*:**

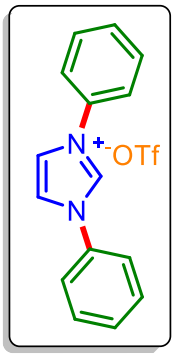

White solid (88 mg, 68% yield); m.p. 153–157 °C. ^{1}H NMR (400 MHz, DMSO-d_6) δ 10.28 (t, J = 1.7 Hz, 1H), 8.52 (d, J = 1.6 Hz, 2H), 7.88–7.85 (m, 4H), 7.68–7.63 (m, 4H), 7.60–7.55 (m, 2H).; ^{13}C{^{1}H} NMR (101 MHz, DMSO-d_6) δ 134.7, 134.6, 130.2, 130.1, 122.1, 122.0. ^{19}F NMR (471 MHz, DMSO-d_6) δ –77.97. IR (neat, cm^{-1}) 3128, 1552, 1285, 1257, 1147, 1120, 1067, 1060, 849, 755. HRMS (ESI) $[M - OTf]^+$ calcd for $C_{15}H_{13}N_2^+$ 221.1079, found 221.1091.

***3-Phenyl-1-vinyl-1H-imidazol-3-ium trifluoromethanesulfonate (10da)*:**

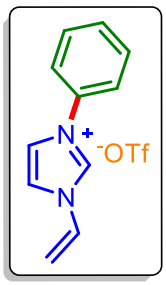

Brown liquid (89 mg, 79% yield); ^{1}H NMR (500 MHz, DMSO-d_6) δ 9.97 (s, 1H), 8.33 (dt, J = 18, 2.0 Hz, 2H), 7.74–7.72 (m, 2H), 7.59 (t, J = 7.8 Hz, 2H), 7.54–7.51 (m, 1H), 7.23 (dd, J = 15.5, 9 Hz, 1H), 6.01 (dd, J = 15.7, 2.4 Hz, 1H), 5.46 (dd, J = 9, 2.5 Hz, 1H).; ^{13}C{^{1}H} NMR (101 MHz, DMSO-d_6) δ 134.6, 134.5, 130.2, 130.1, 128.8, 122.03, 121.99, 120.1, 109.8. ^{19}F NMR (471 MHz, DMSO-d_6) δ –78.03. IR (neat, cm^{-1}) 3133, 1559, 1228, 1217, 1148, 1146, 1053, 1018, 859, 756. HRMS (ESI) $[M - OTf]^+$ calcd for $C_{11}H_{11}N_2^+$ 171.0922, found 171.0948.

***1,3-Di(naphthalen-2-yl)-1H-imidazol-3-ium trifluoromethanesulfonate (10cj)*:**

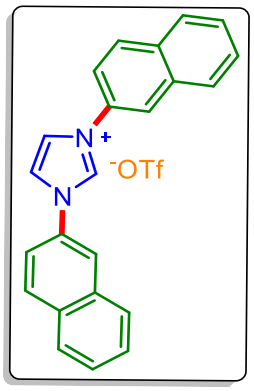

Light brown solid (112 mg, 68% yield); m.p. 146–148 °C. ^{1}H NMR (500 MHz, DMSO-d_6) δ 10.57 (s, 1H), 8.74–8.72 (m, 2H), 8.55-8.54 (m, 2H), 8.28 (d, J = 8.5 Hz, 2H), 8.11–8.05 (m, 6H), 7.73–7.67 (m, 4H).; ^{13}C{^{1}H} NMR (126 MHz, DMSO-d_6) δ 134.9, 132.8, 132.5, 132.1, 130.3, 128.2, 128.01, 127.97, 127.78, 122.1, 120.5, 119.7. ^{19}F NMR (471 MHz, DMSO-d_6) δ –77.76. IR (neat, cm^{-1}) 3123, 1558, 1229, 1221, 1138, 1131, 1051, 1011, 852,

746. HRMS (ESI) $[M - OTf]^+$ calcd for $C_{23}H_{17}N_2^+$ 321.1392, found.

***1,3-Bis(4-methoxyphenyl)-1H-imidazol-3-ium trifluoromethanesulfonate (10cb)*:**

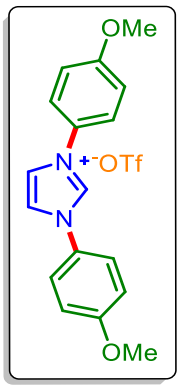

Light brown solid (99 mg, 66% yield); m.p. 145–149 °C. ^{1}H NMR (500 MHz, DMSO-d_6) δ 10.05 (s, 1H), 8.36 (d, J = 2 Hz, 2H), 7.73 (d, J = 9.0 Hz, 4H), 7.15 (d, J = 9.0 Hz, 4H), 3.77 (s, 6H).; ^{13}C{^{1}H} NMR (126 MHz, DMSO-d_6) δ 160.2, 133.9, 127.8, 123.7, 122.0, 115.2, 55.8. ^{19}F NMR (471 MHz, DMSO-d_6) δ –77.75. IR (neat, cm^{-1}) 3123, 1561, 1227, 1216, 1149, 1143, 1042, 1017, 852, 750. HRMS (ESI) $[M - OTf]^+$ calcd for $C_{17}H_{17}N_2O_2^+$ 281.1290, found 281.1315.

***1,3-Bis(4-chlorophenyl)-1H-imidazol-3-ium trifluoromethanesulfonate (10cf)*:**

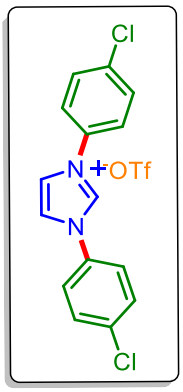

Light brown solid (104 mg, 68% yield); m.p. 150–153 °C. ^{1}H NMR (500 MHz, DMSO-d_6) δ 10.38 (s, 1H), 8.53 (d, J = 1.6 Hz, 2H), 7.92 (d, J = 8.8 Hz, 4H), 7.76 (d, J = 8.8 Hz, 4H).; ^{13}C{^{1}H} NMR (126 MHz, DMSO-d_6) δ 135.1, 134.7, 133.5, 130.2, 124.0, 122.0. ^{19}F NMR (471 MHz, DMSO-d_6) δ –77.76. IR (neat, cm^{-1}) 3133, 1569, 1247, 1213, 1149, 1147, 1023, 1017, 812, 759. HRMS (ESI) $[M - OTf]^+$ calcd for $C_{15}H_{11}Cl_2N_2^+$ 289.0299, found 289.0356.

***1,3-Diphenylquinoxalin-2(1H)-one (11)*:**

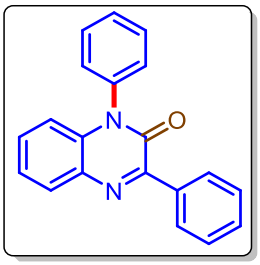

White solid (47 mg, 79% yield); m.p. 180–185 °C. ^{1}H NMR (500 MHz, $CDCl_3$) δ 8.40 (m, 2H), 8.00–7.98 (m, 1H), 7.64 (t, J = 7.5 Hz, 2H), 7.57 (t, J = 7.5 Hz, 1H), 7.48–7.45 (m, 3H), 7.35–7.34 (m, 4H), 6.70–6.68 (m, 1H).; ^{13}C{^{1}H} NMR (126 MHz, $CDCl_3$) δ 154.69, 154.67, 136.3, 135.9, 134.4, 133.2, 130.6, 130.4, 130.2, 130.1, 129.9, 129.6, 128.5, 128.2, 124.0, 115.5. IR (neat, cm^{-1}) 3065, 1657, 1597, 1581, 1457, 1291, 1216, 1150, 1073, 754. HRMS (ESI) $[M + H]^+$ calcd for $C_{20}H_{15}N_2O^+$ 299.1179, found 299.1172.

***1,3,4,8,9-Pentaphenyl-1H-benzo[ij]imidazo[2,1,5-de]quinolizin-10-ium trifluoromethanesulfonate (12)*:**

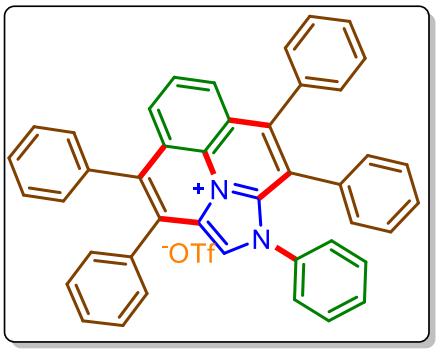

Dark brown gummy solid (128 mg, 89% yield); ^{1}H NMR (500 MHz, $CDCl_3$) δ 7.73 (d, J = 4.5 Hz, 2H), 7.65 (t, J = 4.7 Hz, 1H), 7.61 (s, 1H), 7.52–7.48 (m, 3H), 7.40–7.35 (m, 5H), 7.33–7.26 (m, 9H), 7.18 (t, J = 7.7 Hz, 1H), 7.08 (t, J = 7.7 Hz, 2H), 7.00 (d, J = 7.5 Hz, 2H), 6.89 (t, J = 7.5 Hz, 1H), 6.82 (t, J = 7.5 Hz, 2H).; ^{13}C{^{1}H} NMR (126 MHz, $CDCl_3$) δ 147.3, 137.9, 135.2, 134.7, 134.4, 134.0, 132.9, 131.7, 131.0, 130.6, 130.4, 129.95, 129.05, 128.92, 128.91, 128.8, 128.6, 128.6, 128.5, 128.2, 128.1, 128.0, 127.9, 127.1, 126.8, 126.6, 126.2, 125.5, 125.3, 124.6, 119.6. ^{19}F NMR (471 MHz, DMSO-d_6) δ –78.37. IR (neat, cm^{-1}) 3141, 1558, 1257, 1200, 1142, 1101, 1028, 1013, 802, 769. HRMS (ESI) [M – OTf]$^{+}$ calcd for $C_{43}H_{29}N_2^{+}$ 573.2325, found 573.2360.

III.10. NMR Spectra

1,3-Diphenyl-1,2-dihydroquinoxalin-2-ol (3aa): ^{1}H NMR ($CDCl_3$, 500 MHz)

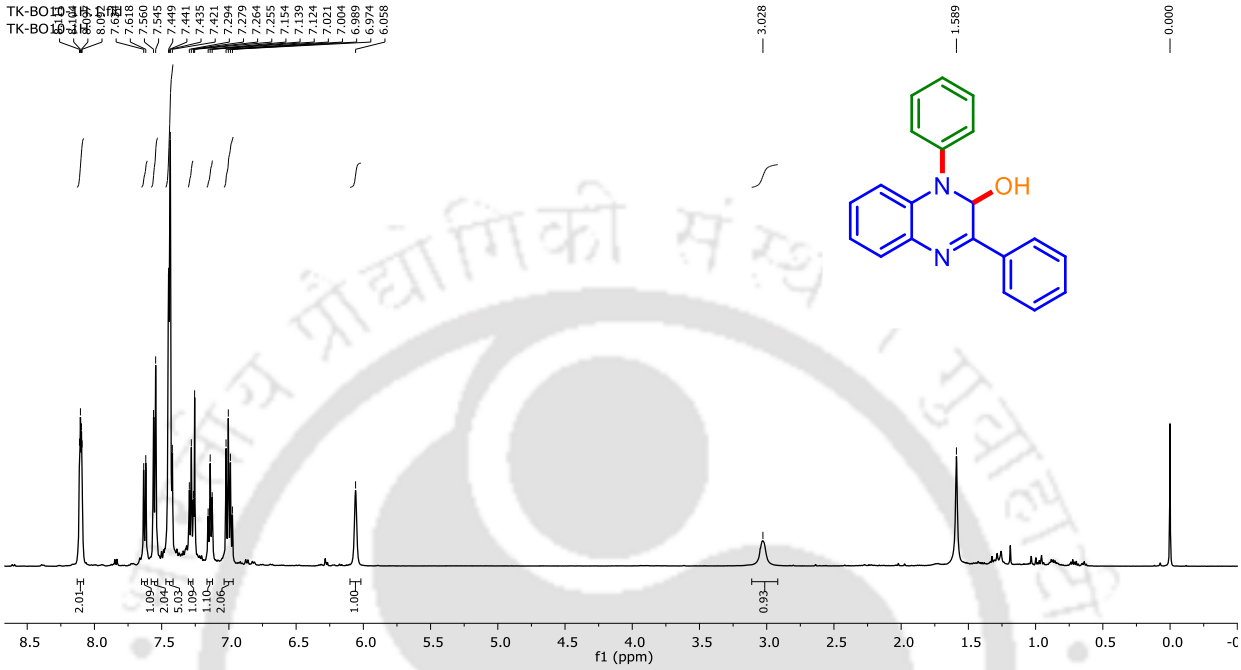

1,3-Diphenyl-1,2-dihydroquinoxalin-2-ol (3aa): $^{13}C\{^{1}H\}$ NMR ($CDCl_3$, 101 MHz)

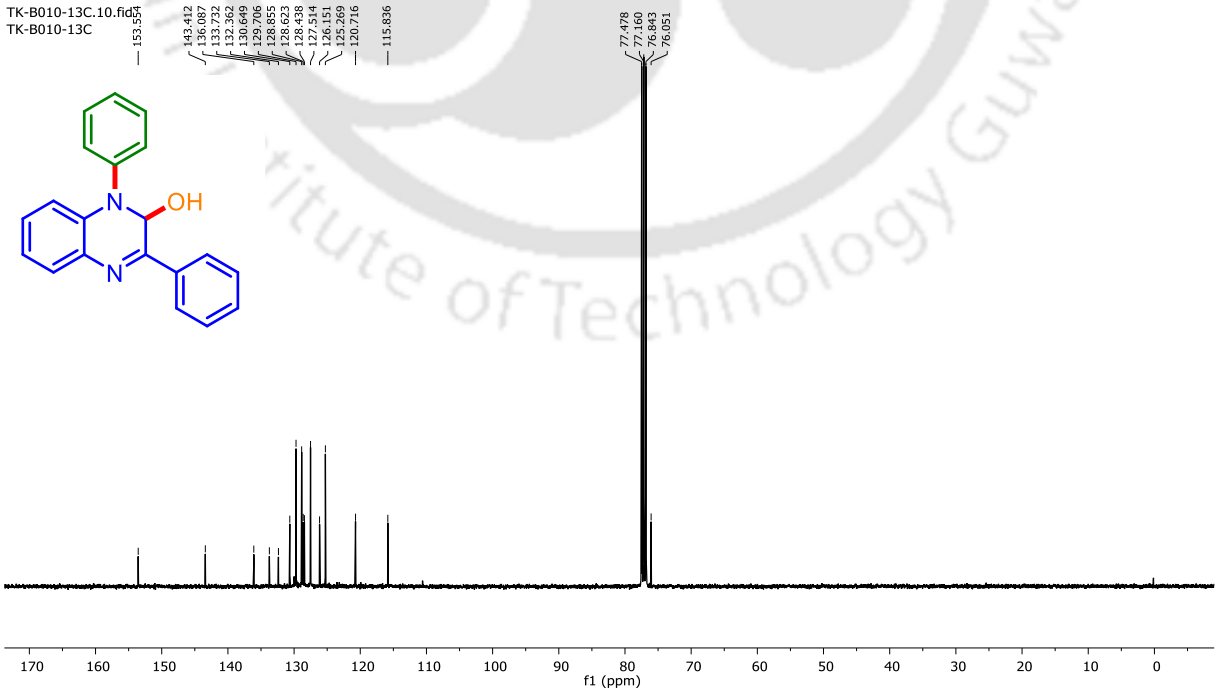

1-Phenyl-3-(*p*-tolyl)-1,2-dihydroquinoxalin-2-ol (3ca): ^{1}H NMR ($CDCl_3$, 500MHz)

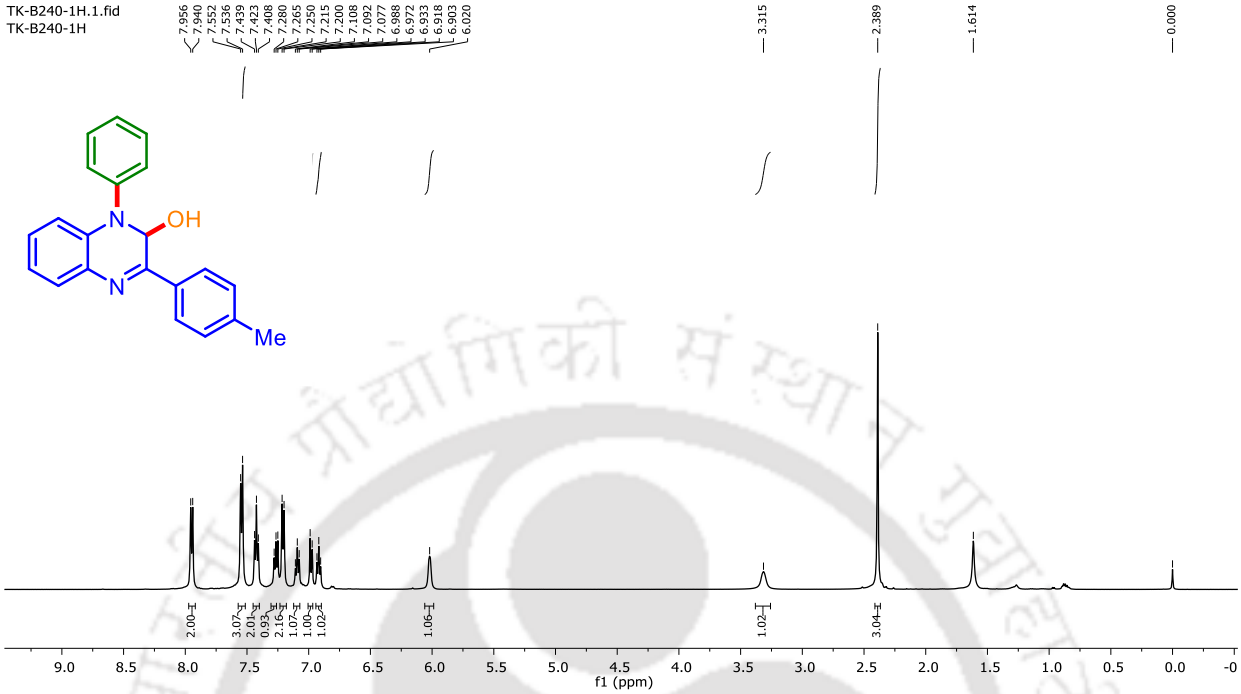

1-Phenyl-3-(*p*-tolyl)-1,2-dihydroquinoxalin-2-ol (3ca): $^{13}C\{^{1}H\}$ NMR ($CDCl_3$, 126 MHz)

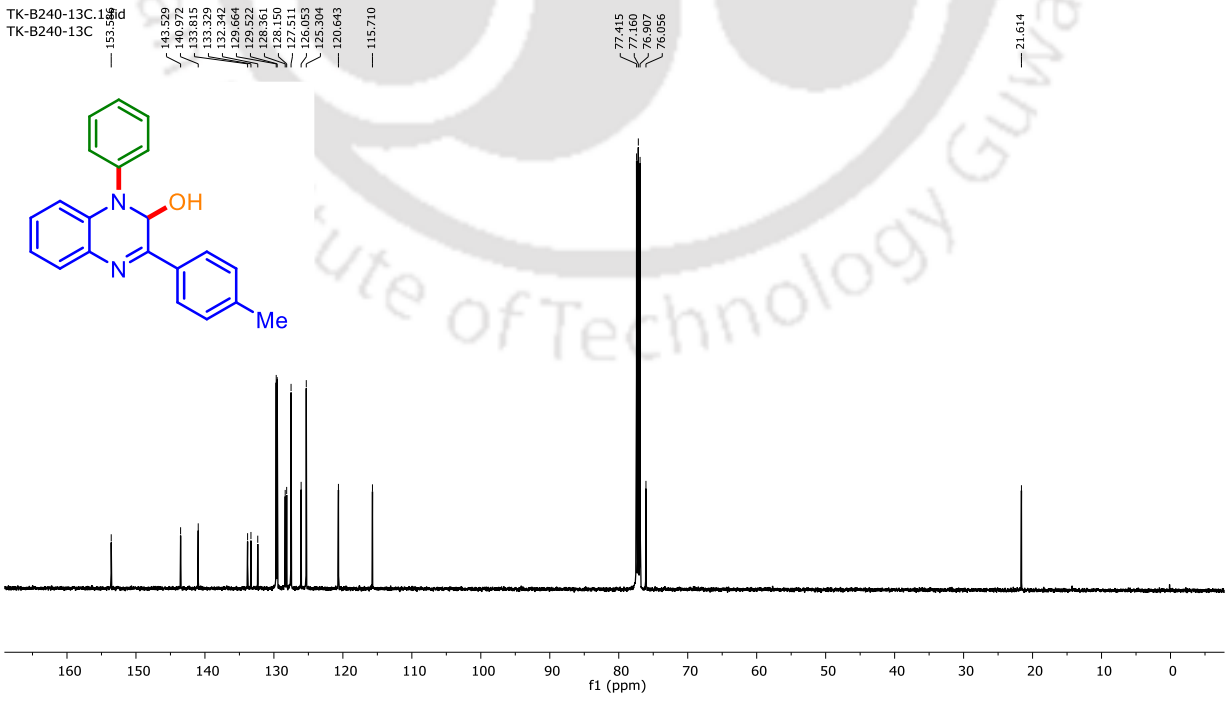

1-Phenyl-3-(*m*-tolyl)-1,2-dihydroquinoxalin-2-ol (3ja): ^{1}H NMR ($CDCl_3$, 500MHz)

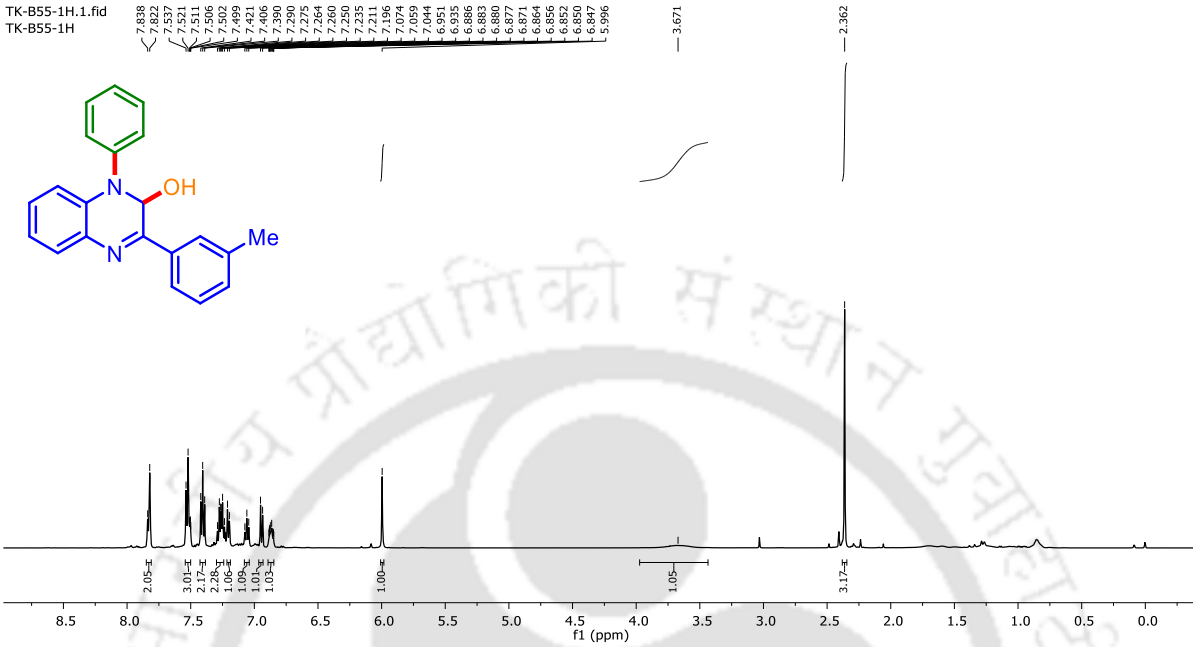

1-Phenyl-3-(*m*-tolyl)-1,2-dihydroquinoxalin-2-ol (3ja): ^{13}C{^{1}H} NMR ($CDCl_3$, 126 MHz)

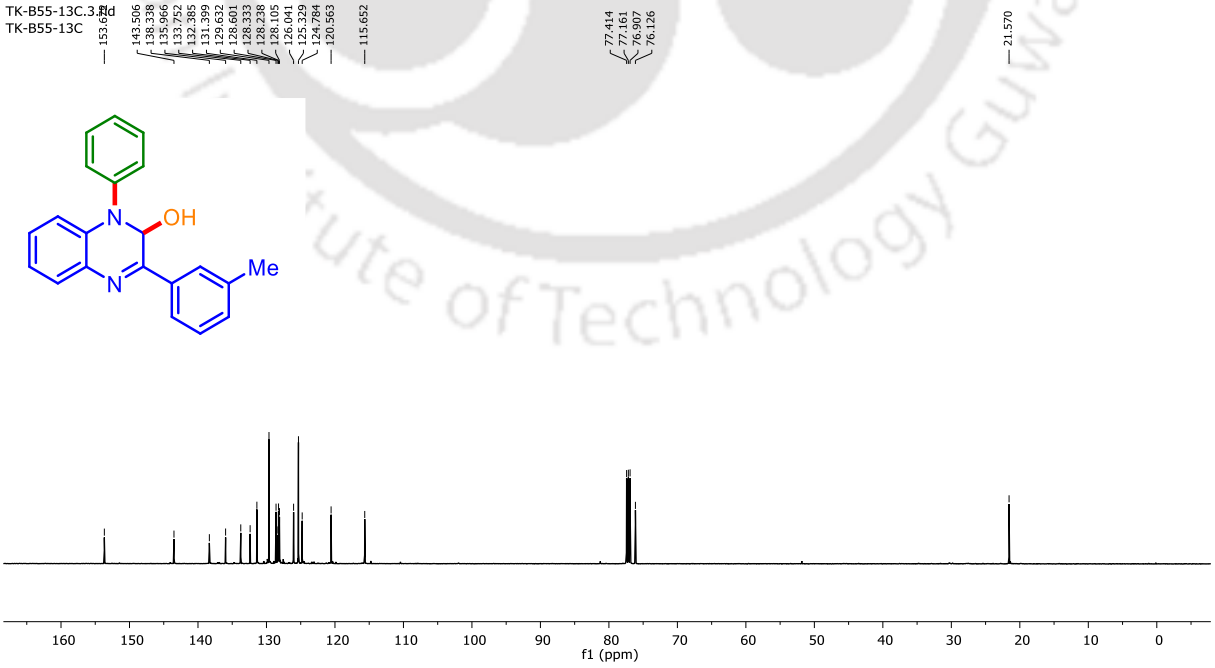

3-(2-Fluorophenyl)-1-phenyl-1,2-dihydroquinoxalin-2-ol (3ka): ^{1}H NMR ($CDCl_3$, 500MHz)

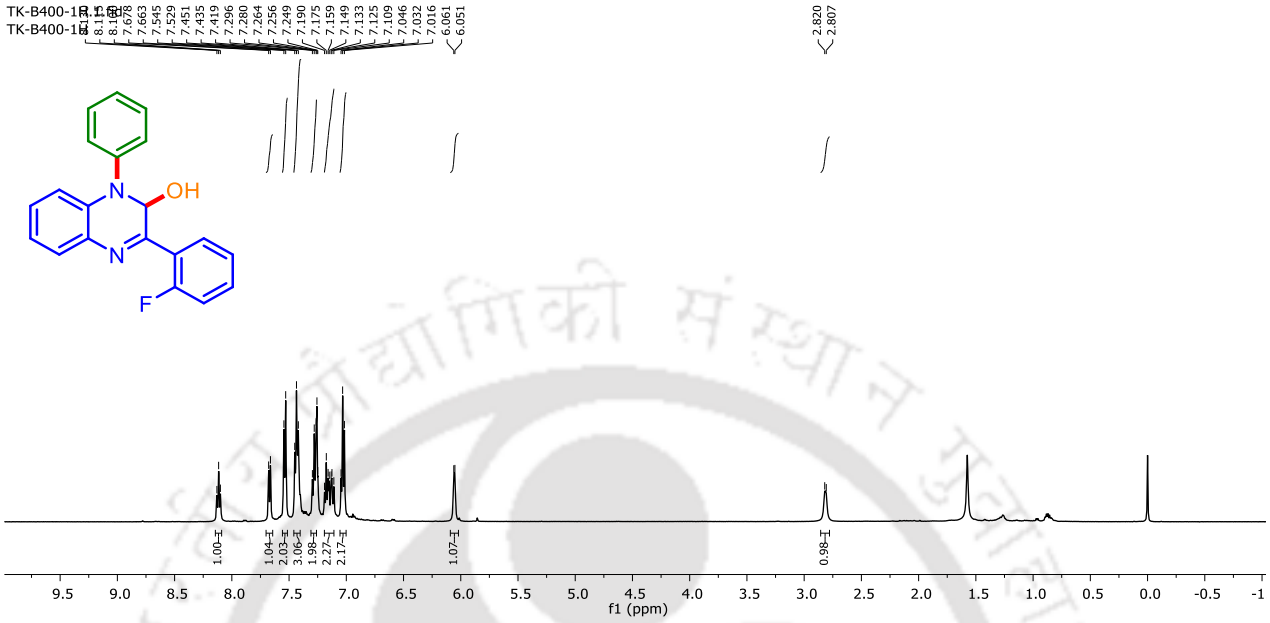

3-(2-Fluorophenyl)-1-phenyl-1,2-dihydroquinoxalin-2-ol (3ka): ^{13}C{^{1}H} NMR ($CDCl_3$, 101 MHz)

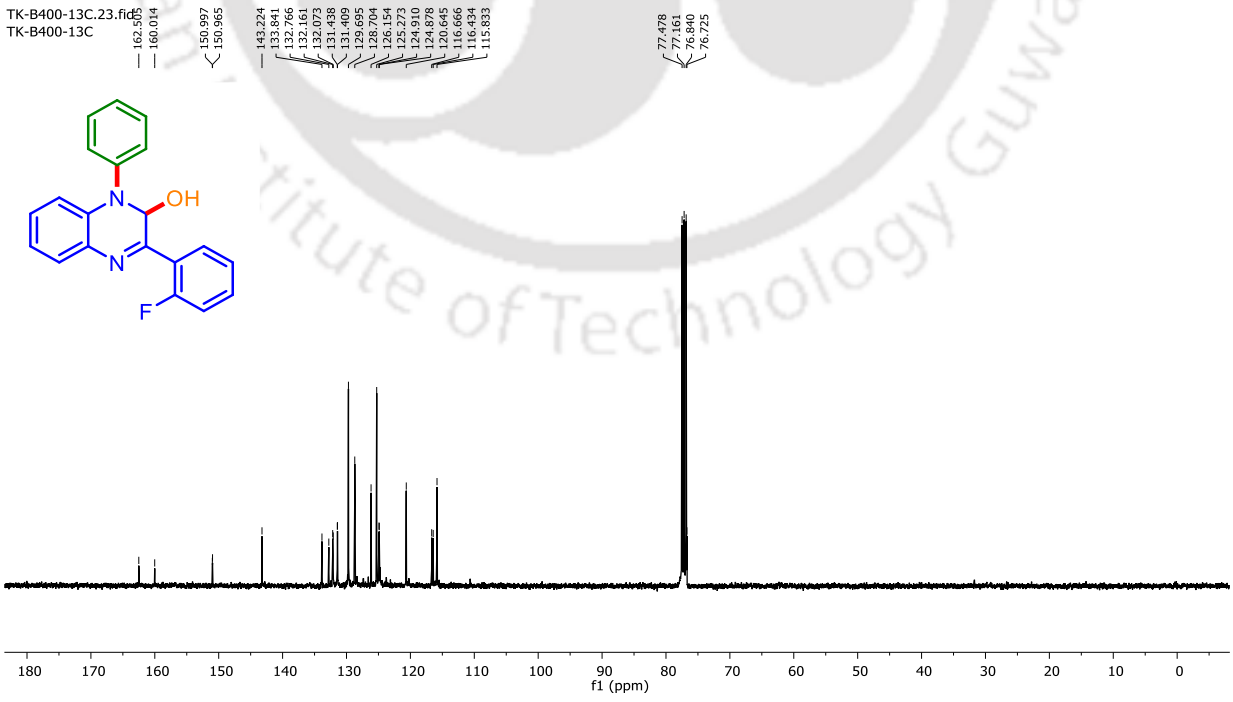

3-(2-Fluorophenyl)-1-phenyl-1,2-dihydroquinoxalin-2-ol (3ka): ^{19}F NMR ($CDCl_3$, 376 MHz)

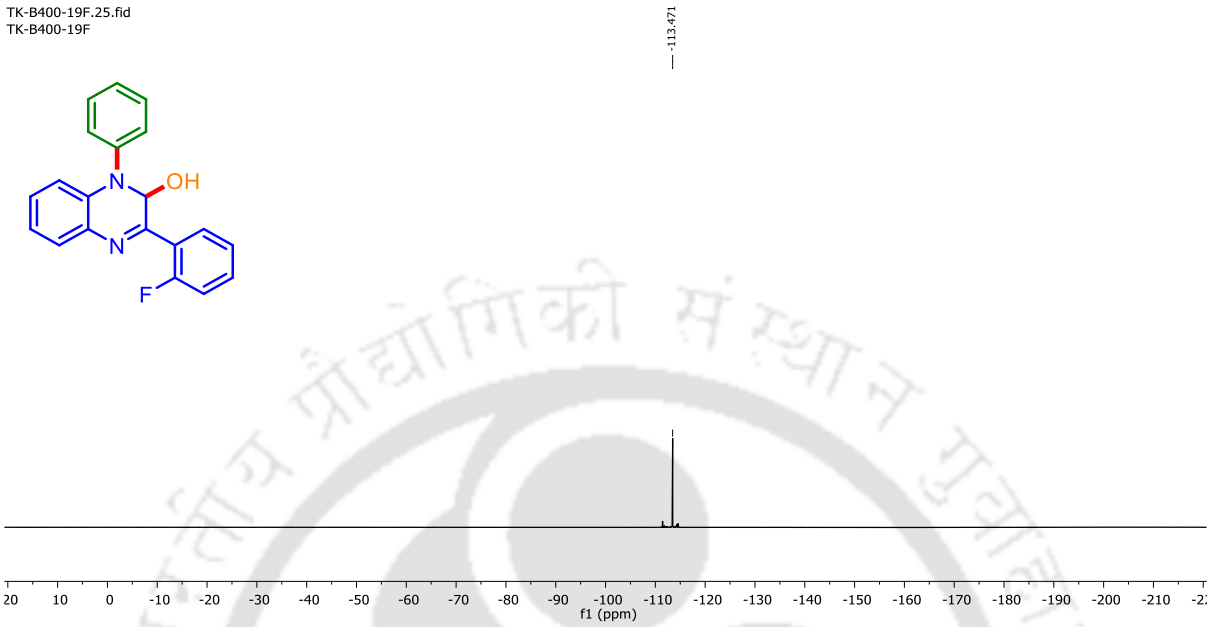

1-Phenyl-3-(thiophen-2-yl)-1,2-dihydroquinoxalin-2-ol (3ma): ^{1}H NMR ($CDCl_3$, 500MHz)

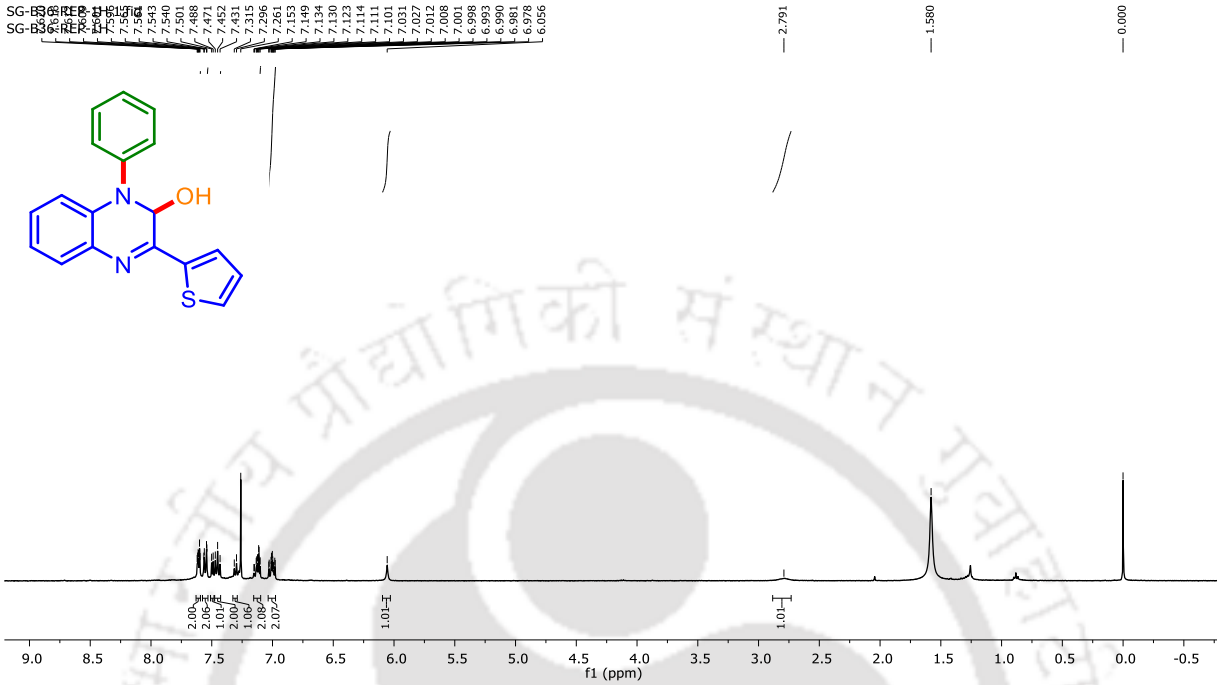

1-Phenyl-3-(thiophen-2-yl)-1,2-dihydroquinoxalin-2-ol (3ma): ^{13}C{^{1}H} NMR ($CDCl_3$, 126 MHz)

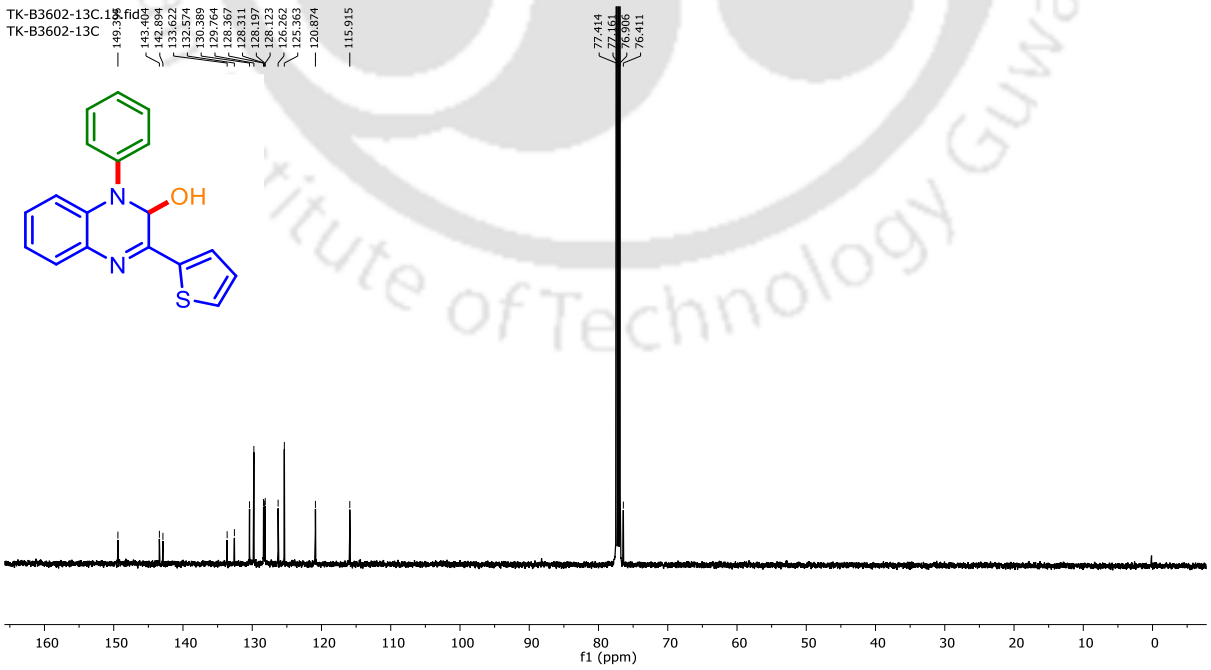

1-(4-Methoxyphenyl)-3-phenyl-1,2-dihydroquinoxalin-2-ol (3ab): ^{1}H NMR ($CDCl_3$, 500 MHz)

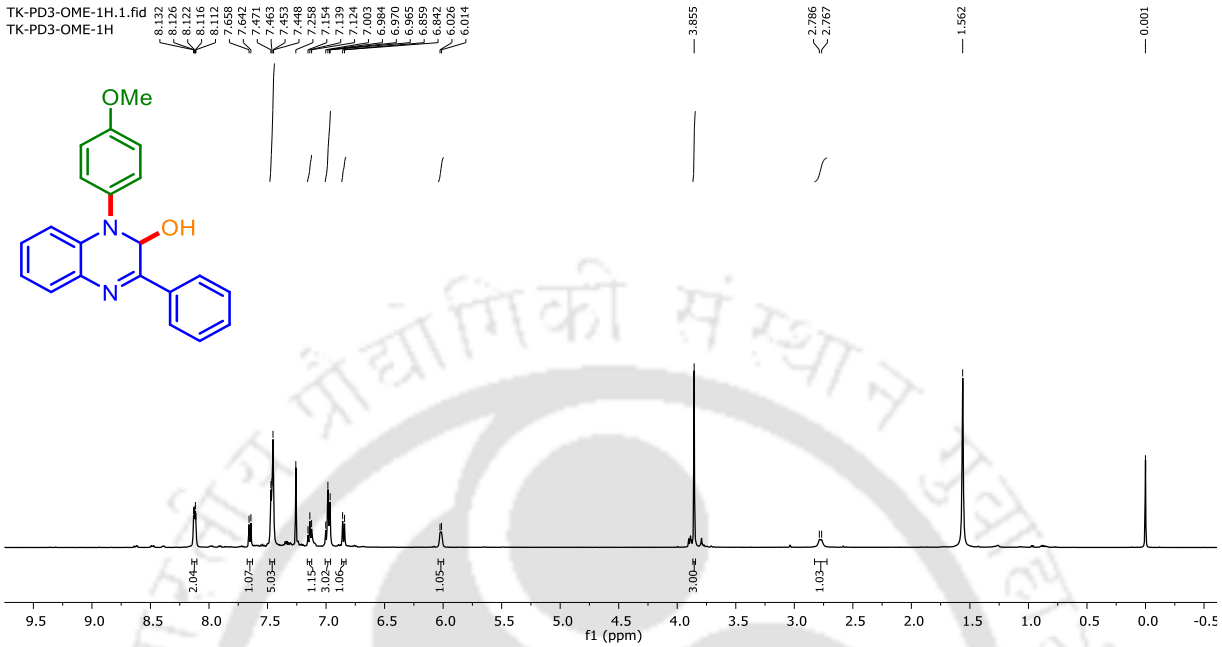

1-(4-Methoxyphenyl)-3-phenyl-1,2-dihydroquinoxalin-2-ol (3ab): ^{13}C{^{1}H} NMR ($CDCl_3$, 126 MHz)

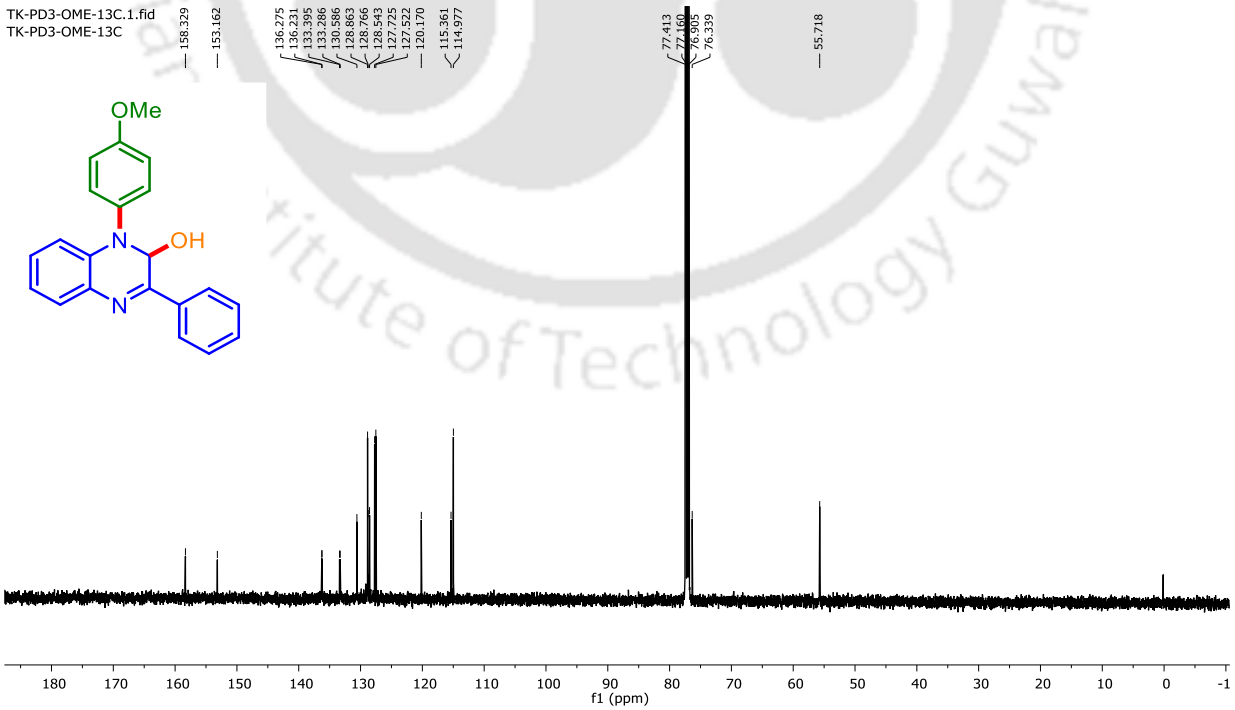

(1*S*, 2*R*, 5*S*)-2-Isopropyl-5-methylcyclohexyl 4-((*S*)-3-hydroxy-4-phenyl-3,4-dihydroquinoxalin-2-yl)benzoate (3oa): ^{1}H NMR ($CDCl_3$, 500 MHz)

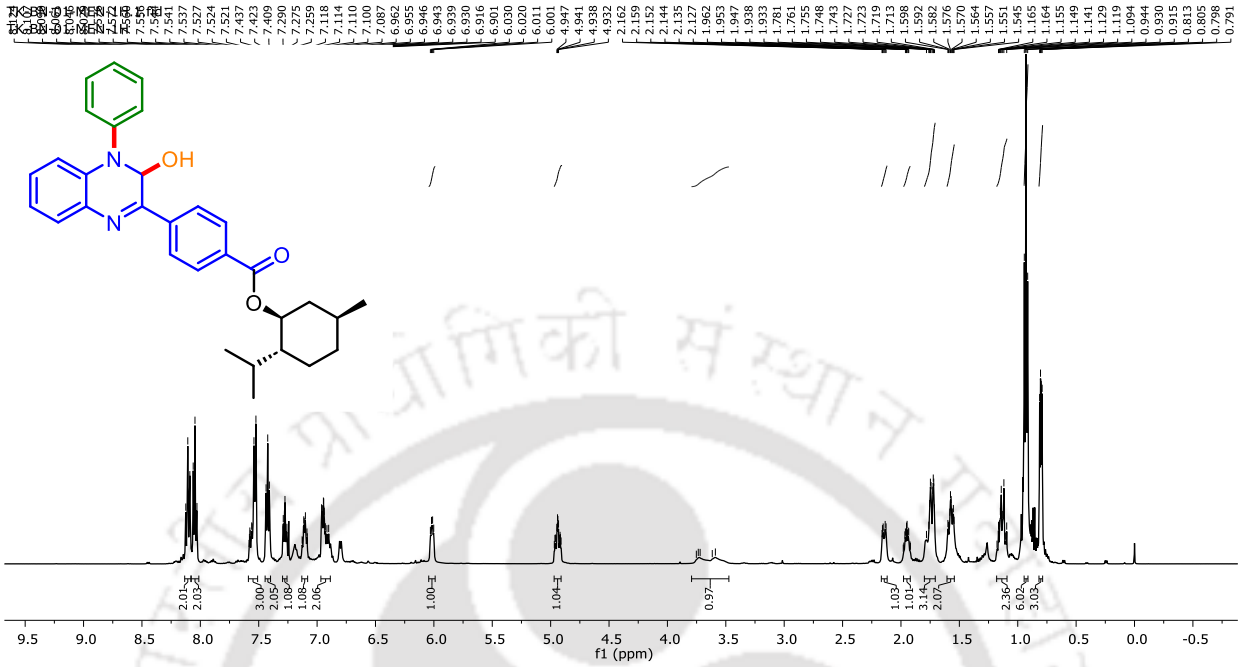

(1*S*, 2*R*, 5*S*)-2-Isopropyl-5-methylcyclohexyl 4-((*S*)-3-hydroxy-4-phenyl-3,4-dihydroquinoxalin-2-yl)benzoate (3oa): ^{13}C{^{1}H} NMR ($CDCl_3$, 126 MHz)

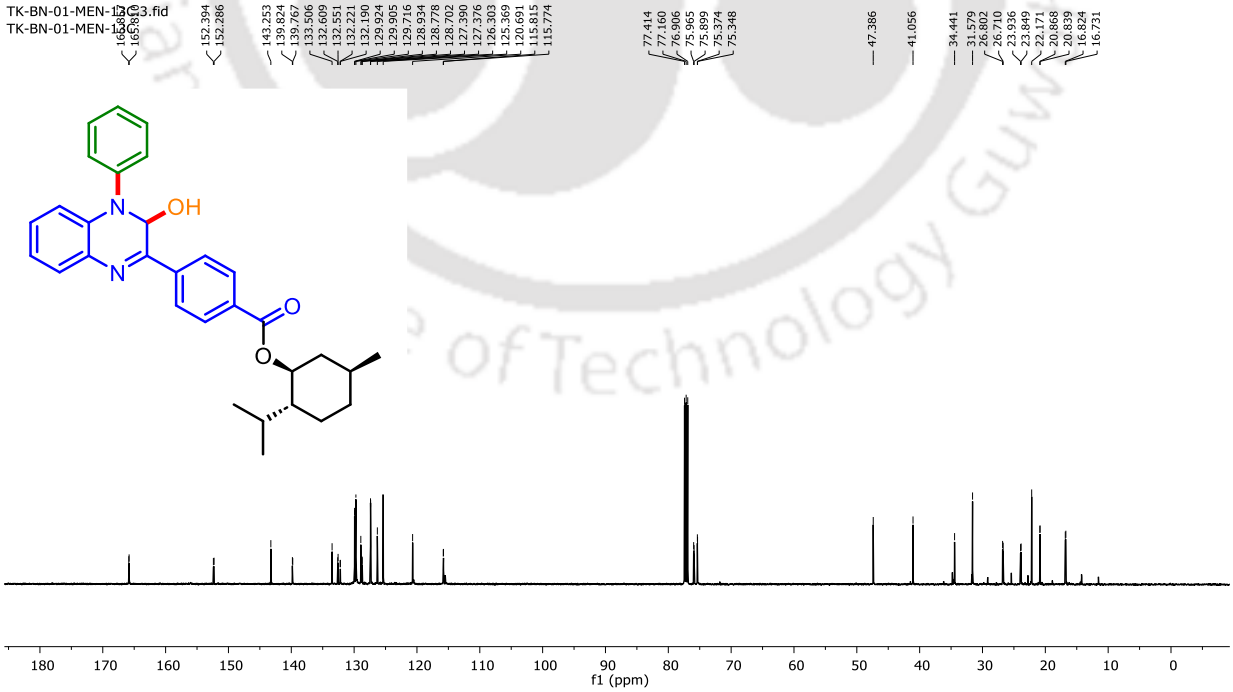

2-Phenylisoquinolin-2-ium trifluoromethanesulfonate (7'): ^{1}H NMR (DMSO-d$_6$, 400 MHz)

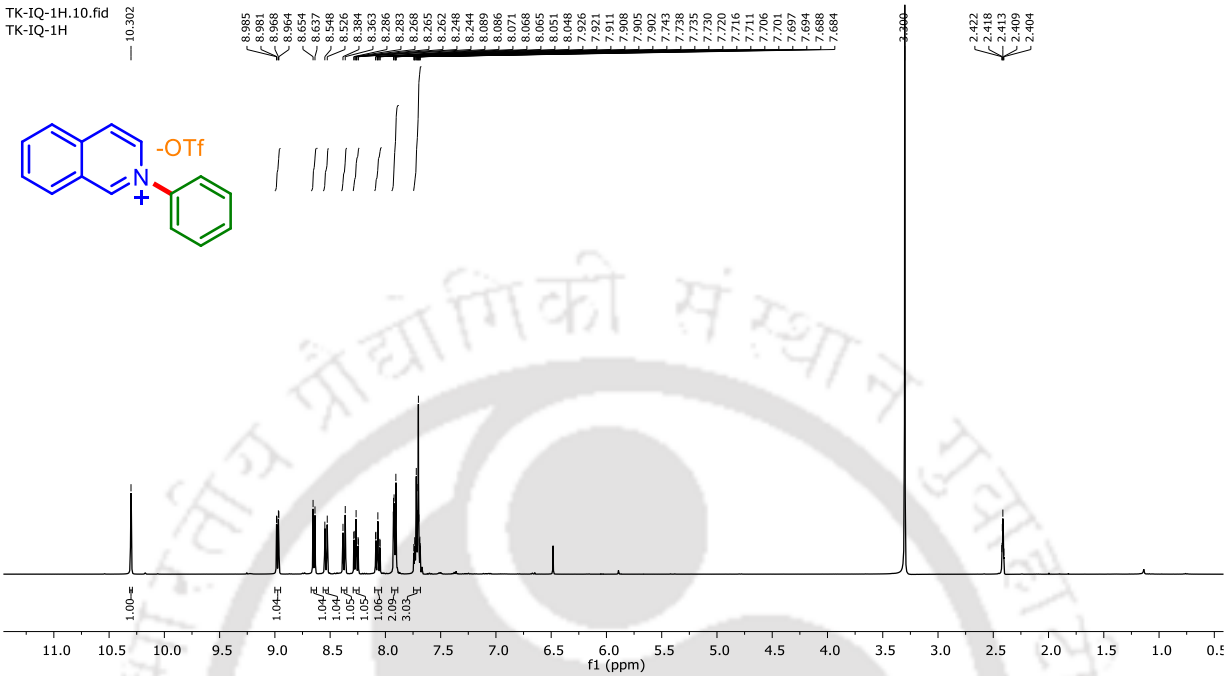

2-Phenylisoquinolin-2-ium trifluoromethanesulfonate (7'): ^{13}C{^{1}H} NMR (DMSO-d$_6$, 101 MHz)

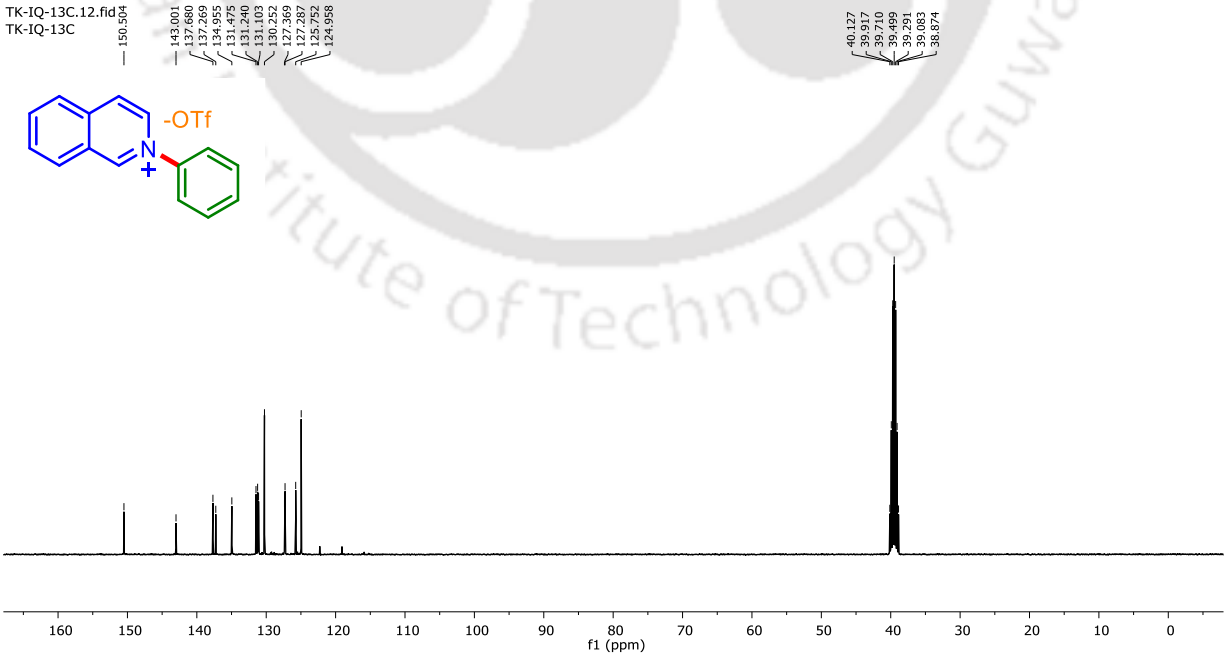

2-Phenylisoquinolin-2-ium trifluoromethanesulfonate (7'): ^{19}F NMR (DMSO-d$_6$, 471 MHz)

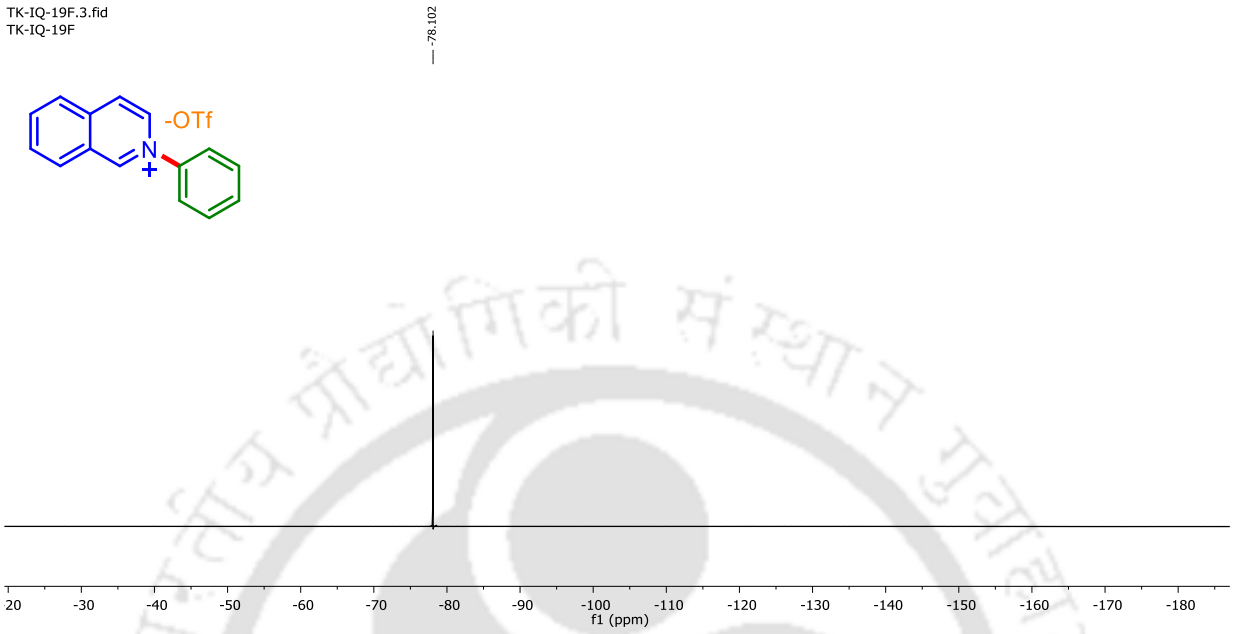

2-Phenylquinoline (8'): ^{1}H NMR ($CDCl_3$, 600 MHz)

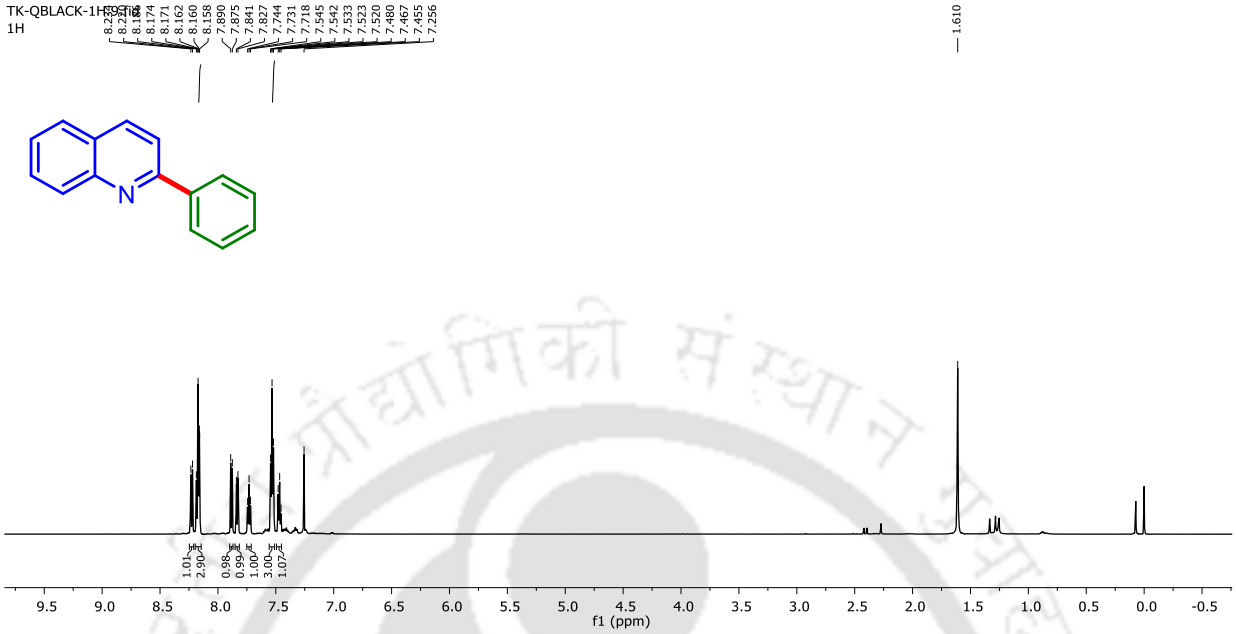

2-Phenylquinoline (8'): ^{13}C{^{1}H} NMR ($CDCl_3$, 151 MHz)

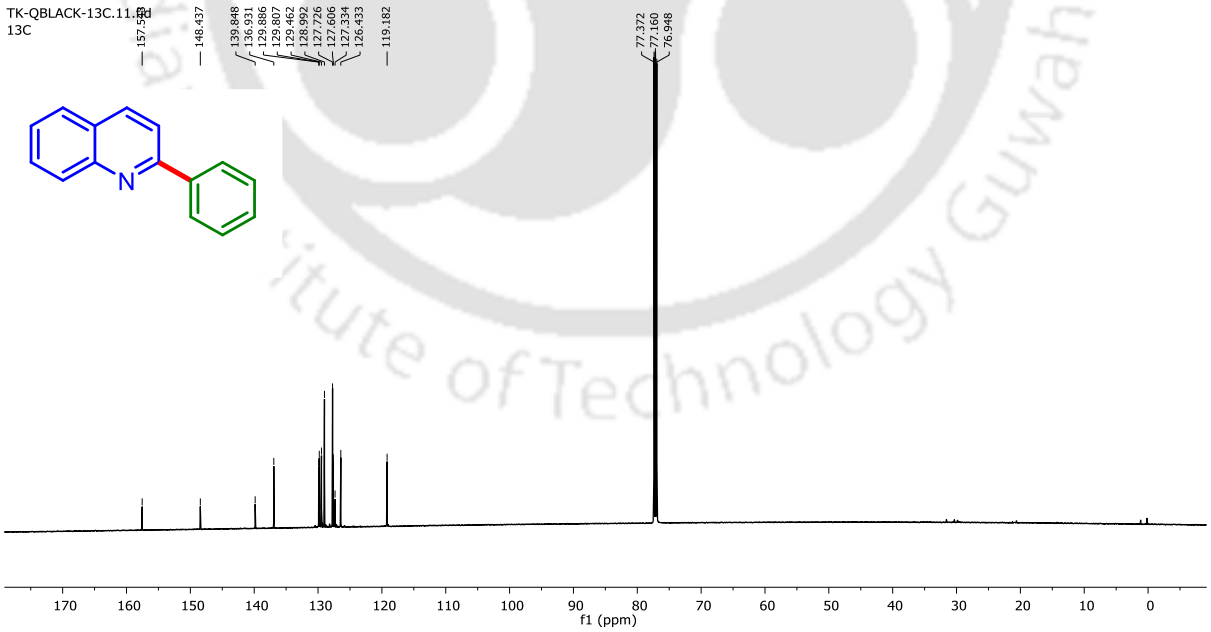

5-Methyl-1,3-diphenyl-1*H*-benzo[*d*]imidazol-3-ium trifluoromethanesulfonate (10aa): ^{1}H NMR (DMSO-d$_6$, 500 MHz)

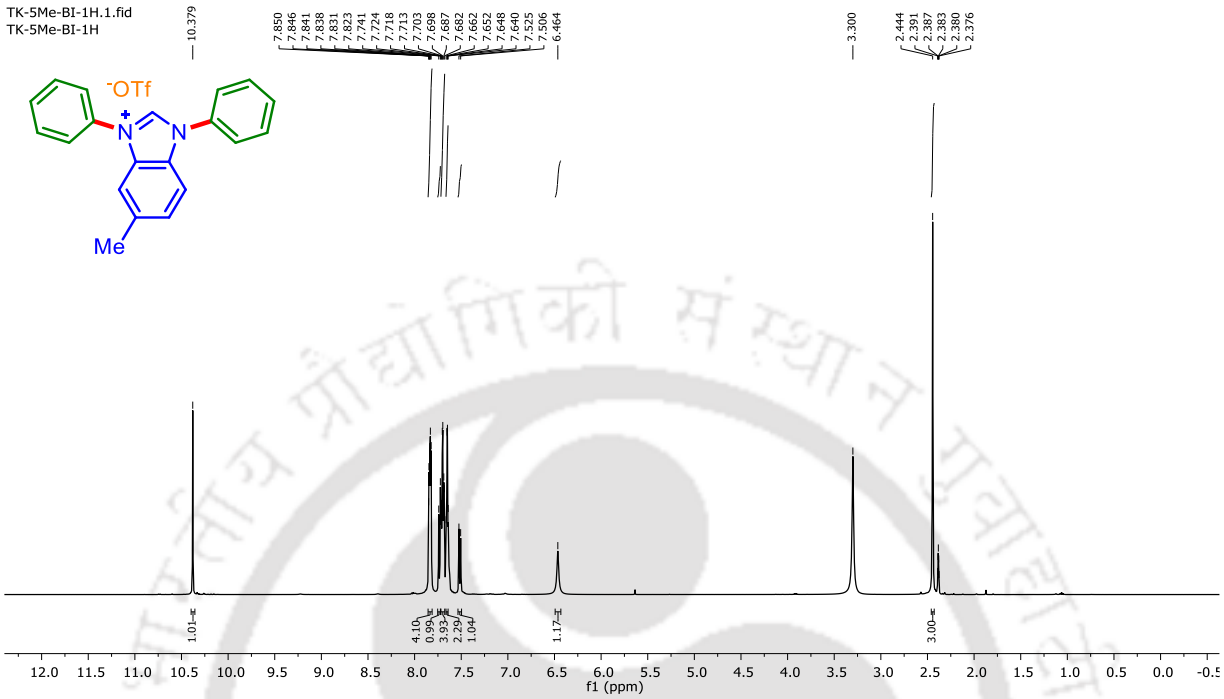

5-Methyl-1,3-diphenyl-1*H*-benzo[*d*]imidazol-3-ium trifluoromethanesulfonate (10aa): ^{13}C{^{1}H} NMR (DMSO-d$_6$, 126 MHz)

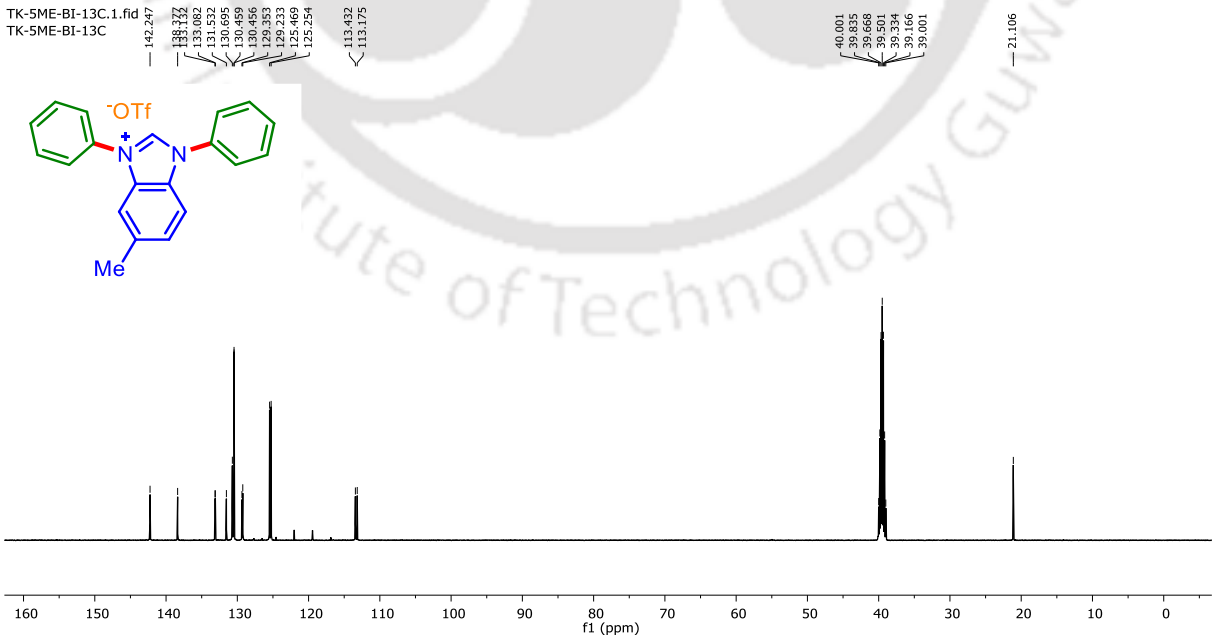

5-Methyl-1,3-diphenyl-1*H*-benzo[*d*]imidazol-3-ium trifluoromethanesulfonate (10aa): ^{19}F NMR (DMSO-d$_6$, 471 MHz)

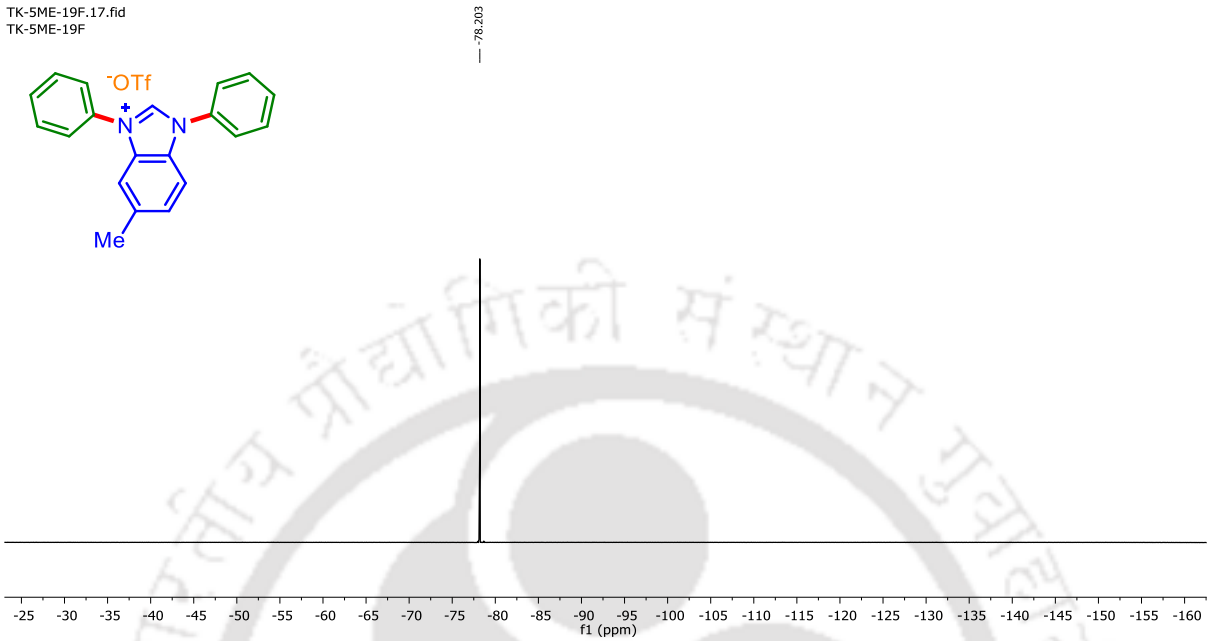

1,3-Diphenyl-1*H*-imidazol-3-ium trifluoromethanesulfonate (10ca): ^{1}H NMR (DMSO-d$_6$, 400 MHz)

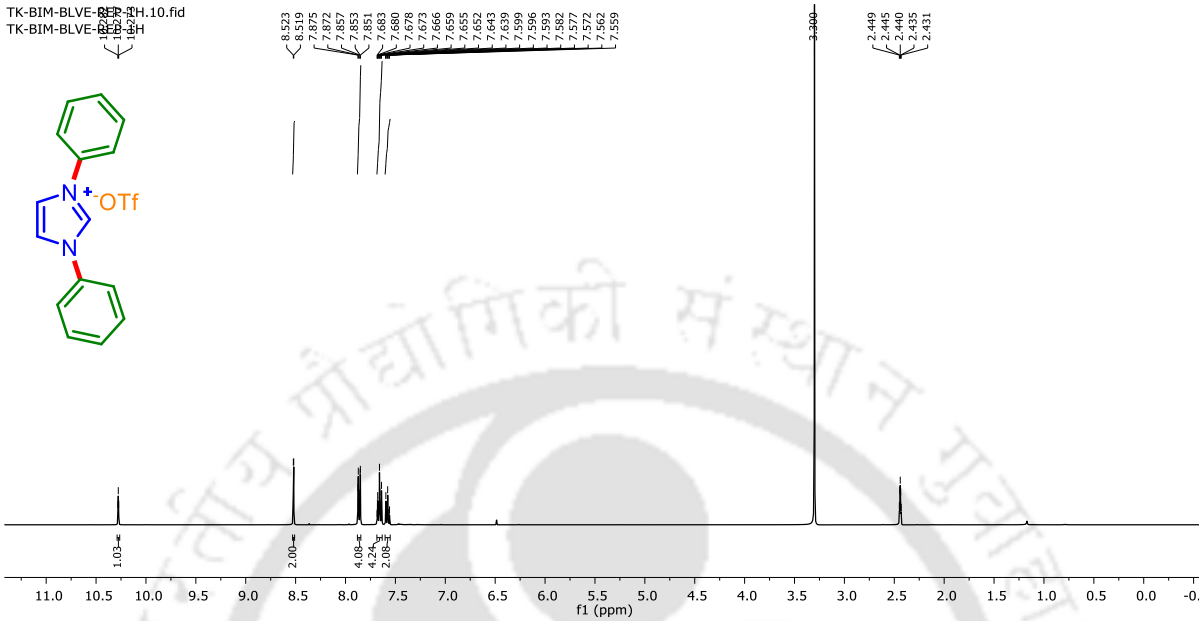

1,3-Diphenyl-1*H*-imidazol-3-ium trifluoromethanesulfonate (10ca): ^{13}C{^{1}H} NMR (DMSO-d$_6$, 101 MHz)

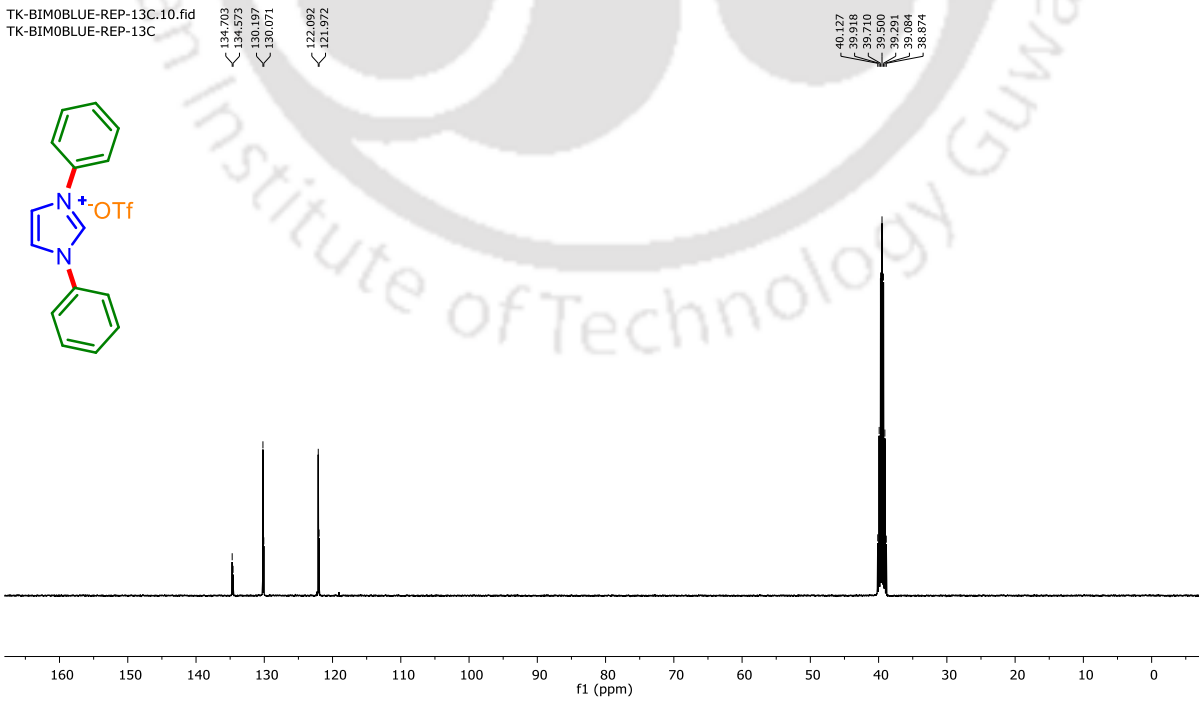

1,3-Diphenyl-1*H*-imidazol-3-ium trifluoromethanesulfonate (10ca): ^{19}F NMR (DMSO-d_6, 471 MHz)

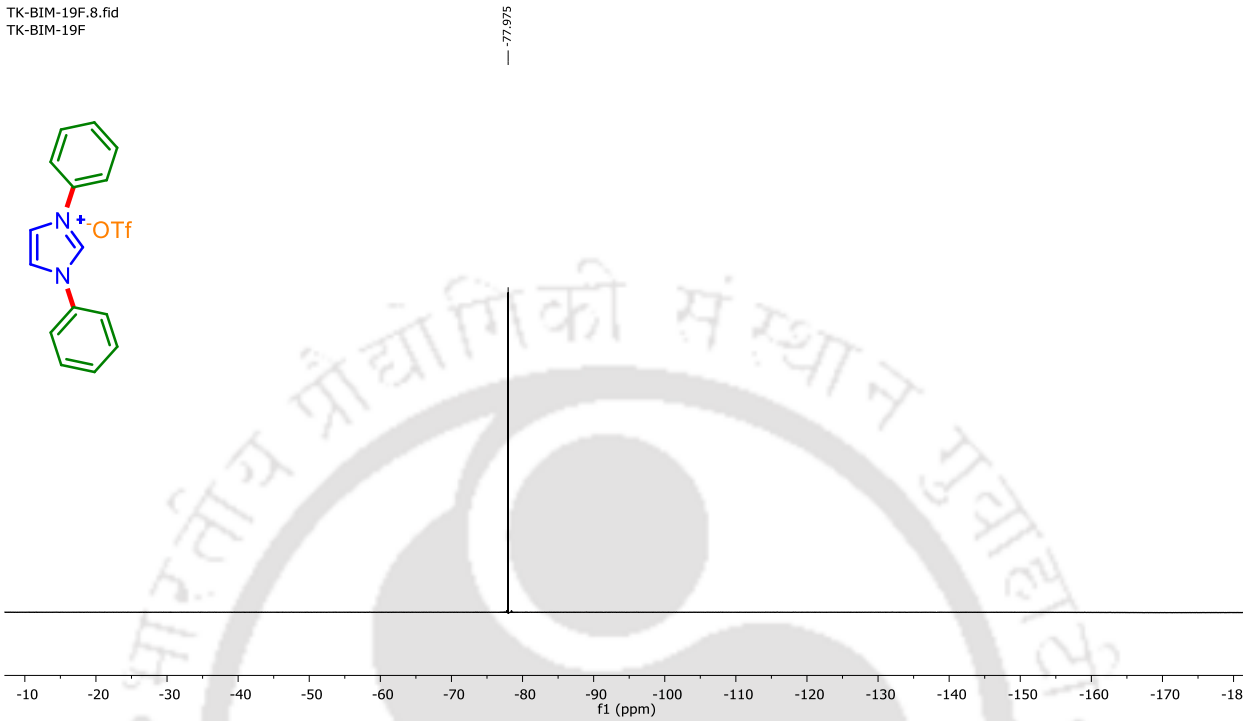

1,3-Diphenylquinoxalin-2(1*H*)-one (11): ^{1}H NMR ($CDCl_3$, 500 MHz)

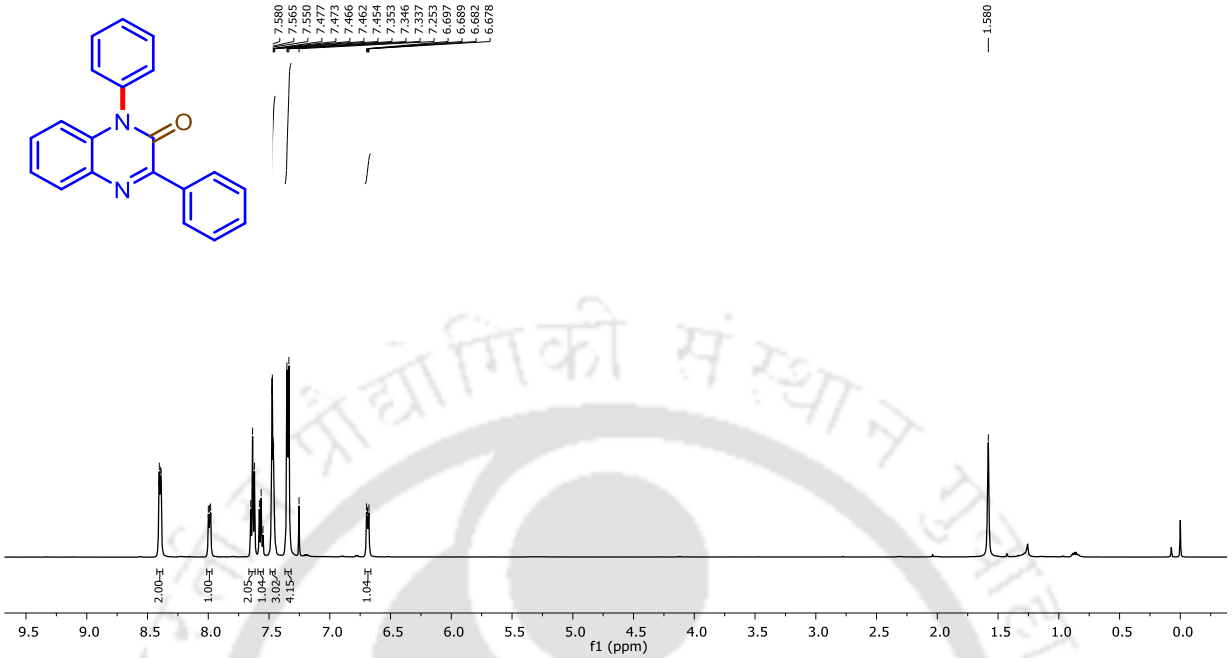

1,3-Diphenylquinoxalin-2(1*H*)-one (11): ^{13}C{^{1}H} NMR ($CDCl_3$, 126 MHz)

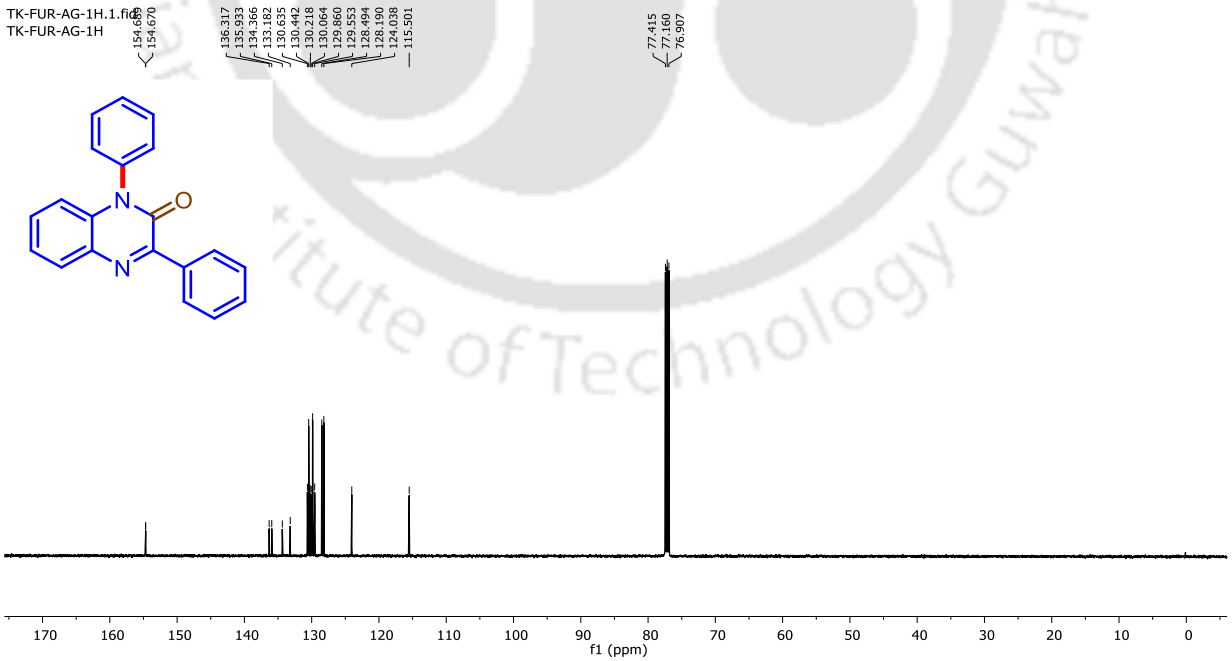

1,3,4,8,9-Pentaphenyl-1*H*-benzo[*ij*]imidazo[2,1,5-*de*]quinolizin-10-ium trifluoromethanesulfonate (12): ^{1}H NMR ($CDCl_3$, 500 MHz)

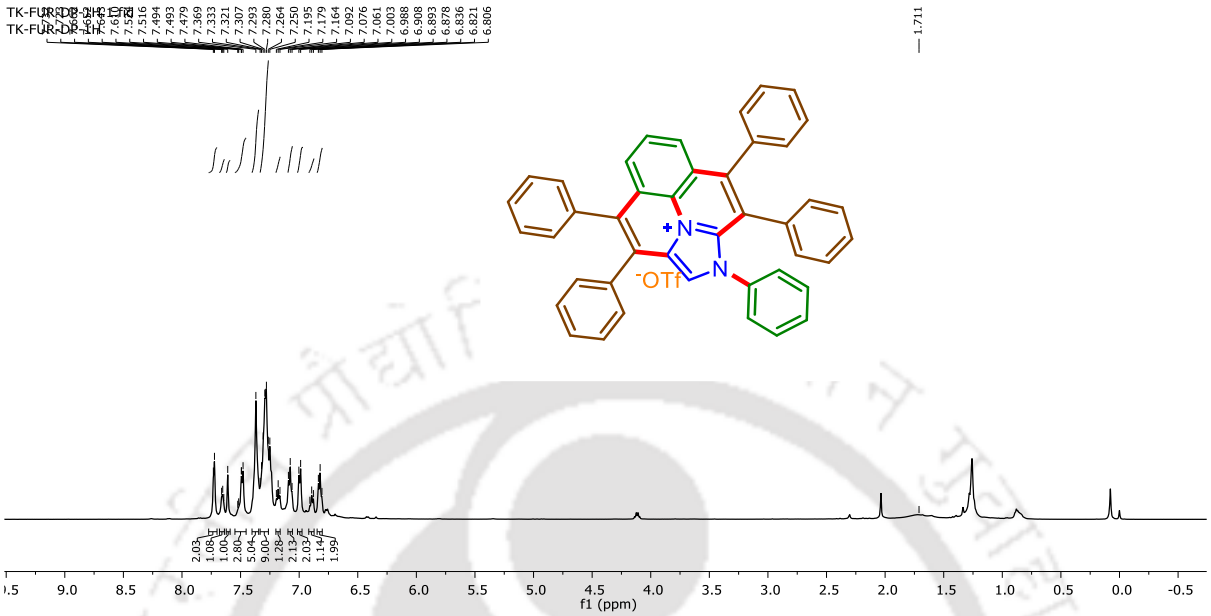

1,3,4,8,9-Pentaphenyl-1*H*-benzo[*ij*]imidazo[2,1,5-*de*]quinolizin-10-ium trifluoromethanesulfonate (12): ^{13}C{^{1}H} NMR ($CDCl_3$, 126 MHz)

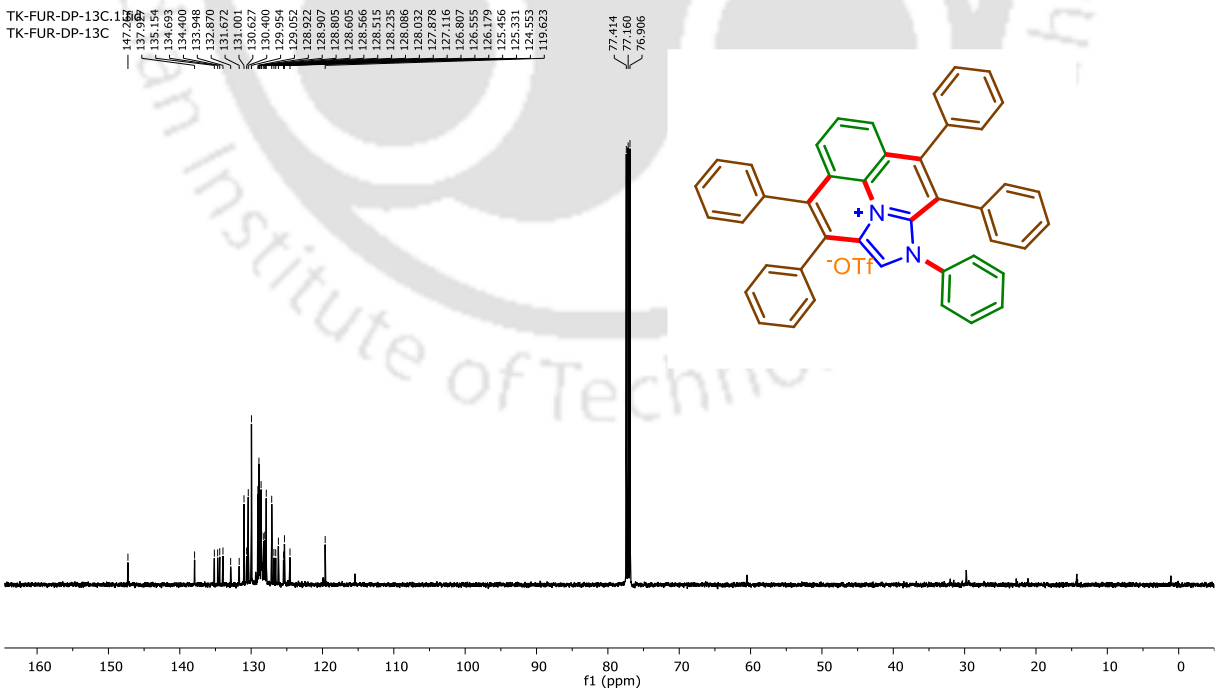

1,3,4,8,9-Pentaphenyl-1*H*-benzo[*ij*]imidazo[2,1,5-*de*]quinolizin-10-ium trifluoromethanesulfonate (12): ^{19}F NMR ($CDCl_3$, MHz)

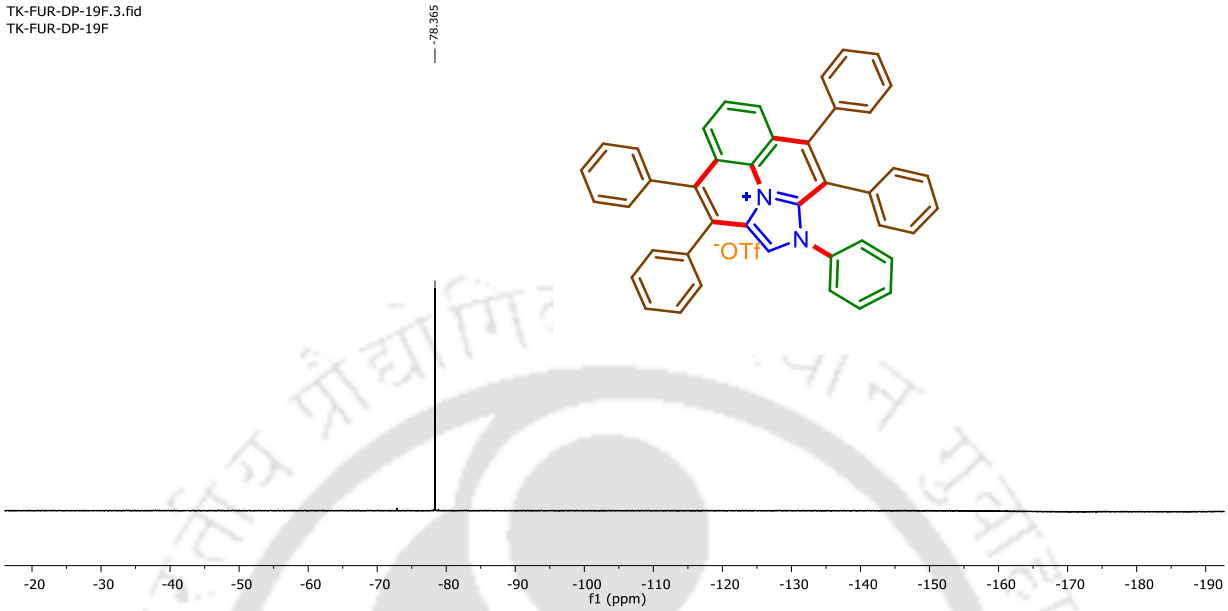

Photo-Induced 1,2-Thiohydroxylation of Maleimide Involving Disulfide and Singlet Oxygen

IV

Chapter

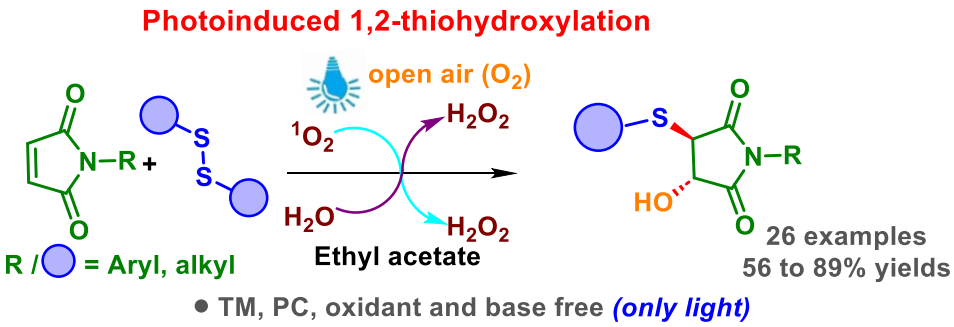

ABSTRACT

A visible light-driven di-functionalization of maleimide with disulfide and in situ-generated singlet oxygen offers selective 1,2-thiohydroxylation under additive-free conditions. Here the disulfide plays the dual role of photosensitizer and the coupling reagent. Notably, the hydroxyl functionality originates from the in situ generated singlet oxygen followed by HAT from H_2O (moisture).

Reference:

Khandelia, T.; Ghosh, S.; Panigrahi, P.; Mandal, R.; Boruah D.; Patel, B. K. *Chem. Commun.*, **2023**, *59*, 11196.

IV.1. Introduction

The recent era of contemporary organic synthesis has witnessed the rapid broadening of photo-catalysis as a robust synthetic itinerary.[1] It offers sustainable eco-friendly conditions to access drugs, natural products, and agrochemicals. Many such strategies are associated with developing biologically and functionally pertinent organosulfur compounds.[2,3] Among them, the organosulfur having alkyl-aryl C–S and vicinal C–S/C–O linked candidates have generated much attention due to their prevalence in many commercial drugs (Figure IV.1.1.1). In this regard, the intricate structure of sulfur compounds and their multiple valences have attracted researchers to synthesize numerous sulfur-linked targets using thiols as one of the precursors.[4] But the stench and toxic behavior of thiols and the requirement of oxidant and metal for the generation of thiyl radical make this route unfavourable for accessing C–S bonds. To overcome this, disulfides have been used as an alternative thiolating reagent to facilitate C–S bond formation.[5] Thus a sustainable mild disulfide mediated protocol is highly looked for.

The alkene di-functionalization strategy opens up a new avenue to access complex molecular entities via the simultaneous installation of two distinct functionalities. Lately, this strategy rapidly evolves under metal and photo catalysis to synthesize numerous functional materials.[6] Despite notable advancements in this arena, the di-functionalization of maleimide under sustainable photocatalysis is highly sought after. As maleimides and succinimides are biologically pertinent scaffolds therefore great efforts have been devoted towards their functionalization.[7] Apart from this, maleimides are also explored as powerful di-functionalization handles to access substituted maleimides.

IV.1.1. Importance of Organosulfur Molecules Having Alkyl-Aryl C–S and Vicinal C–S/C–O Bonds

The organosulfur molecules having alkyl-aryl C–S and vicinal C–S/C–O bonds are prevalent in numerous biologically important structures. Some of the examples are antifungal drug butoconazole, anti-hyperlipidemic drug probucol, antiviral drug lamivudine, prostate cancer treating drug casodex, antagonist of ErB, antibiotic cleocin and antibacterial drug bithionol (Figure IV.1.1.1.).

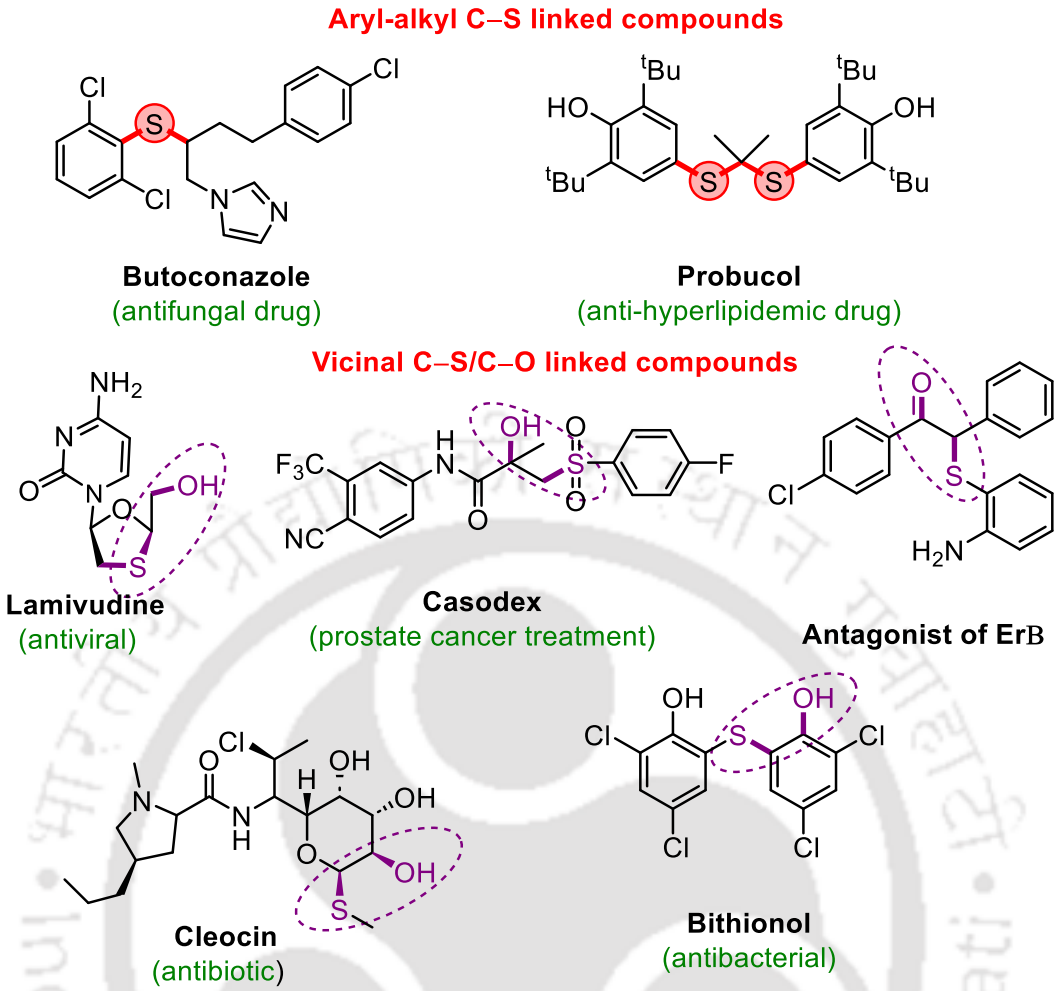

Figure IV.1.1.1. *Representative sulfur containing drug candidates*

IV.1.2. Preceding Reports of Thermal and Photocatalyzed Di-functionalization of Maleimide

In 2022, Zhao *et. al.* achieved seleno-sulfonation of maleimide using sulfonyl hydrazides, diphenyl diselenide and $Cu(CH_3CN)_4PF_6$ as the catalyst. The reaction utilizes *tert*-butyl hydroperoxide as oxidant (Scheme IV.1.2.1).[8]

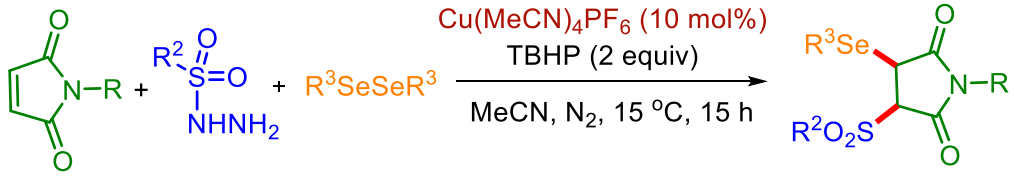

Scheme IV.1.2.1. *Cu(I)-catalyzed selenosulfonation of maleimide*

In 2020, Wu *et. al.* reported a Cu(I) catalyzed oxidative thioamination of maleimide with secondary amines and Bunte salt. The reaction proceeds via the formation of reactive enaminone and subsequent intermolecular alkenyl C–H thiolation at 100 ºC (Scheme IV.1.2.2).[9]

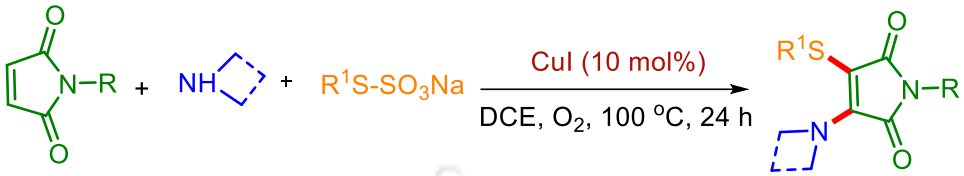

Scheme IV.1.2.2. *Cu(I)-catalyzed thioamination of maleimide*

Besides such metal catalysis considering photoinduced di-functionalizations, in 2019, Melchiorre *et. al.* reported a photoinduced di-functionalization of maleimide under a radical-mediated process. The protocol utilizes thiocarbamate salt as a catalyst (photo absorbing species) and alkyl chloride and heteroaromatic fragments as the bifunctional moiety (Scheme IV.1.2.3).[10]

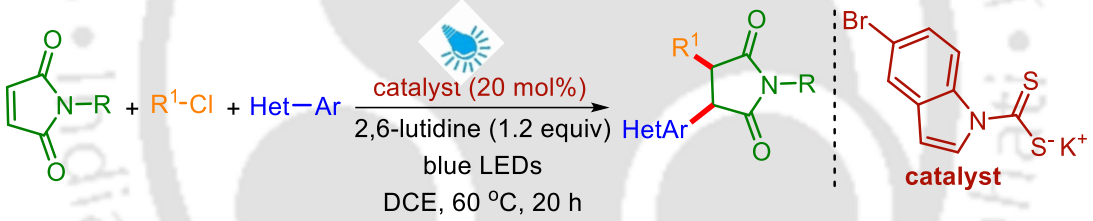

Scheme IV.1.2.3. *Photo-induced di-functionalization of maleimide*

IV.1.3. Present Strategy for Photo-Induced Di-functionalization of Maleimide

The photochemical approach most often uses organic or inorganic photocatalysts. Under the irradiation of light of appropriate wavelength organic disulfides undergo homolytic cleavage, generating thiyl radical (RS•) which can add across C=C double bond. Due to the intrinsic electron transfer and radical generating ability, thiyl radicals are powerful hydrogen atom transfer (HAT) catalysts in a photo redox process.[11] Despite the remarkable achievements, to the best of our knowledge the di-functionalized succinimides are less scrutinized under sustainable photocatalysis. This aforementioned conundrum and our continuous effort to functionalize maleimides,[12] encouraged us to envision a di-functionalization of maleimide under a sustainable additive-free photocatalysis. With this quest in mind, N-phenylmaleimide (**1a**) (1 equiv.) and 1,2-bis(4-methoxyphenyl)disulfane (**2a**) (0.5 equiv., λ_{ab} = 400–440 nm,

Figure IV.4.1.6) in ethyl acetate were reacted under blue light ($\lambda_{em,max}$ = 419 nm, Figure IV.4.1.6) irradiation. To our delight, a di-functionalized product, thio-hydroxylated maleimide (**3aa**) in trans selective form was obtained in 86% (Scheme IV.1.3.1) as confirmed by spectroscopic techniques (^{1}H, ^{13}C NMR).

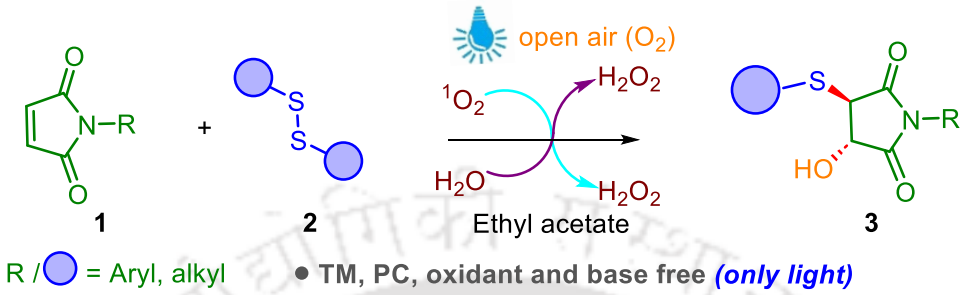

Scheme IV.1.3.1. *Photoinduced 1,2-thiohydroxylation of maleimide*

The structure of the obtained product (3*S*,4*R*)-3-hydroxy-4-((4-methoxyphenyl)thio)-1-phenylpyrrolidine-2,5-dione (**3aa**) was further confirmed by single crystal X-ray analysis (Scheme IV.3.1). Here, the incorporation of hydroxyl functionality is unprecedented which may serve as the handle for further organic transformations.[13]

IV.2 Optimization of Reaction Conditions

Table IV.2.1. *Optimization of reaction conditions*[a]

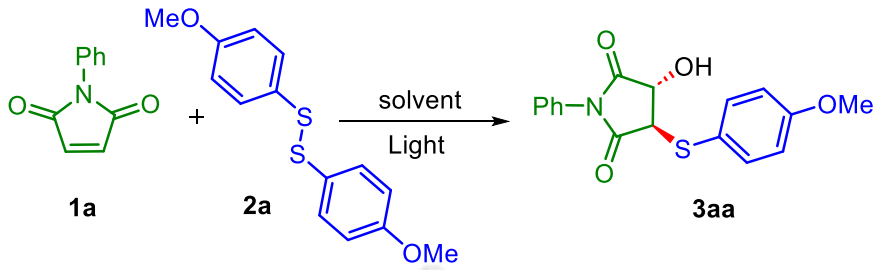

Sl. No.	Deviation from standard conditions	Yield of **3aa** (%)[b]
1.	None	86
2.	$CHCl_3$ instead of ethyl acetate	63
3.	DCE instead of ethyl acetate	60
4.	DCM instead of ethyl acetate	65
5.	TFE instead of ethyl acetate	71
6.	1,4 dioxane instead of ethyl acetate	30
7.	Toluene instead of ethyl acetate	40
8.	PhCl instead of ethyl acetate	20
9.	EtOH instead of ethyl acetate	55
10.	0.6 and 0.75 equivalents of **2a**	86 and 87
11.	No light	0
12.	Green LEDs instead of blue LEDs	0

[a]Reaction Conditions: **1a** (0.25 mmol), **2a** (0.125 mmol), solvent (2 mL) for 9 h under 5W x 4 blue LEDs ($\lambda_{em,max}$ = 419 nm) in an open air. [b]Isolated yield.

Although the yield was quite good (86%), a series of optimization studies were carried out to improve it further. Initially, various solvents were screened such as $CHCl_3$, dichloroethane (DCE), dichloromethane (DCM), tetrafluoroethanol (TFE), 1,4-dioxane, toluene, PhCl, EtOH, (entry 2–9, Table IV.2.1.). But there was no improvement in the yield and ethyl acetate turned out to be the best solvent. Upon increasing the loading of 1,2-*bis*(4-methoxyphenyl)disulfane (**2a**) to 0.6 and 0.75 equiv there was no further enhancement in the yield (entry 10, Table IV.2.1.). Also, there was no reaction in the absence of light and under green LEDs (entry 11-12, Table IV.2.1.). Thus, the optimized condition found was *N*-phenylmaleimide (**1a**, 1 equiv) and 1,2-*bis*(4-methoxyphenyl)disulfane (**2a**, 0.5 equiv) in ethyl acetate under the exposure of blue light (4 x 5W, $\lambda_{em,max}$ = 419 nm) in an open air.

IV.3. Substrate Scope of the Protocol

By executing the optimized reaction condition, the scope of this strategy was extended towards diversely substituted maleimides and disulfides (Scheme IV.3.1). At first, the scope of maleimide was checked keeping 1,2-bis(4-methoxyphenyl)disulfane (**2a**) as the standard disulfide. Various substituted N-phenylmaleimide (**1b-1d**) delivered product **3ba-3da** in good yields (84−89%). Next, N-benzylmaleimide (**1e**), N-cyclohexylmethyl (**1f**) and substituted N-benzylmaleimides (**1g-1i**) all gave products **3ea-3ia** in decent yields (78−85%). Also, N-alkylated short and long-chain maleimides underwent efficient thiohydroxylation to provide products **3ja-3qa** in good yields (74−89%). A free NH containing maleimide (**1r**) also gave the corresponding difunctionalized product **3ra** (in 85% yield). Further, maleimides derived from 4-phenylbutan-2-amine (**1s**), phenylbutylamine (**1t**), phenylethylamine (**1u**), thiophenethyl amine (**1v**), all successfully yielded their thio-hydroxy products **3sa-3va** (78−89% yields). To check the scalability of the reaction, **3aa** was synthesized in 2 mmol scale with an isolated yield of 79% (Scheme IV.3.1).

Next, the scope of disulfide was checked with N-phenyl maleimide (**1a**) as the standard reacting partner (Scheme IV.3.2). It was observed that unsubstituted, mono and disubstituted disulfides, delivered the corresponding products **3ab-3ae** in moderate yields (56−77%). It was also observed that dialkyldisulfides like 1,2-di-tert-butyldisulfane, dipropyl disulfide failed to react under the standard protocol because of the inability to form corresponding alkyl thiyl radical. Also, heterocyclic disulfides such as 1,2-bis(furan-2-ylmethyl)disulfane, 1,2-di(thiophen-2-yl)disulfane, 1,2-di(pyridin-2-yl)disulfane were analyzed, but they failed to deliver the corresponding hydroxy thiolated product (Scheme IV.3.2). This may be attributed to the reduced nucleophilicity of the thiyl radical for heterocyclic disulfides due to the presence of additional hetero atoms. The non reactivity of 1,2-diphenylditellane is due to its inability to form corresponding phenyltelluro radical.

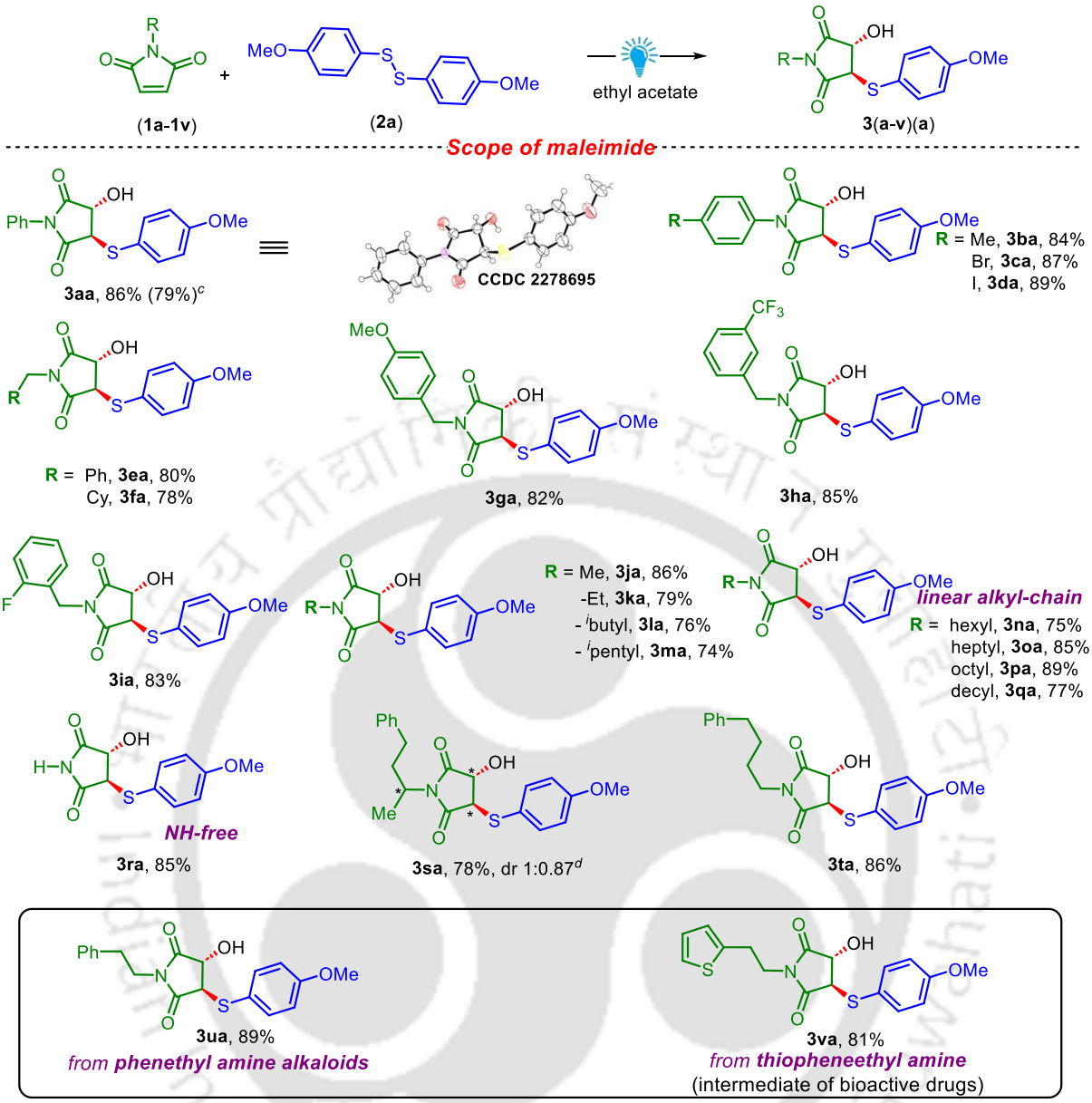

[a]Reaction conditions: **1** (0.25 mmol), **2** (0.125 mmol), ethylacetate (2 mL) for 9 h in an open-air under 5W x 4 blue LEDs ($\lambda_{em,\ max}$ = 419 nm). [b]Isolated yield. [c]Reaction performed at 2 mmol scale. [d]based on ^{1}H NMR analysis.

Scheme IV.3.1. *Scope of maleimide*[a, b]

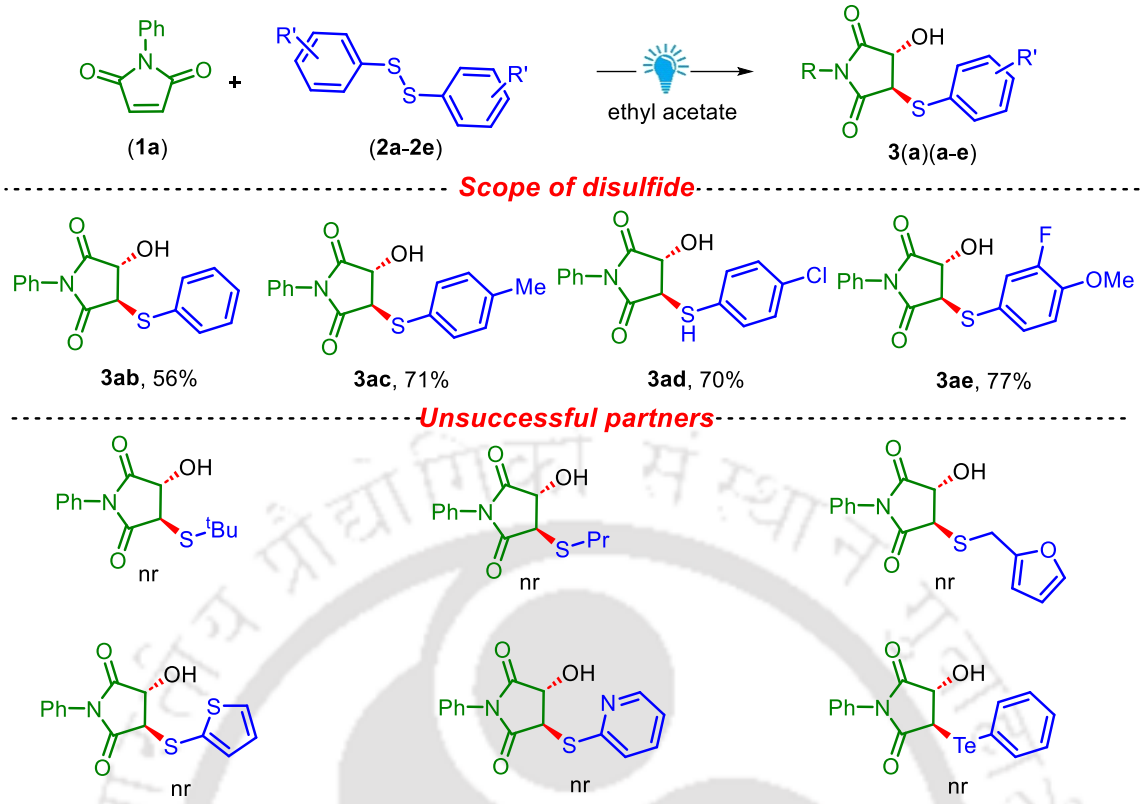

[a]Reaction conditions: **1** (0.25 mmol), **2** (0.125 mmol), ethylacetate (2 mL) for 9 h in an open-air under 5W x 4 blue LEDs ($\lambda_{em,max}$ = 419 nm). [b]Isolated yield.

Scheme IV.3.2. *Scope of disulfide*[a, b]

IV.4. Study of Mechanistic Pathway

IV.4.1. Control Experiments

In order to elucidate the mechanism of thio hydroxylation, a few studies were carried out.

(a) Reaction in Dark

The standard reaction was conducted in the absence of light (Scheme IV.4.1.1). The reaction did not proceed, thereby suggesting the requirement of light.

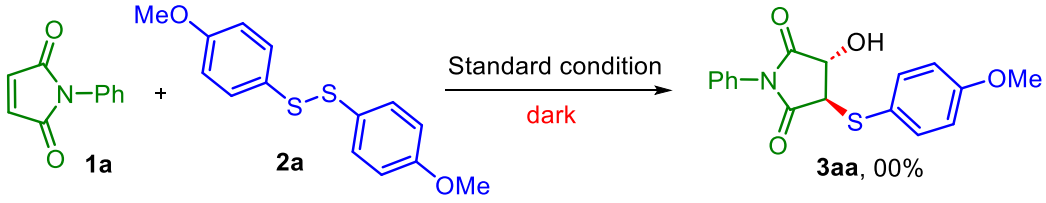

Scheme IV.4.1.1. *Reaction in dark*

(b) Radical Scavenging Experiment

The formation of hydroxyl-thiolated product (**3aa**) was largely quenched in the presence of radical quenchers BHT, TEMPO and 1,1-DPE (Scheme IV.4.1.2). The corresponding thio-TEMPO adduct (**4**) was also detected by HRMS analysis of the reaction aliquot (Figure IV.4.1.1), which supports the radical nature of the reaction.

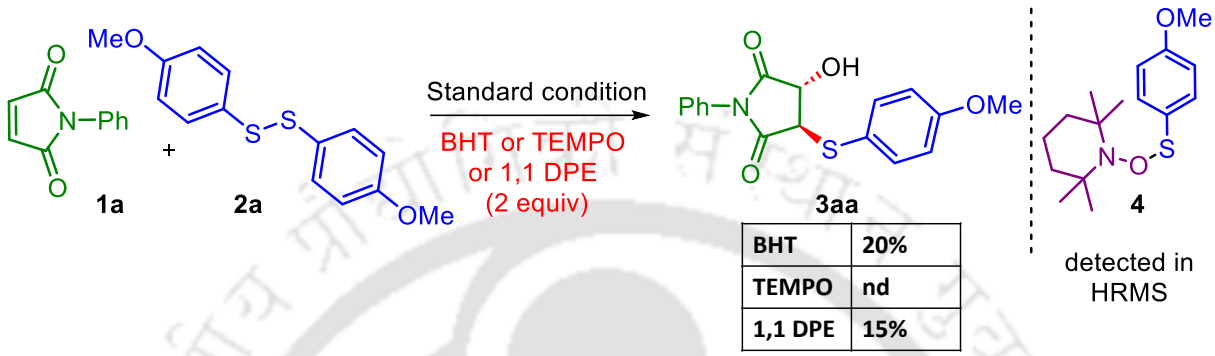

BHT	**20%**
TEMPO	**nd**
1,1 DPE	**15%**

Scheme IV.4.1.2. *Radical scavenging experiment*

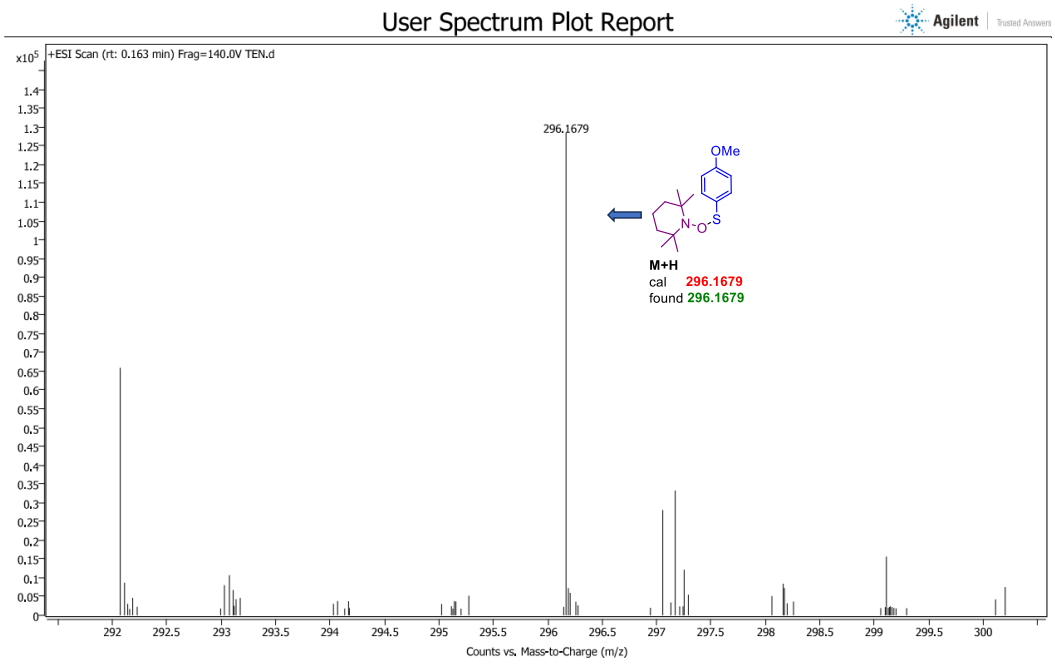

Figure IV.4.1.1. *Detection of thio-TEMPO adduct **4** in HRMS*

(c) Experiment for Studying the Role of Singlet Oxygen ($^1O_2$)

➢ **Influence of Singlet Oxygen ($^1O_2$) Quencher DABCO**

In the presence of singlet oxygen ($^1O_2$) quencher such as DABCO, the reaction failed to proceed (Scheme IV.4.1.3.). Thereby suggesting the active involvement of singlet oxygen, which is perhaps generated *in situ*.

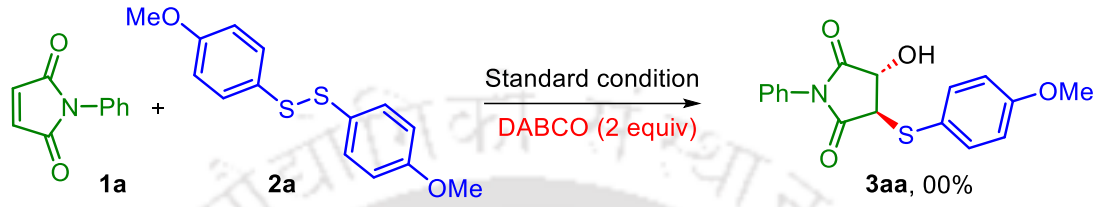

Scheme IV.4.1.3. *Singlet oxygen ($^1O_2$) quenching experiment*

➢ **Singlet Oxygen Trapping Experiment ($^1O_2$)**

The *in situ* generated singlet oxygen ($^1O_2$) was trapped using 1,3-diphenylisobenzofuran (2 equiv.) and the trapped adduct (**5**) was detected by HRMS (Figure IV.4.1.2), confirming the generation and involvement of singlet oxygen (Scheme IV.4.1.4).

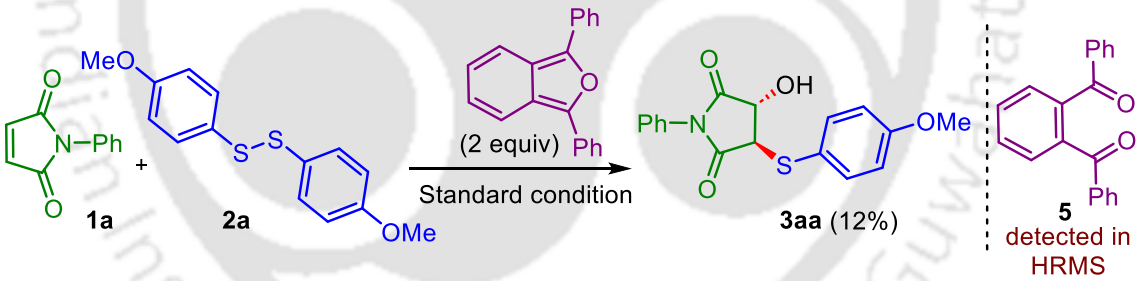

Scheme IV.4.1.4. *Singlet oxygen trapping experiment ($^1O_2$)*

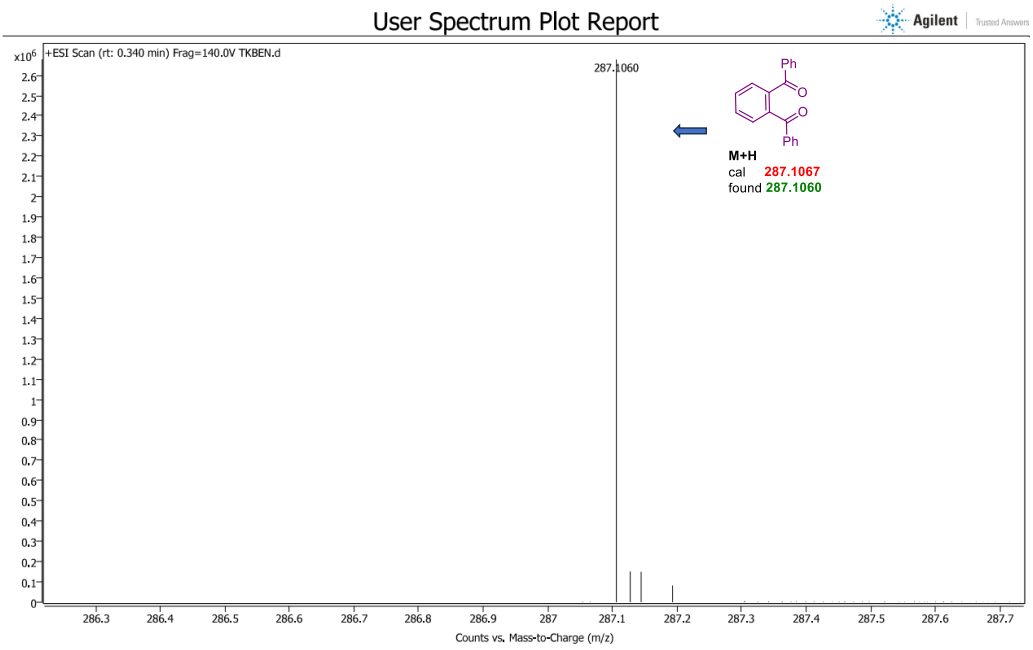

Figure IV.4.1.2. *Detection of singlet oxygen trapped adduct* ***5*** *in HRMS*

(d) Experiment for Detection of any Superoxide Radical Involvement

The presence of *p*-benzoquinone (which is known to quench superoxide radical) failed to suppress the formation of (**3aa**) (Scheme IV.4.1.5). This, rules out the involvement of superoxide radical generation in the reaction medium.

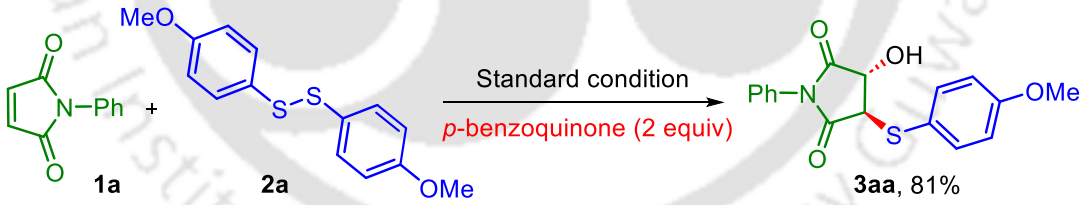

Scheme IV.4.1.5. *Influence of superoxide quencher p-benzoquinone*

(e) Experiment for Investigation of the Source of Hydroxyl Oxygen

In order to find out the origin of oxygen in the hydroxyl functionality in (**3aa**), few experiments were performed

- **Standard Reaction in the Presence of H_2O^{18}**

A standard reaction was carried out in the presence of H_2O^{18} (10 equiv) (Scheme IV.4.1.6). From the labelling experiment, no ^{18}O-labelled product (**3aa**) could be detected, thus confirming the non-involvement of moisture, either from the atmosphere or solvent.

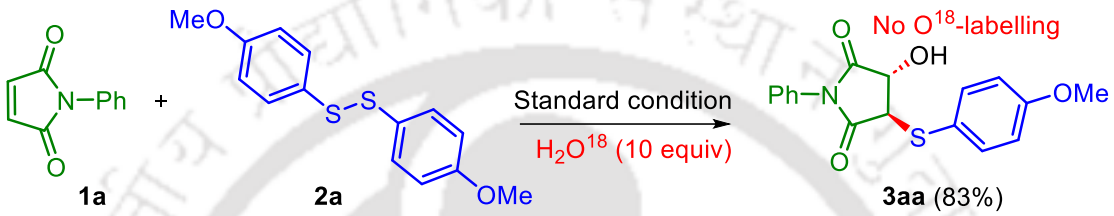

Scheme IV.4.1.6. *Standard reaction in the presence of H_2O^{18}*

- **Reaction Under Dry Conditions**

The standard reaction under Argon atmosphere largely suppressed the formation of **3aa**, suggesting the participation of oxygen (Scheme IV.4.1.7).

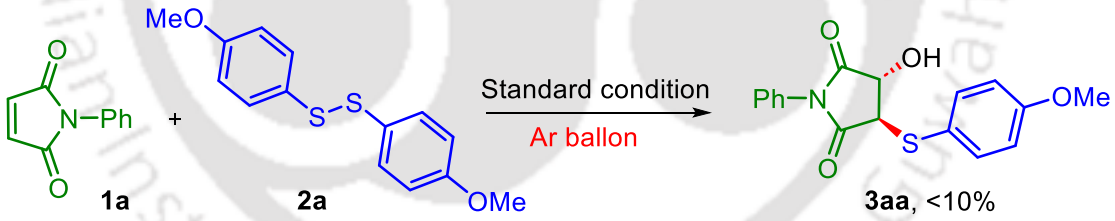

Scheme IV.4.1.7. *Reaction under dry conditions*

(f) Reaction with Thiol in Lieu of Disulfide

When thiol (**6a**) was used as a limiting reagent in lieu of disulfide (**2a**), a Michael adduct (**6aa**) was isolated as the major product (75%) and **3aa** was obtained in a minor amount (18%) (Scheme IV.4.1.8). The insignificant amount of product (**3aa**) formed is originating from the disulfide (**2a**) obtained from oxidation of thiol (**6a**).

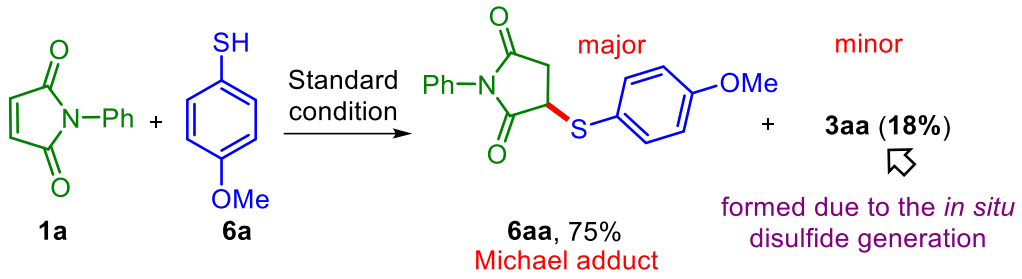

Scheme IV.4.1.8. *Reaction with thiol*

Thus, in this protocol, the disulfide plays the dual role of limiting reagent and also facilitates the singlet oxygen formation.

(g) Detection of Intermediate in HRMS

In order to detect the intermediates, the crude reaction aliquot (2 h) of **3aa** was subjected to HRMS analysis. One of the intermediates **D** (Scheme IV.4.2.1) was detected during the analysis (Figure IV.4.1.3).

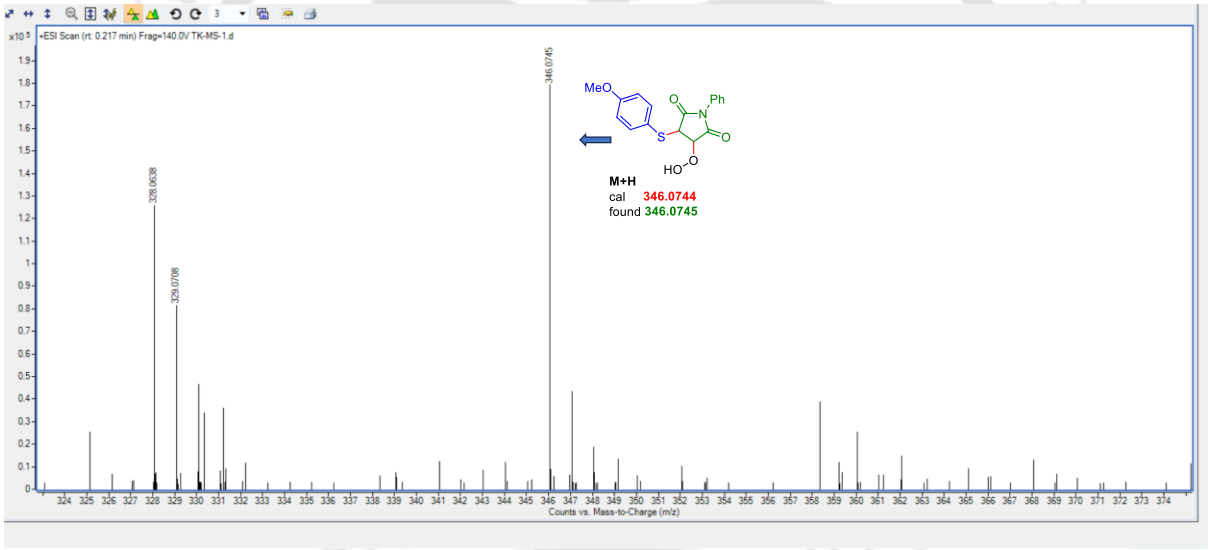

Figure IV.4.1.3. *Detection of intermediate* ***D*** *in HRMS*

(h) Detection of H_2O_2 Release During the Reaction

- **H_2O_2 detection by iodometry**

(a) (b) (c)

Figure IV.4.1.4. *H_2O_2 detection experiment: (a) Reaction mixture after completion (b) Portion of the freshly prepared KI starch solution in 0.02 M H_2SO_4. (c) Appearance of dark blue colour due to the formation of I_2-starch complex (H_2O_2 detected).*

- **(ii) H_2O_2 Detection in a Typical Reaction with $KMnO_4$.**

$$KMnO_4 + 3H_2O_2 \longrightarrow 2MnO_2 + 2KOH + 3O_2 + 2H_2O$$

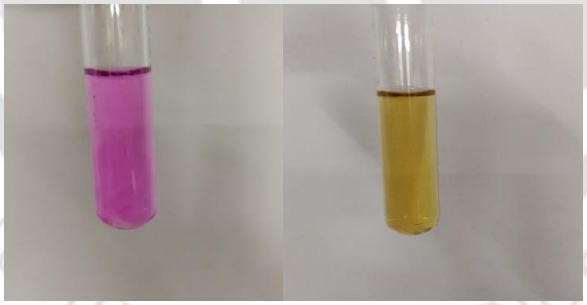

(a) (b)

Figure IV.4.1.5. *(a) $KMnO_4$ solution (b) $KMnO_4$ solution after addition of reaction mixture.*

(i) Study of Light Absorption: UV- vis and Emission Spectra

The absorbance spectra of 1,2-*bis*(4-methoxyphenyl)disulfane (**2a**) has been recorded which show an absorbance in the region 400–440 nm. Also, the emission spectra of blue LED have

been recorded, which has a maximum emission at 419 nm. The absorbance spectra of **2a** and the emission spectra of blue LED overlap each other as shown in Figure IV.4.1.6.c.

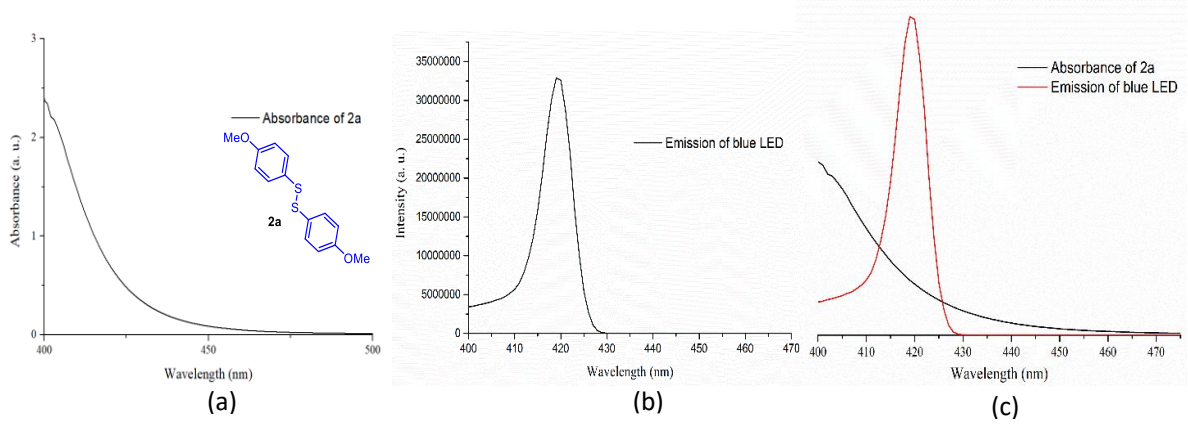

Figure IV.4.1.6. *(a) UV-vis absorbance of 1,2-bis(4-methoxyphenyl)disulfane (**2a**) in Ethyl acetate at a concentration of 0.05 M at room temperature. (b) Emission spectra of blue LED. (c) spectral overlap of UV-vis absorption spectrum of **2a** and emission spectra of blue LED*

IV.4.2. Mechanism

Based on the mechanistic studies in section IV.4.1 and literature precedence[5,11] a plausible reaction mechanism is depicted in Scheme IV.4.2.1. Initially, under blue light irradiation, the disulfide (**2a**) (λ_{ab} = 400–440 nm, Figure IV.4.1.6) is excited and cleaved to thiyl radical (**A**) with the generation of singlet oxygen ($^1O_2$) from triplet oxygen ($^3O_2$). The thiyl radical **A** then underwent radical addition to the C=C bond of N-phenyl maleimide **1a** to form the radical species **B**. The radical **B** then reacts with the singlet oxygen to afford a peroxy radical species **C**. A subsequent protonation from H_2O with the generation of H_2O_2 delivers a peroxy intermediate **D** (detected in HRMS, Figure IV.4.1.3) which subsequently leads to the hydroxyl thiolated adduct **3aa**.[14] The generation of H_2O_2 has been confirmed by iodometric and $KMnO_4$ experiment (Figure IV.4.1.4 and Figure IV.4.1.5). Further, the possibility of ethylacetate serving as the hydrogen atom donor cannot be completely ruled out. But the fact that this reaction proceeds with equal ease in other solvents such as $CHCl_3$ (63%), DCE (60%), DCM (65%), TFE (71%) (Table IV.2.1) supports our proposition of water as the source of hydrogen atom.

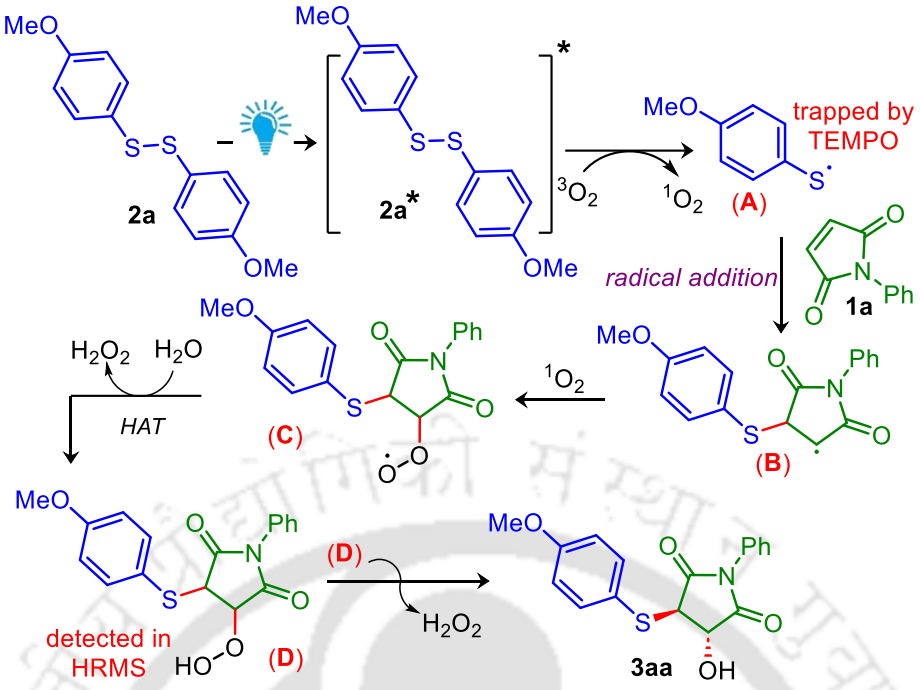

Scheme IV.4.2.1. *Plausible mechanism*

IV.5 Conclusion

In summary, a visible-light-induced 1,2-thiohydroxylation of maleimides has been accomplished using disulfides in green solvent ethyl acetate under mild conditions. The hydroxyl group originates from the singlet oxygen generated *in situ* from the atmospheric oxygen and photo activated disulfide. The mechanism involves the formation of peroxy radical followed by HAT from H_2O via water oxidation. External photocatalyst free, decent yield and 1,2-thiohydroxylation in a simple ease technique are salient features of this protocol.

IV.6 Experimental Section

IV.6.1. General Information and Instrumentation

All chemicals were obtained from commercial sources and were used without further purification. The starting material **1** was synthesized according to previously described method.[15] Reactions were monitored via TLC, prepared using silica gel 60 F_{254} (0.25 mm), and were detected under UV light at 254 nm. The chromatography separation was carried out using 60−120 mesh-sized silica gel. Ethyl acetate/ hexane mixtures were used as the eluent. ^1H, ^{13}C, and ^{19}F NMR spectra were recorded in 500, and 400 MHz NMR in deuterated solvents, and the chemical shifts (δ) are given in ppm. The ^1H spectra were referenced to TMS (0 ppm) for $CDCl_3$; for ^{13}C $CDCl_3$ (77.16 ppm). IR spectra were recorded neat using an FT-IR spectrometer.

HRMS was recorded using ESI (Q-TOF type mass analyzer) in positive modes. UV−vis experiment was performed in 1 mL quartz cuvettes with a path length equal to 1 cm. Photoluminescence was carried out in 1 mL quartz cuvettes.

- **Light Information and Reaction Setup**

Philips 4 x 5 W white LED bulbs ($\lambda_{em,max}$ = 419 nm) were used as the light source for this light-promoted reaction and no filter was used. A borosilicate 10 mL vial was used as the reaction vessel. The distance from the light source to the irradiation vessel was ~3−5 cm. Regular fan was used to ventilate the area to maintain the room temperature (27−30 ºC). The reaction set-up for this photochemical reaction is shown below (Figure IV.6.1.1)

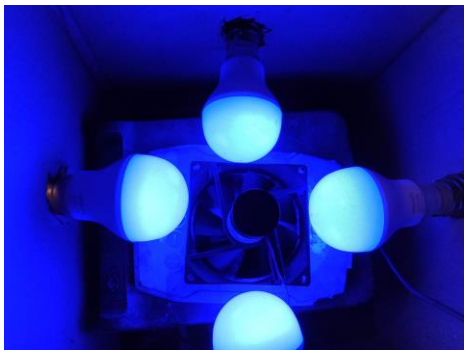

Figure IV.6.1.1. *Photochemical reaction set-up*

IV.6.2. Reaction Procedure

IV.6.2.1. General Procedure for the Synthesis of 3aa

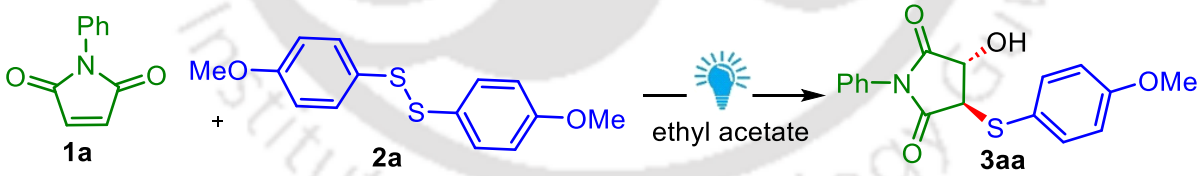

An oven-dried 10 mL vial was charged with *N*-phenylmaleimide (**1a**) (0.25 mmol, 43 mg), 1,2-*bis*(4-methoxyphenyl)disulfane (**2a**) (0.125 mmol, 35 mg), a magnetic stir bar in ethyl acetate (2 mL) and was stirred at room temperature in an open-air for 9 h under the irradiation of 4 x 5 W blue LEDs ($\lambda_{em,max}$ = 419 nm) approximately at a distance of ~3−5 cm. The progress of the reaction was monitored via TLC. After completion of the reaction, the solvent was removed by rotary evaporation. The reaction mixture was then mixed with water (10 mL) and extracted with ethyl acetate (2 × 15 mL). The organic layer was dried over anhydrous sodium sulfate and was evaporated under reduced pressure. The residue so obtained was then purified

over column chromatography by eluting with hexane: ethyl acetate (83:17) mixture to afford the desired product **3aa** as grey solid in 86% yields (71 mg).

IV.6.2.2. Procedure for the Synthesis of 3aa in 2 mmol Scale

An oven-dried 10 mL vial was charged with *N*-phenylmaleimide (**1a**) (2 mmol, 346 mg), 1,2-*bis*(4-methoxyphenyl)disulfane (**2a**) (1 mmol, 278 mg), a magnetic stir bar in ethyl acetate (3 mL) and was stirred at room temperature in an open-air for 9 h under the irradiation of 4 x 5 W blue LEDs ($\lambda_{em,max}$ = 419 nm) approximately at a distance of ~3−5 cm. The progress of the reaction was monitored via TLC. After completion of the reaction, the solvent was removed by rotary evaporation. The reaction mixture was then mixed with water (10 mL) and extracted with ethyl acetate (2 × 15 mL). The organic layer was dried over anhydrous sodium sulfate and was evaporated under reduced pressure. The residue so obtained was then purified over column chromatography by eluting with hexane: ethyl acetate (83:17) mixture to afford the desired product **3aa** as grey solid in 79% yields (519 mg).

IV.6.2.3. Procedure for Mechanistic Studies

(a) Procedure for Radical Scavenging Experiment

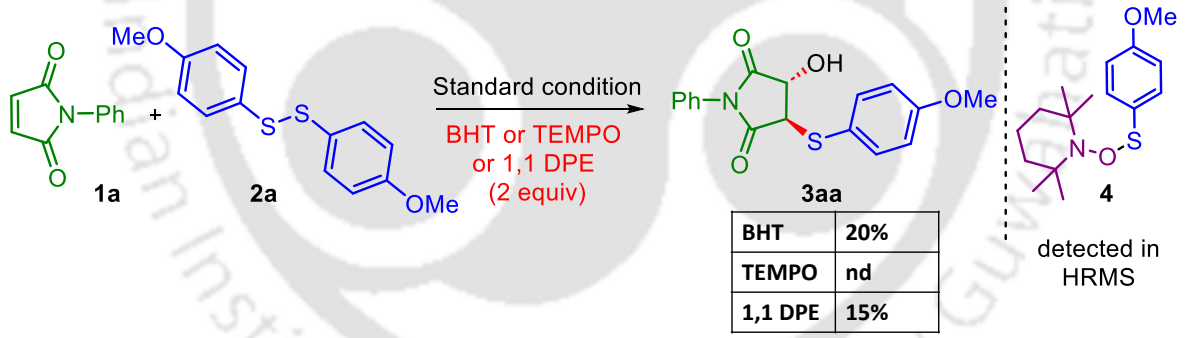

BHT	20%
TEMPO	nd
1,1 DPE	15%

An oven-dried 10 mL vial was charged with *N*-phenylmaleimide (**1a**) (0.25 mmol, 43 mg), 1,2-*bis*(4-methoxyphenyl)disulfane (**2a**) (0.125 mmol, 35 mg), BHT (2 equiv, 0.5 mmol, 110 mg) or TEMPO (2 equiv, 0.5 mmol, 78 mg) or 1,1-diphenylethylene (DPE) (2 equiv, 0.5 mmol, 90 mg) a magnetic stir bar in ethyl acetate (1.5 mL) and was stirred at room temperature in an open-air for 9 h under the irradiation of 4 x 5 W blue LEDs ($\lambda_{em,max}$ = 419 nm) approximately at a distance of ~3−5 cm. The solvent was removed by rotary evaporation. The reaction mixture was then mixed with water (10 mL) and extracted with ethyl acetate (2 × 15 mL). The organic layer was dried over anhydrous sodium sulfate and was evaporated under reduced pressure. The residue so obtained was then purified over column chromatography by eluting with

hexane: ethyl acetate (83:17) mixture to afford the product **3aa** as grey solid in 16 mg (20% yield) for BHT, 0 mg (0% yield) for TEMPO and 12 mg (15% yield) for DPE. These results support the radical nature of the reaction.

(b) Procedure for Detection of Singlet Oxygen and Superoxide:

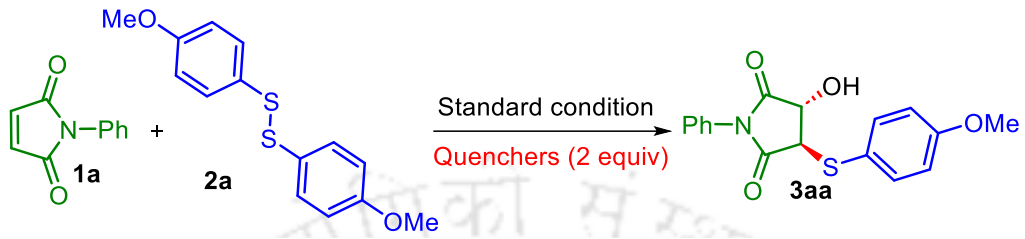

Quencher (2 equiv)	Role	Yield%
DABCO	Singlet oxygen quencher	00
p-benzoquinone	Superoxide quencher	81%

An oven-dried 10 mL vial was charged with *N*-phenylmaleimide (**1a**) (0.25 mmol, 43 mg), 1,2-*bis*(4-methoxyphenyl)disulfane (**2a**) (0.125 mmol, 35 mg), DABCO (2 equiv, 0.5 mmol, 56 mg) or *p*-benzoquinone (2 equiv, 0.5 mmol, 54 mg), a magnetic stir bar in ethyl acetate (1.5 mL) and was stirred at room temperature in an open-air for 9 h under the irradiation of 4 x 5 W blue LEDs ($\lambda_{em,max}$ = 419 nm) approximately at a distance of ~3−5 cm. The solvent was removed by rotary evaporation. The reaction mixture was then mixed with water (10 mL) and extracted with ethyl acetate (2 × 15 mL). The organic layer was dried over anhydrous sodium sulfate and was evaporated under reduced pressure. The residue so obtained was then purified over column chromatography by eluting with hexane: ethyl acetate (83:17) mixture to afford the product **3aa** as grey solid in 0 mg (0% yield) for DABCO and 66 mg (81% yield) for *p*-benzoquinone. The failure to obtain the product **3aa** in the presence of DABCO confirms the involvement of the singlet oxygen in the reaction and for *p*-benzoquinone, the 81% yield of **3aa** suggests non-involvement of superoxide in the reaction.

(c) Procedure for Singlet Oxygen Trapping

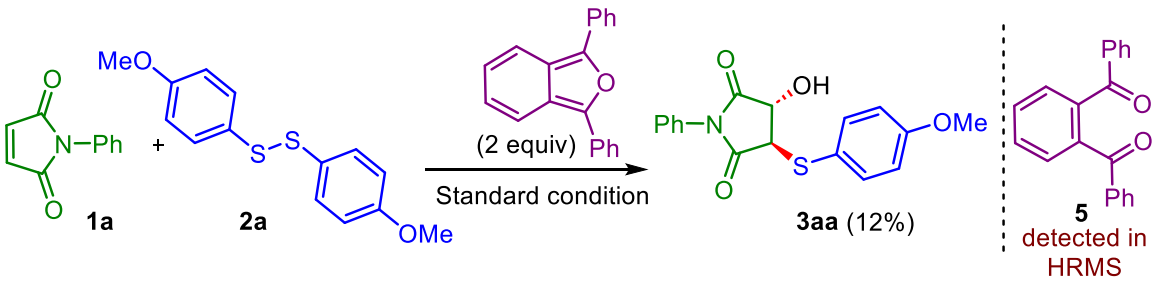

An oven-dried 10 mL vial was charged with *N*-phenylmaleimide (**1a**) (0.25 mmol, 43 mg), 1,2-*bis*(4-methoxyphenyl)disulfane (**2a**) (0.125 mmol, 35 mg), 1,3-diphenylisobenzofuran (2 equiv, 0.5 mmol, 135 mg) a magnetic stir bar in ethyl acetate (1.5 mL) and was stirred at room temperature in an open-air for 9 h under the irradiation of 4 x 5 W blue LEDs ($\lambda_{em,max}$ = 419 nm) approximately at a distance of ~3−5 cm. The solvent was removed by rotary evaporation. The reaction mixture was then mixed with water (10 mL) and extracted with ethyl acetate (2 × 15 mL). The organic layer was dried over anhydrous sodium sulfate and was evaporated under reduced pressure. The residue so obtained was then purified over column chromatography by eluting with hexane: ethyl acetate (83:17) mixture to afford the product **3aa** as grey solid in 12% yields (10 mg) and 1,2-phenylene*bis*(phenylmethanone) (**5**) was detected in HRMS analysis of the crude reaction mixture.

(d) Procedure for Investigation of the Source of Hydroxyl Oxygen

- **Standard Reaction in the Presence of H_2O^{18}**

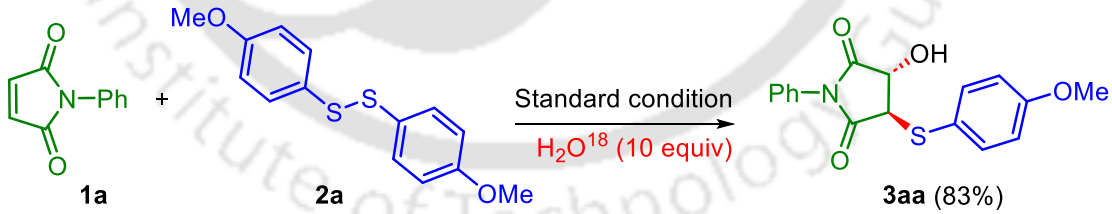

An oven-dried 10 mL vial was charged with *N*-phenylmaleimide (**1a**) (0.25 mmol, 43 mg), 1,2-*bis*(4-methoxyphenyl)disulfane (**2a**) (0.125 mmol, 35 mg), H_2O^{18} (10 equiv, 2.5 mmol, 50 mg) a magnetic stir bar in ethyl acetate (1.5 mL) and was stirred at room temperature for 9 h under the irradiation of 4 x 5 W blue LEDs ($\lambda_{em,max}$ = 419 nm) approximately at a distance of ~3−5 cm. The solvent was removed by rotary evaporation. The reaction mixture was then purified over column chromatography by

eluting with hexane: ethyl acetate (83:17) mixture to afford the product **3aa** as grey solid in 83% yields (68 mg). No H_2O^{18} labelled **3aa** was detected.

➢ **Reaction Under Dry Conditions**

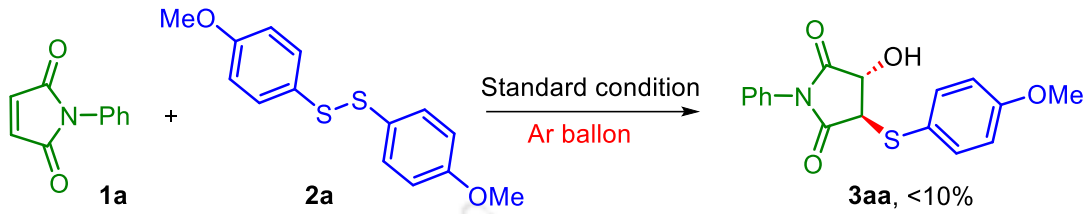

An oven-dried 10 mL vial was charged with *N*-phenylmaleimide (**1a**) (0.25 mmol, 43 mg), 1,2-*bis*(4-methoxyphenyl)disulfane (**2a**) (0.125 mmol, 35 mg), a magnetic stir bar in dry ethyl acetate (1.5 mL) and was stirred at room temperature for 9 h under an argon atmosphere under the irradiation of 4 x 5 W blue LEDs ($\lambda_{em,max}$ = 419 nm) approximately at a distance of ~3−5 cm. The solvent was removed by rotary evaporation. The reaction mixture was then purified over column chromatography by eluting with hexane: ethyl acetate (83:17) mixture to afford the product **3aa** in 7% yield.

(e) Procedure for Reaction with Thiol in Lieu of Disulfide

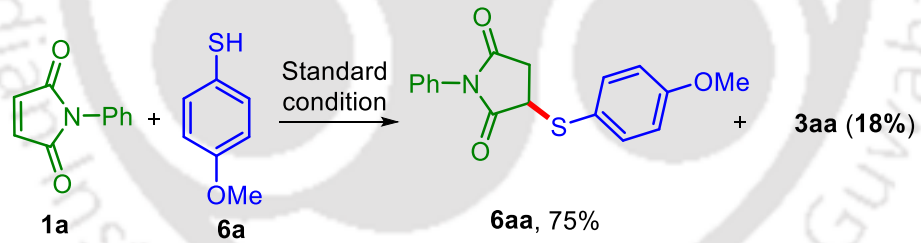

An oven-dried 10 mL vial was charged with *N*-phenylmaleimide (**1a**) (0.25 mmol, 43 mg), 4-methoxybenzenethiol (**6a**) (0.25 mmol, 35 mg), a magnetic stir bar in ethyl acetate (1.5 mL) and was stirred at room temperature in an open air for 9 h the irradiation of 4 x 5 W blue LEDs ($\lambda_{em,max}$ = 419 nm) approximately at a distance of ~3−5 cm. The solvent was removed by rotary evaporation. The reaction mixture was then mixed with water (10 mL) and extracted with ethyl acetate (2 × 15 mL). The organic layer was dried over anhydrous sodium sulfate and was evaporated under reduced pressure. The residue so obtained was then purified over column chromatography by eluting with hexane: ethyl acetate (88:12) mixture to afford the product **6aa** in 75% yield (58 mg) and **3aa** in 18% yields (14 mg).

(f) Procedure for Detection of H_2O_2 Release During the Reaction

- **H_2O_2 detection by iodometry**

An oven-dried 10 mL vial was charged with *N*-phenylmaleimide (**1a**) (0.25 mmol, 43 mg), 1,2-*bis*(4-methoxyphenyl)disulfane (**2a)** (0.125 mmol, 35 mg), a magnetic stir bar in ethyl acetate (2 mL) and was stirred at room temperature in an open-air for 9 h under the irradiation of 4 x 5 W blue LEDs ($\lambda_{em,max}$ = 419 nm) approximately at a distance of ~3−5 cm. In a separate test tube, KI-starch solution was prepared by adding aqueous solution of KI (0.2 mmol in 1.5 mL H_2O), 0.02 M H_2SO_4 (1 ml) and 0.5 mL of freshly prepared starch solution. To a portion of the reaction mixture, the freshly prepared KI-starch solution was added and stirred vigorously. Instantly, the aqueous solution turned to dark blue colour (Figure IV.4.1.4.c) indicating the presence of H_2O_2.

- **H_2O_2 detection in a typical reaction with $KMnO_4$.**

An oven-dried 10 mL vial was charged with *N*-phenylmaleimide (**1a)** (0.25 mmol, 43 mg), 1,2-*bis*(4-methoxyphenyl)disulfane (**2a)** (0.125 mmol, 35 mg), a magnetic stir bar in ethyl acetate (2 mL) and was stirred at room temperature in an open-air for 9 h under the irradiation of 4 x 5 W blue LEDs ($\lambda_{em,max}$ = 419 nm) approximately at a distance of ~3−5 cm. . In a separate test tube, $KMnO_4$ solution was prepared by adding $KMnO_4$ (300 μM) in H_2O. A portion of the reaction mixture was added to the $KMnO_4$ solution (Figure IV.4.1.5.a). Instantly, the aqueous solution turned to pale yellow colour (Figure IV.4.1.5.b) indicating the presence of H_2O_2.

IV.6.3. Crystallographic Description

Crystal data were collected with Bruker Smart Apex-II CCD diffractometer using graphite monochromated MoK_α radiation (λ = 0.71073 Å) at 298 K for **3aa**. Cell parameters were retrieved using SMART[a] software and refined with SAINT[a] on all observed reflections. Data reduction was performed with the SAINT software and corrected for Lorentz and polarization effects. Absorption corrections were applied with the program SADABS.[b] The structure was solved by direct methods implemented in SHELX-2014[c] program and refined by full-matrix least-squares methods on F2. All non-hydrogen atomic positions were located in difference Fourier maps and refined anisotropically. The hydrogen atoms were placed in their geometrically generated positions.

a. SMART V 4.043 Software for the CCD Detector System; Siemens Analytical Instruments Division: Madison, WI, 2008.

b. SAINT Plus (v 6.14) Bruker AXS Inc., Madison, WI, 2008.

c. Sheldrick, G. M. SHELXL-2014, Program for the Refinement of Crystal Structures; University of Göttingen: Göttingen (Germany), 1997.

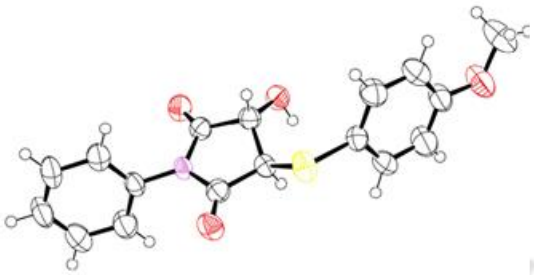

Figure IV.6.3.1. *ORTEP diagram of* ***3aa*** *with ellipsoid probability 50%*

Table IV.6.3.1. *Crystal Data table for* ***3aa***

Empirical formula	$C_{17}H_{15}NO_4S$
CCDC number	2278695
Formula weight	329.36
Temperature	298 (2)
Wavelength	0.71073 Å
Crystal system	orthorhombic
Space group	P 21 21 21
Unit cell dimensions	a = 5.2038(7) Å, b = 13.8139(17) Å, c = 21.853(3) Å α = 90°, β = 90°, γ = 90°
Volume	1570.9(3) $Å^3$
Z	4
Density (calculated)	1.393 g/cm^{-3}
Absorption coefficient	0.226
F(000)	688
Theta range for data collection	1.744 to 24.991°
Index ranges	–6 < = h < = 6, –16 < = k < = 16, –25< = l < = 25
Reflections collected	37567
Refinement method	Full-matrix least-squares on F2
Data / restraints / parameters	2765/ 0/ 212
Goodness-of-fit on F2	0.895
Final R indices [I>2sigma(I)]	0.0594, wR2 = 0.1401
R indices (all data)	0.1223, wR2 = 0.1804

IV.7. References

1. (a) Holmberg-Douglas, N.; Nicewicz, D. A. *Chem. Rev*. **2022**, *122*, 1925; (b) Zhou, Q.; Zou, Y.; Lu, L.; Xiao, W. *Angew. Chem., Int. Ed*. **2019**, *58*, 1586; (c) Candish, L.; Collins, K. D.; Cook, G. C.; Douglas, J. J.; Gómez-Suárez, A.; Jolit, A.; Keess, S. *Chem. Rev*. **2022**, *122*, 2907.

2. (a) Blum, S. P.; Hofman, K.; Manolikakes, G.; Waldvogel, S. R. *Chem. Commun*. **2021**, *57*, 8236; (b) Tilby, M. J.; Dewez, D. F.; Pantaine, L. R. E.; Hall, A.; Martínez-Lamenca, C.; Willis, M. C.; *ACS Catal*. **2022**, *12*, 6060; (c) Hell, S. M.; Meyer, C. F.; Misale, A.; Sap, J. B. I.; Christensen, K. E.; Willis, M. C.; Trabanco, A. A.; Gouverneur, V. *Angew. Chem., Int. Ed*. **2020**, *59*, 11620.

3. (a) Ilardi, E. A.; Vitaku, E.; Njardarson, J. T. *J. Med. Chem*., **2014**, *57*, 2832; (b) Mishra, A.; Ma, C.-Q.; Bauerle, P. *Chem. Rev*. **2009**, *109*, 1141; (c) Scott, K. A.; Njardarson, J. T. *Top. Curr. Chem*. **2018**, *376*, 5; (d) Wang, N.; Saidhareddy, P.; Jiang, X. *Nat. Prod. Rep*. **2020**, *37*, 246. (e) Feng, M.; Tang, B.; Liang, S. H.; Jiang, X. *Curr Top Med Chem*. **2016**, *16*, 1200. (f) Wang, M.; Jiang, X. *ACS Sustainable Chem. Eng*. **2022**, *10*, 671.

4. (a) Yuan, J.; Ma, X.; Yi, H.; Liu, C.; Lei, A. *Chem. Commun*. **2014**, *50*, 14386; (b) Sandfort, F.; Knecht, T.; Pinkert, T.; Daniliuc, C. G.; Glorius, F. *J. Am. Chem. Soc*. **2020**, *142*, 6913; (c) Pramanik, M.; Choudhuri, K.; Mathuri, A.; Mal, P. *Chem. Commun*. **2020**, *56*, 10211; (d) Pramanik, M.; Choudhuri, K.; Chakraborty, S.; Ghosh, A.; Mal, P. *Chem. Commun*. **2020**, *56*, 2991.

5. (a) Teders, M.; Henkel, C.; Anhauser, L.; Strieth-Kalthoff, F.; Gómez-Suárez, A.; Kleinmans, R.; Kahnt, A.; Rentmeister, A.; Guldi, D.; Glorius, F. *Nat. Chem*. **2018**, *10*, 981; (b) Qin, Y.; Han, Y.; Tang, Y.; Wei, J.; Yang, M. *Chem. Sci*. **2020**, *11*, 1276; (c) Kim, J.; Kang, B.; Hong, S. H. *ACS Catal*., **2020**, *10*, 6013.

6. (a) Dong, B.; Shen, J.; Xie, L.-G. *Org. Chem. Front*. **2023**, *10*, 1322; (b) Kosobokov, M. D.; Zubkov, M. O.; Levin, V. V.; Kokorekin, V. A.; Dilman, A. D. *Chem. Commun*. **2020**, *56*, 9453; (c) Kostromitin, V. S.; Levin, V. V.; Dilman, A. D. *J. Org. Chem*. **2023**, *88*, 6252; (d) Giri, R.; Kc, S. *J. Org. Chem*., **2018**, *83*, 3013; (e) Khandelia, T.; Ghosh, S.; Patel, B. K. *Chem. Commun*. **2023**, *59*, 2118.

7. (a) Liu, S. L.; Ye, C.; Wang, X. *Org. Biomol. Chem*. **2022**, *20*, 4837; (b) Manoharan, R.; Jeganmohan, M. *Asian J. Org. Chem*. **2019**, *8*, 1949.

8. Ruan, H. L.; Deng, Y. X.; Li, Z. J.; Zhao, S. Y. *J. Org. Chem*. **2022**, *87*, 15661.

9. Shi, S.; Ma, Y.; Zhou, J.; Li, J.; Chen, L.; Wu, Ge. *Org. Lett*. **2020**, *22*, 1863.

10. Cuadros, S.; Horwitz, M. A.; Chaput, B. S.; Melchiorre, P. *Chem. Sci*. **2019**, *10*, 5484.

11. Patehebieke, Y. *Beilstein J. Org. Chem*. **2020**, *16*, 1418.

12. (a) Ghosh, S.; Khandelia, T.; Patel, B. K. *Org. Lett.* **2021**, *23*, 7370; (b) Khandelia, T.; Ghosh, S.; Panigrahi, P.; Shome, R.; Ghosh, S. S.; Patel, B. K. *J. Org. Chem*. **2021**, *86*, 16948; (c) Ghosh, S.; Khandelia, T.; Panigrahi, P.; Mandal, R.; Patel, B. K. *Org. Lett*. **2023**, *25*, 3806.

13. Dobereiner, G. E.; Crabtree, R. H. *Chem. Rev*. **2010**, *110*, 681.

14. Li, H.; Xie, F.; Zhang, M. T. *ACS Catal*. **2021**, *11*, 68.

15. Mandal, R.; Emayavaramban, B.; Sundararaju, B. *Org. Lett*. **2018**, *20*, 2835.

IV.8. Spectral Data

***(3S,4R)-3-Hydroxy-4-((4-methoxyphenyl)thio)-1-phenylpyrrolidine-2,5-dione (3aa)*:**

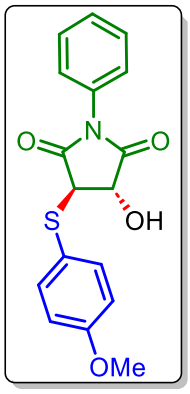

Grey solid (71 mg, 86% yield), m.p. 140–143 °C; purified over a column of silica gel (17% ethyl acetate in hexane); ^{1}H NMR (500 MHz, $CDCl_3$) δ 7.56 (d, J = 8.5 Hz, 2H), 7.46–7.43 (m, 2H), 7.41–7.38 (m, 1H), 7.14 (d, J = 7.0 Hz, 2H), 6.88 (d, J = 9.0 Hz, 2H), 4.62 (d, J = 4.0 Hz, 1H), 3.98 (d, J = 5.0 Hz, 1H), 3.81 (s, 3H), 3.30 (s, 1H); ^{13}C{^{1}H} NMR (126 MHz, $CDCl_3$) δ 174.7, 171.6, 161.2, 137.6, 131.3, 129.4, 129.2, 126.3, 120.3, 115.2, 72.9, 55.6, 53.7. IR (neat, cm^{-1}) 3155, 3054, 1599, 1489, 1452, 1328, 1258, 1049, 758, 696. HRMS (ESI) $[M + H]^+$ calcd for $C_{17}H_{16}NO_4S^+$ 330.0795, found 330.0796.

***(3S,4R)-3-Hydroxy-4-((4-methoxyphenyl)thio)-1-(p-tolyl)pyrrolidine-2,5-dione (3ba)*:**

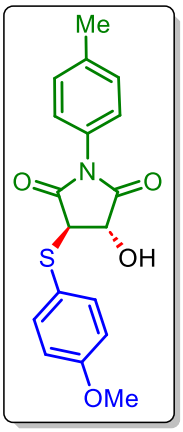

White solid (72 mg, 84% yield); m.p. 137–140 °C; purified over a column of silica gel (16% ethyl acetate in hexane); ^{1}H NMR (500 MHz, $CDCl_3$) δ 7.55 (d, J = 8.5 Hz, 2H), 7.24 (d, J = 8.0 Hz, 2H), 7.01 (d, J = 8.0 Hz, 2H), 6.88 (d, J = 8.0 Hz, 2H), 4.62–4.60 (m, 1H), 3.97 (d, J = 5.0 Hz, 1H), 3.81 (s, 3H), 3.39 (s, 1H), 2.37 (s, 3H); ^{13}C{^{1}H} NMR (126 MHz, $CDCl_3$) δ 174.9, 171.8, 161.2, 139.4, 137.6, 130.0, 128.6, 126.1, 120.3, 115.2, 72.9, 55.6, 53.7, 21.4. IR (neat, cm^{-1}) 3388, 1699, 1591, 1493, 1395, 1245, 1178, 1024, 798, 730. HRMS (ESI) $[M + H]^+$ calcd for $C_{18}H_{18}NO_4S^+$ 344.0951, found 344.0946.

***(3S,4R)-1-(4-Bromophenyl)-3-hydroxy-4-((4-methoxyphenyl)thio)pyrrolidine-2,5-dione (3ca)*:**

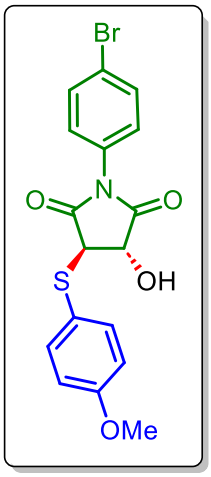

White solid (88 mg, 87% yield); m.p. 180–182 °C; purified over a column of silica gel (16% ethyl acetate in hexane); ^{1}H NMR (500 MHz, $CDCl_3$) δ 7.57 (d, J = 8.5 Hz, 2H), 7.54 (d, J = 8.5 Hz, 2H), 7.06 (d, J = 8.5 Hz, 2H), 6.88 (d, J = 8.5 Hz, 2H), 4.63–4.61 (m, 1H), 3.97 (d, J = 5.0 Hz, 1H), 3.81 (s, 3H), 3.15 (s, 1H); ^{13}C{^{1}H} NMR (126 MHz, $CDCl_3$) δ 174.3, 171.3, 161.3, 137.6, 132.6, 132.5, 130.2, 127.7, 123.1, 121.4, 120.1, 115.3, 73.0, 55.6, 53.6. IR (neat, cm^{-1}) 3389, 1705, 1592, 1491, 1392, 1244, 1177, 1014, 828, 767. HRMS (ESI) $[M + H]^+$ calcd for $C_{17}H_{15}BrNO_4S^+$ 407.9900, found 407.9900.

***(3S,4R)-3-Hydroxy-1-(4-iodophenyl)-4-((4-methoxyphenyl)thio)pyrrolidine-2,5-dione (3da)*:**

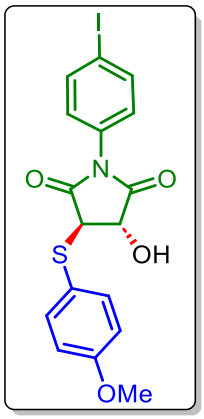

Light yellow solid (101 mg, 89% yield); m.p. 191–196°C; purified over a column of silica gel (17% ethyl acetate in hexane); ^{1}H NMR (400 MHz, $CDCl_3$) δ 7.77 (d, J = 8.4 Hz, 2H), 7.54 (d, J = 8.8 Hz, 2H), 6.91 (d, J = 8.8 Hz, 2H), 6.87 (d, J = 8.8 Hz, 2H), 4.61 (d, J = 5.2 Hz, 1H), 3.97 (d, J = 4.8 Hz, 1H), 3.81 (s, 3H), 3.40 (s, 1H); ^{13}C{^{1}H} NMR (126 MHz, $CDCl_3$) δ 174.2, 171.3, 161.3, 138.5, 137.6, 131.0, 127.9, 120.1, 115.3, 94.7, 73.0, 55.6, 53.6. IR (neat, cm^{-1}) 3442, 1705, 1591, 1489, 1396, 1244, 1177, 1101, 1006, 764. HRMS (ESI) $[M + H]^+$ calcd for $C_{17}H_{15}INO_4S^+$ 455.9761, found 455.9762.

***(3S,4R)-1-Benzyl-3-hydroxy-4-((4-methoxyphenyl)thio)pyrrolidine-2,5-dione (3ea)*:**

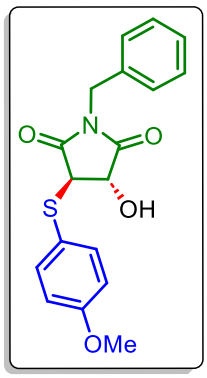

Brown solid (69 mg, 80% yield); m.p. 126–130 °C; purified over a column of silica gel (17% ethyl acetate in hexane); ^{1}H NMR (500 MHz, $CDCl_3$) δ 7.41 (d, J = 8.5 Hz, 2H), 7.27–7.26 (m, 3H), 7.20–7.18 (m, 2H), 6.73 (d, J = 9.0 Hz, 2H), 4.59 (q, J = 14.7 Hz, 2H), 4.44 (d, J = 5.0 Hz, 1H), 3.81 (d, J = 5.0 Hz, 1H), 3.77 (s, 3H), 3.46 (s, 1H); ^{13}C{^{1}H} NMR (126 MHz, $CDCl_3$) δ 175.4, 172.2, 160.9, 137.4, 135.0, 128.8, 128.7, 128.2, 120.2, 115.1, 72.7, 55.5, 53.6, 42.9. IR (neat, cm^{-1}) 3352, 1696, 1589, 1499, 1399, 1242, 1171,1082, 1023, 817. HRMS (ESI) $[M + H]^+$ calcd for $C_{18}H_{18}NO_4S^+$ 344.0951, found 344.0951.

***(3S,4R)-1-(Cyclohexylmethyl)-3-hydroxy-4-((4-methoxyphenyl)thio)pyrrolidine-2,5-dione (3fa)*:**

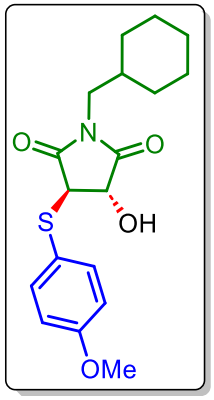

Yellow liquid (68 mg, 78% yield); purified over a column of silica gel (15% ethyl acetate in hexane); ^{1}H NMR (500 MHz, $CDCl_3$) δ 7.51 (d, J = 8.5 Hz, 2H), 6.85 (d, J = 9.0 Hz, 2H), 4.48–4.46 (m, 1H), 3.80 (d, J = 5.5 Hz, 1H), 3.79 (s, 3H), 3.29 (dd, J = 7.3, 2.3 Hz, 2H), 3.13 (d, J = 3.0 Hz, 1H), 1.62–1.52 (m, 4H), 1.41 (d, J = 12.9 Hz, 1H), 1.31 (d, J = 11.5Hz, 1H), 1.15–1.06 (m, 3H), 0.87 – 0.79 (m, 2H); ^{13}C{^{1}H} NMR (126 MHz, $CDCl_3$) δ 175.9, 172.4,

161.1, 137.7, 120.2, 115.1, 72.6, 55.5, 53.7, 45.4, 36.0, 30.6, 30.5, 26.2, 25.7, 25.6. IR (neat, cm^{-1}) 3056, 1586, 1483, 1320, 1167, 1011, 975, 692, 677. HRMS (ESI) $[M + H]^+$ calcd for $C_{18}H_{24}NO_4S^+$ 350.1421 , found 350.1422.

***(3S,4R)-3-Hydroxy-1-(4-methoxybenzyl)-4-((4-methoxyphenyl)thio)pyrrolidine-2,5-dione (3ga)*:**

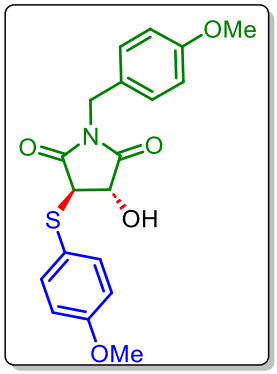

White solid (76 mg, 82% yield); m.p. 112–116 °C; purified over a column of silica gel (20% ethyl acetate in hexane); ^1H NMR (500 MHz, $CDCl_3$) δ 7.40 (d, J = 8.5 Hz, 2H), 7.16 (d, J = 9.0 Hz, 2H), 6.78 (d, J = 8.5 Hz, 2H), 6.73 (d, J = 8.5 Hz, 2H), 4.53 (q, J = 14.0 Hz, 2H), 4.41 (d, J = 4.0 Hz, 1H), 3.79 (d, J = 4.0 Hz, 1H), 3.78 (s, 3H), 3.77 (s, 3H), 3.37 (s, 1H); $^{13}C\{^1H\}$ NMR (126 MHz, $CDCl_3$) δ 175.4, 172.2, 160.9, 159.5, 137.3, 130.3, 127.3, 120.3, 115.1, 114.1, 72.8, 55.42, 55.38, 53.6, 42.4. IR (neat, cm^{-1}) 3376, 1708, 1593, 1511, 1395, 1293, 1249, 1175, 1027, 828. HRMS (ESI) $[M + H]^+$ calcd for $C_{19}H_{20}NO_5S^+$ 374.1057, found. 374.1054.

***(3S,4R)-3-Hydroxy-4-((4-methoxyphenyl)thio)-1-(3-(trifluoromethyl)benzyl)pyrrolidine-2,5-dione (3ha)*:**

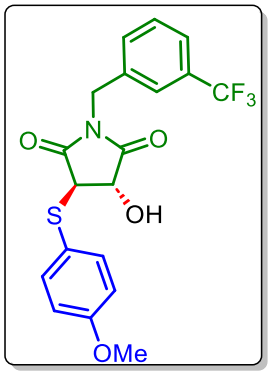

Brown solid (87 mg, 85% yield); m.p. 147–148 °C; purified over a column of silica gel (19% ethyl acetate in hexane); ^1H NMR (500 MHz, $CDCl_3$) δ 7.55 (d, J = 5.5 Hz, 2H), 7.42–7.39 (m, 4H), 6.74 (d, J = 9.0 Hz, 2H), 4.65 (q, J = 13.5 Hz, 2H), 4.47–4.45 (m, 1H), 3.83 (d, J = 5.0 Hz, 1H), 3.77 (s, 3H), 3.22 (s, 1H); $^{13}C\{^1H\}$ NMR (126 MHz, $CDCl_3$) δ 175.0, 172.1, 161.1, 137.4, 135.9, 132.2, 131.3 (d, J = 32.4 Hz), 129.4, 125.7 (q, J = 21.3 Hz), 125.2 (q, J =3.6 Hz), 122.9, 120.0, 115.1, 72.7, 55.4, 53.6, 42.5. ^{19}F NMR (471 MHz, $CDCl_3$) δ -62.6. IR (neat, cm^{-1}) 3066, 1588, 1489, 1333, 1166, 1011, 865, 677. HRMS (ESI) $[M + H]^+$ calcd for $C_{19}H_{17}F_3NO_4S^+$ 412.0825, found 412.0829.

***(3S,4R)-1-(2-Fluorobenzyl)-3-hydroxy-4-((4-methoxyphenyl)thio)pyrrolidine-2,5-dione (3ia)*:**

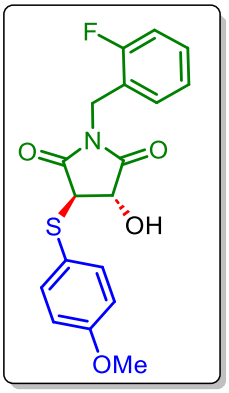

Brown liquid (75 mg, 83% yield); purified over a column of silica gel (18% ethyl acetate in hexane); ^{1}H NMR (500 MHz, $CDCl_3$) δ 7.44 (d, J = 9.0 Hz, 2H), 7.25–7.23 (m, 1H), 7.02–7.01 (m, 2H), 6.77 (d, J = 9.0 Hz, 2H), 6.70 (d, J = 1.0 Hz, 1H), 4.68 (q, J = 12.7 Hz, 2H), 4.48 (d, J = 5.0 Hz, 1H), 3.84 (d, J = 5.0 Hz, 1H), 3.79 (s, 3H), 3.39 (s, 1H); ^{13}C{^{1}H} NMR (126 MHz, $CDCl_3$) δ 175.1, 171.9, 161.0, 137.5, 135.3, 130.1 (d, J = 3.5 Hz), 130.0 (d, J = 8.2 Hz), , 124.3 (d, J = 3.7 Hz), 121.7 (d, J = 14.5 Hz), 120.2, 115.7 (d, J = 21.3 Hz), 115.1, 72.6, 55.5, 53.7, 36.7 (d, J = 4.7 Hz,). ^{19}F NMR (471 MHz, $CDCl_3$) δ -116.9. IR (neat, cm^{-1}) 3414, 1710, 1590, 1492, 1344, 1244, 1170, 1098, 830, 752. HRMS (ESI) $[M + H]^+$ calcd for $C_{18}H_{17}FNO_4S^+$ 362.0857, found 362.0856.

***(3S,4R)-3-Hydroxy-4-((4-methoxyphenyl)thio)-1-methylpyrrolidine-2,5-dione (3ja)*:**

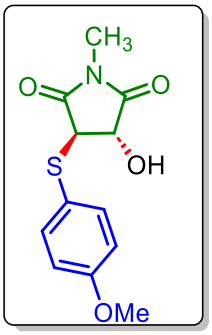

Brown solid (57 mg, 86% yield); m.p. 93–95 °C; purified over a column of silica gel (15% ethyl acetate in hexane); ^{1}H NMR (400 MHz, $CDCl_3$) δ 7.50 (d, J = 8.8 Hz, 2H), 6.86 (d, J = 8.8 Hz, 2H), 4.47 (d, J = 4.8 Hz, 1H), 3.84 (d, J = 4.8 Hz, 1H), 3.80 (s, 3H), 3.44 (s, 1H), 2.95 (s, 3H); ^{13}C{^{1}H} NMR (126 MHz, $CDCl_3$) δ 175.8, 172.7, 161.0, 137.2, 120.5, 115.1, 72.9, 55.5, 53.8, 25.4. IR (neat, cm^{-1}) 3327, 1683, 1590, 1492, 1444, 1285, 1240, 1092, 1029, 776, 629. HRMS (ESI) $[M + H]^+$ calcd for $C_{12}H_{14}NO_4S^+$ 268.0638, found 268.0634.

***(3S,4R)-1-Ethyl-3-hydroxy-4-((4-methoxyphenyl)thio)pyrrolidine-2,5-dione (3ka)*:**

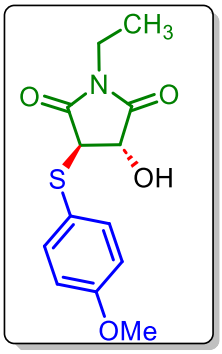

Brown liquid (55 mg, 79% yield); purified over a column of silica gel (16% ethyl acetate in hexane); ^{1}H NMR (500 MHz, $CDCl_3$) δ 7.50 (d, J = 9.0 Hz, 2H), 6.85 (d, J = 9.0 Hz, 2H), 4.45 (d, J = 5.0 Hz, 1H), 3.81 (d, J = 5.0 Hz, 1H), 3.80 (s, 3H), 3.51 (q, J = 7.2 Hz, 2H), 3.45 (s, 1H), 1.07 (t, J = 7.3 Hz, 3H); ^{13}C{^{1}H} NMR (126 MHz, $CDCl_3$) δ 13C NMR (126 MHz, CDCl3) δ 175.6, 172.4, 161.0, 137.3, 120.5, 115.1, 72.9, 55.5, 53.6, 34.4, 12.9. IR (neat, cm^{-1}) 3066, 2967, 1606, 1589, 1473, 1278, 1015, 956, 745, 694. HRMS (ESI) $[M + H]^+$ calcd for $C_{13}H_{16}NO_4S^+$ 282.0795, found 282.0790.

***(3S,4R)-3-Hydroxy-1-isobutyl-4-((4-methoxyphenyl)thio)pyrrolidine-2,5-dione (3la)*:**

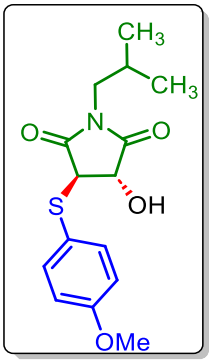

Brown solid (59 mg, 76% yield); m.p. 143–145 °C; purified over a column of silica gel (17% ethyl acetate in hexane); ^{1}H NMR (500 MHz, $CDCl_3$) δ 7.50 (d, J = 9.0 Hz, 2H), 6.85 (d, J = 8.5 Hz, 2H), 4.46 (d, J = 5.0 Hz, 1H), 3.82 (d, J = 5.0 Hz, 1H), 3.79 (s, 3H), 3.28 (s, 1H), 3.27–3.26 (m, 2H), 1.94–1.89 (m, 1H), 0.79 (d, J = 6.5 Hz, 3H), 0.73 (d, J = 6.5 Hz, 3H); ^{13}C{^{1}H} NMR (126 MHz, $CDCl_3$) δ 176.0, 172.5, 161.1, 137.6, 120.4, 115.1, 72.6, 55.5, 53.7, 46.6, 27.1, 20.0, 19.9. IR (neat, cm^{-1}) 3120, 1567, 1484, 1446, 1335, 1226, 1098, 975, 742, 699. HRMS (ESI) $[M + H]^+$ calcd for $C_{15}H_{20}NO_4S^+$ 310.1108, found 310.1107.

***(3S,4R)-3-Hydroxy-1-isopentyl-4-((4-methoxyphenyl)thio)pyrrolidine-2,5-dione (3ma)*:**

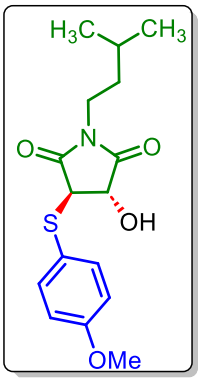

Brown solid (60 mg, 74% yield); m.p. 165–169 °C; purified over a column of silica gel (16% ethyl acetate in hexane); ^{1}H NMR (500 MHz, $CDCl_3$) δ 7.50 (d, J = 8.5 Hz, 2H), 6.85 (d, J = 9.0 Hz, 2H), 4.46 (d, J = 4.5 Hz, 1H), 3.80 (d, J = 4.5 Hz, 1H), 3.79 (s, 3H), 3.53 (s, 1H), 3.46 (t, J = 7.5 Hz, 2H), 1.41–1.35 (m, 1H), 1.34–1.28 (m, 2H), 0.88 (d, J = 3.5 Hz, 3H), 0.87 (d, J = 3.5 Hz, 3H); ^{13}C{^{1}H} NMR (126 MHz, $CDCl_3$) δ 175.7, 172.4, 161.0, 137.5, 120.5, 115.1, 72.9, 55.5, 53.7, 37.9, 36.3, 25.9, 22.35, 22.34. IR (neat, cm^{-1}) 3137, 1581, 1478, 1388, 1336, 1101, 976, 896, 711,

698. HRMS (ESI) $[M + H]^+$ calcd for $C_{16}H_{22}NO_4S^+$ 324.1264, found. 324.1268.

***(3S,4R)-1-Hexyl-3-hydroxy-4-((4-methoxyphenyl)thio)pyrrolidine-2,5-dione (3na)*:**

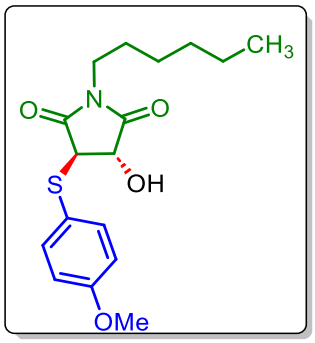

Brown liquid (63 mg, 75% yield); purified over a column of silica gel (15% ethyl acetate in hexane); ^{1}H NMR (500 MHz, $CDCl_3$) δ 7.50 (d, J = 9.0 Hz, 2H), 6.85 (d, J = 9.0 Hz, 2H), 4.46–4.44 (m, 1H), 3.81–3.80 (m, 1H), 3.79 (s, 3H), 3.44 (t, J = 7.3 Hz, 2H), 3.19 (s, 1H), 1.47–1.40 (m, 2H), 1.27–1.20 (m, 4H), 1.17–1.12 (m, 2H), 0.87 (t, J = 6.7 Hz, 3H); ^{13}C{^{1}H} NMR (126 MHz, $CDCl_3$) δ 175.7, 172.4, 161.1, 137.5, 120.4, 115.1, 72.8, 55.5, 53.7, 39.5, 31.4, 27.6, 26.4, 22.6, 14.1. IR (neat, cm^{-1}) 3419, 1701, 1589, 1492, 1398, 1289, 1174, 1026, 829, 632. HRMS (ESI) $[M + H]^+$ calcd for $C_{17}H_{24}NO_4S^+$ 338.1421, found 338.1418.

***(3S,4R)-1-Heptyl-3-hydroxy-4-((4-methoxyphenyl)thio)pyrrolidine-2,5-dione (3oa)*:**

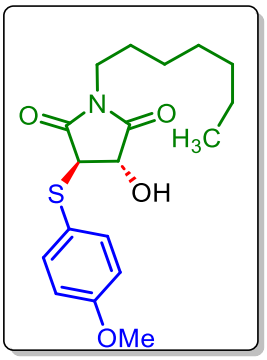

Brown liquid (75 mg, 85% yield); purified over a column of silica gel (18% ethyl acetate in hexane); ^{1}H NMR (500 MHz, $CDCl_3$) δ 7.50 (d, J = 8.5 Hz, 2H), 6.85 (d, J = 8.5 Hz, 2H), 4.45 (d, J = 2.5 Hz, 1H), 3.80 (d, J = 2.5 Hz, 1H), 3.79 (s, 3H), 3.44 (t, J = 7.5 Hz, 2H), 3.25 (s, 1H), 1.48–1.41 (m, 2H), 1.31–1.21 (m, 6H), 1.16–1.10 (m, 2H), 0.87 (t, J = 7.0 Hz, 3H); ^{13}C{^{1}H} NMR (126 MHz, $CDCl_3$) δ 175.7, 172.4, 161.0, 137.5, 120.4, 115.1, 72.8, 55.5, 53.7, 39.5, 31.8, 28.9, 27.6, 26.7, 22.7, 14.2. IR (neat, cm^{-1}) 3157, 1581, 1485, 1454, 1236, 1087, 1044, 934, 747, 697. HRMS (ESI) $[M + H]^+$ calcd for $C_{18}H_{26}NO_4S^+$ 352.1577, found 352.1571.

***(3S,4R)-3-Hydroxy-4-((4-methoxyphenyl)thio)-1-octylpyrrolidine-2,5-dione (3pa)*:**

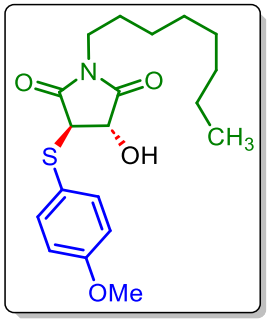

Brown liquid (81 mg, 89% yield); purified over a column of silica gel (18% ethyl acetate in hexane); ^{1}H NMR (500 MHz, $CDCl_3$) δ 7.50 (d, J = 9.0 Hz, 2H), 6.85 (d, J = 8.5 Hz, 2H), 4.45 (d, J = 3.0 Hz, 1H), 3.80 (d, J = 3.0 Hz, 1H), 3.79 (s, 3H), 3.44 (t, J = 7.3 Hz, 2H), 3.31 (s, 1H), 1.47–1.40 (m, 2H), 1.30–1.21 (m, 8H), 1.16–1.10 (m, 2H), 0.88 (t, J = 7.0 Hz, 3H); ^{13}C{^{1}H} NMR (126

MHz, $CDCl_3$) δ 175.8, 172.5, 161.0, 137.4, 120.4, 115.1, 72.8, 55.5, 53.7, 39.5, 31.9, 29.22, 29.17, 27.6, 26.8, 22.7, 14.2. IR (neat, cm^{-1}) 3419, 1702, 1591, 1492, 1398, 1246, 1172, 1030, 830, 632. HRMS (ESI) $[M + H]^+$ calcd for $C_{19}H_{28}NO_4S^+$ 366.1734, found 366.1734.

***(3S,4R)-1-Decyl-3-hydroxy-4-((4-methoxyphenyl)thio)pyrrolidine-2,5-dione (3qa)*:**

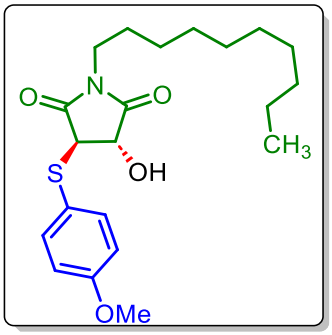

Brown liquid (76 mg, 77% yield); purified over a column of silica gel (17% ethyl acetate in hexane); ^1H NMR (400 MHz, $CDCl_3$) δ 7.50 (d, J = 8.8 Hz, 2H), 6.85 (d, J = 8.8 Hz, 2H), 4.45 (d, J = 4.4 Hz, 1H), 3.80 (d, J = 3.0 Hz, 1H), 3.78 (s, 3H), 3.44 (t, J = 7.4 Hz, 2H), 3.20 (s, 1H), 1.46–1.42 (m, 2H), 1.29–1.20 (m, 12H), 1.17–1.12 (m, 2H), 0.88 (t, J = 6.8 Hz, 3H); $^{13}C\{^1H\}$ NMR (126 MHz, $CDCl_3$) δ 175.7, 172.4, 161.0, 137.4, 120.4, 115.1, 72.8, 55.5, 53.7, 39.5, 32.0, 29.7, 29.6, 29.4, 29.2, 27.6, 26.8, 22.8, 14.3. IR (neat, cm^{-1}) 3421, 1702, 1591, 1492, 1399, 1246, 1173, 1030, 829, 632. HRMS (ESI) $[M + H]^+$ calcd for $C_{21}H_{32}NO_4S^+$ 394.2047, found 394.2049.

***(3S,4R)-3-Hydroxy-4-((4-methoxyphenyl)thio)pyrrolidine-2,5-dione (3ra)*:**

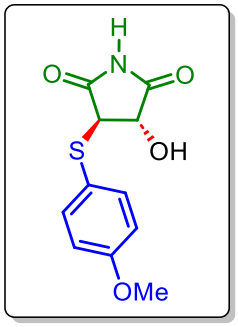

Brown liquid (54 mg, 85% yield); purified over a column of silica gel (20% ethyl acetate in hexane); ^1H NMR (500 MHz, $CDCl_3$) δ 8.11 (s, 1H), 7.52 (d, J = 9.0 Hz, 2H), 6.87 (d, J = 9.0 Hz, 2H), 4.48 (d, J = 6.0 Hz, 1H), 3.89 (d, J = 5.5 Hz, 1H), 3.81 (s, 3H), 3.30 (s, 1H); $^{13}C\{^1H\}$ NMR (126 MHz, $CDCl_3$) δ 13C NMR (126 MHz, CDCl3) δ 175.1, 171.8, 161.1, 137.4, 135.3, 115.3, 73.5, 55.5, 54.9. IR (neat, cm^{-1}) 3241, 2933, 1608, 1488, 1429, 1291, 1181, 1012, 930, 759. HRMS (ESI) $[M + H]^+$ calcd for $C_{11}H_{12}NO_4S^+$ 254.0482, found 254.0483.

***3-Hydroxy-4-((4-methoxyphenyl)thio)-1-(4-phenylbutan-2-yl)pyrrolidine-2,5-dione (3sa)*:**

Light yellow solid (75 mg, 78% yield); dr 1:0.87; m.p. 100–104 °C; purified over a column of silica gel (17% ethyl acetate in hexane); ^1H NMR (500 MHz, $CDCl_3$) δ 7.49 (d, J = 8.0 Hz, 4H),

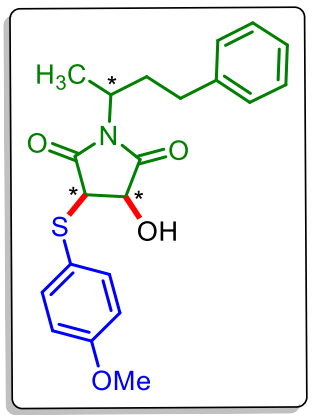

7.25–7.23 (m, 4H), 7.19–7.14 (m, 2H), 7.07 (t, J = 8.0 Hz, 4H), 6.81 (d, J = 8.5 Hz, 4H), 4.31–4.27 (m, 2H), 4.22–4.15 (m, 2H), 3.71 (s, 3H), 3.67 (s, 3H), 3.63 (d, J = 5.5 Hz, 1H), 3.57 (d, J = 5.5 Hz, 1H), 3.26–3.23 (m, 2H), 2.48–2.43 (m, 2H), 2.38 – 2.14 (m, 4H), 1.91–1.83 (m, 2H), 1.30 (d, J = 7.0 Hz, 3H), 1.27 (d, J = 7.0 Hz, 3H); $^{13}C\{^1H\}$ NMR (126 MHz, $CDCl_3$) δ 175.87, 175.86, 172.4, 160.99, 160.97, 141.0, 140.9, 137.5, 137.4, 128.6, 128.5, 128.4, 126.22, 126.19, 120.6, 120.5, 115.07, 115.06, 72.31, 72.27, 55.44, 55.36, 53.64, 53.62, 49.2, 49.0, 33.9, 33.8, 33.2, 33.0, 18.2, 18.0. IR (neat, cm^{-1}) 3385, 1689, 1590, 1491, 1367, 1246, 1166, 1028, 826, 699. HRMS (ESI) $[M + H]^+$ calcd for $C_{21}H_{24}NO_4S^+$ 386.1421, found 386.1425.

(3S,4R)-3-Hydroxy-4-((4-methoxyphenyl)thio)-1-(4-phenylbutyl)pyrrolidine-2,5-dione (3ta):

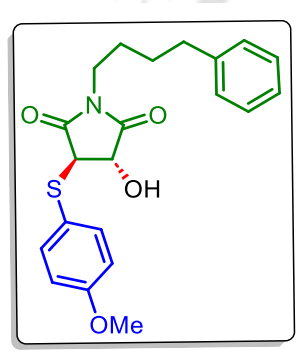

Brown liquid (83 mg, 86% yield); purified over a column of silica gel (17% ethyl acetate in hexane); ^1H NMR (500 MHz, $CDCl_3$) δ 7.48 (d, J = 9.0 Hz, 2H), 7.27 (t, J = 6.8 Hz, 2H), 7.18 (t, J = 7.5 Hz, 1H), 7.13 (d, J = 7.5 Hz, 2H), 6.79 (d, J = 9.0 Hz, 2H), 4.44 (d, J = 5.5 Hz, 1H), 3.80 (d, J = 5.5 Hz, 1H), 3.75 (s, 3H), 3.71 (s, 1H), 3.46 (t, J = 6.5 Hz, 2H), 2.56 (t, J = 7.0 Hz, 2H), 1.50–1.49 (m, 4H); $^{13}C\{^1H\}$ NMR (126 MHz, $CDCl_3$) δ 175.9, 172.5, 161.0, 141.8, 137.4, 128.5, 126.0, 120.3, 115.1, 72.6, 55.5, 53.7, 39.1, 35.2, 28.4, 27.1. IR (neat, cm^{-1}) 3420, 1700, 1591, 1492, 1396, 1245, 1146, 1029, 829, 740. HRMS (ESI) $[M + H]^+$ calcd for $C_{21}H_{24}NO_4S$ 386.1421 , found 386.1427.

***(3S,4R)-3-Hydroxy-4-((4-methoxyphenyl)thio)-1-phenethylpyrrolidine-2,5-dione (3ua)*:**

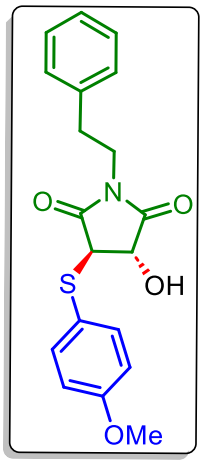

Brown solid (80 mg, 89% yield); m.p. 153–155 °C; purified over a column of silica gel (17% ethyl acetate in hexane); ^{1}H NMR (500 MHz, $CDCl_3$) δ 7.50 (d, J = 9.0 Hz, 2H), 7.25–7.20 (m, 3H), 7.08 (d, J = 6.5 Hz, 2H), 6.86 (d, J = 8.5 Hz, 2H), 4.37 (d, J = 3.0 Hz, 1H), 3.79 (s, 3H), 3.76 (d, J = 5.5 Hz, 1H), 3.69 (t, J = 7.6 Hz, 2H), 3.33 (s, 1H), 2.83–2.73 (m, 2H); ^{13}C{^{1}H} NMR (126 MHz, $CDCl_3$) δ 175.5, 172.2, 161.1, 137.44, 137.37, 128.9, 128.7, 127.0, 120.5, 115.1, 72.6, 55.5, 53.7, 40.5, 33.5. IR (neat, cm^{-1}) 3078, 1681, 1508, 1336, 1287, 1156, 1114, 984, 835, 756, 685. HRMS (ESI) $[M + H]^+$ calcd for $C_{19}H_{20}NO_4S^+$ 358.1108, found 358.1107.

***(3S,4R)-3-Hydroxy-4-((4-methoxyphenyl)thio)-1-(2-(thiophen-2-yl)ethyl)pyrrolidine-2,5-dione (3va)*:**

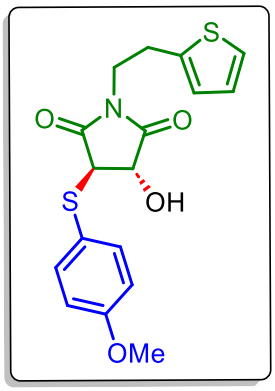

Brown solid (73 mg, 81% yield); m.p. 120–124 °C; purified over a column of silica gel (18% ethyl acetate in hexane); ^{1}H NMR (400 MHz, $CDCl_3$) δ 7.50 (d, J = 8.8 Hz, 2H), 7.13 (dd, J = 4.8, 1.2 Hz, 1H), 6.90–6.87 (m, 1H), 6.86 (d, J = 8.4 Hz, 2H), 6.70 (d, J = 2.8 Hz, 1H), 4.41 (d, J = 4.0 Hz, 1H), 3.80 (s, 3H), 3.78 (d, J = 4.0 Hz, 1H), 3.72 (t, J = 7.2 Hz, 2H), 3.11 (s, 1H), 3.05–3.00 (m, 2H); ^{13}C{^{1}H} NMR (126 MHz, $CDCl_3$) δ 175.3, 172.1, 161.1, 139.3, 137.4, 127.2, 126.0, 124.5, 120.5, 115.2, 72.7, 55.5, 53.8, 40.6, 27.5. IR (neat, cm^{-1}) 3317, 2965, 1600, 1511, 1478, 1370, 1264, 964, 746, 681. HRMS (ESI) $[M + H]^+$ calcd for $C_{17}H_{18}NO_4S_2^+$ 364.0672, found 364.0675.

***(3S,4R)-3-Hydroxy-1-phenyl-4-(phenylthio)pyrrolidine-2,5-dione (3ab)*:**

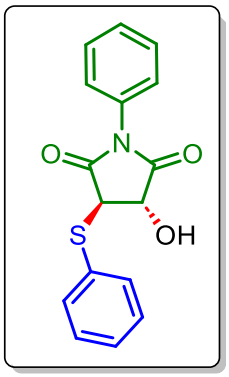

White solid (42 mg, 56% yield); m.p. 148–151 °C; purified over a column of silica gel (15% ethyl acetate in hexane); ^{1}H NMR (500 MHz, $CDCl_3$) δ 7.64–7.62 (m, 3H), 7.46 (t, J = 7.5 Hz, 2H), 7.40–7.37 (m, 4H), 7.19–7.17 (m, 1H), 4.66–4.65 (m, 1H), 4.13 (d, J = 5.5 Hz, 1H), 3.30 (s, 1H); ^{13}C{^{1}H} NMR (126 MHz, $CDCl_3$) δ 174.6, 171.5, 134.6, 129.7, 129.5, 129.42, 129.41, 129.2, 126.3, 125.6, 119.9, 73.4, 53.3. IR (neat, cm^{-1}) 3172, 1476, 1461, 1239,

1166, 1037, 968, 637. HRMS (ESI) $[M + H]^+$ calcd for $C_{16}H_{14}NO_3S^+$ 300.0689, found 300.0710.

***(3S,4R)-3-Hydroxy-1-phenyl-4-(p-tolylthio)pyrrolidine-2,5-dione (3ac)*:**

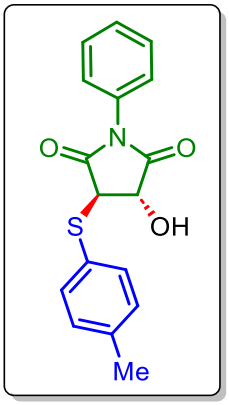

White solid (56 mg, 71% yield); m.p. 141–148 °C; purified over a column of silica gel (16% ethyl acetate in hexane); ^{1}H NMR (500 MHz, $CDCl_3$) δ 7.50 (d, J = 7.5 Hz, 2H), 7.45 (t, J = 7.5 Hz, 2H), 7.41 (d, J = 7.5 Hz, 1H), 7.18–7.15 (m, 4H), 4.63 (d, J = 5.0 Hz, 1H), 4.05 (d, J = 5.5 Hz, 1H), 3.36 (s, 1H), 2.36 (s, 3H); ^{13}C{^{1}H} NMR (126 MHz, $CDCl_3$) δ 174.7, 171.6, 140.1, 135.2, 131.3, 130.5, 129.4, 129.2, 126.7, 126.3, 73.1, 53.4, 21.4. IR (neat, cm^{-1}) 3372, 1676, 1351, 1320, 1208, 1026, 928, 738, 655. HRMS (ESI) $[M + H]^+$ calcd for $C_{17}H_{16}NO_3S^+$ 314.0845, found 314.0851.

***(3R,4S)-3-((4-Chlorophenyl)thio)-4-hydroxy-1-phenylpyrrolidine-2,5-dione (3ad)*:**

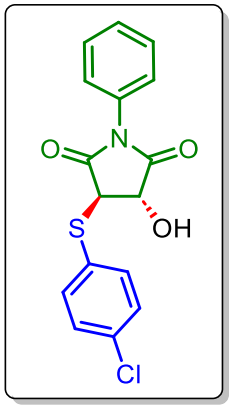

White solid (58 mg, 70% yield); m.p. 156–159 °C; purified over a column of silica gel (19% ethyl acetate in hexane); ^{1}H NMR (400 MHz, $CDCl_3$) δ 7.57 (d, J = 8.4 Hz, 2H), 7.47– .46 (m, 2H), 7.44–7.41 (m, 1H), 7.34 (d, J = 8.4 Hz, 2H), 7.21 (d, J = 7.2 Hz, 2H), 4.63 (d, J = 5.6 Hz, 1H), 4.12 (d, J = 5.6 Hz, 1H), 3.43 (s, 1H); ^{13}C{^{1}H} NMR (126 MHz, $CDCl_3$) δ 174.4, 171.3, 135.9, 135.7, 131.1, 129.8, 129.5, 129.4, 129.3, 126.2, 73.3, 53.5. IR (neat, cm^{-1}) 3072, 1676, 1651, 1369, 1158, 1028, 938, 688, 599. HRMS (ESI) $[M + H]^+$ calcd for $C_{16}H_{13}ClNO_3S^+$ 334.0305, found 334.0303.

***(3R,4S)-3-((3-Fluoro-4-methoxyphenyl)thio)-4-hydroxy-1-phenylpyrrolidine-2,5-dione (3ae)*:**

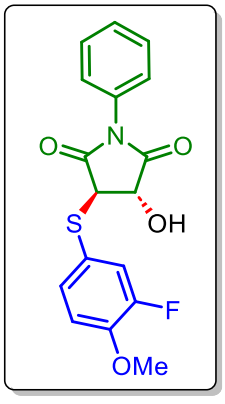

White solid (67 mg, 77% yield); m.p. 149–154 °C; purified over a column of silica gel (23% ethyl acetate in hexane); ^{1}H NMR (500 MHz, $CDCl_3$) δ 7.47 (t, J = 7.5 Hz, 2H), 7.42–7.38 (m, 3H), 7.20 (d, J = 7.5 Hz, 2H), 6.94 (t, J = 9.0 Hz, 1H), 4.61 (d, J = 5.0 Hz, 1H), 4.03 (d, J = 5.0 Hz, 1H), 3.90 (s, 3H), 3.37 (s, 1H); ^{13}C{^{1}H} NMR (126 MHz, $CDCl_3$) δ 174.5, 171.4, 149.5 (d, J = 10.3 Hz),

132.2 (d, J = 3.7 Hz), 131.2, 129.5, 129.31, 129.27, 126.2, 123.1 (d, J = 18.5 Hz), 121.3 (d, J = 6.7 Hz), 113.9 (d, J = 2.3 Hz), 72.9, 56.4, 53.8. ^{19}F NMR (471 MHz, $CDCl_3$) δ -132.4. IR (neat, cm^{-1}) 3172, 1523, 1445, 1329, 1165, 1127, 858, 738, 635. HRMS (ESI) $[M + H]^+$ calcd for $C_{17}H_{15}FNO_4S^+$ 348.0700, found 348.0696.

***3-((4-Methoxyphenyl)thio)-1-phenylpyrrolidine-2,5-dione (6aa)*:**

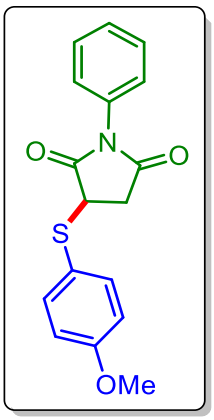

Brown liquid (58 mg, 75% yield; purified over a column of silica gel (11% ethyl acetate in hexane); ^{1}H NMR (500 MHz, $CDCl_3$) δ 7.51 (d, J = 8.5 Hz, 2H), 7.44–7.41 (m, 2H), 7.37 (d, J = 7.5 Hz, 1H), 7.04 (d, J = 7.5 Hz, 2H), 6.88 (d, J = 9.0 Hz, 2H), 4.03 (dd, J = 9.5, 3.5 Hz, 1H), 3.81 (s, 3H), 3.31 (q, J = 9 Hz, 1H), 2.90 (dd, J = 19.0, 3.5 Hz, 1H); ^{13}C{^{1}H} NMR (126 MHz, $CDCl_3$) δ 174.8, 173.8, 161.4, 137.9, 131.7, 129.3, 128.9, 126.5, 119.7, 115.2, 55.6, 44.7, 36.4. IR (neat, cm^{-1}) 3163, 1514, 1455, 1314, 1115, 1107, 755, 631, 601. HRMS (ESI) $[M + H]^+$ calcd for $C_{17}H_{16}NO_3S^+$ 314.0845, found 314.0844.

IV.9. NMR Spectra

(3*S*,4*R*)-3-Hydroxy-4-((4-methoxyphenyl)thio)-1-phenylpyrrolidine-2,5-dione (3aa): ^{1}H NMR ($CDCl_3$, 500 MHz)

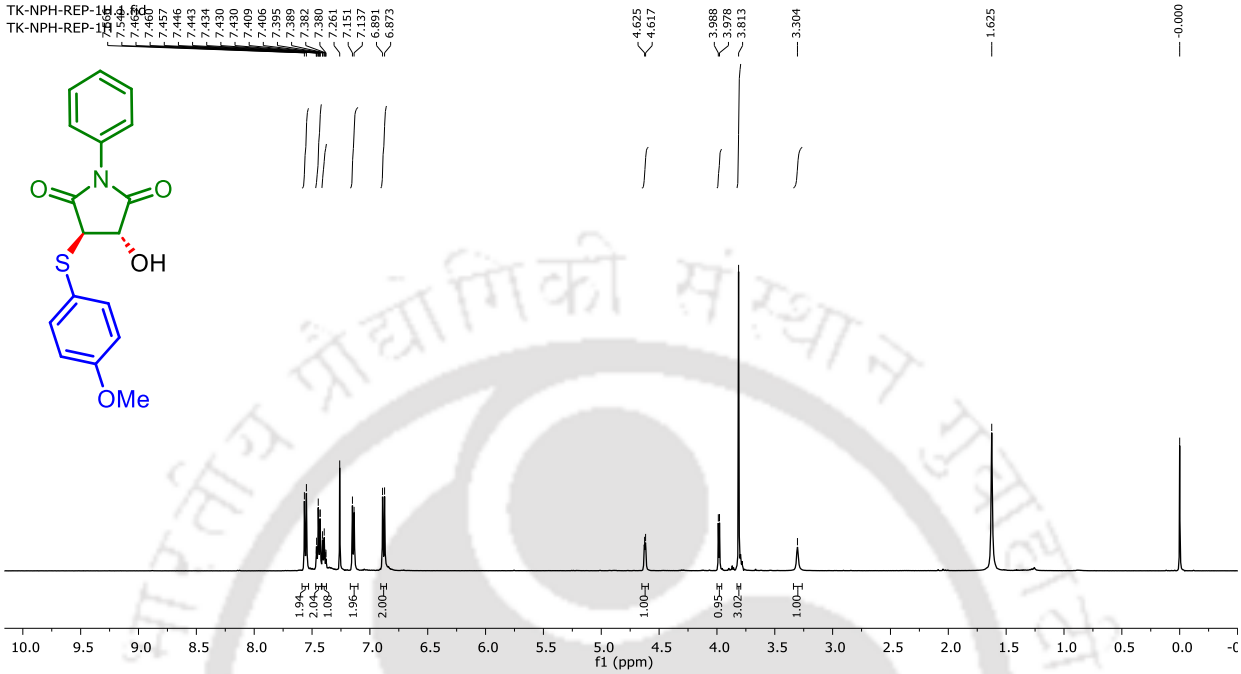

(3*S*,4*R*)-3-Hydroxy-4-((4-methoxyphenyl)thio)-1-phenylpyrrolidine-2,5-dione (3aa): ^{13}C{^{1}H} NMR ($CDCl_3$, 126 MHz)

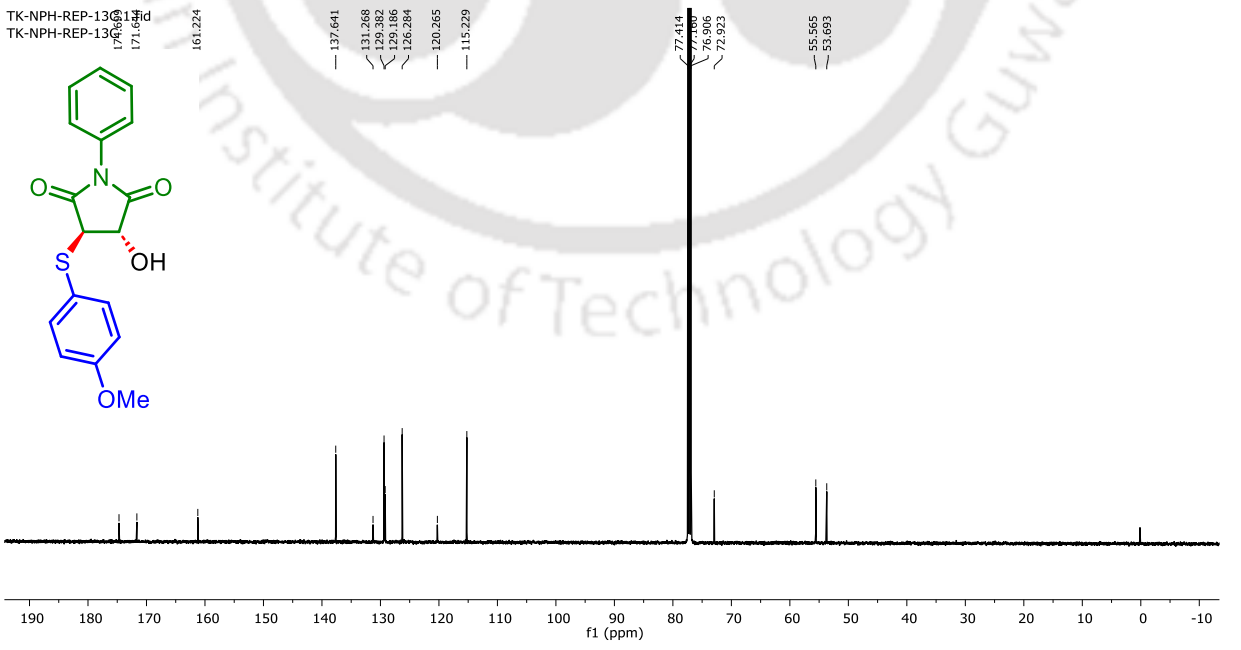

(3*S*,4*R*)-3-Hydroxy-4-((4-methoxyphenyl)thio)-1-(*p*-tolyl)pyrrolidine-2,5-dione (3ba): ^{1}H NMR ($CDCl_3$, 500 MHz)

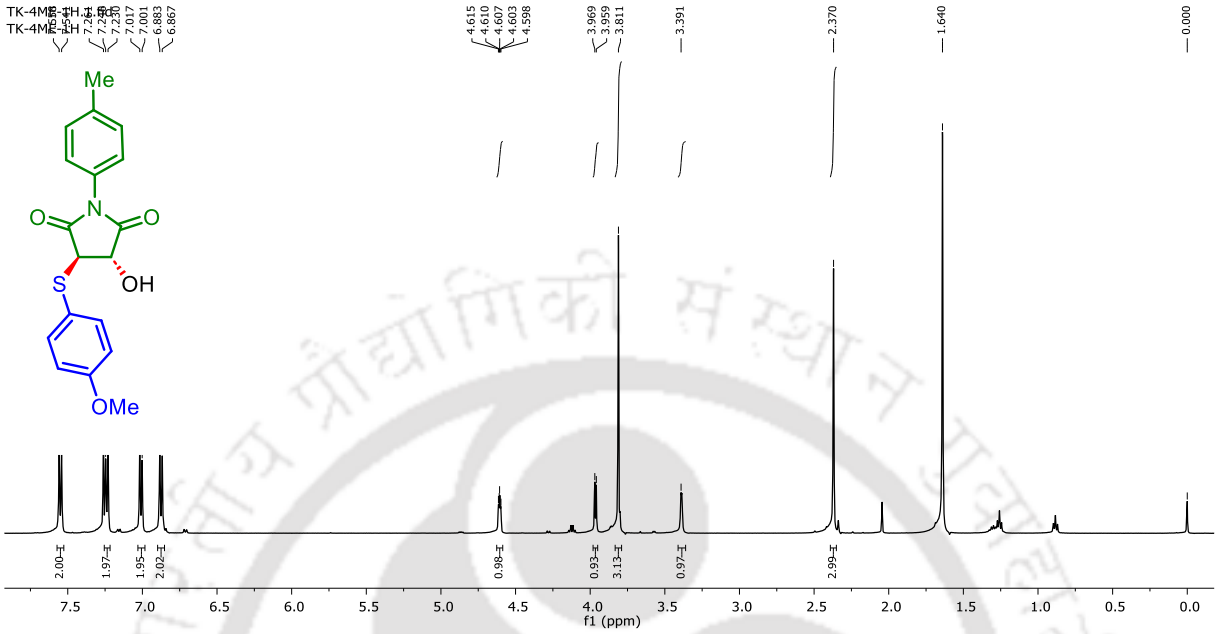

(3*S*,4*R*)-3-Hydroxy-4-((4-methoxyphenyl)thio)-1-(*p*-tolyl)pyrrolidine-2,5-dione (3ba): ^{13}C{^{1}H} NMR ($CDCl_3$, 126 MHz)

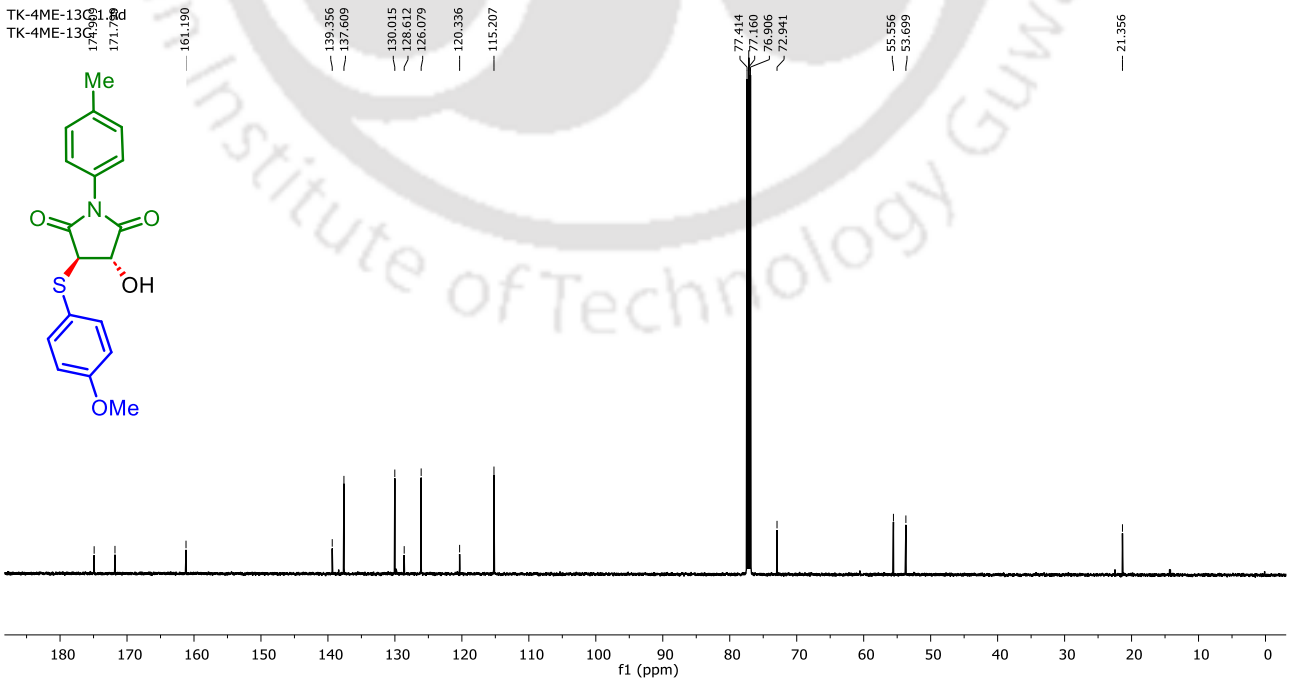

(3*S*,4*R*)-1-Benzyl-3-hydroxy-4-((4-methoxyphenyl)thio)pyrrolidine-2,5-dione (3ea): ^{1}H NMR ($CDCl_3$, 500 MHz)

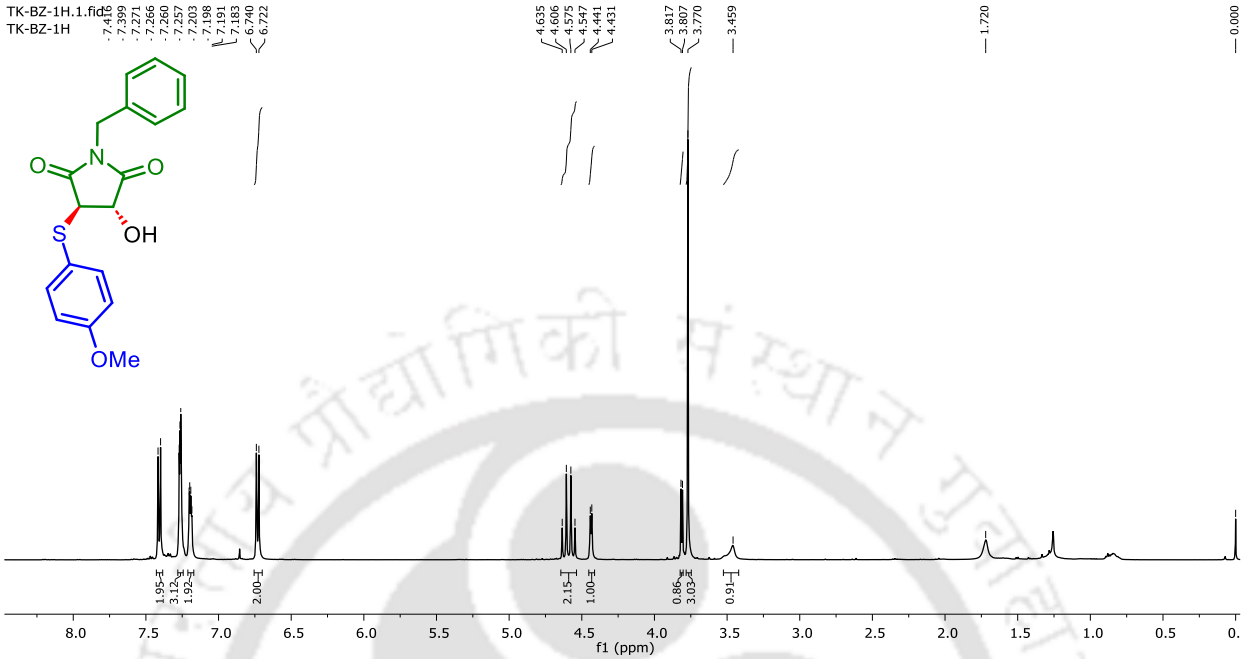

(3*S*,4*R*)-1-Benzyl-3-hydroxy-4-((4-methoxyphenyl)thio)pyrrolidine-2,5-dione (3ea): ^{13}C{^{1}H} NMR ($CDCl_3$, 126 MHz)

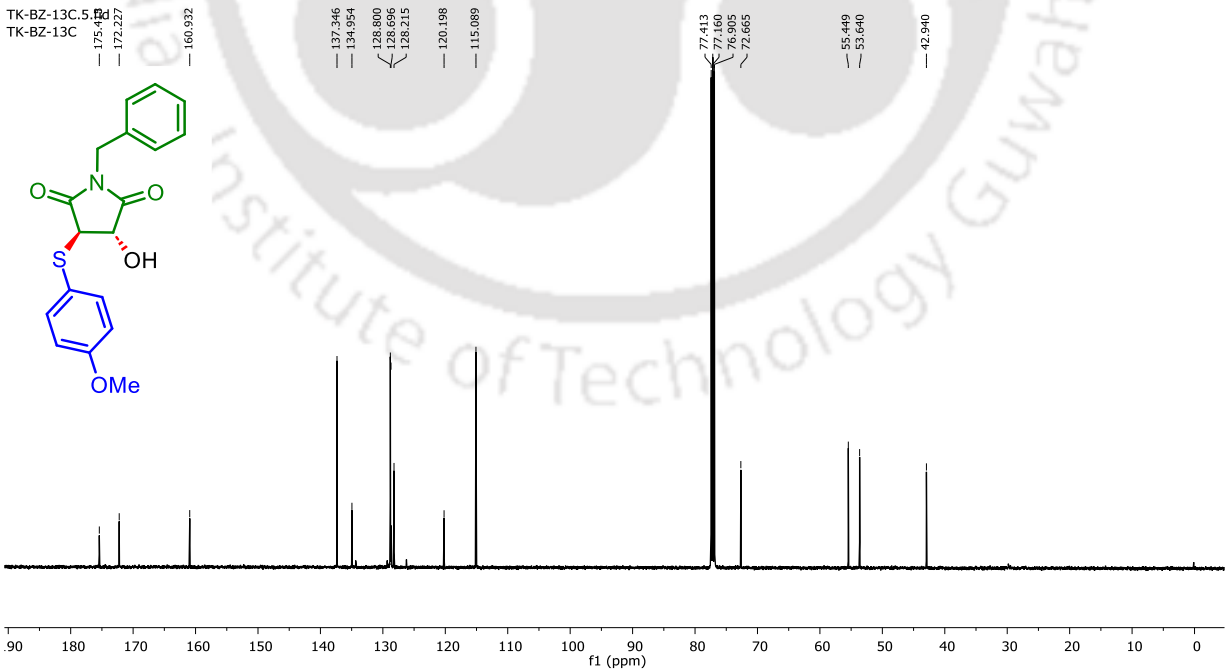

(3*S*,4*R*)-1-(2-Fluorobenzyl)-3-hydroxy-4-((4-methoxyphenyl)thio)pyrrolidine-2,5-dione (3ia): ^{1}H NMR ($CDCl_3$, 500 MHz)

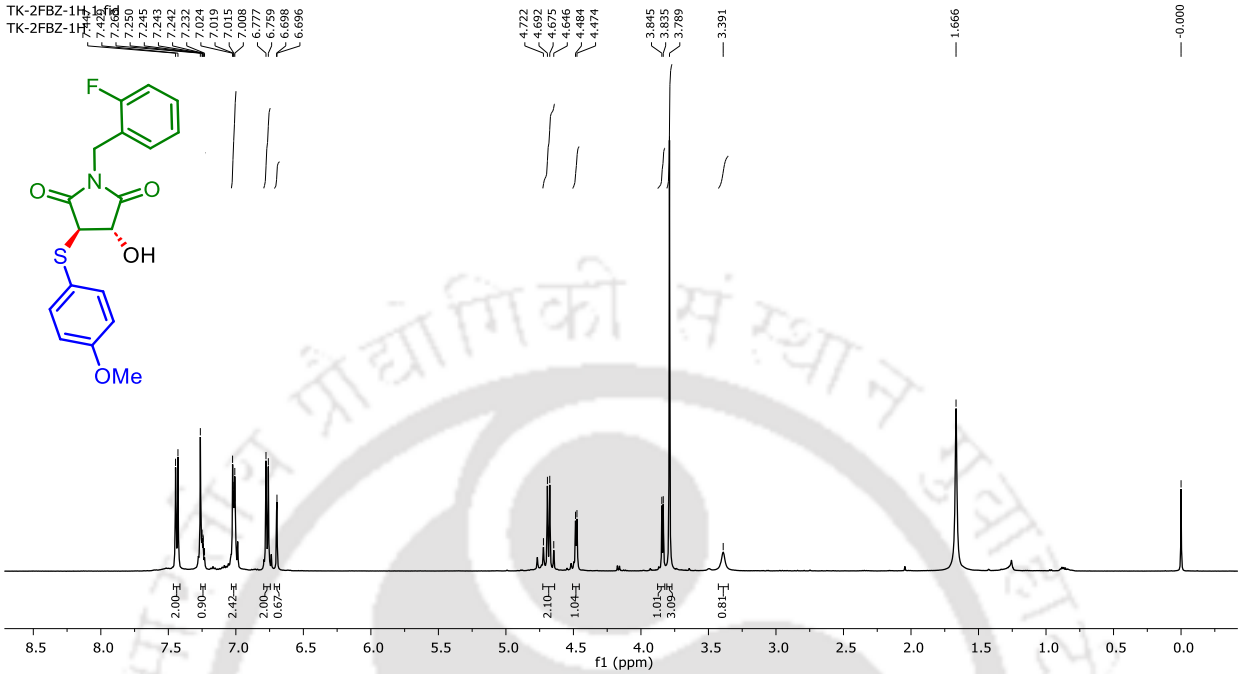

(3*S*,4*R*)-1-(2-Fluorobenzyl)-3-hydroxy-4-((4-methoxyphenyl)thio)pyrrolidine-2,5-dione (3ia): ^{13}C{^{1}H} NMR ($CDCl_3$, 126 MHz)

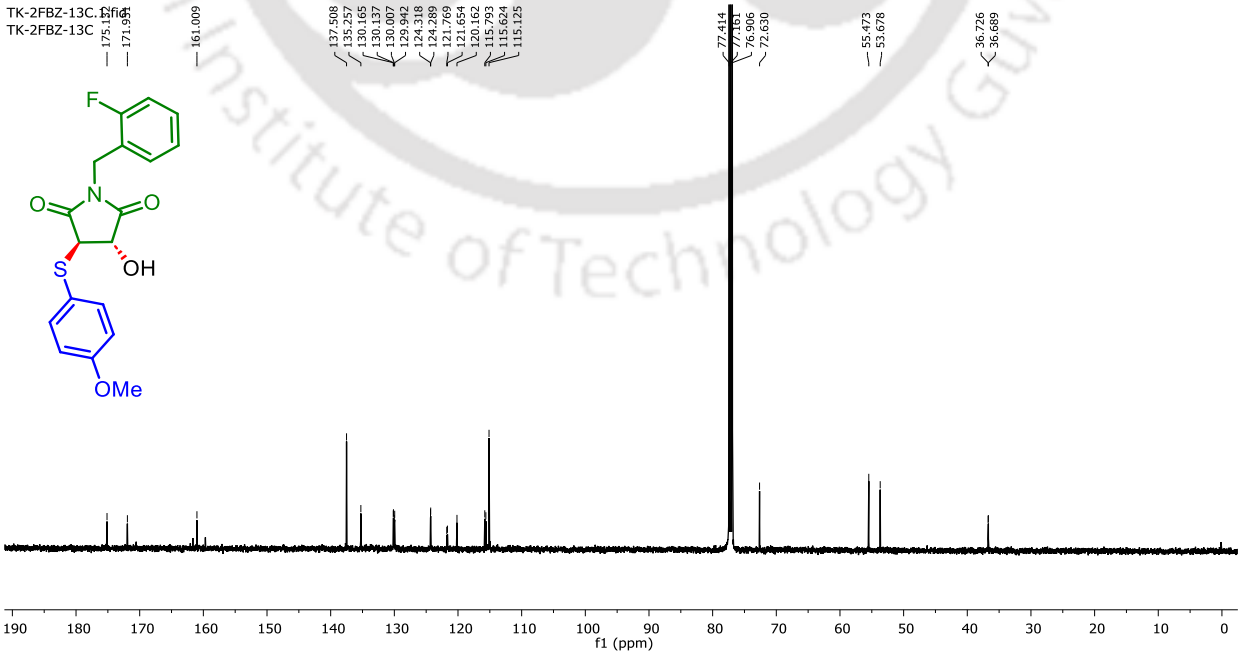

(3*S*,4*R*)-1-(2-Fluorobenzyl)-3-hydroxy-4-((4-methoxyphenyl)thio)pyrrolidine-2,5-dione (3ia): ^{19}F NMR ($CDCl_3$, 471 MHz)

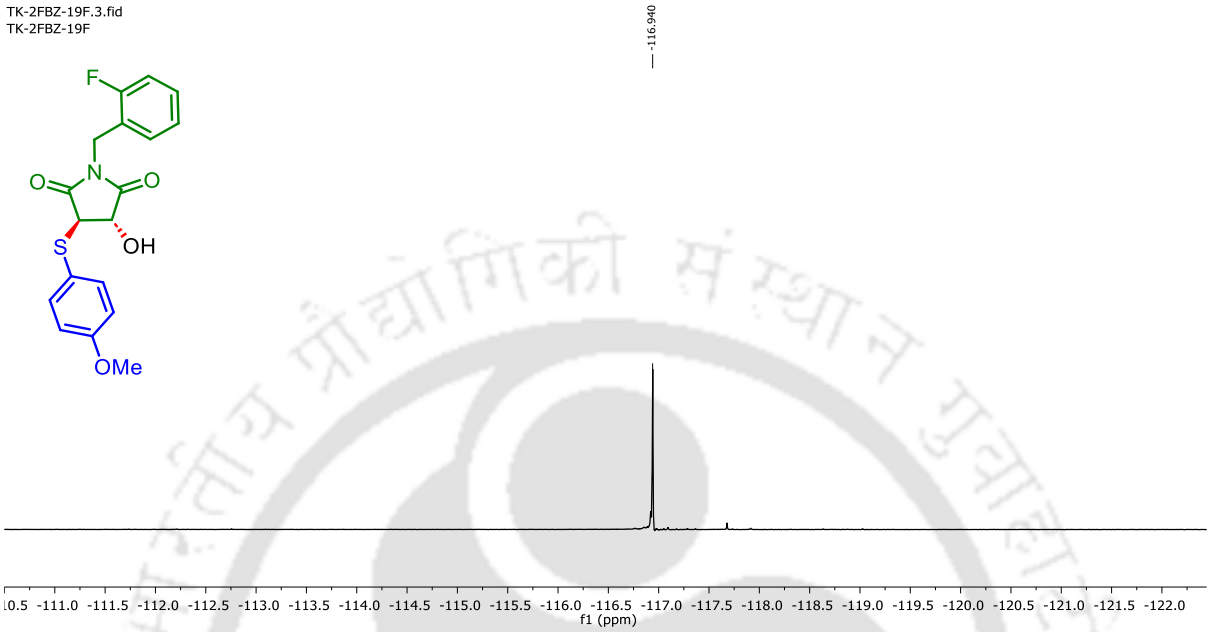

(3*S*,4*R*)-3-Hydroxy-4-((4-methoxyphenyl)thio)-1-methylpyrrolidine-2,5-dione (3ja): ^{1}H NMR ($CDCl_3$, 400 MHz)

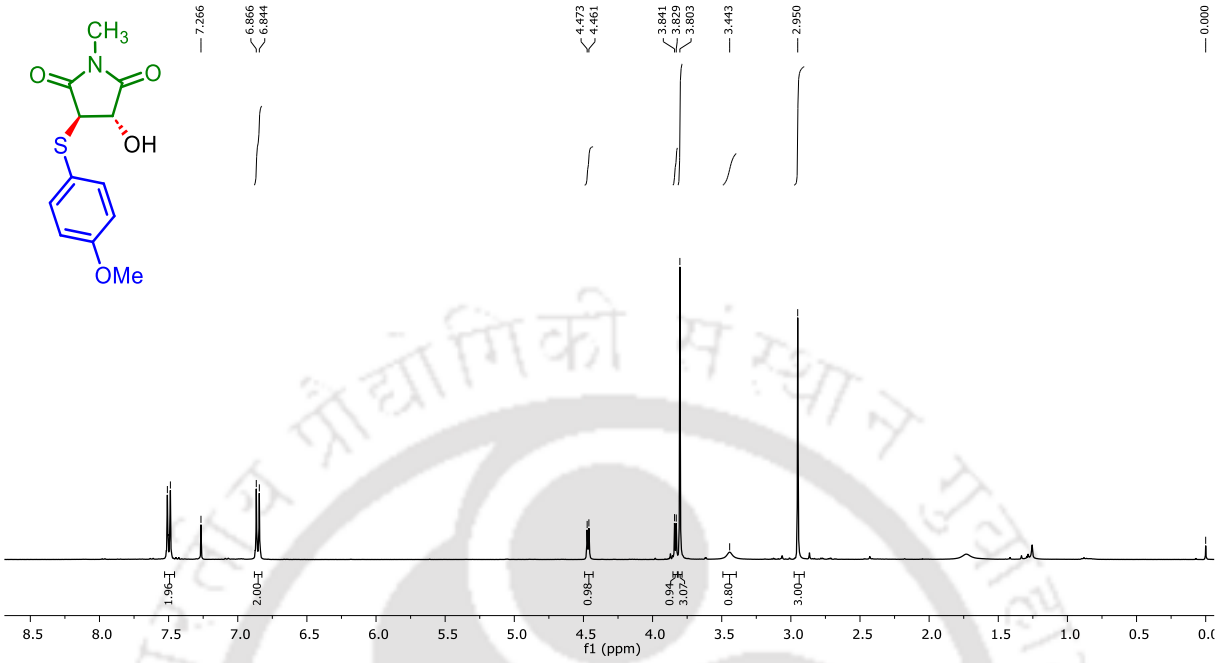

(3*S*,4*R*)-3-Hydroxy-4-((4-methoxyphenyl)thio)-1-methylpyrrolidine-2,5-dione (3ja): ^{13}C{^{1}H} NMR ($CDCl_3$, 126 MHz)

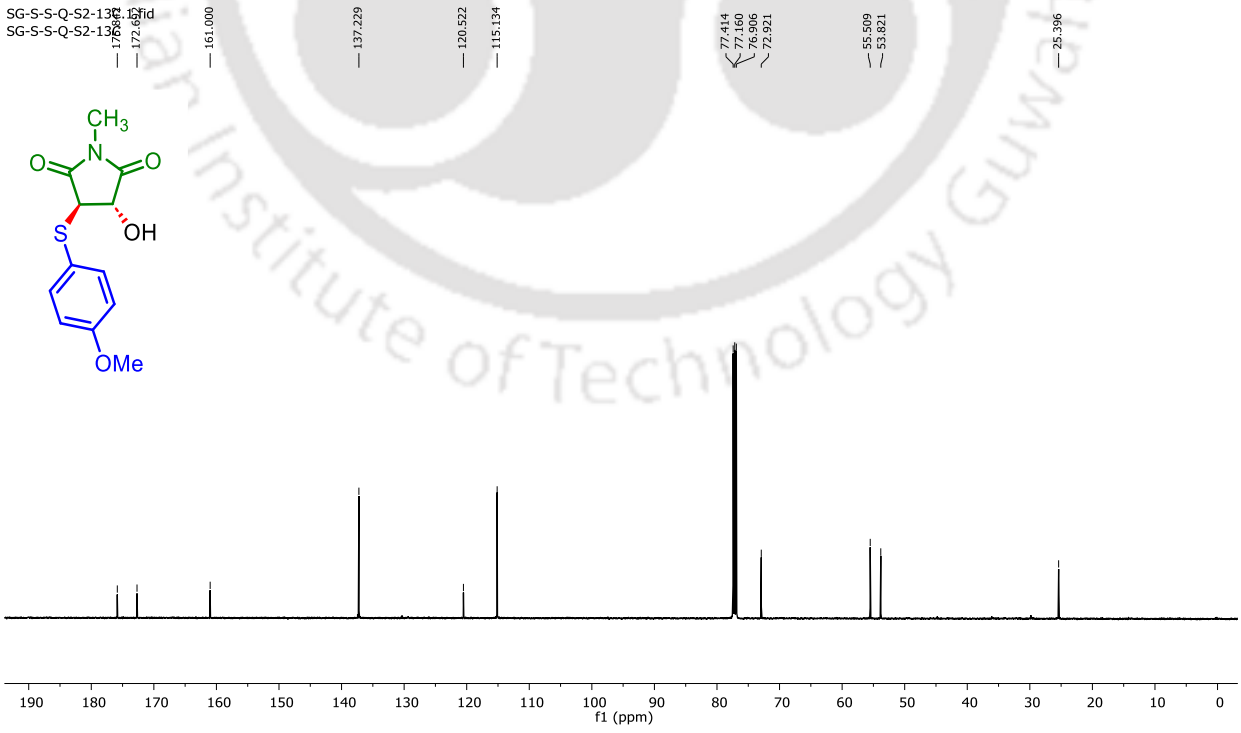

(3*S*,4*R*)-3-Hydroxy-4-((4-methoxyphenyl)thio)-1-octylpyrrolidine-2,5-dione (3pa): ^{1}H NMR ($CDCl_3$, 500 MHz)

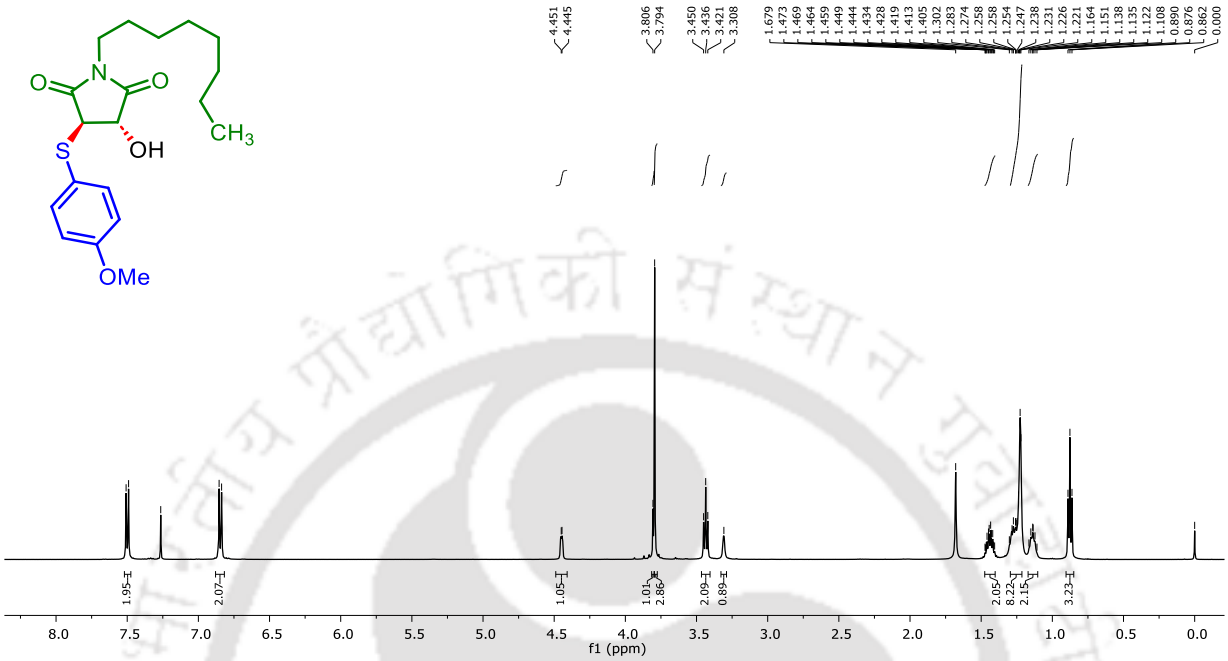

(3*S*,4*R*)-3-Hydroxy-4-((4-methoxyphenyl)thio)-1-octylpyrrolidine-2,5-dione (3pa): ^{13}C{^{1}H} NMR ($CDCl_3$, 126 MHz)

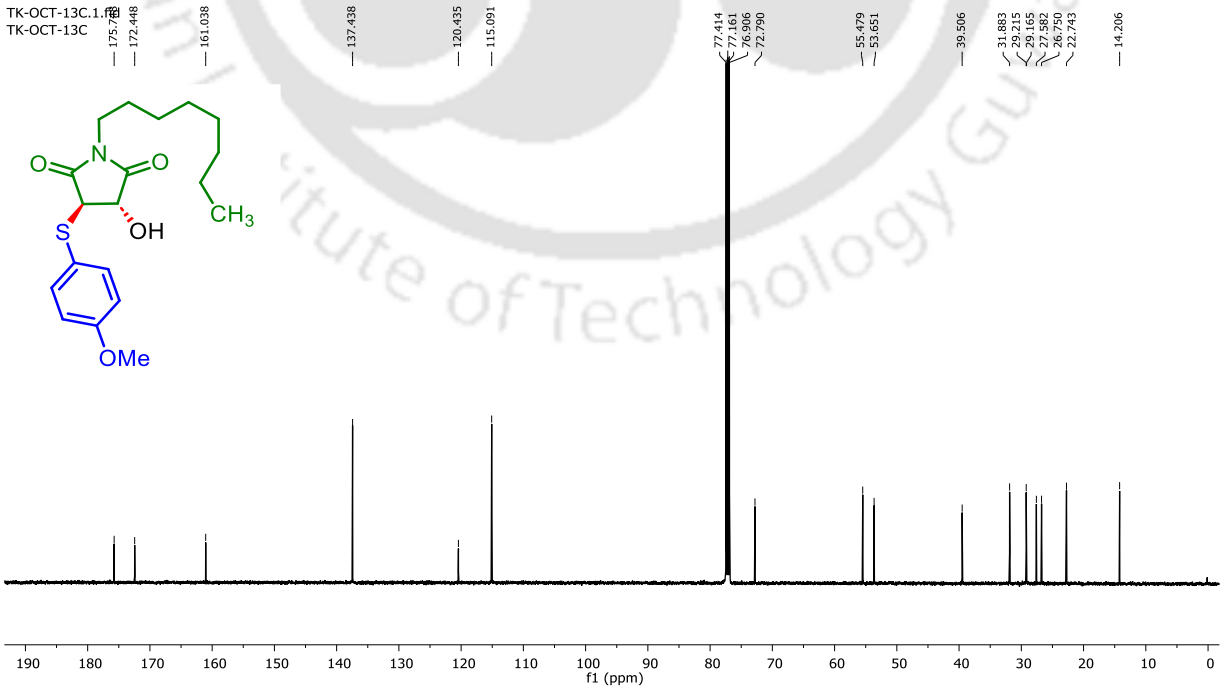

(3*S*,4*R*)-3-Hydroxy-4-((4-methoxyphenyl)thio)pyrrolidine-2,5-dione (3ra): ^{1}H NMR (CDCl$_3$, 500 MHz)

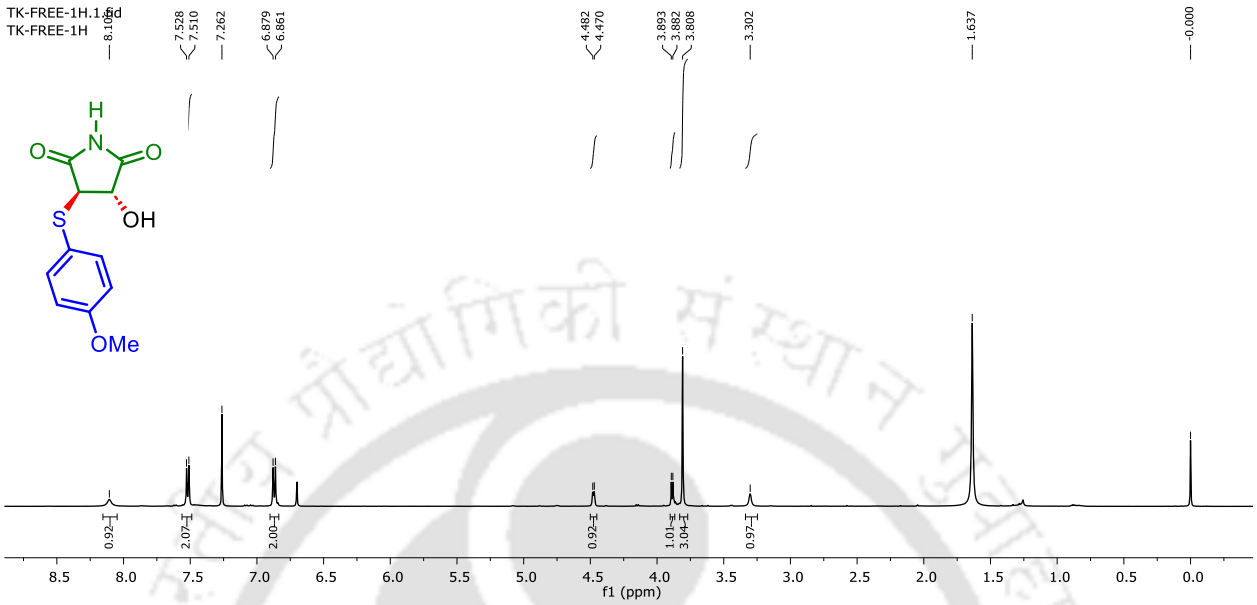

(3*S*,4*R*)-3-Hydroxy-4-((4-methoxyphenyl)thio)pyrrolidine-2,5-dione (3ra): ^{13}C{^{1}H} NMR (CDCl$_3$, 126 MHz)

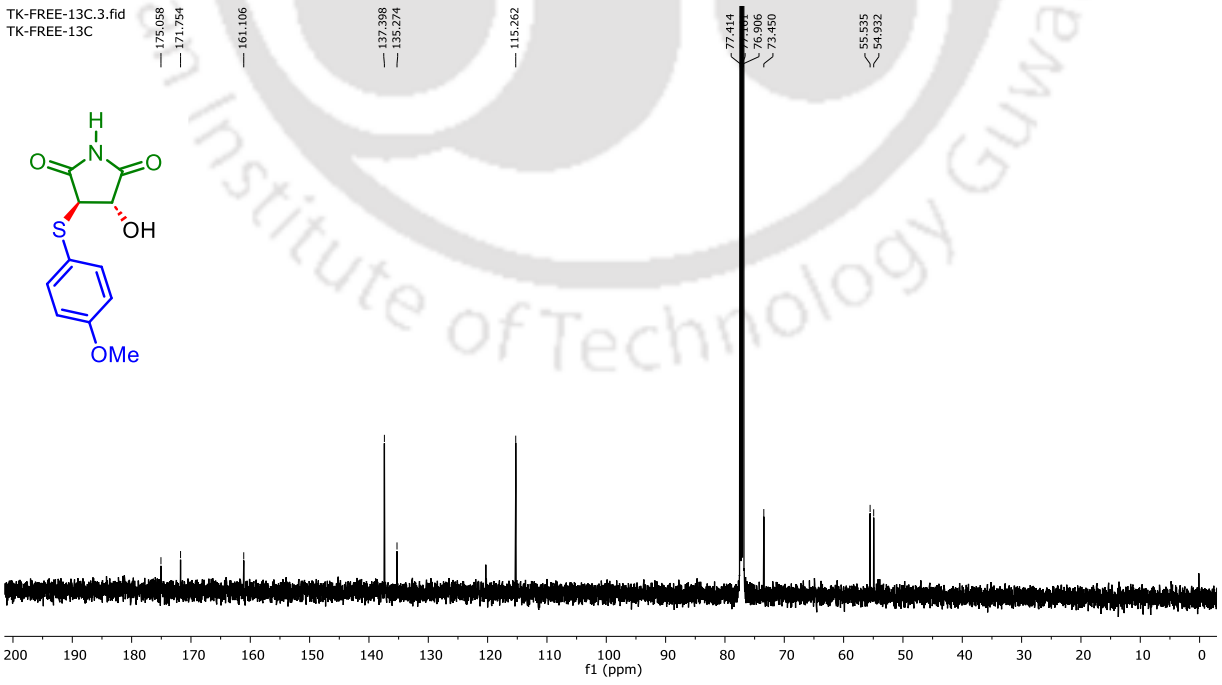

(3*S*,4*R*)-3-Hydroxy-4-((4-methoxyphenyl)thio)-1-phenethylpyrrolidine-2,5-dione (3ua): ^{1}H NMR ($CDCl_3$, 500 MHz)

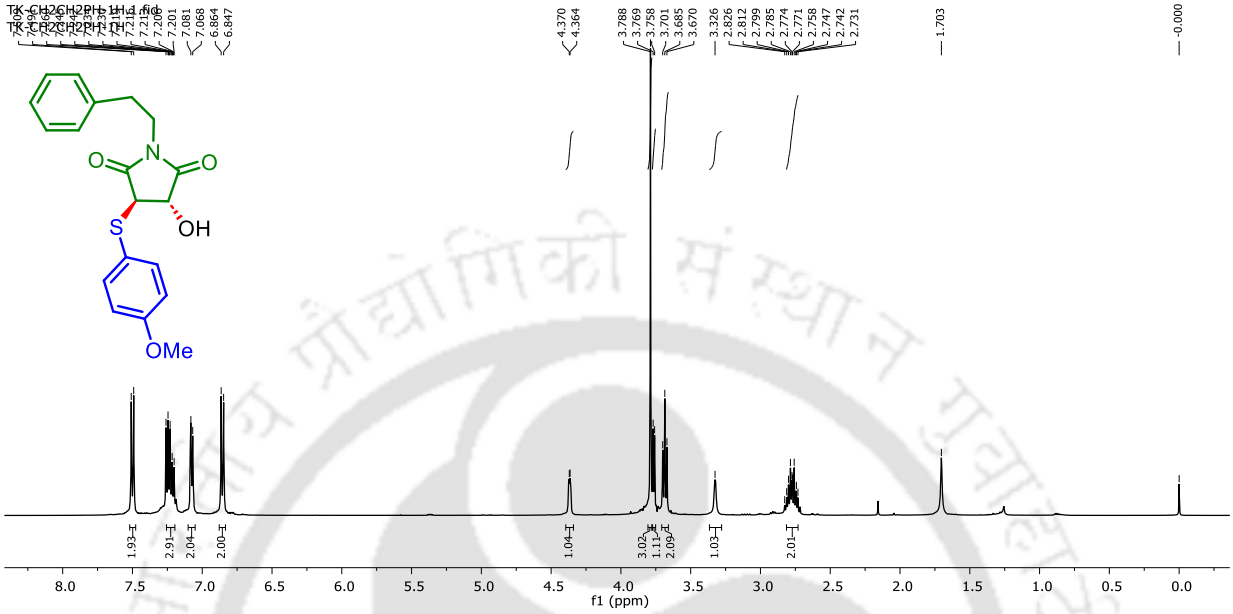

(3*S*,4*R*)-3-Hydroxy-4-((4-methoxyphenyl)thio)-1-phenethylpyrrolidine-2,5-dione (3ua): ^{13}C{^{1}H} NMR ($CDCl_3$, 126 MHz)

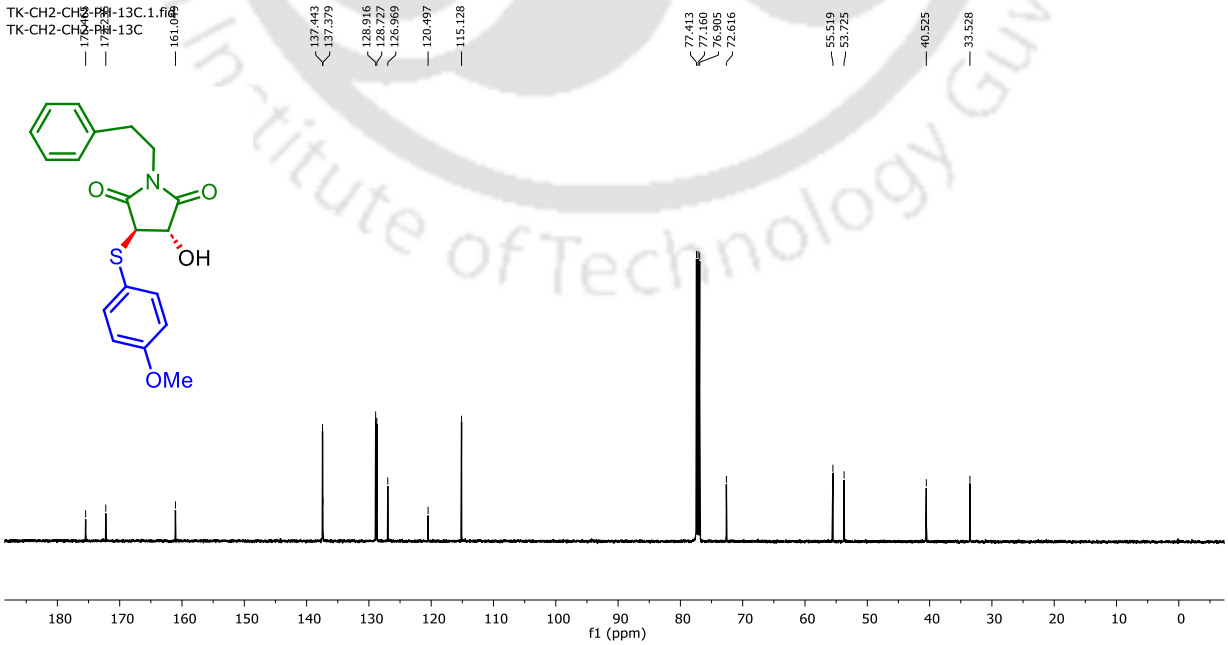

(3*S*,4*R*)-3-Hydroxy-1-phenyl-4-(*p*-tolylthio)pyrrolidine-2,5-dione (3ac): ^{1}H NMR ($CDCl_3$, 500 MHz)

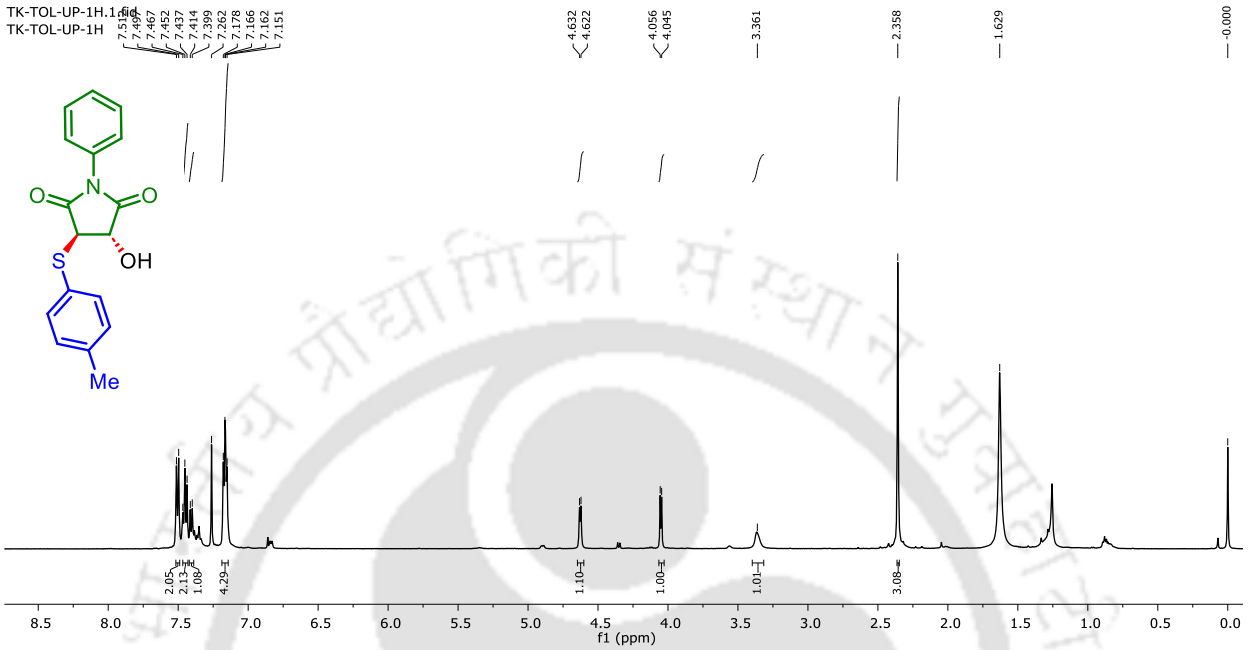

(3*S*,4*R*)-3-Hydroxy-1-phenyl-4-(*p*-tolylthio)pyrrolidine-2,5-dione (3ac): ^{13}C{^{1}H} NMR ($CDCl_3$, 126 MHz)

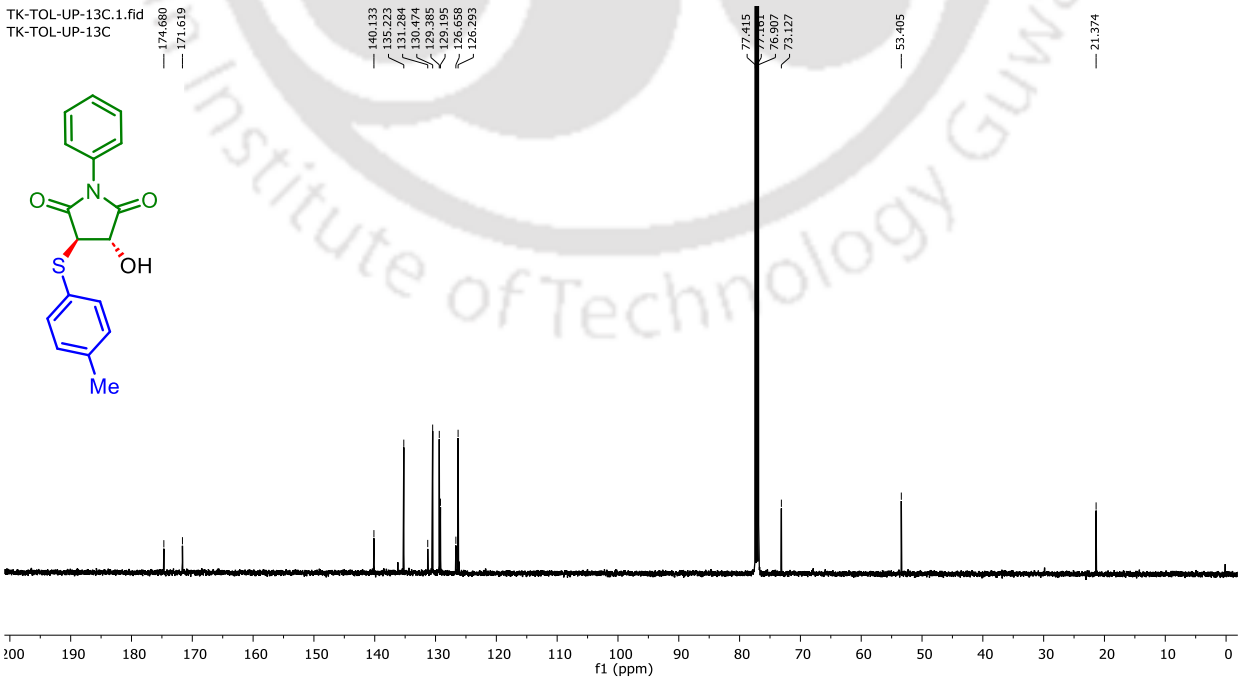

List of Publications:

(i) **Khandelia, T.**; Ghosh, S.; Panigrahi, P.; Shome, R.; Ghosh, S. S.; Patel, B. K. Copper(I)-Mediated Cascade Annulation via Dual C–H/C–H Activation: Access to Benzo[*a*]carbazolic AEEgens. *J. Org. Chem.* **2021**, *86*, 16948. https://doi.org/10.1021/acs.joc.1c02109

(ii) **Khandelia, T.**; Ghosh, S.; Patel, B. K. Dearomative bis-functionalization of quinoxalines and bis-N-arylation of (benz)imidazoles via Cu (II) mediated addition of boronic acids. *Chem. Commun.* **2023**, *59*, 2118. DOI: 10.1039/D2CC06399A

(iii) **Khandelia, T.**; Ghosh, S.; Panigrahi, P.; Mandal, R.; Boruah D.; Patel, B. K. Photo-induced 1,2-thiohydroxylation of maleimide involving disulfide and singlet oxygen. ***Chem. Commun.***, **2023**, *59*, 11196. DOI: 10.1039/D3CC03296E

(iv) **Khandelia, T.**; Patel, B. K. Carbon nanotube-based oil-water separation. Book chapter published by Elsevier. ISBN: 978-0-323-89978-9.

(v) **Khandelia, T.**; Ghosh, S.; Patel, B. K. Cross-Dehydrogenative Coupling Involving Aldehydes for C(sp^2)–C(sp^2) Bond Formation. Book chapter published by Thieme. ISBN: 978-3-13-245524-5. DOI 10.1055/b000000640

(vi) Ghosh, S.; **Khandelia, T.**; Patel, B. K. Solvent-Switched Manganese(I)-Catalyzed Regiodivergent Distal vs Proximal C–H Alkylation of Imidazopyridine with Maleimide. *Org. Lett.* **2021**, *23*, 7370. https://doi.org/10.1021/acs.orglett.1c02536

(vii) Ghosh, S.; **Khandelia, T.**; Panigrahi, P.; Mandal, R.; Patel, B. K. Mn(I)-Catalyzed Preferential Electrophilic C3-Maleimidation in Quinoxaline Leading to Spirocyclization and Dehydrogenation of Succinimides. *Org. Lett.* **2023**, *25*, 3806. https://doi.org/10.1021/acs.orglett.3c01350

(viii) Ghosh, S.; **Khandelia, T.**; Mahadevan, A.; Panigrahi, P.; Kumar, P.; Mandal, R.; Boruah, D.; Venkataramani, S.; Patel, B. K. Photo-Induced Generation of Oxygenated Quaternary Centers via EnT Enabled Singlet O2 Addition to C3-Maleimidated Quinoxaline: A Reagent-Less Approach. *Chem. Eur. J.* **2024**, e202400219. https://doi.org/10.1002/chem.202400219

(ix) Panigrahi, P.; Ghosh, S.; **Khandelia, T.**; Mandal, R.; Patel, B. K. Isoxazole as a nitrile synthon: *en routes* to the *ortho*-alkenylated isoxazole and benzonitrile with allyl sulfone catalyzed by Ru(II). *Chem. Commun.*, **2023**, *59*, 10536. DOI: 10.1039/D3CC02996D

(x) Mandal, R.; Ghosh, S.; **Khandelia, T.**; Panigrahi, P.; Patel, B. K. Base-Induced Decarboxylative 1,1-Alkoxy Thiolation via Hydrothiolation of Vinylene Carbonate. *J. Org. Chem.* **2023**, *88*, 16655. https://doi.org/10.1021/acs.joc.3c02036